Developing small molecule antagonists against AM2 receptor for the treatment of pancreatic cancer

By:

Paris Avgoustou

A thesis submitted in partial fulfilment of the requirements for the degree of Doctor of Philosophy

The University of Sheffield
Faculty of Medicine, Dentistry and Health.
Department of Oncology and Metabolism

Submission Date

May 2018

Acknowledgments

Abstract

Pancreatic cancer is the 11th most common cancer type in the UK. The survival rates are among the lowest in the UK which is directly reflected by its mortality rates that keep raising. Existing therapies include surgical removal and cytotoxic chemotherapeutic cocktails which have minimal improvement in life expectancy.

Adrenomedullin (AM) is a multifunctional peptide that exerts its actions through activation of AM receptor a member of GPCR superfamily. The physiological role of AM as an important regulator of blood pressure is well established. However, emerging data suggest its involvement in several aspects of tumour development including cancer cell growth, angiogenesis, cell survival and the communication between the tumour cells and the host microenvironment.

This study aims to develop novel small molecule antagonists against AM2 receptor. Using a structure/knowledge-based drug modelling program, based on published crystal structures of CGRP and AM1 receptors and recently developed CGRP receptor small molecule antagonists we were able to design and screen a large library of potential antagonists.

Novel compounds were screened for their ability to inhibit cAMP production in CGRPr, AM1r, AM2r AMY1r and AMY3r overexpressing cells. This resulted in the development of a primary structural family with high potency and selectivity against AM2 and CGRP receptors. Several members of this family such as SHF-638, showed high selectivity for AM2 receptor when compared with CGRP.

Pharmacological evaluation of SHF-638, using Schild regression analysis, suggested a competitive mode of antagonism. Moreover, SHF-638 was proven as an excellent tool for *in-vitro* and *in-vivo* use. *In-vivo* administration of SHF-638 resulted in significant decrease of breast and pancreatic cancer subcutaneous tumour growth. Inhibition of AM resulted in decrease proliferation, vessel development and increase in necrosis. Decrease in the presence of pancreatic stellate cells was also observed suggesting involvement of AM in the development of desmoplastic structures.

Overall, the findings of this study suggest that blocking the effects of AM not only influences the development and growth of tumors but is also affecting the tumour microenvironment, feature that could potentially be used for overcoming chemotherapeutic resistance.

Table of content

List of figures

Chapter 5

Chapter 6

Chapter 7

Chapter 8

List of tables

List of Abbreviations

ABC – avidin-biotinylated enzyme complex

AC – adenylate cyclase

ADT – adrenotensin

ADME – Absorption, Distribution, Metabolism, and Excretion

AM – adrenomedullin

AM_{1-52} – peptide agonist of adrenomedullin

AM1r – adrenomedullin-1 receptor (CLR + RAMP-2)

AM2 – adrenomedullin-2 peptide (also known as intermedin (IMD))

AM_{22-52} – antagonist fragment of adrenomedullin

AM2r – adrenomedullin-2 receptor (CLR + RAMP-3)

AMY – Amylin

AMY1r – Amylin-1 receptor

AMY3r – Amylin-3 receptor

Arg – Arginine

ATP – adenosine triphosphate

BRET – bioluminescence resonance energy transfer

BSA – bovine serum albumin

Ca2+ – calcium ions

CAFs – cancer associated fibroblasts

cAMP – Cyclic adenosine monophosphate

CGRP – calcitonin gene-related peptide

CGRPa – peptide agonist of CGRP

CGRPr – calcitonin gene-related peptide receptor (CLR + RAMP-1)

CLR – calcitonin receptor-like receptor

CNS – central nervous system

CT – calcitonin

CTR – calcitonin receptor

Cys – Cystine

DAB – 3,3'-diaminobenzidine

DMEM – Dulbecco's modified Eagle medium

DMSO – dimethyl sulfoxide

DPX – distyrene, plasticiser and xylene mixture

ECD – Extracellular domain

ECL – Extracellular loop

ECM – extracellular matrix

EGFR – epidermal growth factor receptor

ERK – extracellular signal-regulated kinase

FBS – fetal bovine serum

FDA – Food and Drug Administration

FP – fluorescence polarization

FRET – fluorescence resonance energy transfer

GFP – green fluorescent protein

GI – Gastrointestinal

Gln – Glutamine

GPCR – G-protein-coupled receptor

H&E – haematoxylin and eosin staining

HBSS – Hank's buffered saline solution

HCC – hepatocellular carcinoma

HEPES – 4-(2-hydroxyethyl)-1-piperazineethanesulfonic acid

HFLFs – human fetal lung fibroblasts

HIF-1α – hypoxia-inducible factor-1α

His – Histidine

HLMVEC – human lymphatic microvascular endothelial cells

HTS – high-throughput screening

IBMX - 3-isobutyl-1-methylxanthine

ICL – intracellular loop

IHC – immunohistochemistry

IMD – intermedin (also known as adrenomedullin-2 peptide (ADM-2))

IP1 – myo-Inositol 1 phosphate

IP – intraperitoneal

IV – intravenous

IVIS – *in vivo* imaging system

MAPK – mitogen-activated protein kinase

MEK – mitogen-activated protein kinase kinase

MNC – mononuclear cell

MR-proADM – mid-regional pro-adrenomedullin

NF-κB – Nuclear factor-κB

NO – nitric oxide

O/E – Overexpressing

PAMP – pro-adrenomedullin peptide

PBS – phosphate-buffered saline

Phe – Phenylalanine

PI – phosphatidylinositol

PI3K – phosphatidylinositol 3'-kinase

PK – pharmacokinetics

PKA – protein kinase A

PKC – protein kinase C

PLC – phospholipase C

P.O – oral administration

PPB – plasma protein binding

Pro – proline

PSCs – pancreatic stellate cells

RAMP – receptor activity-modifying protein

RET – Resonance energy transfer

RFU – relative fluorescence units

ROI – region of interest

RPMI – Roswell Park Memorial Institute

RT – room temperature

SD – standard deviation

SEM – standard error of the mean

SP – substrate P

TAE – Tris-acetate EDTA

TBS – Tris-buffered saline

TE – Tris-EDTA

TM – Transmembrane

TMD – Transmembrane domain

TR-FRET – time resolved fluorescence resonance energy transfer

TRPA1 – transient receptor potential channel A1

Try – Tryptophan

VEGF – Vascular endothelial growth factor

VSMCs – vascular smooth muscle cells

SAR – structure–activity relationship

SB – subcutaneously

αSMA – alpha-smooth muscle actin

List of Residues

D – Aspartic acid	K – Lysine
E – Glutamic acid	P – Proline
F – Phenylalanine	Q – Glutamine
G – Glycine	R – Arginine
W – Tryptophan	T – Threonine
Y – Tyrosine	V – Valine

Chapter 1: General introduction

Chapter 1: General Introduction

1.1 Pancreas and pancreatic cancer

The pancreas is a flat and pear-shaped gland (~15cm long, in humans) that consist of endocrine (made up of α, β, γ and δ cells) and exocrine (made up of acinar, centroacinar and duct cells) compartments (Cano et al., 2007). Upon food intake, the exocrine cells are responsible for releasing digestive fluids which contain enzymes that facilitate the breakdown of food and absorption of nutrients by the intestine. The endocrine cells, which are normally arranged in clusters known as islets of Langerhans, release hormones (such as insulin, amylin, somatostatin, pancreatic polypeptide and glucagon) that control the use and storage of these nutrients (energy fuels) by the body during various metabolic processes (Cano et al., 2007, Folias and Hebrok, 2013). These functions make the pancreas an important organ for several physiological processes such as the regulation of blood glucose, glucose metabolism and food digestion.

There are several diseases associated with the pancreas and its abnormal function including type I and II diabetes mellitus, pancreatitis and pancreatic cancer. According to Cancer Research UK statistics, pancreatic cancer is the 11th most common cancer type in the UK (12th in men and 9th in women), with approximately 9600 new cases (3% of all cancer cases) in both sexes in 2014. The incidence rates of the disease have significantly increase by ~14% during the last few decades and are projected to rise by ~6% in the next 20 years (2014-2035). Figure 1.1 below illustrates the incidence rates of the twenty most common cancer types in the UK in 2014. Moreover, pancreatic cancer is the fourth most common cause of cancer related deaths in women (~ 4400 deaths in 2014) and the fifth in men (~ 4400 deaths in 2014) making it the fifth most common cause of cancer related deaths in the UK (Cancer Research UK, 2014). Furthermore, in a study published in 2015 in which Malvezzi and colleagues compared cancer related deaths with standardised death rates, pancreatic cancer was found to be the only type of cancer with an increase in the predicted cancer deaths and mortality rates in both male (4%) and female (5%) between 2009 and 2015 in Europe (Malvezzi et al., 2015). In the United States,

studies have predicted that pancreatic cancer will likely climb up to second from fourth place (above breast, prostate and colorectal cancer) in cancer related deaths only behind lung cancer by 2030 (figure 1.2 below) (Rahib et al., 2014). This is directly reflected by the survival of pancreatic cancer which is considered one of the lowest in the world. More specifically, according to data obtain by Cancer Research UK approximately a fifth of the patients (21%) (both men and women) survive for one year post diagnosis, a percentage which then falls dramatically to less than a 3% survival at five years and approximately to 1% survival at ten year (Cancer research UK, 2014c). Figure 1.3 below shows one-, five- and ten-year survival rates of common cancers in the UK with pancreatic cancer to be at the bottom with the lowest rates (Cancer research UK, 2014b).

There are two main categories of pancreatic cancer, the exocrine tumours that originate from exocrine cells, and the endocrine tumours that originate from endocrine cells. Approximately 90% of them are malignant ductal adenocarcinomas which belong to the exocrine carcinoma family (Bornman and Beckingham, 2001). Most of the cases of pancreatic cancer are presented to the clinic with non-specific symptoms such as abdominal pain, weight loss, nausea, fatigue and painless jaundice. These symptoms occur after the establishment of the tumour (unresectable disease) which is often related with poor prognosis or terminal disease (Bond-Smith et al., 2012). Symptoms such as muscle wasting, enlarged supraclavicular lymph node and back pain usually suggest advance disease and still worse prognosis (Bornman and Beckingham, 2001).
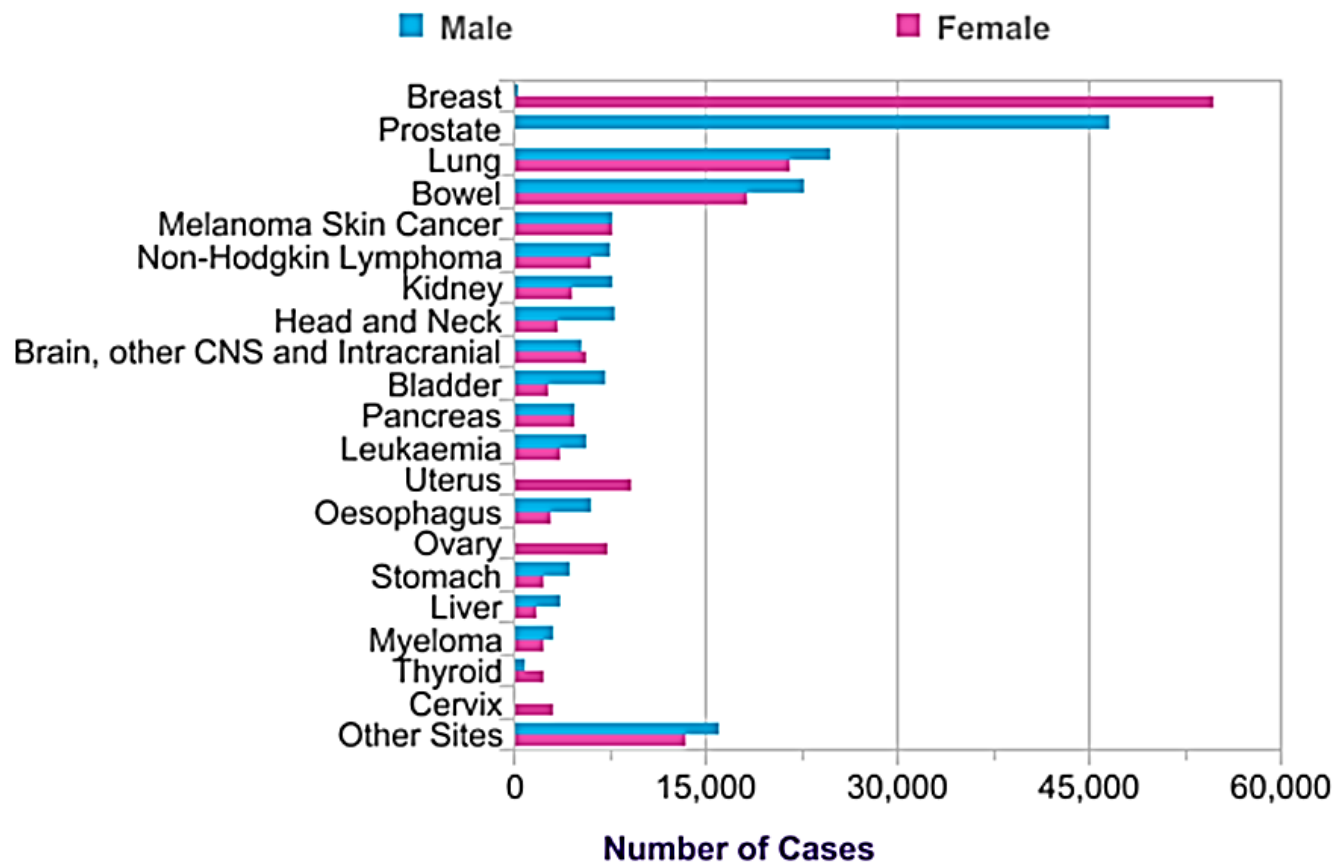
Figure 1.1: Incidence rates of the twenty most common cancer types in the UK. Graphical representation (histogram) of the incidence rates of most common cancer types in both male and female population in the UK in 2014. Pancreatic cancer is the 11th most common cancer in the UK with ~9600 new cases. Adapted from (Cancer research UK, 2014a).
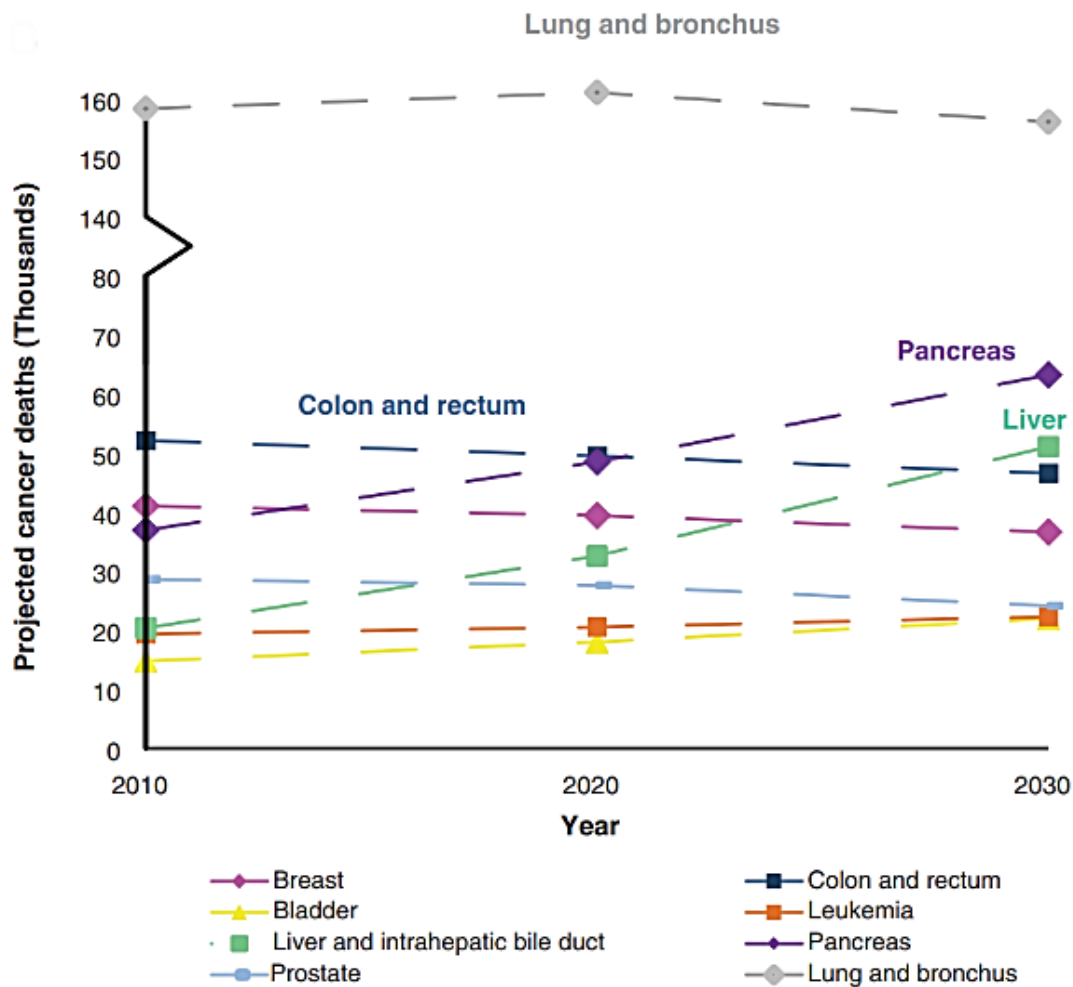
Figure 1.2: Projected cancer related deaths in the United States. Graphical illustration of the predicted cancer related deaths in the United States over a period of 20 years (2010-2030). It is estimated that pancreatic cancer will overcome both breast and colorectal cancer and become the second most common cause of cancer related deaths in the US by 2030. Figure modified from Rahib et al., 2014, with permission from Elsevier.
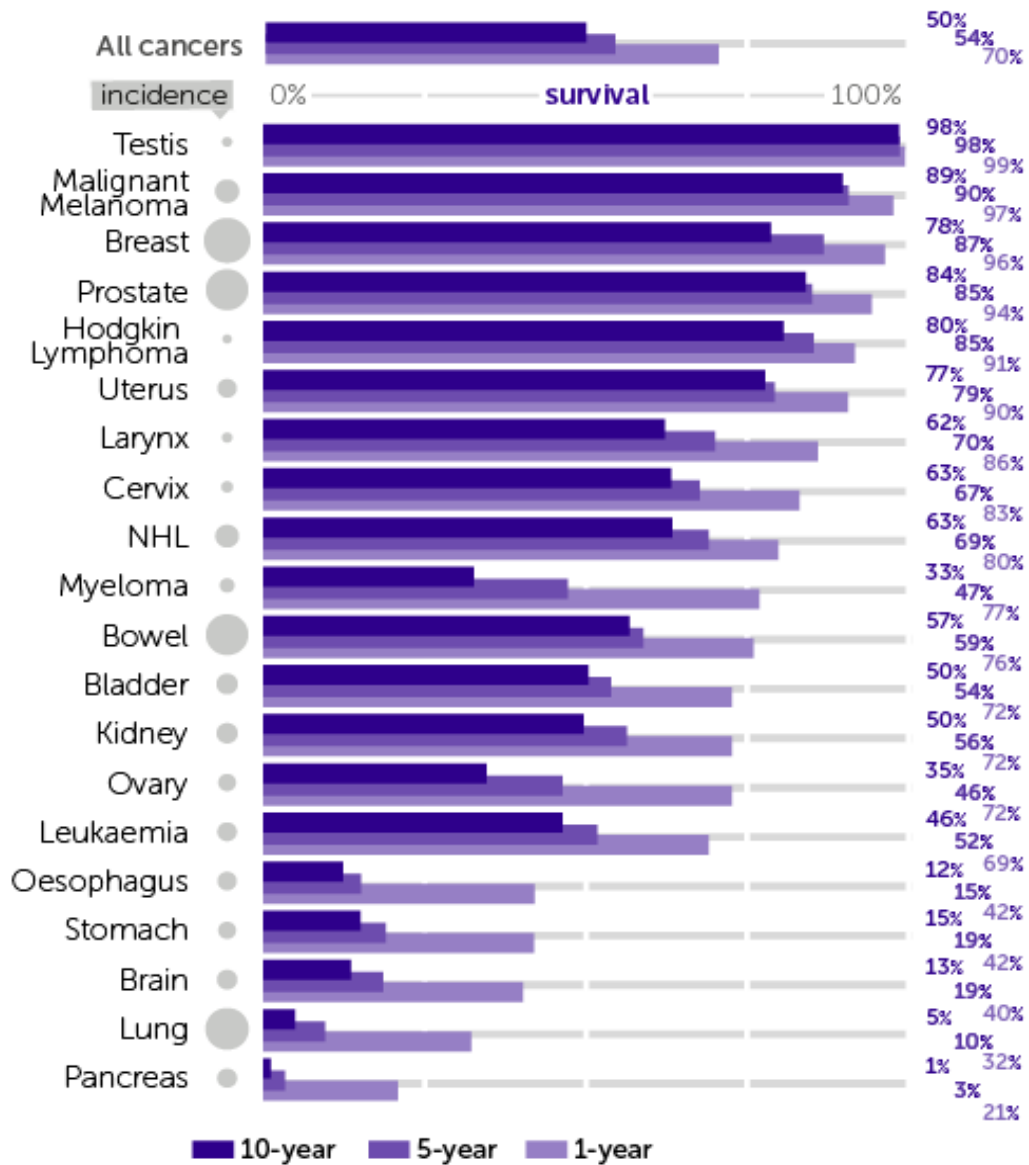
Figure 1.3: One-, five- and ten-year survival rates of common cancers in the UK.
Graphical representation of the survival rates of the most common cancer types in the UK. Survival rates of pancreatic cancer remain the lowest in the UK with no significant improvement in the last decade. Adapted from (Cancer research UK, 2014b)

1.2 Current treatment for pancreatic cancer

1.2.1 Surgery and conventional chemotherapy

Surgery is considered the main treatment option for pancreatic carcinomas. However, treating pancreatic cancer can be challenging mainly because more than 80% of the patients present with non-resectable tumours, locally advanced tumours or metastatic disease (mainly liver) leaving only palliative care, focusing on improving quality of life, as the main treatment option (Pierantoni *et al.*, 2008). Palliative treatment may include bile duct stenting or partial removal of the tumour to reduce the symptoms, but with no hope of a remission of disease. Following surgery or in patients with non-resectable tumours other treatment options are available including radiotherapy and adjuvant chemotherapy that aims to reduce recurrence risk and/or improve survival (Li et al., 2015b), although increases in lifespan are generally insignificant.

One of the most common treatment option is the use of potent cytotoxic chemotherapeutics alone or in combination (i.e. FOLFIRINOX which consists of **FOL** – folinic acid, **F** – fluorouracil (5FU), **IRIN** – irinotecan, **OX** – oxaliplatin.). Currently the preferred chemotherapeutic is Gemcitabine (originally an antiviral agent), is a nucleoside analogue which targets DNA synthesis of cancer cells. More specifically, Gemcitabine replaces cytidine (nucleic acids building blocks) during DNA replication making DNA polymerases unable to proceed (a process called masked chain-termination), reducing tumour growth and promoting apoptosis. Another target of Gemcitabine is ribonucleotide reductase, an enzyme important for DNA replication and repair (Lawrence et al., 2003). The combination of gemcitabine with other chemotherapeutic agents for the treatment of advanced pancreatic cancer has been studied in several randomised control trials with controversial results. Such agents include Capecitabine (pro-drug)/Fluorouracil (antimetabolite) (Cunningham et al., 2009), cisplatin (Heinemann et al., 2006) and oxaliplatin (Louvet et al., 2005) (platinums), irinotecan (Neri et al., 2009) and exatecan (Abou-Alfa et al., 2006) (topoisomerase I inhibitors) as well as paclitaxel (Von Hoff et al., 2013) and docetaxel (taxanes - mitotic inhibitors). Most of these combinations had mildly beneficial effects for the patients when compared to the gemcitabine alone group. However,

some show minimal or no significant improvement in life extension. This suggests that combining anticancer drugs with different mechanisms of action can improve the efficacy and effectiveness of chemotherapy.

1.2.2 Molecular targeted therapy

The development of targeted therapies, that specifically target pathways involved in the progression of cancer (i.e. EGFR (epidermal growth factor receptor), VEGF (Vascular endothelial growth factor)), in the form of small molecules or antibodies has given oncologists new tools for the treatment of pancreatic cancer. For example, in a phase II trial, the combination of nimotuzumab (a monoclonal antibody that binds only cells that over-express EGFR) with gemcitabine and cisplatin was associated with significant improvement in a small group of patients (six patients with stable disease) that failed to respond after first-line standard chemotherapy (Strumberg et al., 2012). Moreover, the combination Erlotinib, another tyrosine kinase inhibitor (EGFR), with gemcitabine increased the progression free survival of patients when compared with gemcitabine alone (Moore et al., 2007). Furthermore, the combination of Bevacizumab (angiogenesis inhibitor targeting VEGF) with gemcitabine and/or Erlotinib has shown promising but not significant results when compared with placebo in both advanced (Kindler et al., 2005) and metastatic (Van Cutsem et al., 2009) disease.

Despite advances in the development of new therapeutic agents that have improved the outcome of several types of cancer, prognosis of pancreatic cancer remains very poor. Moreover, only 3% of the patients that undergo surgery will survive for five years (Bond-Smith *et al.*, 2012, De La Cruz *et al.*, 2014). Furthermore, delivery of chemotherapeutic agents is quite challenging in patients with pancreatic cancer due to the nature of the disease that is characterized by the formation of dense fibrous and connective tissue around the tumours that consists of alpha (α)-smooth-muscle actin (α-SMA) positive cancer associated fibroblasts (CAFs) or activated pancreatic stellate cells (PSCs), immune cells and extracellular matrix (ECM) proteins (Pandol et al., 2009). This shows the desperate need for more effective drugs that will improve patients' quality of life and potentially treat their disease. This requires deeper

understanding of the mechanisms and pathways that are related with the development of pancreatic cancer.

1.3 G-protein coupled receptors

G-protein-coupled receptors (GPCRs), a superfamily of seven transmembrane domain receptors that consists of more than 800 members (Pierce et al., 2002, Hauser et al., 2017) is one of the most prominent target family for drug development (~34% of all approved Food and Drug Administration (FDA) drugs – 475 drugs (Hauser et al., 2017, Overington et al., 2006)). This superfamily is subdivided into seven distinct families/classes (A-F, although, D and E are not found in humans) based on sequence similarity (members of each classes normally share ~ 25% homology) and the ligands with which they interact (Eglen and Reisine, 2009, Hauser et al., 2017, Isberg et al., 2016). Calcitonin and calcitonin-like receptor families both belong to Class B subfamily alongside with parathyroid hormone and corticotropin-releasing hormone receptors (Pierce et al., 2002).

1.3.1 Adrenomedullin (AM) peptide

Adrenomedullin (AM) is a 52-amino acid multifunctional peptide that belongs to the calcitonin family of peptides together with calcitonin gene related peptide (CGRP), calcitonin (CT) and amylin (AMY) based on their homology (Poyner et al., 2002, Westermark, 2011). AM was firstly isolated by Kitamura et al. in 1993 from a human pheochromocytoma, and it was found to have a single disulphide bond between residues 16 and 21 and an amidated tyrosine at its carboxyl terminus (Kitamura et al., 1993a). The peptide was found to be synthesized as part of a larger gene precursor (located at chromosome 11) known as pre-pro-adrenomedullin which consists of 185 residues in both humans (Kitamura et al., 1993b) and rats (Sakata et al., 1993) and of 188 amino acids in pigs (Kitamura et al., 1994). The first step of AM production is the removal of 21 amino acids (signal peptide) at the amino-terminus of pre-pro-adrenomedullin during its transport across the cell membrane. This leads to the formation of pro-adrenomedullin which is then cleaved further by endogenous peptidases resulting in the creation of four physiologically distinct

peptides: PAMP (pro-adrenomedullin N-terminal 20 peptide, preproAM22–41), Mid-regional (MR)-proAM (PreproAM45–92), AM (PreproAM95–146), and ADT (adrenotensin or PreproAM153–185) (Hinson et al., 2000, Qi et al., 2002). Schematic illustration of the biosynthesis of the peptides is shown in figure 1.4 below. Adrenomedullin was thought to be expressed by vascular endothelial cells (Fernandez-Sauze et al., 2004). However, several studies have found the expression of AM in most tissues of the body and in several normal and cancer cell types (Hinson et al., 2000). Expression of AM was found in many other mammalian species including rat, mouse, pig, dog and bovine as well as fish (Hinson et al., 2000). A closely related peptide known as adrenomedullin 2 (AM2) or intermedin (IMD) was discovered in 2004 showing generally similar effects with AM peptide (Roh et al., 2004, Takei et al., 2004).
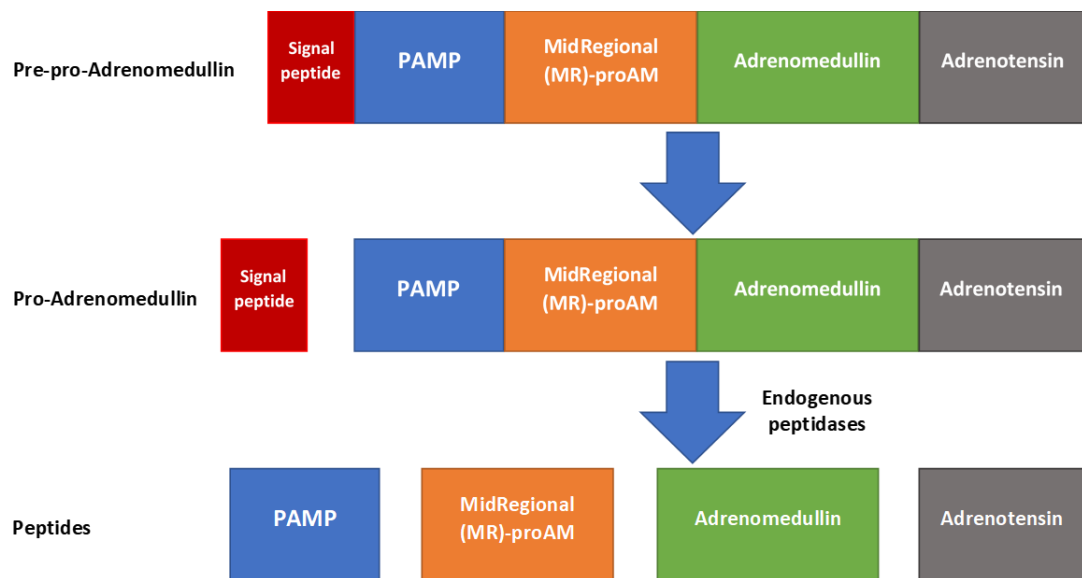
Figure 1.4: Schematic illustration of the biosynthesis of Pre-pro-adrenomedullin derived peptides. The first step of AM production is the removal of 21 amino acids (signal peptide) at the amino-terminus of pre-pro-adrenomedullin. This leads to the formation of pro-adrenomedullin which is cleaved by endogenous peptidases forming four distinct peptides: PAMP, Mid-regional (MR)-proAM, AM, and adrenotensin (ADT).

1.3.2 Calcitonin gene related peptide (CGRP)

CGRP is a 37-amino acid neuropeptide located in both central and peripheral neurons. As mentioned above CGRP belongs to the calcitonin family of peptides alongside with AM, AMY and CT (Poyner et al., 2002, Westermark, 2011). The discovery of CGRP emerged from studies aiming to clone and analyse human calcitonin precursor mRNA (CALC I gene) secreted by the C-cells of the thyroid (Craig et al., 1982). Subsequent studies have shown that calcitonin precursor generates two mRNAs encoding for calcitonin and CGRP (Amara et al., 1982, Rosenfeld et al., 1983). There are mainly two isoforms of CGRP, αCGRP and βCGRP which are also referred to in the literature as CGRP I and CGRP II. The two isoforms have analogous structures (~90% homology- differing by only three amino acids) and similar biological activities. However, they are coded for two separate genes (Amara et al., 1985). αCGRP is synthetized from CALC I gene which as described above can undergo splicing and produce either CT or αCGRP peptides. βCGRP is known to be synthesized from a separate gene called CALC II (Steenbergh et al., 1986). αCGRP is considered as the main isoform of the gene that is in the central and peripheral nervous system. Studies have shown that the β isoform is mainly found in the enteric nervous system (Mulderry et al., 1985). Similarly to adrenomedullin, αCGRP mRNA (produced by CALC I gene) is first translated to produce a larger precursor hormone known as pre-CGRP (consisting of 121-amino acids), which is then cleaved at both the N- and C-terminus leading to the synthesis of a mature 37-amino acid peptide (αCGRP), a N-terminus peptide and a C-terminus peptide (Russell et al., 2014). For the αCGRP mRNA to be produced and lead to the synthesis of CGRP, expression of exons 5 and 6 on the CALC I gene is required. On the other hand, if exon 4 is expressed this will lead to the production of pre-CT and therefore the synthesis of CT peptide (mainly in the thyroid) (Russell et al., 2014). Schematic illustration of the gene splicing of CT and CGRP is shown in figure 1.5 below.

Calcitonin mRNA

Poly (A) tail

| 5' Non-coding exon | C1 | C2 | Calcitonin coding exon |

Common coding regions

CGRP mRNA

Poly (A) tail

| 5' Non-coding exon | C1 | C2 | CGRP coding exon | CGRP 3' non-coding exon |

Common coding regions

Translation

Thyroid "C" cells → Pre-Calcitonin (135-amino acids)

Neuronal cells → Pre-CGRP (121-amino acids)

H₂N — | Common region + 6aa | Calcitonin (33aa) | 16aa | — COOH

H₂N — | Common region + 4aa | CGRP (37aa) | 4aa | — COOH

Post-Translational processing

| N-terminus peptide | Calcitonin (33aa) | C-terminus peptide |

| N-terminus peptide | CGRP (37aa) | C-terminus peptide |

Figure 1.5: Schematic illustration of the synthesis of calcitonin and CGRP peptides. In neuronal cells, αCGRP mRNA is translated to produce a larger precursor hormone, pre-CGRP. This is then cleaved at both the N- and C-terminus forming a mature 37-amino acid peptide (αCGRP), a N-terminus peptide and a C-terminus peptide. Similarly, CT peptide is synthesised after the translation of calcitonin mRNA in the thyroid ''C'' cells which leads to the formation of pre-calcitonin. After post-translational processing, pre-calcitonin is cleaved to 33-amino acid CT peptide, a N-terminus peptide and a C-terminus peptide. Modified from (Russell et al., 2014).

1.4 Calcitonin receptor-like receptor (CLR) family

AM and CGRP peptides exert their actions through their binding on AM and CGRP receptors respectively. Both receptors belong to the CLR family, a member of Class B GPCR superfamily. CLR, a seven-transmembrane domain (461-amino acid) protein, was discovered during the early 90s by studies that identified a novel receptor closely related to calcitonin receptor (CTR) (~96% sequence homology with the rat and ~56% homology with the human proteins) which was however unresponsive to CGRP stimulation when expressed in cell lines (Chang et al., 1993, Fluhmann et al., 1995). Later, in 1996 the expression of the same cloned receptor in human embryonic kidney cells (HEK293) had as a result the increase (60-fold) of cAMP (Cyclic adenosine monophosphate) production upon CGRP stimulation. This response led to the

discovery of a protein that was found to be endogenously expressed by HEK293 cells (Aiyar et al., 1996). This protein was later named, receptor activity modifying protein (RAMP) and recognised as an important regulator in receptor trafficking and pharmacology (McLatchie et al., 1998).

RAMPs are accessory proteins that can modulate the function of GPCRs upon binding. There are three known mammalian RAMPs (RAMP 1, 2 and 3), all consist of a single transmembrane domain, with an extracellular ~90-100 amino acid long N-terminus domain (depending on the family member) and a short (9 amino acids) C-terminus domain (Sexton et al., 2001). The use of a homology search led to the observation that the three RAMP members share 31% homology in their primary sequence and 56% similarity in their secondary structure (McLatchie et al., 1998). Their co-expression with CLR, led to the formation of three functionally distinct receptors. Association of RAMP-1 with CLR produces a receptor for CGRP (CGRPr), heterodimerization of CLR with RAMP-2 produces the Adrenomedullin 1 receptor (AM1r) and association with RAMP-3 produces the Adrenomedullin 2 receptor (AM2r) (McLatchie et al., 1998). A schematic illustration of the heterodimerization of RAMPs and CLR can be found in figure 1.6 below. Interaction of the three different RAMPs with the two variants of the closely related to CLR, CTR (CTRa and CTRb) produces six distinct human AMY receptors (AMYr) (Hay et al., 2004). The other member of the AM peptide family, AM2 or IMD, was found to be more potent on CGRP receptor but less potent on AM1r and AM2r when compared to AM peptide (Bell and McDermott, 2008, Weston et al., 2016). Table 1.1 below summarises the rank order of agonist potency of all the members of calcitonin family of receptors. The structural characteristics of the RAMP and receptor binding and the role of RAMPs on receptor activation and pharmacology will be discussed in chapter 4.
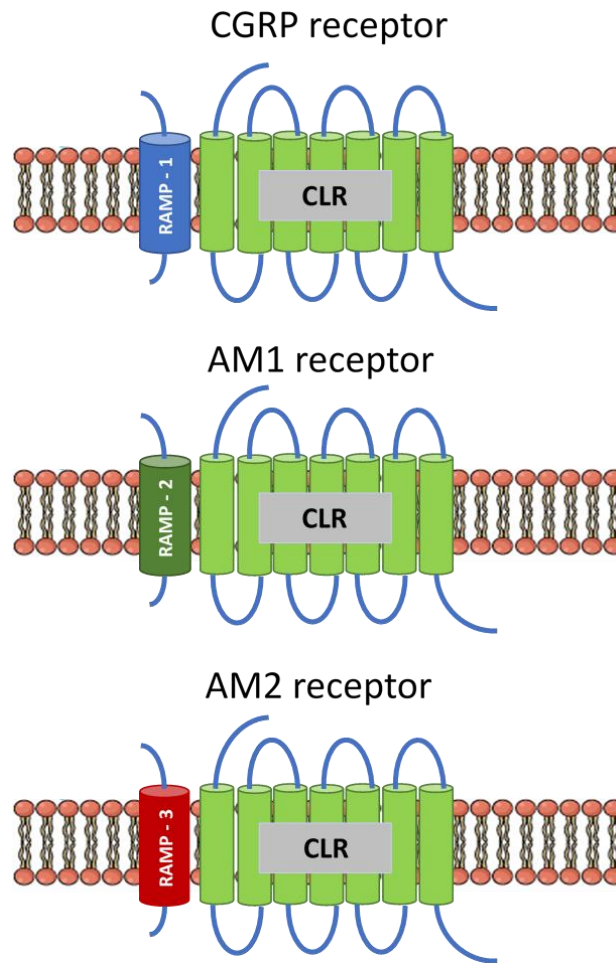
Figure 1.6: Schematic illustration of the heterodimerization of RAMPs and CLR.
CLR binds with RAMP1 to form a CGRP receptor and with RAMP2 and RAMP3 to form two functionally distinct AM receptors (AM1 and AM2).

Table 1.1: Rank order of agonist potency (Calcitonin receptor family)

Receptor	Composition	Rank order of agonist potency
CGRPr	CLR + RAMP1	αCGRP > IMD = AM ≥ AMY ≥ CT
AM1r	CLR + RAMP2	AM > αCGRP > IMD > AMY > CT
AM2r	CLR + RAMP3	AM = IMD > αCGRP > AMY > CT
AMY1r	CTR + RAMP1	AMY ≥ αCGRP > CT > AM
AMY2r	CTR + RAMP2	Poorly characterised
AMY3r	CTR + RAMP3	AMY > αCGRP > AM

1.5 Ligand binding and B Class GPCRs activation – essential components

A model (commonly known as 'two-domain model') that defined the mode of ligand binding and activation of B Class GPCRs was previously described by several groups (Bergwitz et al., 1996, Runge et al., 2003, Al-Sabah and Donnelly, 2003). More specifically, the model suggests that the first interaction occurs between the carboxyl-terminal site of the peptide ligand and the amino-terminal extracellular domain of the receptor. Then the amino-terminal of the ligand binds with the extracellular loops and the seven-transmembrane domain (collectively known as juxtamembrane domain) of the receptor leading to receptor activation and signal transduction (Hoare, 2005). However, the lack of structural information from a full-length member of class B family of GPCRs does not allowed for the complete identification of the essential components involved in ligand binding and receptor activation.

1.5.1 Extracellular domain (ECD)

As the extracellular domain of the receptor is the initial binding site of the ligand it is considered as essential for ligand binding. For this reason, several studies have been focused on the identification and characterization of the ECD of several Class B GPCRs. The role of CLR and RAMPs extracellular domain in the druggability and binding potential of the CLR: RAMPs heterodimeric receptors was explained in the section above. The importance of ECD on ligand binding and receptor activation was suggested in other B-Class GPCRs. More recently, the role of several CTR ECD residues in peptide ligand binding was proposed by Gingell and co-workers. Using a homology model of CTR: RAMP1 receptor using the crystal structure from Booe et al. and alanine mutations Gingell and co-workers were able to identify important residues on CTR and RAMP1 ECD based on their effects on peptide binding (figure 1.7 below) (Gingell et al., 2016).
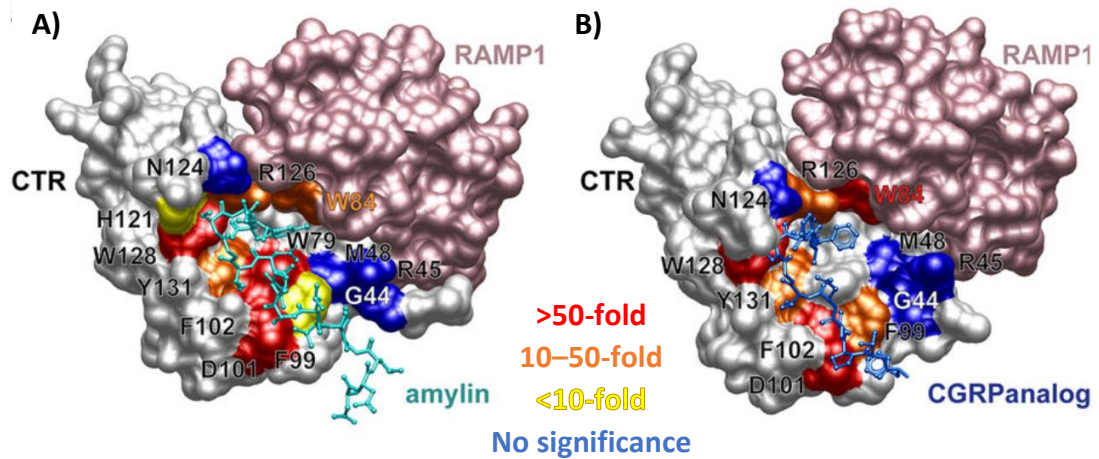
Figure 1.7: Homology model of peptide-bound CTR (White): RAMP1 (Pink) receptor. Illustrates the predicted mode of peptide ligands, **(A)** rAmy (rat AMY, light blue) and **(B)** CGRP$_{27-37}$ (dark blue), binding on AMY1 receptor. The key residues are highlighted with distinct colours depending on their effects on peptide binding defined after alanine substitution. Images from Gingell et al., 2016, reused with permission from Elsevier (creative commons attribution license).

1.5.2 Juxtamembrane domain (Extracellular loops (ECLs) and Transmembrane domains (TMDs))

As mentioned above, the second step of ligand binding involves the interaction of peptide N-terminus with the juxtamembrane domain, although studies of these regions have been proven challenging due to the lack of crystal structures of those domains. The interaction of the ECD with the juxtamembrane domain of the receptor has been suggested to have a significant role in ligand binding. More specifically, mutational analysis of the extracellular residues of rat secretin receptor suggested the presence of a disulphide bridges between the ECD and the second transmembrane domain (TMD2) which are essential for receptor activation (Vilardaga et al., 1997). The first detailed analysis of the function of the ECL1 and ECL3 of the CGRP receptor was conducted by Barwell et al. in 2011 using a combination of alanine and leucine substitution scans. More specifically, the analysis revealed the importance of ECL1 and its associated TM (transmembrane) regions in

the modulation of both ligand binding and the efficacy of αCGRP. ECL3 and its associated TMDs was found to be important in the regulation of cell surface receptor expression (Barwell et al., 2011). In another study, using a combination of mutagenesis and modelling, Woolley and co-workers were able to identify several ECL2 residues (ECL2, R274, W283, D280, D287 and T288) important for the binding of CGRP with its receptor, suggesting the role of ECL2 and its TM regions in the modulation of this interaction (Woolley et al., 2013). More recently, the importance of ECL2 and ECL3 and their adjacent TM regions in the function of CTR receptor was investigated by Dal Maso and colleagues. More specifically, mutations on the ECL2 interconnected network had as a result the increase of peptide efficacy and selectivity for cAMP but did not affect any other signalling pathways (binding affinity, myo-Inositol 1 phosphate (IP1) accumulation and (extracellular signal-regulated kinase) ERK1/2 phosphorylation) tested. This indicated the role of CTR ECL2 in the regulation of Gs/cAMP signalling. Moreover, ECL3 mutations revealed the more complex role of this regions showing distinct ligand and pathway specific effects, indicating the possible use of this region for future implications (agonist or antagonist development) (Dal Maso et al., 2018). Even though, these studies offer a deeper understanding of the role of Juxtamembrane domain, the interaction of RAMPs with receptors such as CLR and CTR (see chapter 4) provide more complexity in the efforts of understanding these interactions.

1.6 Physiological and pathophysiological role of AM and CGRP

As was previously described in the above sections AM and CGRP belong to the calcitonin superfamily of regulatory hormones/peptides. Their activation and action is facilitated by the formation of three distinct receptors comprised of a seven-transmembrane domain B Class GPCR known as CLR and one of the three single transmembrane domain accessory protein known as receptor associate modifying proteins (RAMP 1-3). These receptors are CGRPr, AM1r and AM2r depending on the RAMP isoform involved. The role of AM and CGRP in both physiology and disease will be discussed in the section below.

1.6.1 Calcitonin gene related peptide (CGRP)

1.6.1.1 CGRP and physiological role

CGRP has been found to be involved in several physiological processes in the nervous system, cardiovascular system and other tissues of the body. The peptide is considered as the most potent vasodilator reported with potency ~10 fold greater than prostaglandins, and other vasodilators such as acetylcholine and substance P. It was first described as a potent vasodilator in 1985 when the administration (femtomolar concentrations) of CGRP induced an increase in the blood flow causing reddening of the skin in human and animal (hamster and rabbit) species (Brain et al., 1985). In another study injection of CGRP (picomolar) into human skin had as a result the formation of an erythema which lasted for several hours (Brain et al., 1986). Moreover, systemic administration of CGRP in both normotensive (Gangula et al., 1999) and hypertensive (Itabashi et al., 1988) rats had as a result the reduction of blood pressure. This is thought to be mediated through both nitric oxide (NO) dependent and independent dilatator pathways in peripheral arterial vessels. In addition to vasodilatory effects, intravenous (IV) administration of CGRP had effects in heart rate regulation (inotropic and chronotropic responses) in rats (Ando et al., 1990). Despite the actions described above, studies fail to link CGRP with the physiological regulation of systemic blood pressure. Data from studies using antagonists suggested that inhibition of CGRP did not had significant effects on blood pressure regulation or heart rate (Arulmani et al., 2004, Petersen et al., 2005, Zeller et al., 2008). On the other hand, these data and the perivascular location of CGRP suggests the role of CGRP as a microvascular vasodilator that regulates vascular responsiveness and protects organs from injury. This theory is supported by studies where loss or increase of CGRP causes local responses. For example, loss of CGRP as a response to capsaicin resulted in the formation of skin lesions in rats (Thomas et al., 1994), however, increase of CGRP was linked to blushing syndrome (facial reddening) (Wyon et al., 1998). Moreover, studies have shown that CGRP can have cardio-protection effects against the damage caused during ischemic shock (Chai et al., 2006) and antiplatelet effects (Li et al., 2008).

1.6.1.2 CGRP and pathophysiological conditions

The role of calcitonin gene related peptide in pain and inflammation has been the focus of several studies since the discovery of the peptide. As one of the two main proinflammatory neuropeptides, CGRP together with substrate P (SP) are considered important regulators of neurogenic inflammation. Since SP can promote microvascular permeability and CGRP is an extremely potent vasodilator it is believed that the release these peptides regulates the blood flow and the recruitment of inflammatory cells (oedema formation) in areas of inflammation (Russell et al., 2014). Studies suggested the role of CGRP in the inhibition of lymphocyte differentiation and proliferation (McGillis et al., 1993) and in the regulation of the activity of other inflammatory cells (such as Langerhans cells and macrophages) (Ichinose and Sawada, 1996, He et al., 2000). The role of CGRP in inflammation has been reviewed in detail (Fernandes et al., 2009). Moreover, a recent systematic review found an association between CGRP levels with somatic, visceral, neuropathic, inflammatory and musculoskeletal pain (Schou et al., 2017). Studies suggested the role of CGRP in peripheral and central sensitization and therefore the amplification and transmission of pain signals (Iyengar et al., 2017).

The hypothesis that CGRP is playing a significant role in the pathophysiology of migraine and that inhibition of its actions could be beneficial for the treatment of the disease has been the focus of several studies during the last few decades. Migraine headache is a very common chronic neurovascular disorder that affects a considerable proportion of the adult population worldwide. It is believed that onset of migraine involves the dilation of cranial blood vessels (including carotid arteriovenous anastomoses) (Villalon et al., 2002) and the activation of trigeminovascular system (Goadsby et al., 2002). The presence of CGRP (alongside with SP) in cranial blood vessels and more specifically in trigeminal ganglia was demonstrated almost immediately after the discovery of the peptide (Uddman et al., 1985). As was described and illustrated by several groups CGRP levels are elevated upon stimulation of trigeminal perivascular nerves (after migraine attacks) causing vasodilatation and neurogenic inflammation (promoting migraine related symptoms

including pain) (Goadsby et al., 1988, Goadsby et al., 1990, Edvinsson, 2004). This was supported by studies that showed the elevation of plasma CGRP levels in external jugular venous blood during migraine attacks (Goadsby et al., 1990, Goadsby and Edvinsson, 1994, Gallai et al., 1995). These levels were then normalized by the administration of antimigraine agents such as the triptans. Similarly, in a large study with 45 migraine patients, elevated CGRP plasma levels were significantly decreased after administration of rizatriptan (a serotonin receptor agonist). The decrease of the CGRP levels was correlated by the authors with the relief of migraine symptoms (Stepien et al., 2003). Moreover, IV infusion of CGRP in migraine patients, causes the onset of migraine-like attacks (delayed headache) (Lassen et al., 2002, Lassen et al., 2008). What is more, IV infusion of NO (another potent vasodilator), produced similar delayed migraine-like effects and it was directly associated with a significant increase in plasma CGRP levels (Juhasz et al., 2003). This was supported by a separate, suggesting that these delayed episodes are correlated with increased levels of NO synthase that acts on trigeminal perivascular nerves and causes CGRP release and vasodilation (Akerman et al., 2002). These data in combination with the well documented role of CGRP in pain regulation created the interest of several pharmaceutical organizations in the development of CGRP antagonists (either in the form of antibodies or small molecules).

Inhibiting CGRP and its actions was the first attempt for the development of new therapies for the treatment of acute migraine during the early 2000s. To do so several small molecules or antibodies that target either the peptide or its receptor have been developed in the last few decades by several groups and pharmaceutical companies including small molecules Olcegepant, Telcagepant and MK3207. Further details on the discovery of these molecules and their structural characteristics can be found in chapter 3.

1.6.2 Adrenomedullin (AM)

The expression of AM was reported in most organs, tissues and cells in the body. More specifically, AM expression was reported in the cardiovascular system, adrenal medulla, lung, pancreas, Gastrointestinal (GI) tract, thyroid, skin, liver, kidney, placenta, central nervous system (CNS) and reproductive system (Ichiki et al., 1994, Washimine et al., 1995, Asada et al., 1999, Eto et al., 2003). This broad distribution of the peptide is accounting for its crucial role in multiple physiological and pathophysiological processes. As was reviewed before by others, AM upregulation/expression was found to have beneficial effects in several processes of the organism including angiogenesis, proliferation, prevention of apoptosis and vasodilation (Cheung and Tang, 2012, Kato and Kitamura, 2015). These actions were primarily associated with the protective and beneficial role of AM on the organism, however, studies have shown that these can also lead to development of diseases including cancer (Nikitenko et al., 2006b). The role of AM in different systems and organs and processes of the body as well as its potential role in development and progression of cancer will be discussed in this section.

1.6.2.1 Cardiovascular system and vasodilation

The significant role of AM in the regulation of cardiovascular system was demonstrated in several knockout *in-vivo* studies where embryonic lethality was observed due to cardiovascular defects upon the deletion of functional AM or its receptor components (CLR and RAMP2 but not RAMP3) (Shindo et al., 2001, Dackor et al., 2006, Ichikawa-Shindo et al., 2008). Elevated levels of plasma AM was found in several cardiovascular associated diseases (Wong et al., 2012) including: hypertension (Ishimitsu et al., 1994), heart failure (Nishikimi et al., 1995, Kato et al., 1996), myocardial infarction (Kobayashi et al., 1996, Miyao et al., 1998) and peripheral arterial occlusive disease (Suzuki et al., 2004). AM was also found to have protective effects on the heart. In two *in-vivo* studies Nakamura and co-workers have illustrated that intraperitoneally injection of synthetic AM into a rat model of myocardial infarction was able to increase the survival and decrease the weakening of cardiac function (Nakamura et al., 2002, Nakamura et al., 2004). Similarly,

administration of AM was able to protect rodents from myocardial infarction and injury by ischemia–reperfusion (Kato et al., 2003, Okumura et al., 2004, Hamid and Baxter, 2006). Several mechanisms are being reported to be involved in these protective effects including: suppression of oxidative stress, phosphorylation of Akt and inhibition of muscle cell (myocyte) apoptosis. In clinical trial, IV infusion of AM had a significant improvement in the function of left ventricle in patients with acute myocardial infarction (Kataoka et al., 2010).

AM regulates vasodilation either by activating the cAMP pathway (resulting in elevation of cAMP) and potassium channels leading to vascular smooth muscle cells (VSMCs) relaxation or by stimulating NO production through an endothelium-dependent mechanism (Wong et al., 2012, Kato and Kitamura, 2015, Schoenauer et al., 2017). In-vitro, incubation of rat VSMCs with AM resulted in a significant decrease in FCS-stimulated proliferation of the cells, effect which was correlated with cAMP pathway activation (Kano et al., 1996). Moreover, administration of both AM and sodium nitroprusside (NO donor), had as a result the inhibition of endothelial cell apoptosis (Sata et al., 2000). Administration of NO synthase inhibitor (L-NAME) was able to decrease the vasodilatory effects of AM (Feng et al., 1994). Intravenous infusion of AM resulted in an increase of the cardiac output by reducing vascular resistance and increasing blood flow in patients with Congestive Heart Failure (Nagaya et al., 2000). Furthermore, AM was shown to have a protective role in the development of pulmonary hypertension induced in healthy male SD rats by increased blood flow (Pang et al., 2014). Finally, in a clinical trial the inhalation of AM was able to improve pulmonary hemodynamic profile (such as pulmonary arterial pressure and pulmonary vascular resistance) and exercise capacity in patients with idiopathic pulmonary arterial hypertension when compared with the placebo inhalation group (Nagaya et al., 2004).

1.6.2.2 Angiogenesis

The importance of AM in the regulation of angiogenesis was demonstrated in several studies. Angiogenesis is a complex process that involves the proliferation and migration of endothelial cells leading to the formation and maturation of newly

developed vessels and the remodelling of the extracellular matrix (Jain, 2003). Even though AM exerts its biological actions through two receptor complexes: the CLR-RAMP2 and CLR-RAMP3 complex, studies have shown that CLR-RAMP2 and not RAMP3 complex (Dackor et al., 2007) has significant importance in the regulation of angiogenesis and vascularisation. Several studies indicated that deletion of AM, CLR and RAMP2 genes leads to a common feature of embryo-lethality due to diminished vascular development (Caron and Smithies, 2001, Shindo et al., 2001, Dackor et al., 2006, Ichikawa-Shindo et al., 2008, Koyama et al., 2013). This indicates the distinct physiological roles of CLR-RAMP2 and CLR-RAMP3 (Dackor et al., 2007).

The role of AM in endometrial angiogenesis was demonstrated in 2000 by Nikitenko and colleagues. Using immunohistochemistry, they were able to identify the presence of AM in endometrial endothelial cells both *in-vitro* and *in-vivo*. Moreover, using [methyl-3^H]-Thymidine uptake assays they illustrate the role of AM in the growth of endothelial cells as well (Nikitenko et al., 2000). Furthermore, treatment with AM had as a result the induction of pulmonary arterial endothelial cells sprouting *in-vitro* and the formation new vessel *in-vivo*. It is worth mentioning that these effects were inhibited by the addition of phosphatidylinositol 3'-kinase (PI3K) and ERK1/2 inhibitors suggesting the involvement of Akt and mitogen-activated protein kinase (MAPK) pathways in AM-induced angiogenesis (Kim et al., 2003). Similarly, AM-induced vascular regeneration was inhibited by AM antagonists as well as inhibitors of protein kinase A (PKA) and PI3K (regulators of Akt activation) (Miyashita et al., 2003).

The therapeutic potential of AM as angiogenic regulator was reported by several studies. Administration of AM promoted the growth, migration, and networking of human lymphatic microvascular endothelial cells (HLMVEC) *in-vitro* and increased the blood flow and the formation of lymphatic vessels in tail lymphoedema *in-vivo*. The angiogenic effects of AM were inhibited by cAMP and mitogen-activated protein kinase kinase (MEK) inhibitors suggesting that these changes are mediated partly through the cAMP/MEK/ERK pathway (Jin et al., 2008). In another study, the injection of human AM DNA and human AM DNA-gelatine complex resulted in a significant improvement in a rabbit model of chronic hind limb ischemia (collateral

formation and hind limb perfusion) when compared to gelatine alone (Tokunaga et al., 2004). Similarly, AM administration in combination with bone marrow–derived mononuclear cell (MNC) transplantation was able to increase the MNC differentiation to endothelial cells and the production of mature vessels in rats with hindlimb ischemia when compared to MNC transplantation alone (Iwase et al., 2005). Moreover, topical (in the form of an ointment) administration of AM had beneficial effects in the wound healing process of pressure ulcers in an *in-vivo* mouse model. More specifically, AM increased the formation of granulation tissue as well as the process of angiogenesis and lymph-angiogenesis (Harada et al., 2011)

1.6.2.3 Other physiological actions of AM

Elevated levels of AM and AM1r component (CLR and RAMP2) genes were found in human fetal lung during gestation period (10-24 weeks) suggesting its role in human lung development. Interestingly, RAMP3 gene expression was found to be decreased suggesting diverse functions of AM receptors (Ramos et al., 2014). Furthermore, in an *in-vivo* study AM administration of AM in guinea pigs had as a result the inhibition of antigen-induced microvascular leakage and bronchoconstriction (Ohbayashi et al., 1999). Moreover, administration of AM via three different routes (Intravenous, inhalation and cell-based gene transfer), had beneficial effects in rats (cell-based treatment) and patients with pulmonary hypertension (Nagaya and Kangawa, 2004). Finally, a recent study suggested the role of AM as a protective factor of human fetal lung fibroblasts (HFLFs) against hypoxia-induced pulmonary damage by decreasing fibrosis (Hao et al., 2011).

Studies have found that adrenomedullin is synthesized in the testis, where plays a significant role in sperm maturation, storage and secretion (Santiemma et al., 2001, Hwang et al., 2003, Marinoni et al., 2005). Interestingly, co-expression of CLR and RAMP1/RAMP2 mRNA was found in all regions of rat epididymis (Hwang et al., 2003). Its involvement in the regulation of prostatic blood flow was illustrated in an *in-vivo* study (Shibata et al., 2006). AM was also found to be involved in progesterone production by ovarian cells (Moriyama et al., 2000) and in the development and differentiation of the corpus luteum (Abe et al., 2000). Moreover, elevated levels of

AM were observed in women during pregnancy including decidualization, implantation and placentation (DiIorio et al., 1997, Hu and Cross, 2010, Matson and Caron, 2014). Furthermore. a reduction of AM expression had as a result the disruption of implantation, placentation and fetal growth in mice (Li et al., 2006). These data suggest a key role of AM in the reproductive system.

Both AM and its receptor components were found to be expressed in the central nervous system suggesting its biological action in physiological and pathophysiological processes related to CNS (McLatchie et al., 1998). Lack of AM or reduction of AM production *in-vivo* was correlated with increased brain damage induced by middle cerebral artery occlusion when compared with the wild type mice (Miyamoto et al., 2009, Hurtado et al., 2010) suggesting a protective effect. Moreover, Miyashita and co-workers showed the protective effects of AM both *in-vitro* and *in-vivo.* More specifically, AM inhibited the apoptosis of neuronal cells *in-vitro* reduced brain damage, promoted vascular regeneration and functional recovery *in-vivo* (Miyashita et al., 2006). Mice overexpressing (O/E) circulating AM showed less cognitive decline and better white matter integrity after chronic cerebral hypoperfusion (Maki et al., 2011). Finally, pre-treatment of rats with AM prior induction of cerebral oedema by middle cerebral artery occlusion showed a protective effect by supressing the formation of oedema when compared to $AM_{22\text{-}52}$ antagonist or saline pre-treatment (Kondoh et al., 2011). It was also suggested that AM can mediate these protective actions utilizing several mechanisms including reduction of oxidative stress, increase in angiogenesis and inhibition of neuronal and glia cells apoptosis (Xia et al., 2006, Kondoh et al., 2011).

1.6.3 AM and Cancer

AM contributes to the development and progression of cancer by promoting cancer cells growth (proliferation) and tumour angiogenesis and by inhibiting apoptosis of cancer cells (Martinez et al., 2002, Zudaire et al., 2003). Upregulation AM was reported in several endocrine or endocrine-related tumours as well as other types of tumours. More specifically, AM was associated with the progression of several cancer types including: pancreatic cancer (Ishikawa et al., 2003, Ramachandran et al., 2007, Ramachandran et al., 2009), breast cancer (Oehler et al., 2003, Brekhman

et al., 2011), prostate cancer (Calvo et al., 2002, Berenguer et al., 2008), hepatic cancer (Nakata et al., 2008), renal cancer (Michelsen et al., 2006), lung cancer (Martinez et al., 1995), neuroendocrine carcinomas (Pavel et al., 2006), ovarian cancer (Liu et al., 2009), and many other types (reviewed by (Hay et al., 2011)). Moreover, studies have shown that AM is particularly upregulated by hypoxia and other stimuli including cytokines, promoting angiogenesis and neovascularization (Zudaire et al., 2003, Zhang et al., 2017). The role of AM in the survival of cancer cells under hypoxic conditions, a feature that characterises the microenvironment of several solid tumours (Harris, 2002), was previously illustrated (Oehler et al., 2001, Martinez et al., 2002). It is also shown that AM has an important role in the communication between the tumour cells themselves and between the tumour cells and the host microenvironment promoting tumour growth (Zudaire et al., 2006). Even though AM was found to be expressed in most organs and tissues of the body, in tumours, AM is produced by tumour cells themselves, the vascular epithelium as well as cancer associated cells (such as macrophages and mast cells) (Zudaire et al., 2003, Zudaire et al., 2006, Nikitenko et al., 2006b, Hay et al., 2011).

1.6.3.1 AM and tumour cells growth and survival (proliferation and apoptosis)

Overexpression of AM in breast cancer cell line T47D had as a result the maintenance of cancer cell proliferation and the inhibition of apoptosis, under serum deprivation conditions, when compared to cells that carried the empty plasmid alone. T47D cells O/E AM showed higher levels of oncoproteins including Ras, Raf and MAPKp49 as well as lower levels of pro-apoptotic proteins such as Bax, Bid, and Caspase-8 (Martinez et al., 2002). In the same study, the injection of AM O/E T47D cells *in-vivo* resulted in higher number of xenograft tumours (3 out of 10) compared to cells transfected with the empty vector (0 out of 10) (Martinez et al., 2002). Moreover, overexpression or treatment with AM *in-vitro* reduced the hypoxia-induced apoptosis in endometrial cancer cells by inducing the upregulation of the oncoprotein Bcl-2 (Oehler et al., 2001). The activation of PI3K/Akt signalling pathway was observed after treatment of hepatocellular carcinoma (HCC) cells with AM which

was correlated with an increase in proliferation. These effects were prevented by the use of the AM peptide inhibitor: AM_{22-52} (Park et al., 2008). Furthermore, the use of a polyclonal AM antibody (anti-AM) had as a result the significant reduction in U87 glioblastoma cells (cells with high levels of endogenous AM) proliferation *in-vitro* and in the growth of subcutaneous U87 xenograft *in-vivo* (Ouafik et al., 2002). Moreover, Albertin and colleagues have shown that both endothelin-1 and AM were able to increase the growth of human adrenocortical carcinoma-derived SW-13 cells by promoting proliferation and by inhibiting apoptosis (Albertin et al., 2005). Administration of anti-AM receptor antibodies (alphaAMRs) significantly decreased the glioblastoma (U87) and colorectal (HT-29) tumour cell growth *in-vitro* and supressed the growth of glioblastoma (U87 cells), lung (A549 cells), and colorectal (HT-29 cells) tumour xenografts *in-vivo* (Kaafarani et al., 2009). In a study of cell apoptosis induction by either serum deprivation or chemotherapeutic agent etoposide, AM treatment was able to decrease cell death of prostate cancer cell lines. More specifically, AM decreased cell death in cell lines PC-3 and DU145, but not in LNCaP cells after serum removal. After treatment with etoposide, AM prevented apoptosis in LNCaP and PC-3 cells but not in DU145 cells (Abasolo et al., 2006). During the same treatment, PC-3 cells O/E AM showed a decrease in cleaved PARP (a marker of apoptosis) and no change in the ratio of Bcl-2/Bax complex, when compared with parental PC-3 cells, suggesting a protective role of AM in cancer cell death (Abasolo et al., 2006).

1.6.3.2 AM and tumour angiogenesis/metastasis

The role of AM in angiogenesis under physiological conditions has been shown by several studies. However, it has been reported that this role of AM could be utilised by cancer cells to promote their growth, migration, invasion and therefore metastasis to distant tissues. AM expression in uterine leiomyomas, a benign tumour of the female reproductive system, was related with endothelial cells proliferation and vascularization (Hague et al., 2000). Similarly, increased vascular density was observed after the overexpression of AM in T47D breast cancer cell line both *in-vitro* (aortic ring assay) and *in-vivo* (Martinez et al., 2002). *In-vivo* treatment of pancreatic

cancer cell line (PCI-43) xenografts with AM antagonist (AM_{22-52}), had as a result the significant decrease in tumour growth and blood vessel formation (Ishikawa et al., 2003), suggesting a potential role of AM antagonist for the treatment of pancreatic cancer. Similarly, a reduction in vascular density was also observed in human glioblastoma cells xenografts that were treated with anti-AM polyclonal antibody (Ouafik et al., 2002). Furthermore, a reduction in blood flow recovery as well as in the neovascularisation was observed in both AM knock down (AM+/-) mice and mice treated with AM_{22-52} that also showed significant decrease in subcutaneous tumour growth (sarcoma 180 cells). The effects of AM on tumour angiogenesis and growth were correlated with increase expression of VEGF and activation of Akt *in-vitro* (Iimuro et al., 2004). DIVAA (Directed In Vivo Angiogenesis Assay) analysis of *in-vivo* angiogenesis, induced by injection of human MC leukaemia cell line (HMC-1), have shown that administration of an anti-AM monoclonal antibody (MoAb-G6) have resulted in the inhibition of neovascularisation, supporting the notion that AM plays a significant role in tumour angiogenesis (Zudaire et al., 2006). Recently, immunohistochemical analysis of 56 epithelial ovarian cancer (EOC) tissues, revealed the positive correlation between AM expression and hypoxia-inducible factor-1α (HIF-1α), VEGF and CD34 (marker of cell adhesion) as well as micro-vessel density. Moreover, the expression of HIF-1a and VEGF (important regulators of tumour angiogenesis) in relation with AM was investigated *in-vitro*. Administration of AM or AM_{22-52} on epithelial ovarian cancer cells (CAOV3) caused the upregulation or downregulation of HIF-1a and VEGF, respectively (Zhang et al., 2017).

Other than angiogenesis, AM expression was positively correlated with invasion and metastasis. Analysis of plasma concentration levels in breast cancer patients showed a significant increase in AM levels compared to healthy individuals. This increase was associated with bigger tumour size as well as the presence of lymph node metastasis (Oehler et al., 2003). The expression of AM and its receptor components CLR and RAMP-2 (RAMP-1 and RAMP-3 expression were not investigated) was found in human choriocarcinoma JAr cells and first-trimester cytotrophoblast HTR-8/SV neo cells. Stimulation of these cell lines with AM resulted in an increase in proliferation as well as an increase in their invasion capabilities (Zhang et al., 2005). Moreover,

Nakata and co-workers identify AM as the leading gene in the gene expression profile produced by microarray analysis in primary HCC with intrahepatic metastasis (IM) suggesting its role in the metastatic potential (Nakata et al., 2008). In a study of clear cell renal carcinoma, the expression of AM, CLR and RAMP-2 was found in epithelial compartments of tumour sections whereas RAMP-3 was identified in inflammatory cells that infiltrated the tissue, suggesting a role in the crosstalk between the tumour and the microenvironment. Incubation of two clear cell carcinoma cell lines (BIZ and 786-O) with AM resulted in a significant increase of both invasion and migration. Administration of antibodies (anti-CLR, anti-RAMP2, and anti-RAMP3) that specifically bind to all components of AM receptors as well as AM_{22-52} had as a result a significant decrease in the effects of AM (Deville et al., 2009).

The role of AM in the formation and the development of pancreatic cancer as well as the effects of AM inhibition in the growth of pancreatic tumours *in-vivo* will be discussed in chapter 6.

1.7 Conclusion

Pancreatic cancer is the 11th most common cancer type in the UK with the incidence rates of the disease to have increase significantly during the last few decades. The disease has the lowest survival rates among the most common types of cancer in the UK with only 21% of patients surviving one year after diagnosis. The percentage then falls dramatically to 3% and 1% for five years and ten years survival respectively. (Cancer research UK, 2014c). This is directly reflected by the pancreatic cancer related deaths, as pancreatic cancer is the fifth most common cause of cancer related deaths in the UK (Cancer Research UK, 2014) with its mortality rates to keep raising. What is more, in the US predictions are ranking pancreatic cancer at the second from fourth place (above breast, prostate and colorectal cancer) in cancer related deaths by 2030 (Rahib et al., 2014). These data illustrate the unmet need for the development of novel targets and new therapies which will be more effective than the existing approaches, which mainly involve surgical removal followed by cytotoxic chemotherapeutic cocktails.

An emerging potential target for the development of new therapies for the treatment of pancreatic cancer in AM. AM is multifunctional peptide that belongs to calcitonin family of peptides together with CGRP, CT and AMY (Westermark, 2011). AM exerts its actions through activation of AM receptor a member of Class B GPCR superfamily. AM receptor consists of CLR receptor, a seven-transmembrane domain and one of the three accessory proteins also known as RAMPs, a single-transmembrane domain protein. There are three known mammalian RAMPs (RAMP 1, 2 and 3), co-expression of which with CLR results in the formation of three functionally distinct receptors: CGRPr (CLR + RAMP1), AM1r (CLR + RAMP2) and AM2r (CLR + RAMP3) (McLatchie et al., 1998).

The physiological role of AM as an important regulator of blood pressure is well established. In several in-vivo studies, embryonic lethality was observed due to cardiovascular defects upon the deletion of functional AM or its receptor components (CLR and RAMP2 but not RAMP3) (Shindo et al., 2001, Dackor et al., 2006, Ichikawa-Shindo et al., 2008). This indicates the distinct physiological roles of CLR-RAMP2 and CLR-RAMP3 (Dackor et al., 2007).

On the other hand, AM has been found to be involved in the growth of more than 70% of tumours including pancreatic cancers. Studies have shown the involvement of AM in several aspects of tumour development including cancer cells growth (proliferation), tumour angiogenesis and cancer cell survival (Martinez et al., 2002, Zudaire et al., 2003). Moreover, AM contributes to the development and progression of cancer by facilitating the communication between the tumour cells host microenvironment (such as mast cells) (Zudaire et al., 2006). Several studies have shown that overexpression or treatment with AM resulted in inhibition of apoptosis in several cancer cell lines both *in-vitro* and *in-vivo* (Oehler et al., 2001, Martinez et al., 2002, Abasolo et al., 2006). Moreover, inhibition of AM using AM_{22-52} peptide inhibitor or AM polyclonal antibody resulted in decrease of proliferation of cancer cell lines *in-vitro* and the growth of subcutaneous tumours *in-vivo* (Ouafik et al., 2002, Park et al., 2008, Kaafarani et al., 2009). Furthermore, overexpression of AM in T47D breast cancer cell line was related with increased vascular density both *in-vitro* and *in-vivo* (Martinez et al., 2002). Inhibition of AM resulted in a reduction of

blood vessel formation in pancreatic cancer cell line (PCI-43) xenografts (Ishikawa et al., 2003) as well as in human glioblastoma cells xenografts (Ouafik et al., 2002) suggesting a possible role of AM in vessel development *in-vivo*. Finally, expression of AM was previously correlated with invasion and metastasis (Oehler et al., 2003).

These findings indicate the importance of AM in the development of cancer and the possibility of targeting AM2 receptor for the treatment of the disease. The recently published solved crystal structures of CLR: RAMP1 (CGRP) and CLR: RAMP2 (AM1) receptors as well as the successful development of CGRP receptor small molecule antagonists, formed the basis of our drug discovery program for the development of AM2 receptor specific small molecule antagonists.

1.8 Aim and Objectives

Aim

The principal aim of these study is the development of selective small molecule antagonists against AM2 receptor while not targeting the other members of the calcitonin family of receptors.

Objectives

Objective 1: Develop and optimise a robust screening assay suitable for high-throughput screening purposes.

Objective 2: Investigate the effects of novel small molecule antagonists on receptor activation. Use cAMP cell-based assays to investigate the ability of these antagonists to inhibit the activation of receptors and determine their affinity over the different members of the family.

Objective 3: Determine the suitability of leading compounds to be used in animal studies by establishing their pharmacological (Schild analysis) and *in-vitro* metabolic profiles (ADME studies).

Objective 4: Investigate the pharmacokinetics (PK studies) and the *in-vivo* efficacy of the leading small molecule antagonist.

Chapter 2: General materials and methods

Chapter 2: Materials and methods

2.1 Cell culture techniques

2.1.1 Cells maintenance

All cells were maintained according to the manufacture's instruction in a humidified incubator at 37°C, with 5% CO_2. Cells were normally kept in filter cap T75cm^2 or T175cm^2 flasks or any other size flask or culture plates (according to the needs of the experiments). Cells were passaged or preserved (frozen down) every 2-3 days or when ~70-80% of confluence was reached. Confluency was monitored under an inverted microscope (INVERSO, Medline Scientific Ltd, UK). All material and reagents used for the maintenance of the cells can be found in sections 2.1.1 and 2.1.2 above.

2.1.2 Cell trypsinization/harvesting

In order to harvest the cells either for cell passaging (sub-culturing) or counting to set up an experiment, media was removed from the flasks/plates and cells were washed twice using PBS (phosphate-buffered saline) buffer. TrypLE Express dissociation reagent or Assay-Complete Detachment reagent (see table below for details) was then added to the flask/plate and cells were incubated at 37°C for 2-5 minutes or until all cells were detached from the flask bottom. The reagent was then neutralized with appropriate (equal or more) volume of culture media and the cell suspension was transferred to a 15ml or 50ml centrifuge tube. Cells were then counted if needed or centrifuged at 300 x g for 5 minutes. The resulting cell pellet was re-suspended in 10 ml of media. Appropriate volume of cells (depending on dilution factor and the flask size) was then transferred to a sterile flask or culture plate contained warm culture media. Table 2.2 below shows the various sizes of culture vessels used and the volumes of culture media and dissociation reagents for each size.

Table 2.1: Showing the dissociation reagents used in cell culture techniques

Reagent	Source	Catalogue number
TrypLE Express dissociation reagent	Thermo Fisher scientific (Loughborough, UK)	12605010
Assay-Complete Cell Detachment Reagent	DiscoveRx (Birmingham, UK)	92-0009

Table 2.2: Illustrating the surface area and volumes of culture media and dissociation reagents for various size culture vessels.

Culture vessels	Surface area (cm^2)	Media (mL)	Dissociation reagent (mL)	Neutralization Volume (mL)
Culture Plates				
6-well	9	3.0-5.0	1.0-2.0	2.0
12-well	4	1.0-2.0	0.5-1.0	1.0
24-well	2	0.5-1.0	0.2-0.5	0.5
96-well	0.32	0.1-0.2	0.05-0.1	0.1
Culture Flasks				
T-25	25	3.0-5.0	1.0-2.0	3.0
T-75	75	8.0-12.0	3.0-4.0	6.0-7.0
T-175	175	20-30	5.0-6.0	7.0-8.0

2.1.3 Cell thawing

Following all appropriate safety precautions (wearing mask and gloves) cells were removed from the liquid nitrogen and any pressure was released from the cryo-preserving tube before they immersed in a 37 °C water bath for 30-40 seconds. Cells were then transferred in a 15ml sterile centrifuge tube contained 9ml of the appropriate culture media and centrifuged 300 x g for 5 minutes to form a cell pellet. The resulting cell pellet was re-suspended in 10 ml of media. Appropriate volume of cells (depending on dilution factor and the culture vessel size) was then transferred to a sterile flask/plate contained warm culture media.

2.1.4 Cell counting

A dissociated cell solution was prepared as described in section 2.1.4 above. Before centrifuge the cells at 300 x g for 5 minutes to form a cell pellet, 10μL of the cell suspension were transferred into a sterile 0.5ml microcentrifuge tube and mixed with 10ul of trypan blue (Thermo Fisher Scientific, Catalogue number: 15250-061). The mixture was then transferred to a disposable counting slides and cells were counted using Countess II Automated Cell Counter (Thermo Fisher Scientific).

2.1.5 Cell freezing (cryo-preservation)

A single cell suspension was prepared as described in section 2.1.4 above. However, in the case of transfected cell lines (Section 2.1.2 above) instead of culture media, Assay-Complete Cell Plating Reagent was used for cell suspension. Before cell suspension was centrifuged at 300 x g for 5 minutes to form a pellet, 500ul was removed to be used in cell counting (described in Section 2.1.6 above). The cell pellet was then re-suspended in the appropriate volume of the growth medium supplemented with 10% dimethyl sulfoxide (DMSO) or in Assay-Complete Preserve Freezing Reagent depending on the cell line. 1ml of the cell suspension was then transferred into cryo-preserving tubes which were labelled with cell line, passage number, date and name. Cryo tubes were then stored in -80°C overnight before placing them in liquid nitrogen. Cells were frozen down in $1e^6$ or $2e^6$ depending on the experiment's requirements.

Table 2.3: Showing the reagents used during cell preservation

Reagent	Source	Catalogue number
DMSO (dimethyl sulfoxide)	Sigma Aldrich (Dorset, UK)	D4540
Assay-Complete Preserve 1321N1 Freezing Reagent	DiscoveRx, Birmingham, UK	92-0017FR6S
Assay-Complete Preserve CHO-K1 Freezing Reagent	DiscoveRx, Birmingham, UK	92-0017FR2S
Assay-Complete Cell Plating Reagent	DiscoveRx, Birmingham, UK	93-0563R

2.2 cAMP assays

cAMP is a very important second messenger, used for intracellular signal transduction in many biological processes, derived from adenosine triphosphate (ATP). The conversion of ATP to cAMP is mediated by activation of adenylate cyclase through several GPCRs. The production of cAMP by G-protein couple receptor O/E cell lines after peptide or small molecule stimulation in an agonist or antagonist assays was measured using LANCE® cAMP Assay kit (catalogue number: AD0264) (see figure 2.1 below for details) (Perkin Elmer, Waltham, Massachusetts, United States).
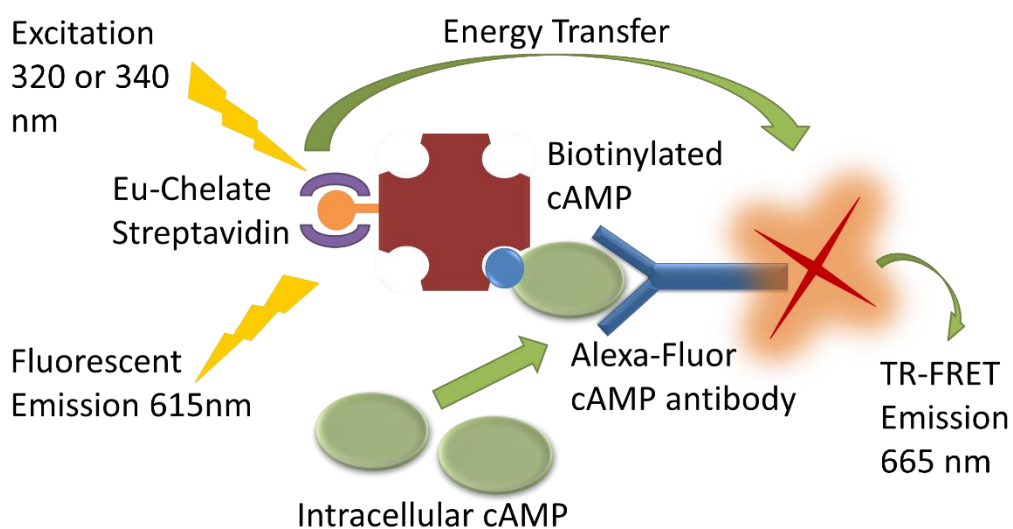
Figure 2.1: LANCE® cAMP Assay kit principle. LANCE® cAMP Assay is based on time resolved fluorescence resonance energy transfer (TR-FRET). As shown on the diagram above a labelled cAMP tracer complex (Europium-Chelate streptavidin/biotinylated cAMP) is competing with intracellular cAMP, for binding sites on Alexa-fluor labelled cAMP-specific antibody. When the cAMP tracer complex is bound with the antibody, energy (340 nm excitation) is transferred from Eu-chelate streptavidin to an Alexa molecule of the antibody which results in TR-FRET emission at 665 nm. The intensity of the emission will then decrease in the presence of intracellular cAMP.

2.2.1 cAMP standard curve protocol

cAMP standard curves were used to evaluate the quality of each assay kit and identify any differences between the different batches of reagents. Moreover, standard dose response curves were used to establish the assay detection window and to optimise different assay parameters (for more details see chapter 3). More detailed illustrations of the agonist and agonist/antagonist competition assays can be found in chapters 3 and 4 respectively (material and methods section).

Serial dilutions (6µl/well) of cAMP standards (see table 2.5 below for dilution details) made in stimulation buffer (see table 2.4 below for buffer formulation) were plated in 384 well OptiPlates (catalogue number: 6007299, Perkin Elmer). Equal volume (6µl/well) of Alexa fluor antibody solution (1:100 concentration in stimulation buffer) was then added to the wells. The plate was then incubated for 30 minutes at room temperature before the addition of 12µl detection mix (Europium-Chelate streptavidin/biotinylated cAMP tracer) (see table 2.6 below for detection mix formulation). Following a 60 minutes incubation period, the plate was then read on the Enspire multimode Plate reader (Perkin Elmer, Waltham, Massachusetts, United States), at; 320/340nm excitation and 615/665nm emission was recorded (see table 2.7 for plate reader settings). During all incubation periods plates were kept covered in the dark.

Table 2.4: Stimulation buffer formulation

Reagent	Volume	Source	Catalogue number
1x HBSS (Ca^{2+}, Mg^{2+}) *	28mL	Thermo Fisher scientific (Loughborough, UK)	24020-117
1M HEPES (pH 7.4) Final conc: 5mM	150ul	Sigma Aldrich (Dorset, UK)	H3375
Stabilizer, 7.5% (BSA) Final conc: 0.1%	400ul	Perkin Elmer (Massachusetts, USA)	CR84-100
250mM IBMX Final conc: 0.5mM	60ul	Sigma Aldrich (Dorset, UK)	I5879

*1x HBSS (Hank's buffered saline solution) with no Ca^{2+} and Mg^{2+} was used in cell-based assays (for cell preparation)
* HEPES (4-(2-hydroxyethyl)-1-piperazineethanesulfonic acid)
* IBMX (3-isobutyl-1-methylxanthine)

Table 2.5: cAMP standard serial dilutions in Stimulation Buffer

Dilution	Final (M) concentration	2X (M) Concentration	Volume of dilution	Stimulation buffer (diluent)
1	$1e^{-6}$	$2e^{-6}$	$3.3\mu l$*	$96.7\mu l$
2	$3e^{-7}$	$6e^{-7}$	$30\mu l$	$70\mu l$
3	$1e^{-7}$	$2e^{-7}$	$30\mu l$	$60\mu l$
4	$3e^{-8}$	$6e^{-8}$	$30\mu l$	$70\mu l$
5	$1e^{-8}$	$2e^{-8}$	$30\mu l$	$60\mu l$
6	$3e^{-9}$	$6e^{-9}$	$30\mu l$	$70\mu l$
7	$1e^{-9}$	$2e^{-9}$	$30\mu l$	$60\mu l$
8	$3e^{-10}$	$6e^{-10}$	$30\mu l$	$70\mu l$
9	$1e^{-10}$	$2e^{-10}$	$30\mu l$	$60\mu l$
10	$3e^{-11}$	$6e^{-11}$	$30\mu l$	$70\mu l$
11	$1e^{-11}$	$2e^{-11}$	$30\mu l$	$60\mu l$
12 (Blank)	-	-	-	$70\mu l$

*of 50µM cAMP standard stock provided in the kit

Table 2.6: Detection mix formulation

Reagent*	Volumes/Steps**
Eu-W8044 labelled streptavidin (Eu-SA)	Dilute 1.5µl of Eu-SA in 25.5µl DB
Biotin cAMP (b-cAMP)	Dilute 5µl of b-cAMP in 25µl DB
cAMP Detection buffer (DB)	Add 25µl of 1) in 3.075mL DB (mix well) Add 25µl of 2) in the solution 3) (mix well)

*All reagents used for the detection mix are included in the assay kit
** This recipe will yield 3.125mL Detection mix

Table 2.7: Plate reader settings for cAMP assays.

Parameter	Instrument Settings
Excitation Filter	Lamp: 111 (UV2 320)
Emission	615 665
Delay Time	70µs
Number of Flashes	100
Window Time	100µs
Total Time	170µs

2.2.2 Peptide ligands and small molecules stock preparation

Various peptide ligands (specific to the receptor of interest) and small molecules (antagonist candidates) were used in our agonist assays and agonist/antagonist competition assays. Their preparation and dilution, was performed according to the manufacturer's instructions and the requirements of each assay.

Human CGRP was obtained from Sigma Aldrich (catalogue number: SCP0060), rat AMY (rAMY) was purchased from Bachem (catalogue number: H-9475) and human AM was purchased from Anaspec (catalogue number: AS-60447). Considering the molecular weights and the properties of each peptide, they were dissolved according to the manufacture's instruction. CGRP was dissolved in 1% acetic acid to produce 60µM stocks, AM and rAMY were dissolved in water to produce 60µM and 1mM stocks respectively. All peptides were dissolved using siliconized tips and they were stored at -20°C as 20µl aliquots in siliconized micro-centrifuge tubes to limit freeze-thaw cycles (see table 2.8 below for more details).

Table 2.8: Special materials used for the preparation of the peptide ligands

Material	Source	Catalogue number
UltraFine™, 0,1 - 10 µl siliconized tips	VWR (Pennsylvania, USA)	613-0336
Bevel Point™, 1 - 200 µl siliconized tips	VWR (Pennsylvania, USA)	613-0278
Siliconized 0.65mL Microcentrifuge Tubes	Sigma Aldrich (Dorset, UK)	T3281-500EA
Siliconized 1.7mL Microcentrifuge Tubes	Sigma Aldrich (Dorset, UK)	T3406-250EA

Small molecules were designed by Sandexis Molecular Design (Kent, UK) and provided by Peakdale Molecular (Derbyshire, UK) and WuXi AppTec (Shanghai, China). Considering their molecular weights and properties, small molecules were dissolved DMSO to produce 20mM solution and sonicated at 37°C for 10 minutes to fully dissolve. The 20mM stocks were dissolved further in DMSO to produce 2mM solution and sonicated at 37°C for 10 minutes, to limit freeze-thaw cycles of the highest compound stocks. To be used in cAMP assays 2mM stocks were dissolved in stimulation buffer to produce 400µM solution and sonicated at 37°C for 10 minutes. All small molecules stocks were stored at -20°C in barcoded screw top 1mL and 0.5mL Matrix tubes (Thermo Fisher scientific, Loughborough, UK).

2.3 Data analysis

Data were analysed and plotted into graphs using Graphpad Prism Version 7.0 (Graphpad software, Inc). In cAMP agonist stimulations, each data set was normalised to the vehicle control as a 0% and the maximum stimulation as a 100%. In agonist and antagonist competition assays each data set was normalised to the vehicle control as a 100% and the EC50 dose of each receptor as a 0%. All data points are presented as the mean of at least three (n=3) independent experiments +/- SEM (standard deviation of the sample mean). To analyse cAMP data a three-parameter logistic equation (for inhibition or stimulation) was used to obtain dose response curves for the data. Data obtained during the in-vivo and post in-vivo (immunohistochemical analysis) studies were presented as mean +/- SD. Where appropriate data were statistically analysed using t-test (parametric or non-parametric) or comparison of fits (for dose response curves), and $p < 0.05$ was considered significant.

2.4 General cell culture materials

Reagent	Source	Catalogue number
Dulbecco's modified Eagle medium (DMEM)	Thermo Fisher scientific (Loughborough, UK)	61965-026
Fetal bovine serum (FBS) – Gibco	Thermo Fisher scientific (Loughborough, UK)	10500-064
Fetal bovine serum (FBS) – Sigma	Sigma Aldrich (Dorset, UK)	12103C
Penicillin/streptomycin (Pen/strep)	Sigma Aldrich (Dorset, UK)	P4333
Assay-Complete 1321N1 Medium 15	DiscoveRx, Birmingham, UK	92-0018GR6
Assay-Complete Serum 15	DiscoveRx, Birmingham, UK	92-0018GR6
Assay-Complete Antibiotics Mix 15 (Pen/Strep/Glutamine, Hygromycin, Geneticin and Puromycin)	DiscoveRx, Birmingham, UK	92-0018GR6
Assay-Complete CHO-K1 Medium 7	DiscoveRx, Birmingham, UK	92-0018GG2
Assay-Complete Serum 7	DiscoveRx, Birmingham, UK	92-0018GG2
Assay-Complete Antibiotics Mix 7 (Pen/Strep/Glutamine, Puromycin and Geneticin)	DiscoveRx, Birmingham, UK	92-0018GG2
PBS (Phosphate-Buffered Saline)	Thermo Fisher scientific (Loughborough, UK)	10010023

2.5 Cell lines

Cell line	Source	Catalogue number	Medium	FCS	Antibiotics
AM2 (1321N1 cells transfected with CALCRL + RAMP-3)	DiscoveRx, Birmingham, UK	95-0169C6	1321N1 Medium 15	Serum 15	Antibiotics Mix 15
CGRP (1321N1 cells transfected with CALCRL + RAMP-1)	DiscoveRx, Birmingham, UK	95-0164C6	1321N1 Medium 15	Serum 15	Antibiotics Mix 15
AM1 (CHO-K1 cells transfected with CALCRL + RAMP-2)	DiscoveRx, Birmingham, UK	93-0270C2	CHO-K1 Medium 7	Serum 7	Antibiotics Mix 7
AMY1 (1321N1 cells transfected with CALCR + RAMP-1)	DiscoveRx, Birmingham, UK	95-0170C6	1321N1 Medium 15	Serum 15	Antibiotics Mix 15
AMY3 (1321N1 cells transfected with CALCR + RAMP-3)	DiscoveRx, Birmingham, UK	95-0166C6	1321N1 Medium 15	Serum 15	Antibiotics Mix 15
178-2 BMA (Mouse prostate cancer cell line)	Dr Timothy C. Thompson*	N/A	DMEM	10% FBS	1% Pen/Strep
PANC 10.05 (Human pancreatic cancer cell line)	ATCC, Middlesex, UK	CRL-2547	RPMI	15% FBS	1% Pen/Strep
MDA-MB-231 (Human breast cancer cell line	ATCC, Middlesex, UK	HTB-26	RPMI	10% FBS	1% Pen/Strep
CFPAC-1 (Human pancreatic cancer cell line)	ATCC, Middlesex, UK	CRL-1918	DMEM	10% FBS	1% Pen/Strep

* University of Texas MD Anderson Cancer Centre

Chapter 3: Assay optimization and quality control

Chapter 3: Assay optimization and quality control

3.1 Introduction

3.1.1 Target of interest – CGRP, AM and AMY receptors signalling

Understanding the mode of action and the signalling pathways activated by the target of interest is one of the most important steps in the development of a robust and successful compound screening assay. GPCRs are some of the most common targets in modern pharmacology due to their widespread expression and their ability to modulate several physiological and pathophysiological processes. Activation of GPCRs normally occurs by endogenous ligands (stimuli) or external signals including proteins, peptides, hormones, amino acids, chemokines,, proteases, neuropeptides, ions and photons (Marinissen and Gutkind, 2001). Upon ligand binding, the receptor rearranges and converts the stimulus into a cellular response (signal transduction). The GPCR will then bind to one of the three subtypes of G proteins (Gα, Gβ and Gγ) and interact with network-related molecules leading to the activation of intracellular processes in a receptor and cell type manner. Some of the internal processes activated include the regulation of cyclic AMP/PKA downstream pathways (via $G\alpha_s/G\alpha_{i/o}$), activation of protein kinase C (PKC), phospholipase C (PLC) activation and elevation of intracellular calcium (Ca^{2+}) via $G\alpha_q$ as well as via activation of Gβγ or β-arrestin-dependent signalling pathways (Hazell et al., 2012).

It is generally accepted that in many cell types, activation of both AM and CGRP receptors results in the activation of adenylate cyclase (AC) that subsequently increases the levels of cAMP (Hay et al., 2003b, Beltowski and Jamroz, 2004). Therefore, measuring cAMP levels, as a marker of receptor activation, is proven as an important tool for characterization of both receptors in several studies (Evans et al., 2000, Hay et al., 2003a, Hay et al., 2006a). Moreover, transfection of cells with both CGRPr and AM1r had as a result the elevation of cAMP levels upon stimulation with AM and CGRP peptides (Kamitani et al., 1999, Buhlmann et al., 1999). Elevation of cAMP levels in VSMC followed by AM stimulation, had as a result the increase of Ca^{2+} efflux leading in relaxation of the vascular cells (Shimekake et al., 1995). Similarly, studies have shown that activation of AMY receptors, members of

calcitonin family alongside CGRP and AM receptors, by AMY and CT peptides results in acute activation cAMP ($G\alpha_s$-coupled)-dependent pathways (Morfis et al., 2008).

However, like most GPCRs, AM, CGRP and AMY receptors can couple with other subtypes of G protein family as well as other protein such as arrestins activating cAMP-independent pathways. In addition to cAMP, AM and CGRP peptides were able to increase the levels of intracellular Ca^{2+} in HEK-293 cells transfected with human CLR and all RAMP members (Kuwasako et al., 2000). A PLCβ1-dependent elevation of free cytosolic calcium levels was also shown upon stimulation of osteoblastic OHS-4 cells by CGRP, in the absence of cAMP (Drissi et al., 1999). Moreover, in addition to an increase in cAMP, AM was able to elevate the levels of intracellular calcium in both bovine aortic endothelial cells and oligodendroglial cells (Shimekake et al., 1995, Uezono et al., 1998). However, decrease of intracellular calcium alongside with a decrease in calcium sensitivity was shown after stimulation of pig coronary arterial smooth muscle with AM, showing a cell type dependent manner (Kureishi et al., 1995). Coupling of AMY receptors with $G\alpha_q$ which resulted in elevation of calcium via PLC dependent pathways was also shown (Morfis et al., 2008).

Even though, engagement of CGRP with other members of the G proteins and the arrestins was shown in recent studies, the extend of this coupling is not clear yet (Heroux et al., 2007, Ritter and Hall, 2009). Studies have suggested the involvement of β-arrestins in CGRP receptor desensitisation and internalisation (Heroux et al., 2007) as well as the CGRP-mediated activation of MAPK (ERK1/2, p38MAPK, JNK) and phosphoinositide 3-kinase (PI3K)/Akt pathways (Nikitenko et al., 2006a, Padilla et al., 2007, Heroux et al., 2007). Moreover, phosphorylation of Akt by AM, CGRP and AMY was recently shown (Nikitenko et al., 2006a, Iemura-Inaba et al., 2008, Visa et al., 2015). Furthermore, activation of MAPK cascades including ERK1/2 and p38MAPK by all three peptides have been observed in several studies (Fritz-Six et al., 2008, Wang et al., 2009, Potes et al., 2012). The interconnectivity of cellular signalling pathways poses a challenge in the identification of the specific G protein responsible for a cellular response.

3.1.2 Assay development – foundation of screening process

The development and screening of new compounds and especially the use of high-throughput screening (HTS) is a complex process of modern drug discovery that involves the use of sophisticated automated systems and advanced detection assays and equipment. Even though HTS is a significant part of most drug development programs, data have shown that new compounds originated from HTS were responsible for ~60% of clinical trial failures indicating the need of improvement in drug discovery (Macarron et al., 2011).

3.1.2.1 Screening approaches

When initiating a compound screening process, it is important to choose the appropriate assay depending on the target of interest. Generally, there are two types of screening approaches in drug discovery the biochemical and cell-based assays. Biochemical assays generally utilise purified specific target proteins such as enzymes (i.e. kinase, proteases) and receptors (i.e. GPCRs, nuclear receptors, kinase receptors, ion channels) to identify the activity or binding potential of compound candidates against the target (Mallender et al., 2006). On the other hand, in the cell-based assays the target could be a specific signalling pathway, a molecule or even the whole cell where the exact target is unknown. More specifically, the response or the potency of a compound is measured in the context of a cell and it is represented as changes in the levels of secondary messengers (i.e. cGMP, cAMP, Ca^{2+}) and differences in cell viability (apoptosis/death) or proliferation (Zhang et al., 2012b).

The use of cell-based assays in drug discovery was significantly increased during the last few decades in an effort to increase the productivity and the success rates of the drug development. In fact, as was reported by Fox et al. in 2006, cell-based assays accounted for more than half (52.6%) of all HTS efforts either as a primary or a secondary screening (Fox et al., 2006). In addition of using cells as a tool to determine the potencies of new compounds, it can provide vital information for the development of the lead candidates such as their effects of cell growth, cytotoxicity or permeability (Zhang et al., 2012b).

3.1.2.2 Cell types

There are generally two types of cells used in drug discovery, primary and engineered cell lines. Even though screening using primary cells is feasible and gives a more realistic approach to the target/disease of interest, culturing the substantial amounts of cells required for compound screening possess some limitations (Johnston, 2002). Therefore, engineered or transfected cells are the main type of cells used in HTS. Relatively high expression of the targeted protein is essential to obtain a sufficient signal output from a cellular-based assay. Therefore, a transient or stable transfection of naïve cells, expression of which is generally low, is required for the upregulation of the gene of interest.

Although transiently transfected cell lines typically rapidly express significantly high levels of targeted protein, the short duration of expression and the transfection inefficiencies (multiple transfection may be required for a HTS) could lead to large variations in the expression levels affecting the quality of screening process (Zhang et al., 2012b). Despite the limitations if sufficient amounts of cells can be produced by transient transfection, this process of cell line generation could be utilised in a HTS. For example, by using cells from a single large-scale transient transfection, Chen and co-workers were able to screen a large chemical library (700,000 compounds) in Ca^{2+} influx and electrophysiological assays identifying several novel transient receptor potential channel A1 (TRPA1) antagonists (Chen et al., 2007). On the other hand, stable cell lines, commonly generated by retroviral infection or plasmid transfection, have lower expression levels than the transient cells, however, their expression is consistent for a long period of time (less variation and reduced cost of transfection) making them more favourable for HTS applications (Johnston, 2002, Zhang et al., 2012b). The use of stable cell lines in various of cell-based HTS assays was reviewed by Paul and Patricia Johnston showing the issues and the advantages of such approaches (Johnston, 2002).

3.1.2.3 Detection methods

There several detection methods commonly used in drug discovery including measurement of cAMP production, quantification of calcium influx, investigation of protein to protein interactions (fluorescence or bioluminescence resonance energy transfer (FRET or BRET)) and the use of reporter genes each one providing a valuable approach for compound screening.

cAMP measurement assays

cAMP is widely used in drug discovery due to its physiological importance as one of the most vital secondary messenger used for several intracellular signal transductions. Numerous technologies have been developed for cAMP measurement. One of them is fluorescence polarization (FP), a homogenous fluorescence assay that is based on molecular movement and rotation of fluorophore-labelled complexes, depending on their interaction with the available molecules of cAMP (Prystay et al., 2001, Allen et al., 2002, Lea and Simeonov, 2011). Another approach that measures the intracellular cAMP, involves the co-expression of cyclic-nucleotide-gated ion channel (CNGC) and a GPCR in the same cell. An increase of intracellular cAMP, upon GPCR activation, results in the activation of CNGCs leading to plasma membrane depolarization which is measured by a fluorescent membrane potential dye (Tang et al., 2006). Enzyme Fragment Complementation (EFC) is another technology used for the measurement of cAMP. The method is based on two recombinant β-galactosidase fragments (enzyme acceptor (EA) and enzyme donor (ED-cAMP)) that when interact they produce a chemiluminescent signal. cAMP produced by the cells is competing with the enzyme donor (ED-cAMP) to bind to the antibody (anti-cAMP) thus is increasing its availability to interact with the acceptor resulting in signal increase (Golla and Seethala, 2002). A similar technology commonly used for the detection of cAMP is based on time resolved fluorescence resonance energy transfer (TR-FRET) (technology explained in more detail below). A labelled cAMP tracer complex (Europium-Chelate streptavidin/biotinylated cAMP) is competing with intracellular cAMP, for binding sites on Alexa-fluor labelled cAMP-specific antibody. When the

cAMP tracer complex is bound with the antibody, energy is transferred from Eu-chelate streptavidin to an Alexa molecule on the antibody which results in TR-FRET emission. The intensity of the emission will then decrease in the presence of intracellular cAMP (Norskov-Lauritsen et al., 2014).

Ca^{2+} mobilization assays

Another second messenger that plays a key role in a wide range of physiological processes including the GPCR-induced signal transduction are Ca^{2+}. Upon activation of such receptors the intracellular Ca^{2+} levels, which are normally maintain at ~100nM, are dramatically increased up to 100-fold in a matter of seconds. This happens either by activation of calcium channels in the plasma membrane that allows extracellular Ca^{2+} to enter or by the release of deposited intracellular Ca^{2+} from the endoplasmic reticulum (ER). Therefore, measuring the intracellular levels of calcium provides a great tool for GPCR targeted compound screening (Ma et al., 2017). There are mainly two categories of indicators used for monitoring intracellular Ca^{2+} levels: photoproteins and chemically synthesized fluorescent indicators. Photoproteins such as aequorin (most commonly used), clytin (phialidin) and obelin are proteins isolated from luminescent marine invertebrates. They can be stably expressed in cells providing a robust and simple screening method. However, the cost and the time required to generate and establish these cell lines are some of the limitations of this technique (Eglen and Reisine, 2008, Ma et al., 2017). Moreover, the use of synthetic fluorescent Ca^{2+} indicators such as Fluo-3, Fluo-4, Quin-2, Indo-1, Rhod-2 and Fura-2 provides a robust assay with an outstanding dynamic and detection range. Normally, a Ca^{2+} indicator containing a lipophilic acetoxymethyl (AM) ester, will enter the cytosol where enzymes (esterases) cleave the lipophilic groups of the AM molecule retaining the indicator into the cell. These indicators, similarly to Ca^{2+} chelators, bind to intracellular Ca^{2+} causing configuration changes to their fluorescent moiety components, leading to an acute change in fluorescence intensity (Woszczek and Fuerst, 2015, Ma et al., 2017). Even though, fluorescent indicators are widely used in drug discovery, the need of additional steps for reagent (dye) loading can potentially decrease the throughput and increase the variation and the complexity of the screening process.

Reporter gene cells-based assays

Reporter genes are often used in the development of cell-based assays in drug discovery mainly due to their efficiency and high sensitivity. The development of such assays requires the stable transfection of both a promoter and a reporter gene into the cells (Roda et al., 2004), which could increase both the cost and the time required for the assay development. The technology is based on the direct or indirect activation of signal transduction, by receptors, kinases or transcription factors that leads to an increase of gene expression. This response has as a result the activation of the promoter (also called regulatory gene), that is specific to the receptor or protein of interest, which then leads to the activation of the reporter gene and subsequently an increase in the production of the reporter protein and signal elevation (Roda et al., 2004, Michelini et al., 2010). There are several reporter genes utilised today including: firefly luciferase derived from Photinus Pyralis, Renilla luciferase derived from Renilla Reniformis (sea pansy), green fluorescent protein (GFP), Beta (β)-galactosidase and Beta (β)-lactamase (Zhang et al., 2012b). The most commonly used reporter genes are the Renilla and firefly luciferase which provide high accuracy and sensitivity. However, the selection of the appropriate reporter gene depends on several factors including the cell line used and the type of experiment/detection method (i.e. cell imaging or plate reading assays) (Michelini et al., 2010). One of the main pitfalls of this method is the high variability in the response due to compound/sample specific effects in the growth/viability of the cells. To resolve this issue, recent technologies that introduced the use of a second reporter gene as a control of cell viability have been developed. The two genes are simultaneously activated by the same stimuli (i.e. receptor activation/inhibition) enabling the quantification of two different outcomes in a single experiment (Adamczyk et al., 2002, Roda et al., 2004, Michelini et al., 2010).

Fluorescence or Bioluminescence resonance energy transfer (FRET or BRET) assays

Assays such as the luminescence reporter genes explained above, are based on the activation of downstream pathways which could cause long response times (hours to days) and delays in the analysis and screening of new compounds. Therefore,

methods that depend on the first step of the receptor activation (i.e. receptor dimerization) are considered more suitable for HTS. Such approaches that are based on protein-protein interactions are FRET or BRET. Resonance energy transfer (RET) is a method that involves two fluorescent/luminescent molecules (a donor and an acceptor fluorophores) with overlapping emission and excitation spectra. When the two molecules are in close proximity (1-10nm), the average distance of most biological interactions, energy from the donor fluorophore it is transferred to the acceptor fluorophore causing light emission (i.e. signal increase) (Jares-Erijman and Jovin, 2003, Hwang et al., 2008b, Michelini et al., 2010).

FRET has been one of the most commonly used cell-based assay for protein-protein interactions in HTS. For example, using a high-throughput cellular FRET assay, Hwang and co-workers were able to screen a library of 480 small molecules, identifying several potent antiviral molecules against poliovirus (PV) (Hwang et al., 2008b). Even though the accuracy and the sensitivity of FRET is particularly high there are some limitations to its application. Auto-fluorescence of cells or fluorescent interferences within the wells from compounds and minor debris could lead to high background noise causing false positive or negative results. Moreover, other limitations include photobleaching of the donor fluorophore, excitation of both donor and acceptor fluorophores due to their overlapping spectrum and the need of an external light source to detect/quantify the interaction (Michelini et al., 2010, Busch et al., 2013).

Time resolved fluorescence (TRF) is a variant of FRET technology that utilizes rare earth ions (such as europium and terbium) with long wavelengths as donor fluorophores. Compared to the conventional fluorescent donor that are relatively short-lived, the use of long-lived donors decreases the fluorescence interferences and the background signal. Several companies have developed cell-based assays utilizing these technologies making them suitable for HTS (Bazin et al., 2001, Janzen, 2014).

3.1.2.4 Other parameters

After choosing the appropriate cell type and detection assay to perform your compound screening, there are several other parameters that need to be optimized to ensure a robust and reproducible assay. One of these parameters is the quality of the cells and the cell culture conditions. Ensuring high quality cells during the entire process of the screening could be challenging considering the number of cells required. The optimal cell culturing conditions including media and cryo-preserving reagents are essential to ensure consistency. A common approach is the cryo-preservation of cells in large batches of the same passage age. This allows the plating of cells directly without the need of thawing and cultivating into flasks or plates before use, increasing assay uniformity and consistency (TerWee et al., 2011). Another approach involves the utilization of division arrested cells using mitomycin C (stops the proliferation without affecting other properties of the cells). This technique ensures that the assays are performed under the same cell cycle phase therefore increasing the accuracy of the screening (Fursov et al., 2005).

Selecting the right plate for the assay is also a key factor when designing and executing a HTS. In cell-based assays 96-well and 384-well plates are commonly used depending on the assay itself. Using a 384-well plate could significantly increase the throughput, however, decrease the signal intensity. Moreover, environmental factors such as humidity and temperature have more significant effect on smaller volumes used in 384- and 1536-well plates. Furthermore, black polystyrene or solid white polystyrene microplates are commonly used in fluorescent or luminescent assays to reduce cross-talk between the wells and background noise (Michelini et al., 2010, Zhang et al., 2012b). When optimizing an assay several other factors are to be considered including cell number, assay volume, incubation/reaction times and reagent concentrations. Depending on the cell type and the volume of the plate/well the number of the cells should be optimized so it gives the highest possible signal (Michelini et al., 2010). What is more, the assay volume mostly depends on the chosen plate and its density (Mayr and Bojanic, 2009). Finally, since most compounds are usually stored in DMSO, which in high concentrations is toxic to cells, compound

concentrations should be considered to avoid cytotoxicity while preserving its activities (Waybright et al., 2009).

3.1.3 Data quality and causes of variability

The ability to produce excellent quality and meaningful data, especially during a single point screening process, is vital for the correct identification of potent compounds. Ideally an assay should be sensitive and able to identify potent from weak compounds with false-negative and false-positive rates to be 0, but no assay can be perfect for all compounds. The quality and the reproducibility of the data produced from such assays can be affected by several factors that introduce variability and inaccuracy. Generally, these variability factors can be divided into two theoretically distinct categories, the unsystematic also called ''random'' variability and the systematic also known as ''traceable'' or ''assignable'' causes (Gunter et al., 2003).

Random sources of variability include slight differences in reagents, variability in sample preparation, differences in geometry of liquid handling tips or any other factors that cannot be predicted. On the other hand, examples of systematic variability include shifts due to evaporation or ageing of the assay reagents or due to faulty equipment (malfunction of pipettes, decay of luminosity of light source), signal trends/shifts associated with specific rows, columns or the edges of the plates due to: variations in incubation time, changes in temperature, errors in liquid handling, cellular toxicity or sample degradation, effects due to differences in measuring/reading times between wells or plates and shifts due to changes of the experimental procedure. Unlike random sources (which if try to correct them could possibly add more noise to your data), systematic variability can be identified and must be corrected/adjusted with the use of appropriate controls on the plates that can be used for either normalization or outlier identification (Gunter et al., 2003, Zhai et al., 2016). These controls deliver also an assay performance monitoring purpose and in combination with statistical or graphical methods are ensuring the quality and minimise the variability of the data.

To assess both the quality of the assay and the signal dynamic range, in 1999 Zhang and colleagues have developed a method of calculating the screening window coefficient also known as Z-factor. As was described in their original paper, Z-factor defines the separation band between the negative and the positive controls of an assay (illustrated in figure 3.1 below) (Zhang et al., 1999). Before the use of the designed assay in a HTS a pilot study with positive and negative controls is required to the suitability of the assay (using Z-factor). Z-factor or Z-value can take any value between 0-1 and is calculated using the following equation as described by Zhang et al.:

$$Z = 1 - \frac{3(SD_P + SD_N)}{|Mean_P - Mean_N|}$$

SD: Standard deviation

P: Positive controls

N: Negative controls

The table below is showing the interpretations for the calculated Z-factor. Depending on the calculated Z-value, re-optimization of the assay or a different detection method should be considered.

Table 3.1: Z-factor Explanation.

Z-factor	Interpretation
1.0	An Ideal assay (SD=0)
between 0.5 and 1.0	An excellent assay (Large separation band).
between 0 and 0.5	A marginal assay (Small separation band).
less than 0	Not ideal for screening purposes (Signal from positive and negative controls could overlap).
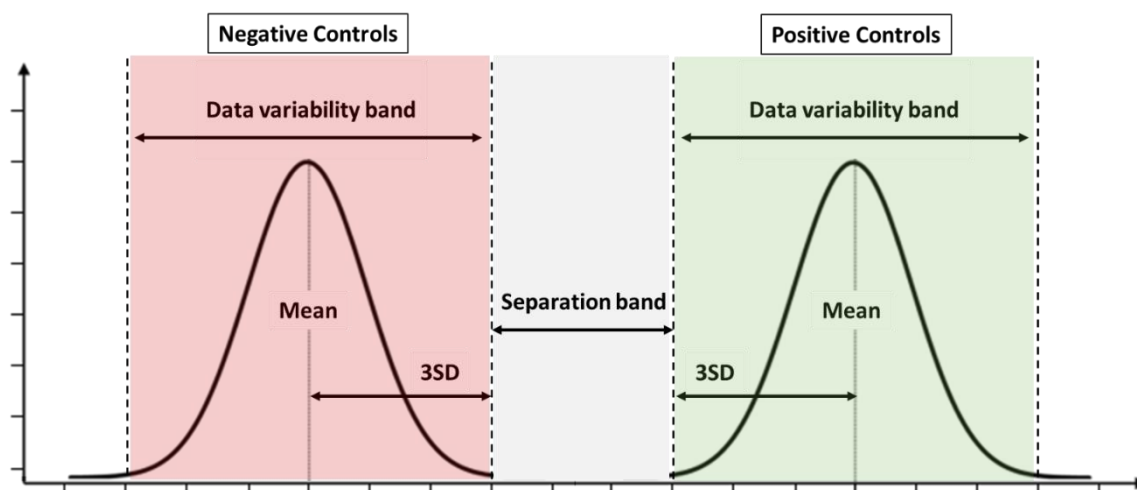
Figure 3.1: Graphical illustration of Z-factor. Z-factor defines the separation band between the negative and the positive controls of an assay. Modified from (Zhang et al., 1999)

3.2 Aim and objectives

Aim

The aim of this chapter was the development and optimization of cAMP production cell-based assay suitable for our high-throughput screening requirements.

Objectives

Objective 1: Determine the optimal cell number for each cell type to be used in cAMP cell-based assay

Objective 2: Optimise the stimulation time required to produce the maximal response after agonist administration

Objective 3: Determine the half maximal response concentration (EC50) of each peptide agonist against their respective overexpressing cell line

Objective 4: Investigate the overall quality and performance of the assay.

3.3 Materials and methods

3.3.1 cAMP assay

The measurement of production of cAMP by various G-protein couple receptor O/E cell lines under different conditions was the experimental basis of this chapter. A list of the cell lines used and a more detailed explanation of the principle of the assay can be found in chapter 2. Figure 3.2 below illustrates the principle of the LANCE® cAMP Assay as shown in chapter 2.2 (catalogue number: AD0264, Perkin Elmer, Waltham, Massachusetts, United States).
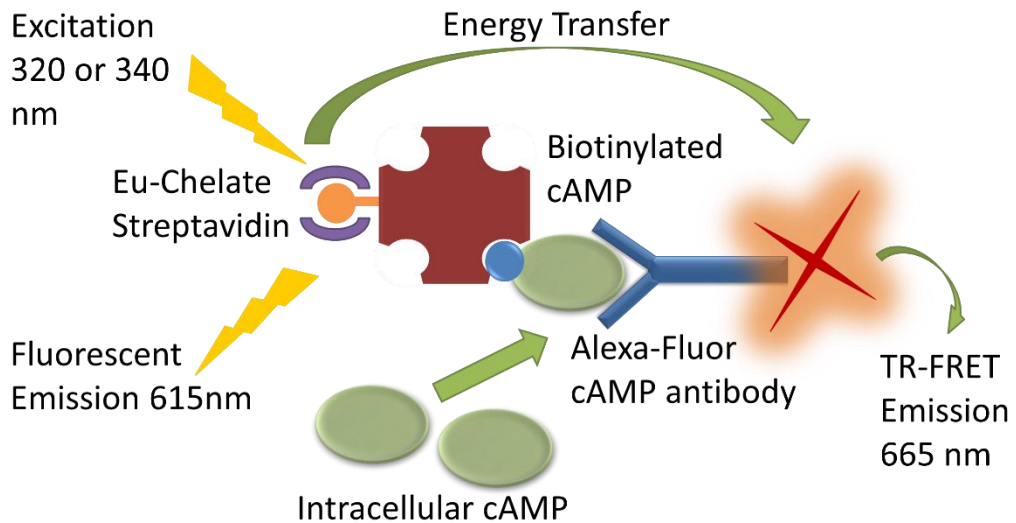
Figure 3.2: LANCE® cAMP Assay kit principle. LANCE® cAMP Assay is based on time resolved fluorescence resonance energy transfer (TR-FRET). As shown on the diagram above a labelled cAMP tracer complex (Europium-Chelate streptavidin/biotinylated cAMP) is competing with intracellular cAMP, for binding sites on Alexa-fluor labelled cAMP-specific antibody. When the cAMP tracer complex is bound with the antibody, energy (340 nm excitation) is transferred from Eu-chelate streptavidin to an Alexa molecule of the antibody which results in TR-FRET emission at 665 nm. The intensity of the emission will then decrease in the presence of intracellular cAMP.

3.3.2 Forskolin Stimulation

Forskolin is a labdane diterpene that is produced and isolated from the roots of Indian Coleus plant. Due to its unique function as a potent, rapid and direct (does not require the activation of any receptor types) activator of adenylyl cyclase, Forskolin has proved to be an important and valuable tool in pharmacology and drug discovery (Insel and Ostrom, 2003). Forskolin stimulation curves were used to determine the optimal cell density for the cell lines used in our drug screening investigations as well as a valuable tool for quality control. cAMP standard curve was also obtained to establish the dynamic range of the assay (see chapter 2 for more details). The optimal cell density was determined based on relationship between the Forskolin dose response curve and the linear phase of the cAMP standard curve. All dose response curves were performed using concentrations ranging from 100uM to 1nM at every half log (see table 3.2 below for dilution details). Data was plotted using Graphpad Prism 7 software in a non-linear three parametric curve.

Serial dilutions (6μl/well) of Forskolin were plated in 384 well OptiPlates (catalogue number: 6007299, Perkin Elmer). Cells were removed from liquid nitrogen and transferred in 37°C water bath until thawed (30-40 seconds). They were then transferred to a 15 ml centrifuge tube with equal amount of warm stimulation buffer (for formulation see chapter 2) and centrifuged for 4 minutes at 300 x g. The stimulation buffer used for re-suspension and preparation of the cells was made with 1x HBSS solution without Calcium and Magnesium (catalogue number: 14170-112, Thermo Fisher Scientific) to ensure equal cell distribution between the wells. The cell pellet was then washed with PBS and centrifuged for 4 minutes at 300 x g. Cells were re-suspended in warm stimulation buffer and counted using Countess II Automated Cell Counter (Thermo Fisher Scientific, Waltham, Massachusetts, United States). Alexa fluor antibody (1:100 concentration) was then added and cells were plated (6μl/well) at different cell densities. Cells were then stimulated for 15 minutes at room temperature and incubated for 60 minutes after the addition of 12μl detection mix (Europium-Chelate streptavidin/biotinylated cAMP tracer) in each well. The plate was then read on the Enspire multimode Plate reader (Perkin Elmer, Waltham, Massachusetts, United States), at; 320/340nm excitation and 615/665nm

emission was recorded. Appropriate controls (0% stimulation: Vehicle control) were included in each plate for data normalization. Figure 3.3 below illustrates the experimental procedure.

Table 3.2: Forskolin serial dilutions in Stimulation Buffer

Dilution	Final (M) concentration	2X (M) Concentration	Volume of dilution	Stimulation buffer (diluent)
1	$1e^{-4}$	$2e^{-4}$	80µl*	120µl
2	$3e^{-5}$	$6e^{-5}$	60µl	140µl
3	$1e^{-5}$	$2e^{-5}$	60µl	120µl
4	$3e^{-6}$	$6e^{-6}$	60µl	140µl
5	$1e^{-6}$	$2e^{-6}$	60µl	120µl
6	$3e^{-7}$	$6e^{-7}$	60µl	140µl
7	$1e^{-7}$	$2e^{-7}$	60µl	120µl
8	$3e^{-8}$	$6e^{-8}$	60µl	140µl
9	$1e^{-8}$	$2e^{-8}$	60µl	120µl
10	$3e^{-9}$	$6e^{-9}$	60µl	140µl
11	$1e^{-9}$	$2e^{-9}$	60µl	120µl
12 (Blank)	-	-	-	140µl

*of 500µM Forskolin working dilution
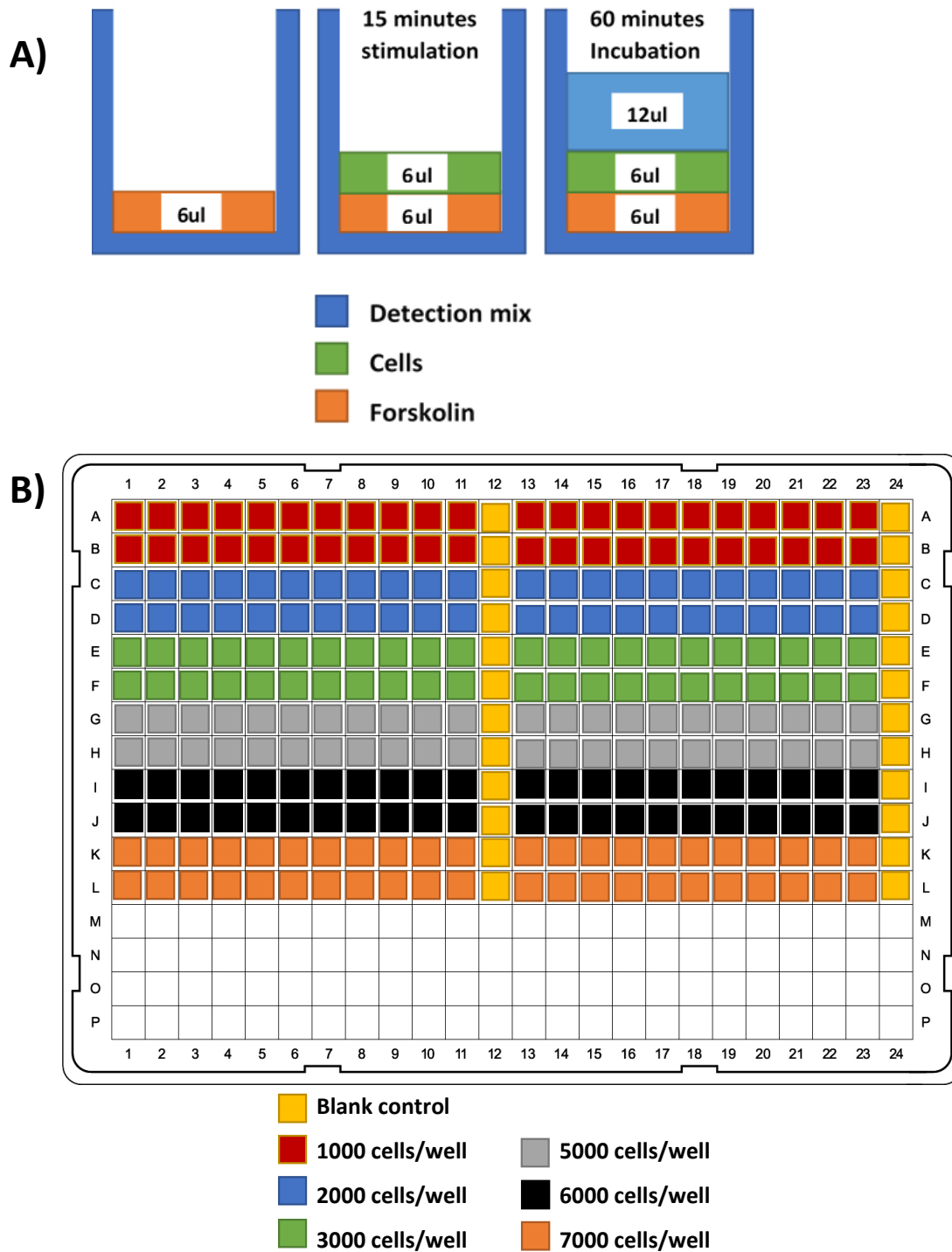
Figure 3.3: A) Illustrates the experimental procedure for measurement of cAMP that is produced by Forskolin stimulation. **B)** Forskolin dilutions were plated in duplicates followed by blank/vehicle controls to determine the optimal cell number.

3.3.3 Agonist stimulation

Similar experimental procedure to the Forskolin stimulation assays was followed to determine the EC_{50} dose of each agonist as well as to evaluate the quality of the assay and the cells during the process of the drug screening. All agonist dose response curves were performed using concentrations ranging from 1uM to 10pM at every half log (See table 3.3 below for dilution details). Data was plotted using Graphpad Prism 7 software in a non-linear three parametric curve.

Serial dilutions (6µl/well) of peptide agonists (CGRP, AM and AMY) were plated in 384 well OptiPlates (catalogue number: 6007299, Perkin Elmer). Cells were removed from liquid nitrogen and transferred in 37°C water bath until thawed almost completely then they were transferred to a 15 ml centrifuge tube with equal amount of warm stimulation buffer (for formulation see chapter 2) and centrifuged for 4 minutes at 1000rpm. Cells were washed with PBS and re-suspended in warm stimulation buffer and counted using Countess II Automated Cell Counter (Thermo Fisher Scientific, Waltham, Massachusetts, United States). Alexa fluor antibody (1:100 concentration) was then added and cells were plated (6µl/well) at desired cell density (2,500 cell/well) following optimisation. Cells were then stimulated with the peptide agonist for 10-45 minutes (for optimization purposes) at room temperature and incubated for 60 minutes after the addition of 12µl detection mix (Europium-Chelate streptavidin/biotinylated cAMP tracer) in each well. The plate was then read on the Enspire multimode Plate reader (Perkin Elmer, Waltham, Massachusetts, United States), at; 320/340nm excitation and 615/665nm emission was recorded. Forskolin stimulation dose response curves were also used for quality control of the cells and the assay itself. Vehicle control: 0% stimulation was also included in each plate for data normalization. Figure 3.4 below illustrates the experimental procedure.

Table 3.3: Peptide ligands serial dilutions in Stimulation Buffer

Dilution	Final (M) concentration	2X (M) Concentration	Volume of dilution	Stimulation buffer (diluent)
1	$1e^{-6}$	$2e^{-6}$	4µl*	116µl
2	$3e^{-7}$	$6e^{-7}$	60µl	140µl
3	$1e^{-7}$	$2e^{-7}$	60µl	120µl
4	$3e^{-8}$	$6e^{-8}$	60µl	140µl
5	$1e^{-8}$	$2e^{-8}$	60µl	120µl
6	$3e^{-9}$	$6e^{-9}$	60µl	140µl
7	$1e^{-9}$	$2e^{-9}$	60µl	120µl
8	$3e^{-10}$	$6e^{-10}$	60µl	140µl
9	$1e^{-10}$	$2e^{-10}$	60µl	120µl
10	$3e^{-11}$	$6e^{-11}$	60µl	140µl
11	$1e^{-11}$	$2e^{-11}$	60µl	120µl
12 (Blank)	-	-	-	140µl

*of 60µM peptide ligand working dilution
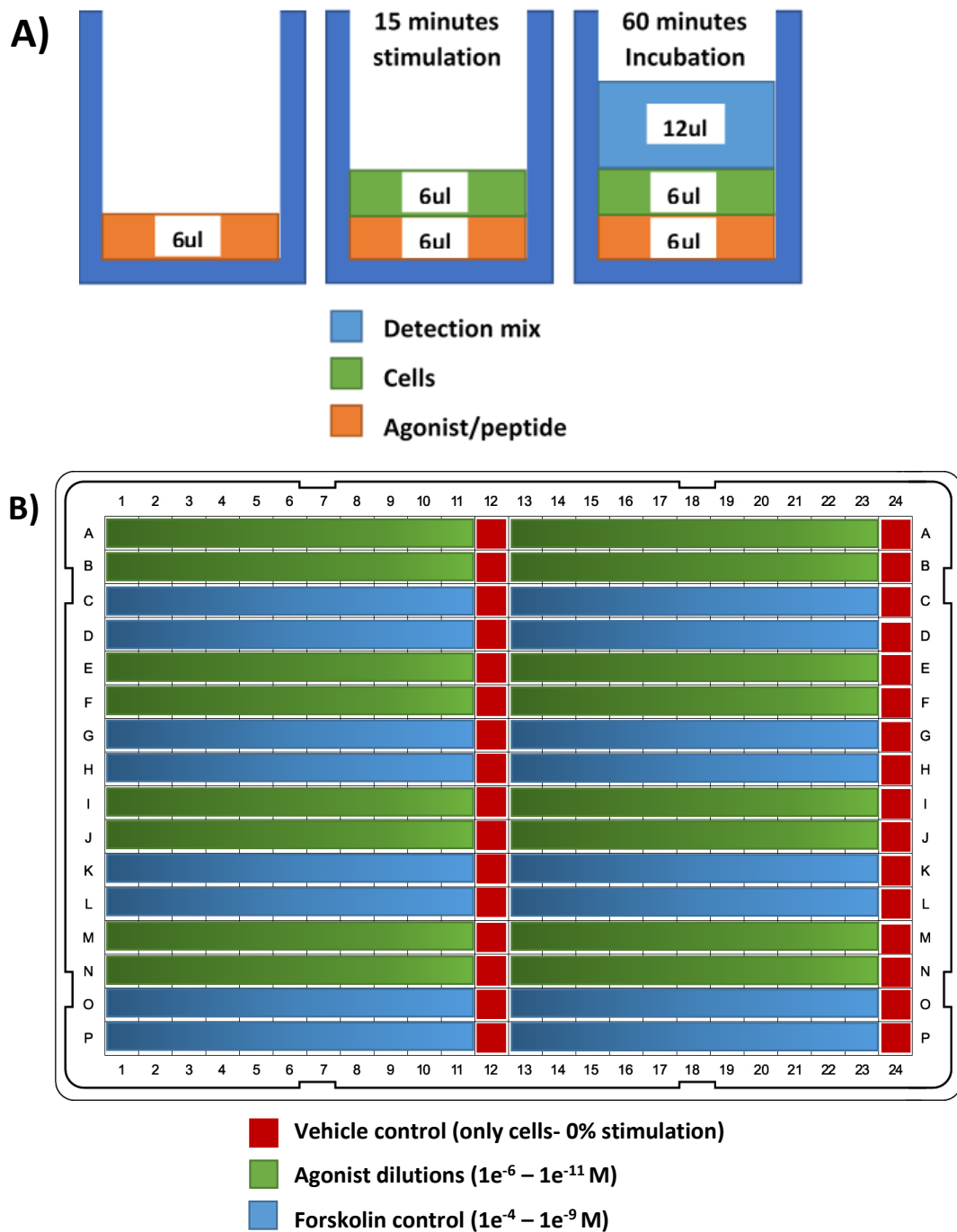
Figure 3.4: A) Illustrates the experimental procedure for measurement of cAMP that is produced by peptide agonist stimulation. **B)** Agonists dilutions were plated in duplicates followed by vehicle controls and Forskolin controls.

3.4 Results

3.4.1 Determination of the optimal cell number

To determine the optimal cell density of the cells used in our screening process cAMP standard curve was first obtained followed the manufacturer's instructions (Perkin Elmer, Waltham, Massachusetts, United States). Subsequently, Forskolin dose response curves using different cell densities (1000, 2000, 3000, 5000, 6000 and 7000 cells/well) were obtained. Figure 3.5 below shows the cAMP standard curve as well as the dose response curves obtained upon the stimulation of AM2r and CGRPr O/E cell lines (cells used in our primary compound screening) with Forskolin. Information about the cells can be found in Chapter 4 (page 44).

As was described in the methods section above, the optimal cell density was chosen based on the coverage of the linear phase of the cAMP standard curve by the Forskolin dose response curve. More specifically, the number of cells that gave the dose response curve that covers most of the linear region of the standard curve was considered as the optimal number. Figure 3.5.A below shows the Forskolin dose response curves obtained with AM2 receptor O/E cells as well as the cAMP standard curve obtained using the same LANCE® cAMP Assay kit. As shown both 2000 and 3000 cells/well provide a dose response that falls within the linear region of the cAMP standard curve. Taking this into account as well as the fact that 2000 cells/well provides a dose response with the largest signal range, we decided on 2500 cells/well as the optimal cell density for AM2r O/E cells.

Comparable results were obtained with CGRPr O/E cells with both 2000 and 3000 cells/well to give a response that covered most of the linear region of the cAMP standard curve (see figure 3.5.B below). Therefore, the same optimal cell number (2500 cells/well) as with the AM2 receptor cells was chosen for CGRP receptor cells. The cAMP standard curve was also used to determine the sensitivity and the dynamic range of the assay which is shown in figure 3.5 below. The assay showed similar sensitivity as the one published by the manufacturer with IC_{50} values in the low nM range (~2nM) and significantly large detection window (dynamic range) of ~3000 relative fluorescence units (RFU).
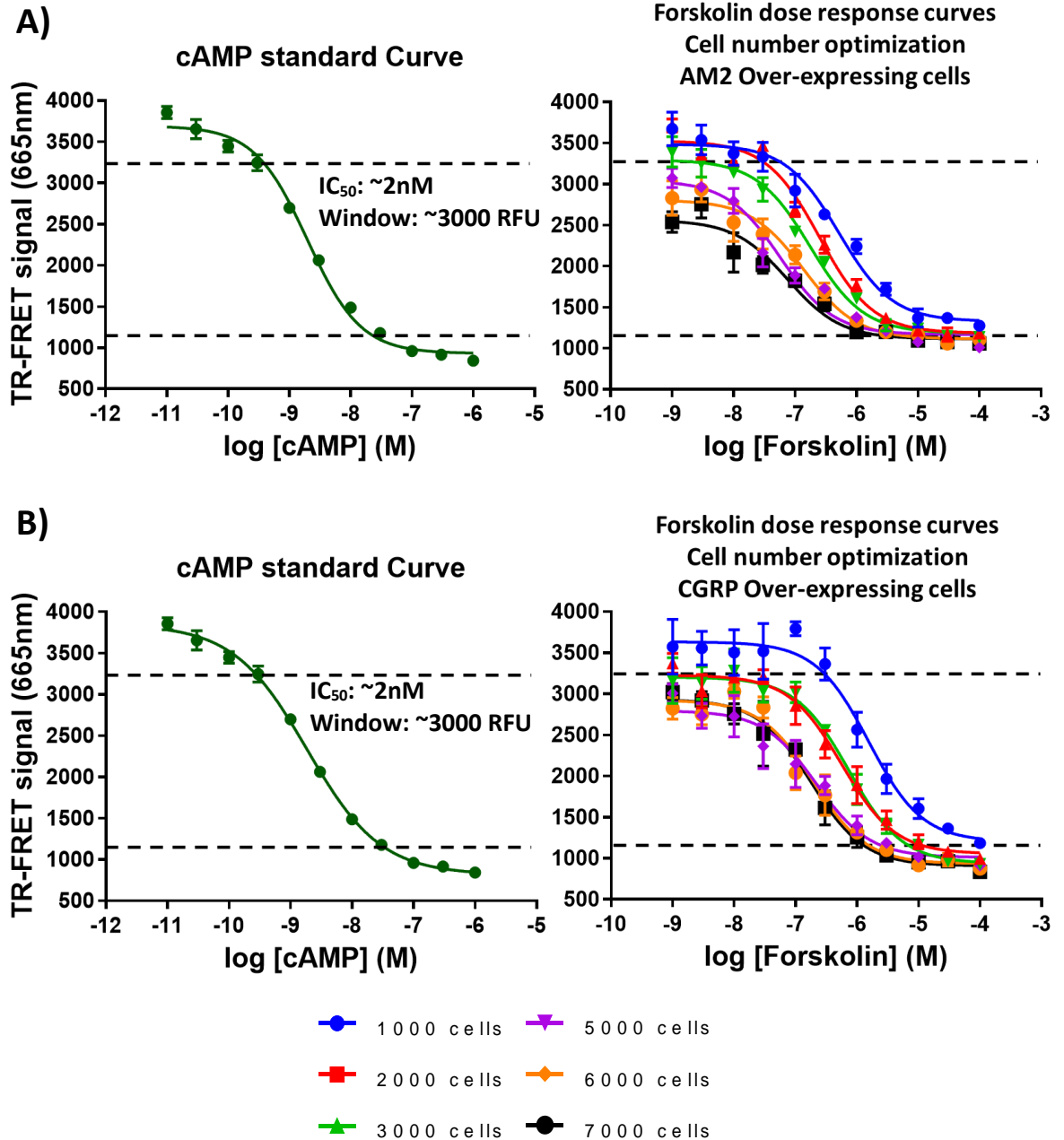
Figure 3.5: Determination of the optimal AM2r and CGRPr O/E cell number. A) Showing the cAMP standard curves used to obtain the dynamic range and sensitivity of the assay and to determine the optimal cell densities **B)** Showing the Forskolin dose response curves obtained by stimulating various densities of AM2r and CGRPr O/E cells.

3.4.2 Optimization of agonist stimulation time

Agonist dose response curves were used to optimise the stimulation parameters of the assay including the time of stimulation. After obtaining the optimal cell density of each cell line, cells were stimulated with the appropriate peptide agonist for 10, 15, 30 or 45 minutes. As shown in the table 3.2 and figure 3.6 below the different stimulation times resulted in similar dose response curves in both AM2r and CGRPr cells. More specifically, when AM2r cells were stimulated with AM_{1-52} (peptide agonist) all four stimulation times yielded similar EC_{50} doses ranging between 5-3nM. Comparable results were observed upon stimulation of CGRPr cells with peptide agonist CGRPa which resulted in EC_{50} values ranging between 1-2nM. However, the best fit values for each stimulation time showed that 15 minutes gives the highest detection window compared with the other time points indicating that 15 minutes is the optimal stimulation time for both cell lines (see table 3.4).

Table 3.4: Best fit values for agonist curves at different stimulation time points.

AM2r Over-expressing cells				
Parameters	**Stimulation time**			
	10 mins	**15 mins**	**30 mins**	**45 mins**
Bottom	1079	**1038**	1102	1193
Top	3562	**3810**	3619	3379
EC_{50}	5.72nM	**5.14nM**	4.30nM	2.71nM
pEC_{50} +/- SEM	8.68 +/- 0.068	8.74 +/- 0.081	8.91 +/- 0.092	8.80 +/- 0.047
Window	2484	**2772**	2516	2186
CGRPr Over-expressing cells				
Parameters	**Stimulation time**			
	10 mins	**15 mins**	**30 mins**	**45 mins**
Bottom	1233	**1297**	1330	1312
Top	2863	**3341**	3086	2831
EC_{50}	2nM	**1.52nM**	1.2nM	1.56nM
pEC_{50} +/- SEM	8.69 +/- 0.095	**8.82 +/- 0.076**	8.92 +/- 0.069	8.81 +/- 0.048
Window	1630	**2043**	1756	1519
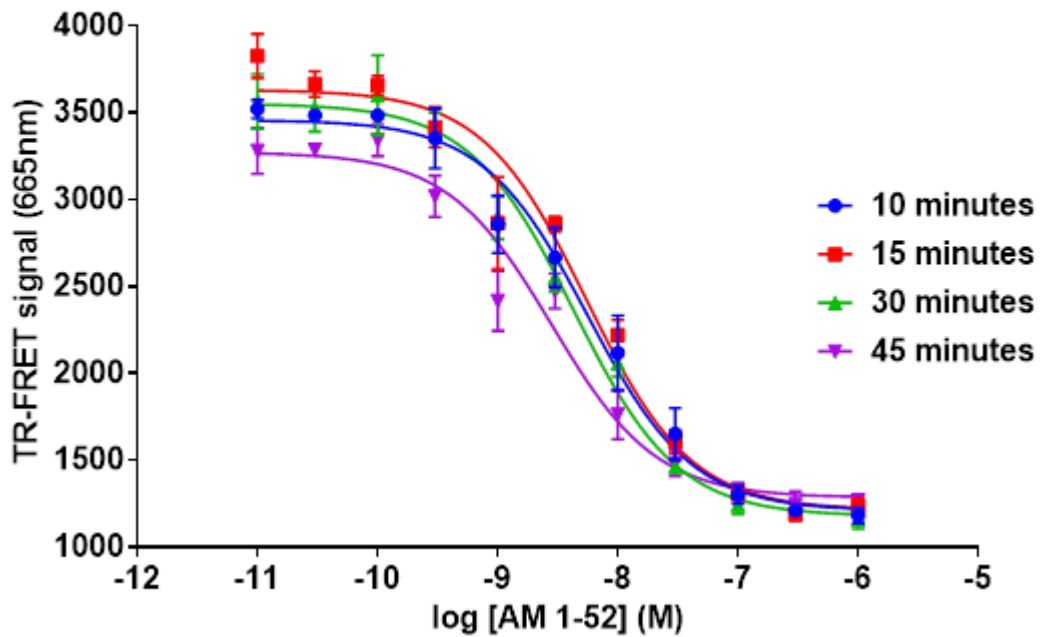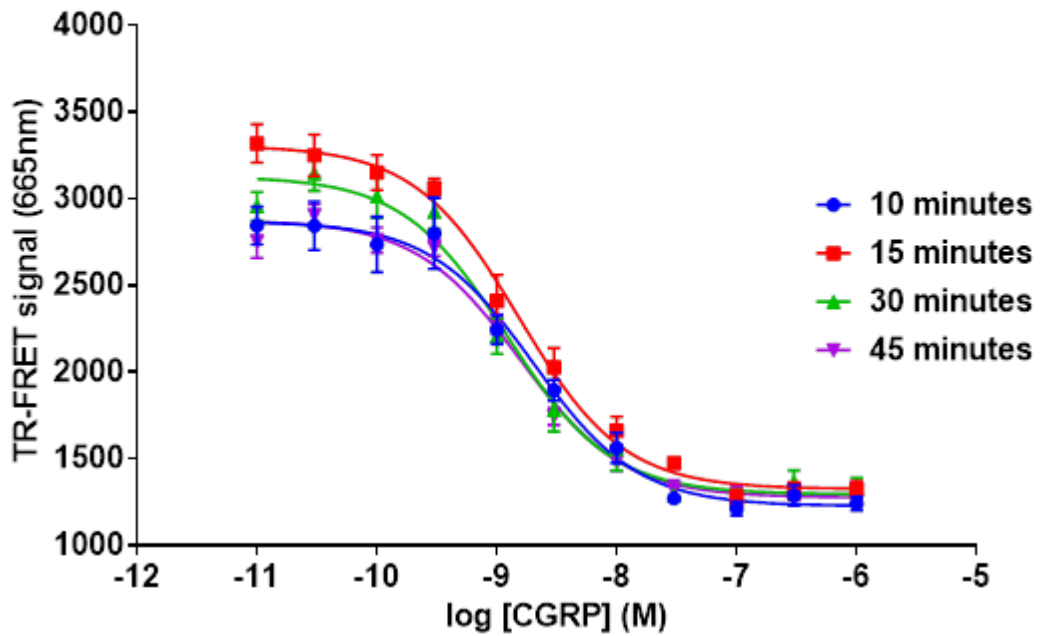
Figure 3.6: Optimization of agonist stimulation time in AM2 and CGRP receptor O/E cells. Showing the agonist dose response curves obtained by the stimulation of AM2r and CGRPr O/E cells by their respective agonist ligand under different stimulation time points.

3.4.3 Determination of half maximal response concentration (EC$_{50}$)

The production of cAMP after stimulation of G-protein couple receptor O/E cells (CGRPr, AM1r, AM2r, AMY1r and AMY3r) by peptide ligands was used to determine the EC$_{50}$ doses of each ligand against their respective cell line. EC$_{50}$ is known as the concentration of the agonist which is responsible for the half maximal response. Knowing the EC$_{50}$ dose of a ligand we are able to test the effects of small molecule antagonists on the production of cAMP by cells stimulated with this dose in an agonist/antagonist competition assay.

Figure 3.7 below shows the dose response curves of CGRP, AM and AMY ligands against CGRPr, AM1r and 2r, and AMY1r and 3r O/E cells respectively. As was mentioned in method section high production of cAMP by the cells is decreasing the TR-FRET signal and vice versa, therefore, higher the signal lower the production of cAMP. Table 3.5 below shows the EC$_{50}$ and pEC$_{50}$ (the negative logarithm of EC$_{50}$) values extracted from each dose response curve as well as the minimum stimulation of cAMP production (lowest TR-FRET signal) and the maximum stimulation (highest TR-FRET signal).

Table 3.5: Best fit values for agonist stimulation of different O/E cells.

Over-expressing Cell lines	Parameters			
	EC$_{50}$	pEC$_{50}$ +/- SEM	Top	Bottom
CGRPr	2.72nM	8.57 +/- 0.063	104.7	0.354
AM1r	4.07nM	8.39 +/- 0.093	102.7	4.504
AM2r	5.15nM	8.29 +/- 0.078	100.8	1.631
AMY1r	0.89nM	9.05 +/- 0.064	97.69	1.307
AMY3r	71.6pM	10.2 +/- 0.050	95.41	1.314
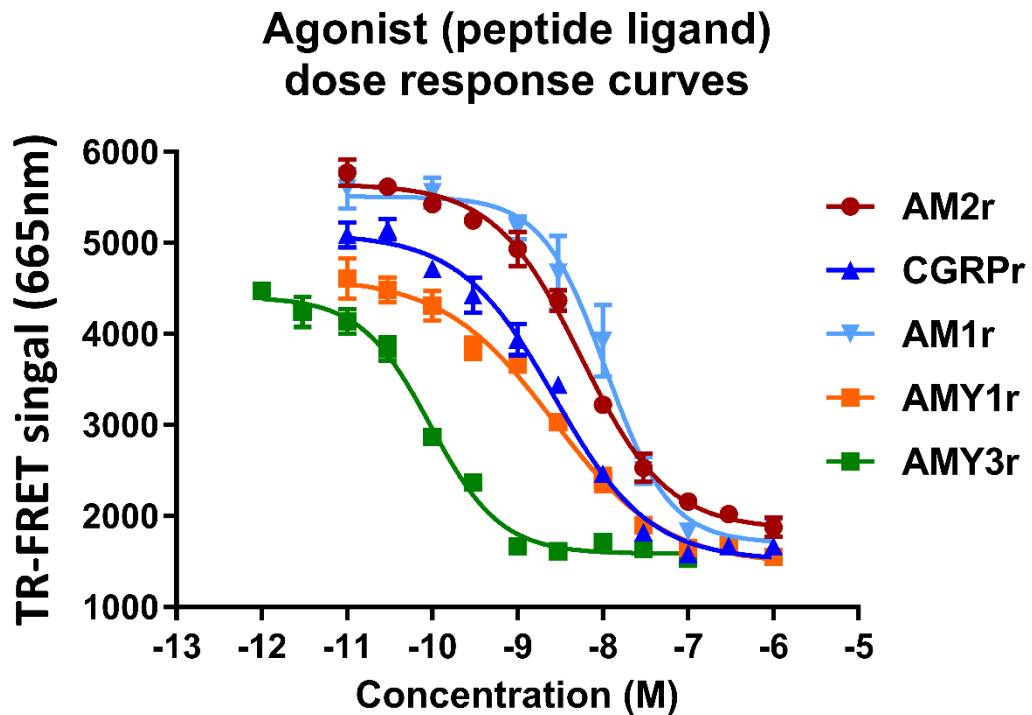
Figure 3.7: Stimulation of overexpressing cells by peptide ligand agonists. Showing the cAMP production (TR-FRET signal) by CGRP, AM1, AM2, AMY1 and AMY3 receptor O/E cells after stimulated by peptide ligands against each receptor.

3.4.4 Overall quality and assay performance

3.4.4.1 Determination of Z-factor

To evaluate both the performance (assay signal window) and the reproducibility of the assay, Z-factor analysis was performed as described by Zhang and colleagues in 1999 (Zhang et al., 1999). Data from two plates each treated with EC_{50} agonist dose (negative) and with vehicle control (positive) were used in this evaluation. The figure 3.8 below illustrates the mean values and SD obtained by stimulation of CGRPr O/E cells, by the EC_{50} dose of CGRPa agonist and vehicle control (buffer). Both the graphical illustration (showing by the separation band) and the mathematical calculation of the assay signal window (Z-factor: 0.74), indicate an extremely robust and consistent assay.
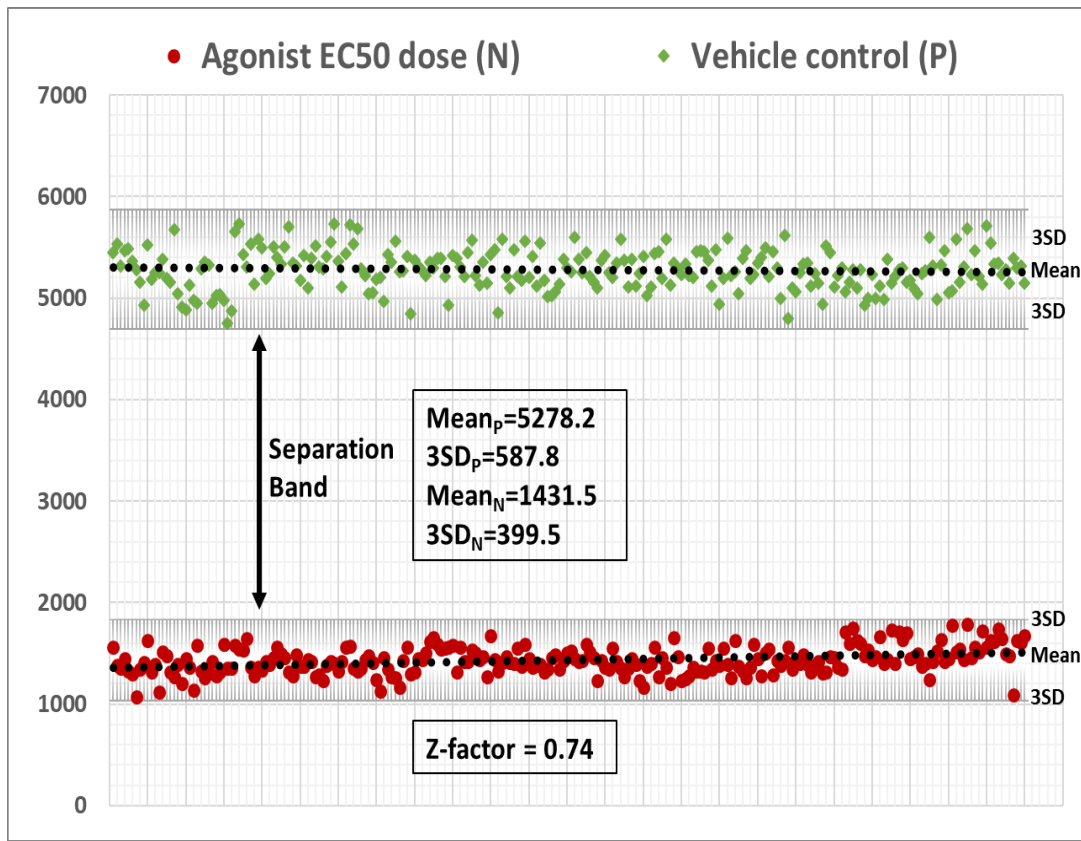
$$Z = \frac{3(SD_P + SD_N)}{|Mean_P - Mean_N|}$$

Z = [3 * (195.9 + 133.2)] / (5278.2 - 1431.5)

Z = 0.74

Figure 3.8: Determination of Z factor. Mathematical and graphical illustration of the signal dynamic range and the quality of the data produced by our High-throughput cell-based TR-FRET cAMP assay.

3.4.4.2 Assay consistency and cell stability

To further evaluate the consistency of the assay and the stability of the transfected cells used in our screening process, agonist dose response curves were regularly performed. The figure 3.9 below shows the agonist dose response curves obtained by stimulation of six different batches (passage age) of AM2r and CGRPr O/E cells by AM_{1-52} and CGRPa respectively. As shown in figure 3.9 below the dose response curves obtained with both cell lines were very consistent. Table 3.6 below shows the EC_{50} and pEC_{50} (the negative logarithm of EC_{50}) values extracted from each dose response curve as well as the minimum stimulation of cAMP production (lowest % of TR-FRET signal) and the maximum stimulation (highest % of TR-FRET signal). When comparing the best fit values of the different passage age cells with the earliest age cells some significant differences were found in CGRPr O/E cells. On the hand, comparison of fits for AM2r O/E cells showed no significant differences. These differences can be possibly explained by the presence of calcitonin or other growth factors in the growth medium of the cells or by the use of frozen instead of live cells.

Table 3.6: Best fit values for agonist stimulation of different passage age cells.

Parameters					
AM2r Cells					
Passage age	EC_{50}	pEC_{50} +/- SEM	**Top**	**Bottom**	**P value**
AM2r p9	5.5nM	8.25 +/- 0.053	100.6	14.58	-
AM2r p12	5.6nM	8.25 +/- 0.056	102.4	6.176	0.93
AM2r p14	6.5nM	8.19 +/- 0.058	102.3	2.959	0.43
AM2r p16	5.5nM	8.26 +/- 0.053	103.0	3.242	0.81
AM2r p17	6.1nM	8.22 +/- 0.096	105.2	7.054	0.76
AM2r p19	7.3nM	8.14 +/- 0.105	105.6	4.653	0.29
CGRPr Cells					
Passage age	EC_{50}	pEC_{50} +/- SEM	**Top**	**Bottom**	**P value**
CGRPr p12	0.7nM	9.14 +/- 0.071	99.81	0.486	-
CGRPr p15	1.1nM	8.95 +/- 0.075	101.8	1.395	0.11
CGRPr p16	2.2nM	8.66 +/- 0.125	105	1.136	<0.0001
CGRPr p18	0.6nM	9.20 +/- 0.071	100.5	1.272	0.33
CGRPr p22	3.6nM	8.44 +/- 0.041	99.07	14.93	<0.0001
CGRPr p23	1.8nM	8.74 +/- 0.062	100.9	10.35	0.0004
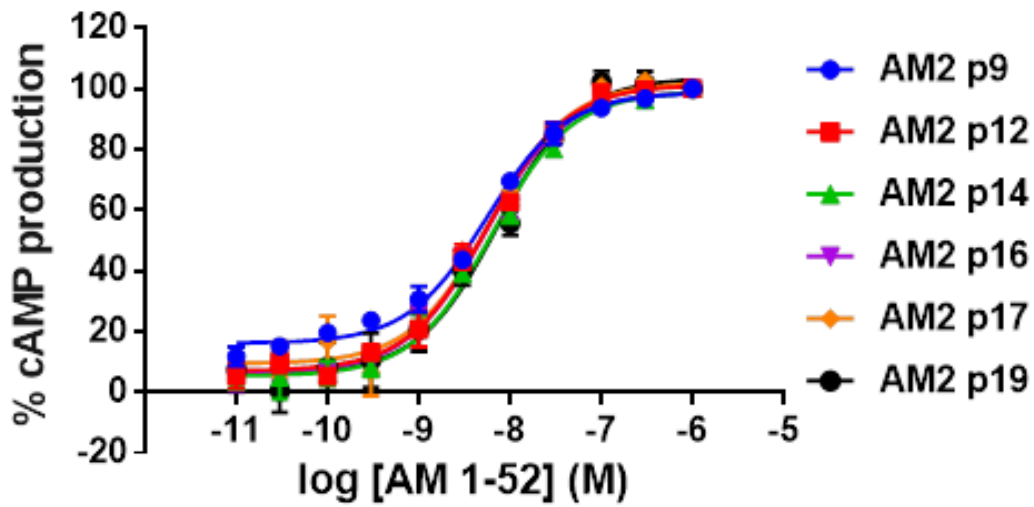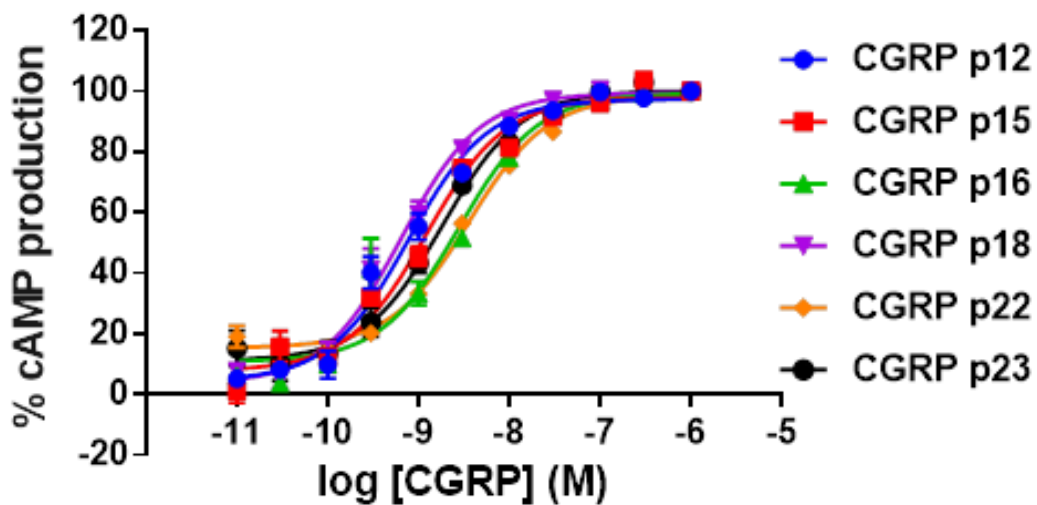
Figure 3.9: Agonist dose response curves run on different passage number AM2r and CGRPr O/E cells. Showing the dose response curves obtained by the stimulation of different passage number AM2r and CGRPr O/E cells by their respective peptide ligand.

3.4.4.3 Evaluating assay variability (Edge effects and DMSO toxicity)

To further assess the quality and consistency of our screening assay, several experiments were performed focusing on possible systematic sources of variability such as differences in signal reading (edge effects) and DMSO toxicity. Firstly, Forskolin dose response curves were used to evaluate the reproducibility of the assay when performed in a whole plate format. In a 384-well plate 16 different Forskolin dose response curves (one in each row) were performed to assess any row specific effects. As shown in the figure 3.10 below, no significant difference was observed, between the different dose response curves, with all EC_{50} doses to be at low uM range. This was supported by the comparison of fits analysis which shown no significant differences (P value: 0.308). Table 3.7 below shows the EC_{50} and pEC_{50} (the negative logarithm of EC_{50}) values extracted from each dose response curve as well as the minimum stimulation of cAMP production (highest % of TR-FRET signal) and the maximum stimulation (lowest % of TR-FRET signal).

Table 3.7: Best fit values for Forskolin dose response curves across the whole plate.

Rows	Parameters				
	EC_{50}	pEC_{50} +/- SEM	Top	Bottom	P value
A	1.38uM	5.86 +/- 0.138	103.3	2.018	-
B	1.35uM	5.87 +/- 0.099	100.9	-3.371	0.12
C	1.25uM	5.90 +/- 0.077	99.83	-0.3359	0.16
D	1.00uM	5.99 +/- 0.059	101.2	1.741	0.38
E	1.06uM	5.98 +/- 0.101	96.7	5.819	0.92
F	0.68uM	6.17 +/- 0.100	96.9	4.566	0.25
G	0.79uM	6.11 +/- 0.147	95.29	3.889	0.79
H	0.86uM	6.07 +/- 0.089	97.22	3.716	0.68
I	0.96uM	6.02 +/- 0.055	102.7	5.167	0.12
J	1.24uM	5.91 +/- 0.103	100.9	1.71	0.82
K	1.30uM	5.89 +/- 0.085	99.78	4.894	0.67
L	0.89uM	6.05 +/- 0.036	97.94	5.262	0.34
M	1.15uM	5.94 +/- 0.054	99.55	6.218	0.55
N	1.25uM	5.90 +/- 0.070	100.7	1.007	0.31
O	0.78uM	6.11 +/- 0.117	94.31	2.632	0.81
P	1.49uM	5.83 +/- 0.099	99.21	2.689	0.52
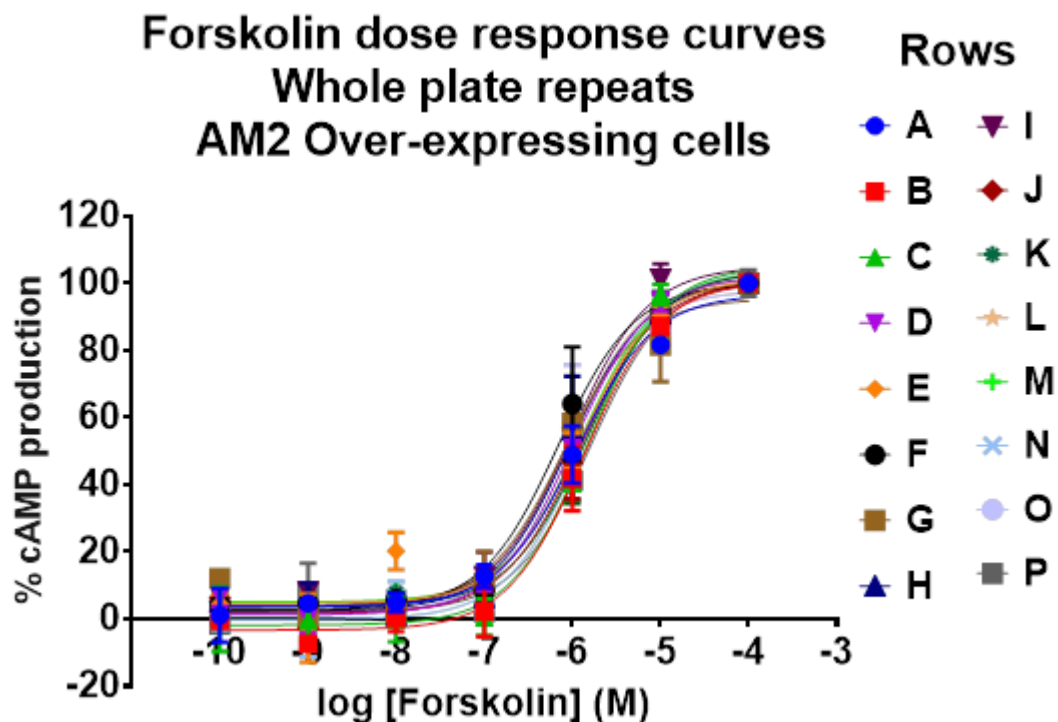
Figure 3.10: Forskolin dose response curves across a whole 384-well plate.
Showing the reproducibility and consistency of the assay after performing 16 Forskolin dose response curves under the same conditions (cell type, cell number and stimulation time) in a single 384-well plate.

Moreover, the consistency and precision (pipetting, plate reader etc.) of the assay was further evaluated by performing whole plate stimulation experiments. In these assays the same number of cells in three whole 384-well plates were exposed to vehicle control. Data obtained were plotted as heat maps to distinguish any row or column specific patterns and any edge effects, which are normally associated with pipetting errors and temperature fluctuations. As shown in the figure 3.11 below, that illustrates the heat maps obtained from three separate plates, no obvious patterns can be identified. All data points are within the range of mean +/- 2SDs.
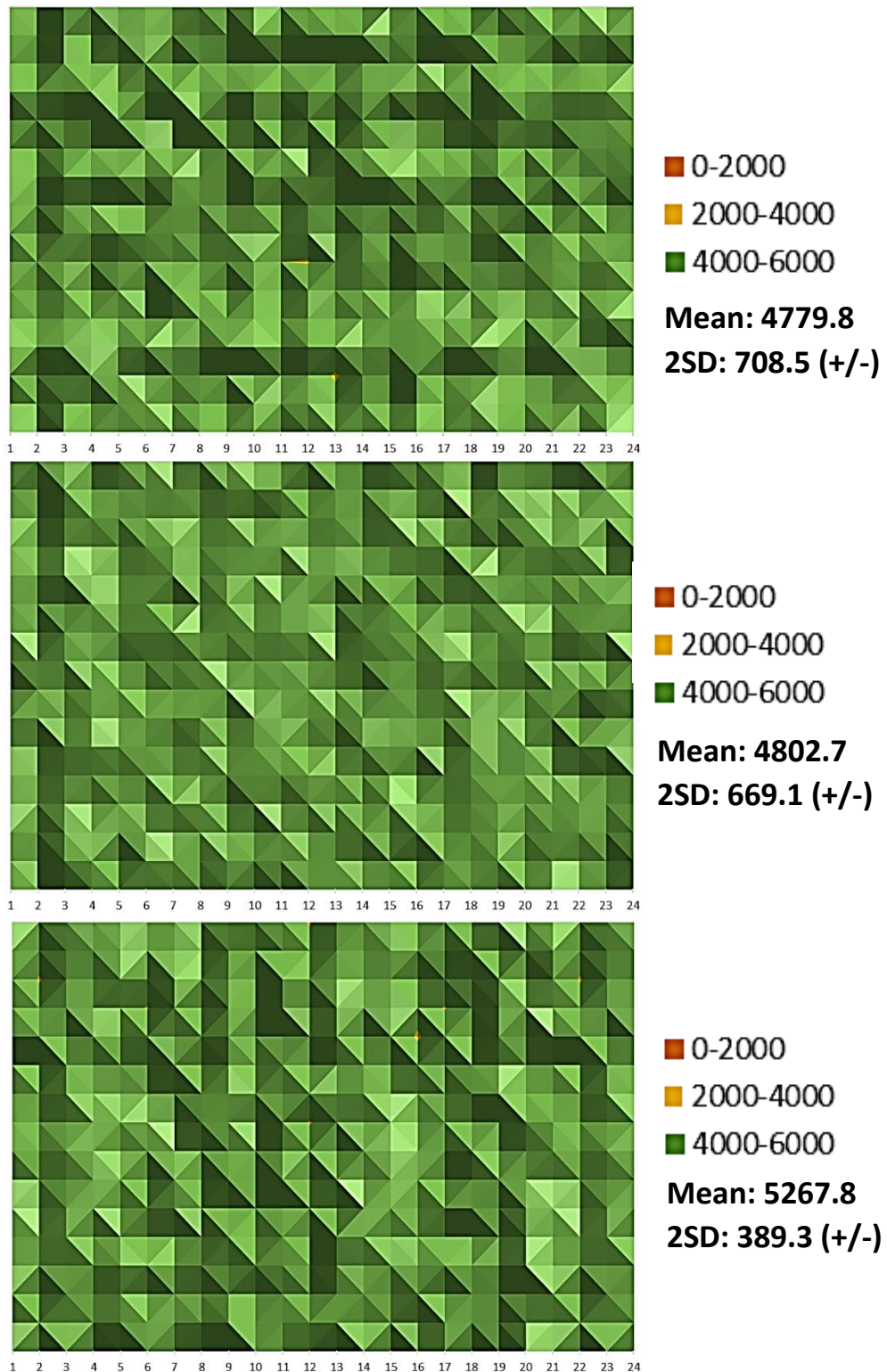
Figure 3.11: Determination of edge effects and/or detection patterns. Illustrating the heat maps of the raw data obtained upon stimulation of AM2r cells with the stimulation buffer.

To investigate the effects of DMSO on the cell stimulation, agonist dose response curves were performed in the presence of various concentrations (0%-5%) of DMSO in the stimulation buffer. In our agonist/antagonist competition cAMP assays (see chapter 4 for more details), DMSO is use as a solvent at a maximum final concentration of 1%. As shown in the figure 3.12 and table 3.8 below, the presence of DMSO had no significant effect on the stimulation of AM2r O/E cells by AM1-52 agonist. Table 3.8 below shows the EC_{50} and pEC_{50} (the negative logarithm of EC_{50}) values extracted from each dose response curve as well as the minimum stimulation of cAMP production (highest % of TR-FRET signal) and the maximum stimulation (lowest % of TR-FRET signal). The P values obtained from the comparison of fits between the dose response curve without any DMSO (0%) and the other dose response curves are also shown on the table.

Table 3.8: Best fit values for agonist stimulation in the presence of DMSO.

%	Parameters				
DMSO	EC_{50}	pEC_{50} +/- SEM	Top	Bottom	P value
0%	21nM	7.67 +/- 0.065	105.4	3.004	-
0.5%	29nM	7.53 +/- 0.058	106	2.834	**0.14**
1%	31nM	7.50 +/- 0.070	98.96	1.102	**0.11**
1.5%	23nM	7.63 +/- 0.073	101.2	-3.251	**0.70**
2.5%	31nM	7.51 +/- 0.082	103.9	-3.405	**0.15**
5%	16nM	7.79 +/- 0.101	100.7	8.163	**0.35**
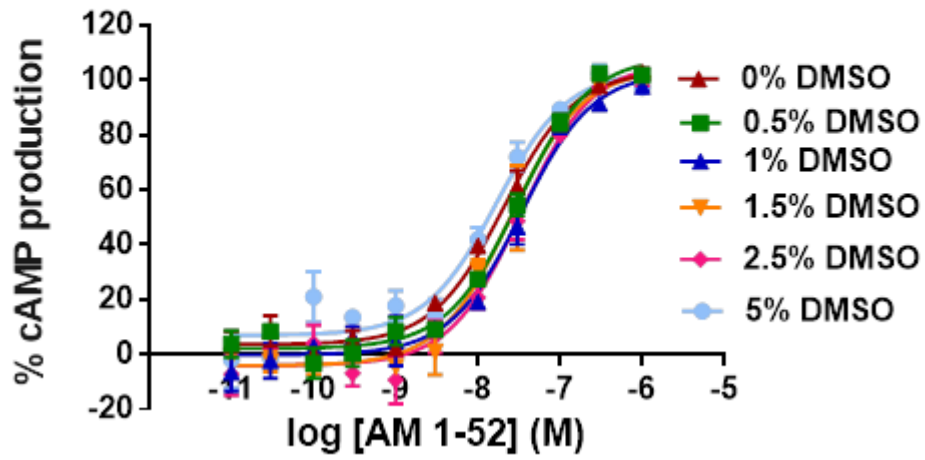
Figure 3.12: DMSO tolerance. Showing the effects of various concentrations of DMSO in the stimulation of AM2r O/E cells by AM_{1-52} ligand.

3.5 Conclusion/Discussion

Drug discovery is a lengthy process that involves the design, development and screening of thousands of new chemicals (compounds). Developing a robust assay that will accurately identify the activity or binding potential of these new compound candidates is the foundation of any HTS process. There are mainly two types of screening approaches that involve the use of either biochemical or cell-based assays. Cell-based assays have increasingly been used during the last few years, mainly due to their ability to provide valuable information (effects on cell growth, cytotoxicity and permeability) for the further development and optimization of the compounds. Choosing the appropriate cell line (primary or engineered) and detection method (cAMP production, calcium influx, protein to protein interactions and the use of reporter genes), based on the target of interest, is an important aspect of the assay development. Moreover, ensuring the consistency of the assay and the quality of the data produced, by identifying and eliminating any source of variability, is crucial to guarantee the correct identification of any lead compounds.

One of the most commonly used detection method in HTS is the measurement of cAMP production, a very important secondary messenger, production of which is triggered upon the activation of various GPCR receptors. The production of cAMP as a measurement of receptor inhibition was previously used successfully for the development of CGRP receptor antagonists. More specifically, a combination of binding studies (assays that utilise radiolabelled ligands to establish binding affinities of potential compounds) and cAMP screening assays was used in three separate high-through put screening programs that led to the discovery of several small molecule antagonists against CGRP receptor, for the treatment of migraine, including Olcegepant (Doods et al., 2000), Telcagepant (Salvatore et al., 2008) and MK-3207 (Salvatore et al., 2010). The Lance TR-FRET cell-based cAMP assay was chosen as the primary screening tool for our drug discovery project. Cells that were stably transfected with our target of interest (AM2r) and closely related receptors (CGRPr, AM1r, AMY1r and AMY3r) were used for the optimization of the assay and the screening process.

Overall, the results of these *in-vitro* experiments illustrate a highly consistent assay, with the ability to produced excellent quality and reproducible data, suitable for HTS purposes. To optimise various aspects of the assay, a series of agonist stimulation assays were performed using primarily AM2r and CGRPr O/E cells (primary screening cell lines). The detection window of the assay was established using the cAMP standard curve provided with the kit. The results have shown a highly sensitive assay (detection of IC_{50} values in the low nM range) and a significantly large detection window (dynamic range) of ~3000 absorbance units (AU) (Figure 3.5).

The optimal cell number for each cell line was determined using Forskolin dose response curves. For both AM2r and CGRPr cells lines 2500 cells/well was selected as the optimal number based on the dose response curves that cover most of the linear region of the standard curve and their dynamic range (Figure 3.5). After the optimal cell number was established, the time of stimulation was optimised using agonist dose response curves. All four stimulation time points used showed similar sensitivity and potency for both the receptors. The optimal stimulation time was determined from the detection window that each time-point yielded, with 15 minutes to be the optimal for both cell lines (Figure 3.6). Following the assay optimization, the EC_{50} dose of each cell line was determined using the respective peptide ligand in an agonist dose response curve. The results suggested that all cell lines are highly sensitive over their respective ligand with all EC_{50} doses to range in low nM (Figure 3.7). This high sensitivity can be explained by the fact that activation of both AM and CGRP receptors will predominantly cause the activation of adenylate cyclase (AC) that subsequently increases the levels of cAMP (Hay et al., 2003b, Beltowski and Jamroz, 2004). Like most GPCRs, AM and CGRP receptors can interact with other subtypes of G protein family as well as other protein such as arrestins activating cAMP-independent pathways. Both receptors were found to be able to increase the release of intracellular calcium, however, this effect was cell type dependent with AM stimulation resulting in a decrease of Ca^{2+} in pig coronary arterial smooth muscle cells (Kureishi et al., 1995). Engagement of CGRP and AM with other members of the G proteins and the arrestins was shown in recent studies, however, the extent of this coupling is not clear yet (Heroux et al., 2007, Ritter and

Hall, 2009) indicating that the use of other cAMP independent pathways as screening tools could be proved insufficient.

To assess the consistency and reproducibility of the assay, agonist stimulation curves were used. A screening window coefficient (Z-factor) of 0.74 was determined using the formula described by Zhang et al. in 1999, indicating an extremely robust and consistent assay, suitable for identifying active compounds ("hits") with high fidelity (Figure 3.8). When different passage numbers of each cell line were tested under the same stimulation conditions, the results showed a consistent EC_{50} values suggesting the stability of the transfection (Figure 3.9). No specific row or column trends were identified when the same Forskolin dose response curve was used on the entire plate (16 rows), with the Forskolin EC_{50} to be extremely consistent between the curves (Figure 3.10). The possible edge effects were tested by running three identical plates of cells that were stimulated with the assay buffer showing no specific trends or patterns (Figure 3.11). Finally, the viability and functionality of the cells was tested in the presence of various concentrations of DMSO. The data showed that these cells were able to tolerate DMSO concentrations between 0.5% and 5%, with no significant difference in their EC_{50} dose when compared with the 0% dose response curve (Figure 3.12).

In conclusion, these data provide confidence of the consistency and reproducibility of this assay and support its use in drug discovery and more specifically in a HTS process.

Chapter 4: Effects of small molecule antagonists on receptor activation

Chapter 4: Effects of small molecule antagonists on receptor activation

4.1 Introduction

4.1.1 Structural characteristics of RAMP and receptor binding

Other than CTR and CLR, RAMPs interact with other members of B Class GPCRs which can be explained by the similar structural characteristics shared between these receptors. The table 4.1 below illustrates the interactions of RAMP with the members of B Class GPCRs and the significance of this interaction (adapted from (Hay and Pioszak, 2016)). Homology and alignment studies have shown that most members of this family share several similarities having a large N-terminal ECD, three ECLs (ECL1, 2 and 3), seven TMDs, three intracellular loops (ICL1, 2 and 3) and a C-terminal extracellular domain (Barwell et al., 2012).

Table 4.1: Summary of interactions between RAMPs and other members of B Class GPCRs and the significance of this interaction (adapted from (Hay and Pioszak, 2016).

GPCRs	RAMP	Receptor formed	Significance
CTR	RAMP 1-3	AMY1, AMY2 and AMY3	Modulates pharmacology
CLR	RAMP 1-3	CGRP, AM1 and AM2	Receptor translocation, internalization and recycling and Pharmacology
PTH1	RAMP 2	Unknown	Unknown
PTH2	RAMP 3	Unknown	Unknown
VPAC1	RAMP 1-3	Unknown	Modulates signalling
VPAC2	RAMP 1-3	Unknown	Modulates signalling
CRF1	RAMP 2	Unknown	Receptor translocation Modulates signalling
Glucagon	RAMP 2	Unknown	Modulates selectivity and pharmacology (Weston et al., 2015)
Secretin	RAMP 3	Unknown	Receptor trafficking (Harikumar et al., 2009)

Mutagenesis studies are often used to identify the importance of specific residues on the binding and activity of the receptors. Such studies have been used and identified residues involved in the binding of RAMPs with CLR as well as ligand interactions (Barwell et al., 2012, Booe et al., 2015). In depth understanding of the interactions between RAMPs and CLR as well as the druggability of the complex (CGRP receptor) was fulfilled by the identification of the crystal structure of the CLR/RAMP1 N-terminal ectodomain heterodimer by ter Haar et al. in 2010. As explained, numerous hydrophobic interactions and hydrogen bonds mainly between the CLR helix αC1 and the RAMP1 helices αR2 and αR3 as well as its C-terminal loop domain are responsible for the stabilization of the heterodimer. The most extensive interactions network was observed between the carbonyl side group of Gln54 of the CLR α-helix and the amine groups of RAMP1 residues Arg102 and Cys104 and between the carbonyl group of CLR residue Gln50 and residues His97, Phe101 and Pro105 of RAMP1 (ter Haar et al., 2010). The importance of these residues was previously described by Kusano et al. in 2008 that showed a reduction of receptor cell surface expression and CGRP ligand binding caused by mutagenesis of residues Cys104, His97 and Phe101 (Kusano et al., 2008).

Moreover, using several CGRP selective small molecule antagonists, ter Harr et al. were able to identify several important residues for antagonist binding and selectivity on the CLR and RAMP1 ECD. An illustration of the location of these residues as wells as the interaction of Olcegepant (selective CGRP antagonist) with the CLR: RAMP1 ECD heterodimer can be found in figure 4.1 below. Upon binding, Olcegepant is causing a 70° rotation of residues Try72 (Try72 shelf also known as W72 bulge) and Arg38 of CLR and an interaction with the dibromotyrosol group of Olcegepant and residues Arg67 of RAMP1 occurs. This causes the formation of a binding pocket which is topped by RAMP1 residue Try74 (shown in figure 4.1B).
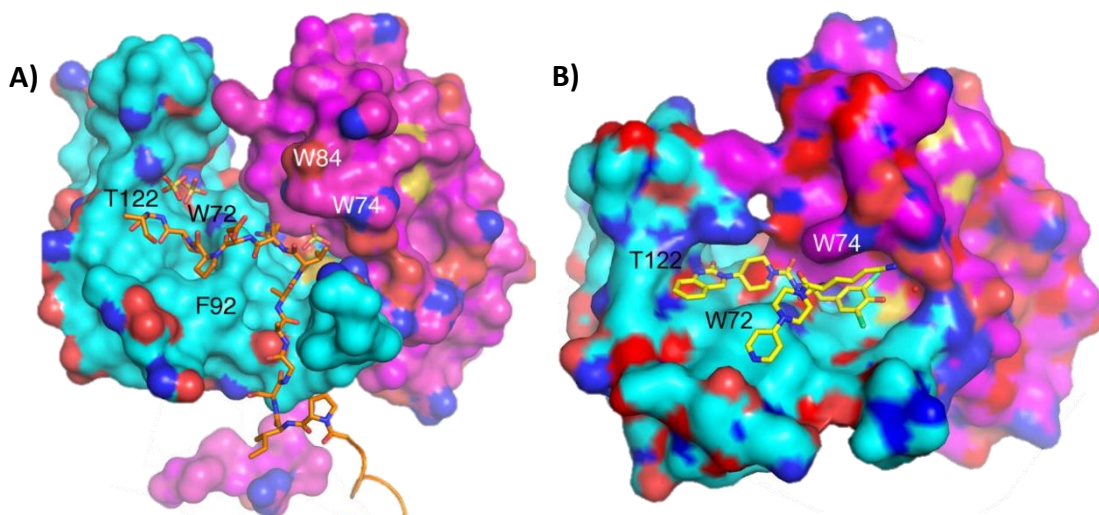
Figure 4.1: CLR: RAMP1 crystal structure and antagonist binding. A) Crystal structure of CLR receptor and RAMP1 (as solved by (ter Haar et al., 2010) including important residues for antagonist binding coloured white on RAMP1 ECD (purple) and black on CLR ECD (blue). **B)** Structure of the Olcegepant (yellow)/CLR/RAMP1 complex including the main interaction points (residues). Image from ter Haar et al. 2010, reused with permission from Elsevier.

The recently published solved crystal structures of CLR: RAMP1 (CGRP) and CLR: RAMP2 (AM1) receptors bound to CGRP$_{27-37}$ and AM$_{25-52}$ respectively, gave further insight into the association of ligands with the CLR: RAMP receptors (Booe et al., 2015). Similarly, to ter Haar et al., Booe and co-workers have shown the presence a hydrophobic patch and pocket that are separated by the Try72 shelf (W72 bulge). Table 4.2 below shows the residues that comprise the pocket and the patch.

Table 4.2: Table illustrates the residues that comprise the CLR pocket and patch.

Residues	Location
CLR Pocket	
D70, G71, W121, T122 and Y124	CLR ECD
W84 and P85	RAMP1 ECD
R97, E101, E105 and P112	RAMP2 ECD
CLR Patch	
F92, F95 and Y124	CLR ECD

Furthermore, these data have suggested the presence of a β-turn on both CGRP and AM peptides that enables them to occupy their respective binding pockets and modulates their interaction with CLR and RAMP residues. More specifically, via its F37 phenyl ring CGRP can interact with CLR residues G71 and W72 as wells as RAMP1 residue W84. As described by ter Haar and co-workers previously, CGRP binds almost entirely on CLR and makes only a single critical contact with RAMP1 ECD (at residue W84) which also includes a hydrophobic interaction with CLR residue F37 (ter Haar et al., 2010). Also, hydrogen bonds are formed between CGRP residue V32 and the W72 bulge of CLR and a main-chain to side-chain connection is made between CGRP T30 and CLR loop 3 D94 residues (Booe et al., 2015).

Similarly, AM residues Y52 and K46 interact with residues R97, E101 and E105 on RAMP2. An extension of a single helical turn allows AM K64 to contact the W72 bulge. It is worth mentioning that the equivalent residue on RAMP1 (W74) was unable to interact with AM. This was explained by the lack of a glutamine residue at position 74 of RAMP1 that discourages AM interaction (Hay and Pioszak, 2016). The importance of residues E101 and F111 (closely positioned to E101 and E105) was previously shown through mutagenesis studies (Moore et al., 2010, Watkins et al., 2014). Using alanine substitutions Booe et al. were able to identify key residues that modulate the binding of the two peptides (figure 4.2 and table 4.3 below).

Table 4.3: Key residues on CLR: RAMP complex that modulate ligand binding.

Peptide ligand	Residue	Location
Calcitonin-Gene Related Peptide (CGRP)	W72, F92, D94, F95, H114, R119, W121, T122 and Y124	CLR
	W84	RAMP1
Adrenomedullin (AM)	W72, F92, F95, W121 and Y124	CLR (essential)
	D94 H114, R119 and T122	CLR (nonessential)
	E101 and F111	RAMP2 (essential)
	R97 and E105	RAMP2 (nonessential)
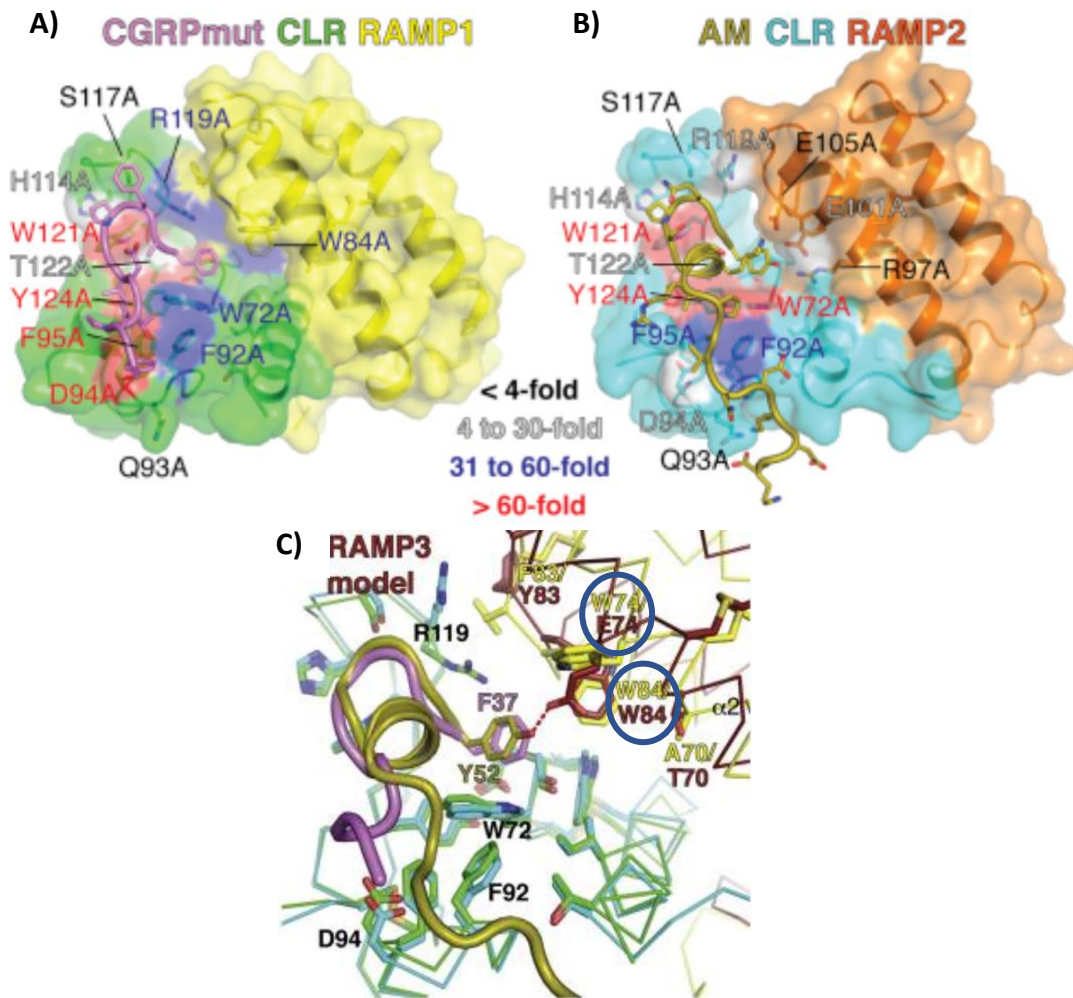
Figure 4.2: Structures of the CGRP- and AM-bound CLR: RAMP1/2 ECD heterodimers. A) Structure of CGRPmut-bound CLR: RAMP1 heterodimer. CLR is coloured green, RAMP1 is coloured yellow and CGRP is coloured purple. **B)** Structure of AM-bound CLR: RAMP2 heterodimer. CLR is coloured blue, RAMP2 is coloured orange and CGRP is coloured brown. The structure residues are coloured according to their effects on ligand potency upon alanine substitution. **C)** A homology model of the AM-bound CLR: RAMP3 ECD heterodimer. Images from Booe et al., 2015, reused with permission from Elsevier (creative commons attribution license).

By analysing the sequence similarities between the RAMP subtypes and by superimposing the crystal structures solved (figure 4.2(A) and (B)), Booe and co-workers were able to generate a homology model of the AM-bound CLR: RAMP3 ECD heterodimer (figure 4.2(C)) in an effort to predict the potential ligand/antagonist

binding site of AM2 receptor complex (Booe et al., 2015). The proposed model shows the interaction of RAMP3 residue E74, which is positioned at the same place as the residue E101 of RAMP2, with the AM peptide residue Y52 by forming a hydrogen bond. Furthermore, it was suggested that the presence of residue W84 on RAMP3, in the same position as in RAMP1, enables the interaction with CGRP peptide residue F37 (phenyl ring) as well as with AM peptide via its Y52 residue (Booe et al., 2015). Similar predictions were previously made by Watkins and co-workers and could potentially explain the increased potency of CGRP peptide on AM2 receptor compared to AM1 receptor (Watkins et al., 2014). These shows the importance of the different RAMPs in receptor pharmacology.

4.1.2 The role of RAMPs on receptor activation/pharmacology

RAMPs are considered as important accessory proteins that can alter and influence the receptor pharmacology and function upon their interaction. The ubiquitous distribution of RAMPs (at least one isoform is detected in all cell lines and tissues tested) indicates their importance in a wide variety of physiological processes (Sexton et al., 2001). Studies have shown that RAMPs are able to alter ligand binding affinity and receptor trafficking, as well as to modulating the signalling (second messenger pathways) of several GPCRs in a receptor-dependent manner (Hay and Pioszak, 2016) (see table 4.1). The interactions of RAMPs with CLR and CTR are the most extensively studied, but, the effects of RAMPs on the pharmacology of other members of B Class GPCRs have been reported as well. When they interact with CLR, RAMPs act as chaperones and enhance cell surface expression and glycosylation of the receptors (McLatchie et al., 1998). In the case of CTR and RAMP interactions, the receptor reaches the cell surface in the absence of RAMPs and then modulates the translocation of the RAMPs to the cell surface, altering the pharmacology of the CTR receptors formed, in a RAMP-dependent manner (Hay et al., 2005, Hay and Pioszak, 2016).

The most distinct example of the modulation of the receptor pharmacology by the RAMPs is the CGRP/AM paradigm and the ability of the different RAMPs to control

ligand binding specificity. More specifically, as described before when CLR binds with RAMP1, the result is a high affinity receptor for CGRP peptide with low affinity for AM. However, this changes dramatically in the presence of RAMP2 which causes a significant decrease in the affinity for CGRP and an increase for AM (~100 fold). When CLR interacts with RAMP3, even though AM has the highest affinity, CGRP can bind to the receptor with moderate affinity and not low depending on the species and the CGRP isoform (could be close to only ~10 fold difference) (Hay et al., 2003a). The presence of different RAMP member can also modulate the formation and the pharmacology of the AMY receptors. For instance, AMY1r formed by the co-expression of CTR and RAMP1 shows high affinity for AMY, salmon CT and CGRP peptides ligands, compared to AMY3r (CTR/RAMP3) that has higher affinity for salmon calcitonin and AMY peptides and lower affinity for CGRP peptide (Poyner et al., 2002, Hay et al., 2015). It is generally accepted that RAMPs increase the affinity of AMY peptide to CT receptors markedly when compared to calcitonin receptors alone (Poyner et al., 2002, Hay et al., 2005).

Even though changes in the pharmacology of CLR and CTR receptors was observed in the presence of different RAMP subtypes, the same is not the case for receptor signalling. The expression of the different RAMPs did not cause any significant changes in cAMP generation, Ca^{2+} internalization or in phosphatidylinositol (PI) hydrolysis by either CLR (Kuwasako et al., 2000) or CTR (Christopoulos et al., 2003) receptors. The presence of RAMP2 and not the other members of the family caused a significant increase in PI hydrolysis when compared to the receptor alone. This was not shown in the cAMP production. Heterodimerization of CLR with the RAMP is considered as obligatory for its transport to the cell surface (chaperone role of RAMP) (McLatchie et al., 1998). Studies using fluorescence cell sorting and confocal imaging suggested that in the presence of RAMPs, CLR receptors were greater in number (McLatchie et al., 1998, Fraser et al., 1999, Kuwasako et al., 2000). Similar results were observed during the cell surface expression and the terminal glycosylation of calcium sensing receptor (a member of C Class GPCRs) in COS-7 cells. The presence of RAMP1 and 3 (not RAMP2) allowed the translocation and glycosylation of the receptor which was not observed in the absence of RAMPs (Hay

et al., 2006b). Moreover, as described by Bomberger et al. in 2005, interaction of the PDZ domain of RAMP3 with the N-ethylmaleimide sensitive factor (NSF) had as a result the recycle of the AM2r compared to the AM1r (lacks the PDZ domain) which undergoes degradation (Bomberger et al., 2005).

The role of RAMPs in receptor functionality as well as their influence on physiological and pathophysiological actions of AM and CGRP was reviewed before (Hay et al., 2016). RAMP deletion or overexpression studies are often used to identify the role of a specific receptor subtype. While RAMP3 knockout mice are viable, RAMP2 knockout mice die in utero suggesting that the two receptors (AM1r and AM2r) have quite distinct functions (Dackor et al., 2007, Yamauchi et al., 2014). The deletion of RAMP1 have shown a variety of differences between the knockout mice and WT (wild type), including differences in angiogenesis (Kurashige et al., 2014), blood pressure regulation (Li et al., 2014) and inflammation response (Tsujikawa et al., 2007) changes which were related mainly to CGRP receptor activity. Moreover, overexpression of RAMP1 in mice led to phenotype related to the role of AMY in blood glucose and body weight regulation (leaner mice, increased metabolic rate and increased body temperature) (Hay and Pioszak, 2016). Furthermore, knockdown of RAMP2 in mice resulted in phenotypes not related to the function of AM1 receptor such as hyperprolactinemia, enlarged pituitary glands, enhanced mammary gland development and skeletal irregularities suggesting new receptor partners of RAMPs (Kadmiel et al., 2011). These data illustrate the role of RAMPs in the modulation of the distinct physiological and pathophysiological functions of the receptors as well as their possible use in the development of selective antagonists for the different members of the family. A well-documented example is the recent development of CGRP receptor antagonists for the treatment of migraine (see section 4.1.3 below).

4.1.3 CGRP receptor antagonists

In the early 2000s, the first screening program for the design and development of small molecule antagonists against CGRP receptor, a member of B class GPCR receptors, was initiated at Boehringer Ingelheim. This led to the development of Olcegepant, the first potent and selective CGRP small molecule antagonist (Doods et al., 2000). Several other small molecule antagonists with similar structural characteristics have been since developed by several groups and pharmaceutical companies including Telcagepant (Salvatore et al., 2008) and MK3207 (Salvatore et al., 2010). The desire to develop CGRP antagonists for the treatment of migraine had as a result the determination of the crystal structure of CLR/RAMP1 extracellular domain heterodimer by ter Haar in 2010 (ter Haar et al., 2010) and the peptide ligand bound CLR/RAMP1 and CLR/RAMP2 structures few years later (Booe et al., 2015).

4.1.3.1 Olcegepant (BIBN4096)

The first research program for the design and development of small molecule antagonists was initiated at Boehringer Ingelheim in early 2000s. Using a high-through put screening method the first potent and selective CGRP antagonist, initially called BIBN4096 (later named Olcegepant), was developed and was nominated for preclinical studies and clinical trials (Doods et al., 2000, Rudolf et al., 2005). The chemical structure of the compound is shown in figure 4.3 below.
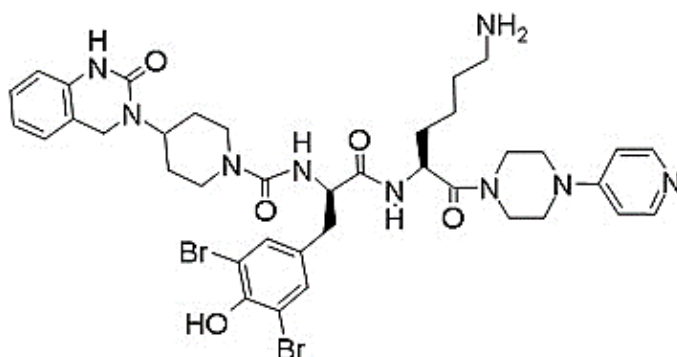
Figure 4.3: Chemical formula/structure of Olcegepant (BIBN4096). Illustrating the chemical structure of the first potent CGRP antagonist developed by Boehringer Ingelheim in early 2000s.

Olcegepant was found to have high binding affinity against the human CGRP receptor (Ki value 0.014nM), however much lower affinity for the rat receptor (Ki value 3.4nM) (Doods et al., 2000). In a subsequent study, the replacement of a single amino acid (lysine 74) in the ECD of RAMP1 component of rat receptor with tryptophan, had as a result the significant increase in affinity of the compound for the rat receptor indicating an a possible crucial interaction of the compound with RAMP1 (Mallee et al., 2002). Several *in-vivo* preclinical studies have been conducted to identify the antimigraine activity of Olcegepant. More specifically, administration of Olcegepant decrease facial blood flow in marmoset monkeys mediated by CGRP (Doods et al., 2000). Moreover, the antagonist was able to decrease the capsaicin-induced carotid haemodynamic changes in anaesthetised pigs (Kapoor et al., 2003). Furthermore, Olcegepant attenuated dilatation of the rat middle meningeal artery induced by CGRP (Petersen et al., 2004).

The first proof of concept clinical trial was conducted by Olesen and co-workers. In a multicentre, double-blinded randomized clinical trial, Olcegepant group had significantly higher response rates compared to the placebo group in all end-points measured including pain-free rate, the rate of sustained response over a period of 24 hours, recurrence rate of a headache and improvement in symptoms (nausea, photophobia, phonophobia). Also no serious adverse effects were reported (Olesen et al., 2004). Despite the promising results, Olcegepant the development of the compound was stopped due to its pharmacokinetics (could only be administrated intravenously). However, these results inspired other groups to search for new more suitable candidates.

4.1.3.2 Telcagepant (MK-0974)

One of these companies that aimed the identification of orally available small molecule antagonists against CGRP receptor suitable for migraine patients was Merck Research Laboratories. A high-through put screening program led to the discovery of a new small molecule antagonist with micromolar activity called

Benzodiazepinone 7 (Williams et al., 2006). Structural modifications and optimization of this compound led to the identification of new highly potent and orally bioavailable (rats: 20% and dogs 35%) compound called MK-0974 (later named Telcagepant). The chemical structure of the compound is shown in figure 4.4 below (Paone et al., 2007).
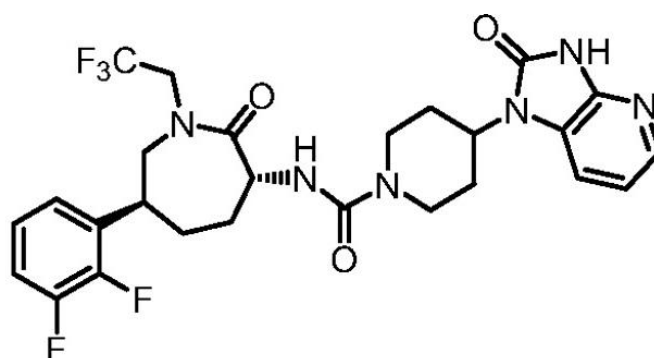
Figure 4.4: Chemical formula/structure of Telcagepant (MK-0974). Illustrating the chemical structure of telcagepant developed by Merck Research Laboratories.

Pharmacological characterization of Telcagepant showed high binding affinity for primate (human and monkey) CGRP receptors (Ki value of 0.77nM and 1.2nM respectively) compared to canine and rat receptors against which it displayed a ~1500-fold lower affinity. High selectivity was also reported over the two closely related human AM1r (>100µM) and AM2r (29µM) (Salvatore et al., 2008). Moreover, Olcegepant decrease the production of cAMP in human CGRP receptor expressing HEK293 cells (IC$_{50}$ ~2.2nM) potency which was decreased by 5-fold with the addition of 50% human serum (Salvatore et al., 2008). Inhibition of Capsaicin-Induced vasodilation was also illustrated (Sinclair et al., 2007, Salvatore et al., 2008).

In a randomized, double-blind dose-ranging (20-600mg) clinical trial the effects of orally administrated MK-0974 were tested against rizatriptan (5-HT$_1$ receptor agonist) and placebo. The effects of the higher doses (300, 400 and 600mg) on pain relief were comparable with those of the commercially available rizatriptan (10mg) and higher than the placebo. Telcagepant was well tolerated with mild side effects

including nausea and dizziness (Ho et al., 2008b). Similarly, oral administration of telcagepant (300mg) showed higher effectiveness than the placebo and the same efficiency with the commercially available zolmitriptan (5mg) in all primary endpoints including pain freedom, pain relief and nonappearances of phonophobia, photophobia and nausea. Moreover, telcagepant was well tolerated and had less associated adverse effects than zolmitriptan (Ho et al., 2008a). Despite the promising data shown in several phase-II and III studies for the treatment of acute migraine the compound was not fully developed due to liver toxicities (transaminase elevations) reported (Tepper and Cleves, 2009, Ho et al., 2014, Ho et al., 2016).

4.1.3.3 MK-3207

Further development and optimization of compound Benzodiazepinone 7 reported earlier by Merck Research Laboratories led to the discovery of MK-3207. The chemical structure of the compound is shown in figure 4.5 below (Salvatore et al., 2010). Similarly, to other CGRP antagonists, MK-3207 had lower binding affinity for rat (K_i = 10nM) and dog (K_i = 10nM) CGRP receptors compared to human (K_i = 0.021nM) and monkey (K_i = 0.024nM) receptors. MK-3207 showed also excellent selectivity profile over AM1, AM2 and AMY3 receptors (> 5,000-fold) and modest selectivity over the AMY1 receptor (30-fold) (Salvatore et al., 2010). Moreover, MK-3207 decrease the production of cAMP a cell-based functional assay (IC50 0.12nM), potency which was slightly decreased to 0.17nM with the addiction of 50% human serum (Bell et al., 2010). In an early *in-vivo* pharmacodynamic study MK-3207 reduced the capsaicin-induced vasodilation (dermal blood flow) at EC_{90} = 7nM (100 times more potent than telcagepant in the same model) (Salvatore et al., 2010).
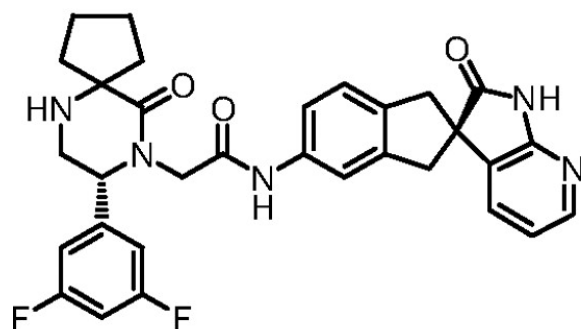
Figure 4.5: Chemical formula/structure of MK-3207. Illustrating the chemical structure of MK-3207 developed by Merck Research Laboratories.

Furthermore, in a multicenter, double-blinded randomized clinical trial, MK-3207 found to be superior to placebo at doses of 10, 100 and 200mg (primary endpoint: pain freedom at 2h). The compound was well tolerated with mild adverse effects to be the same between placebo and MK-3207 (Hewitt et al., 2011). However, in the same study data from an extended Phase I clinical trial were reported showing similar hepatic toxicity profiles as with telcagepant terminating further use of this compound (Hewitt et al., 2011). Table 4.4 below summarizes the pharmacological properties of CGRP antagonists on different species and receptor types.

4.1.3.4 Small molecules antagonists currently under development

Several other compounds have been developed during the last decade with very promising results. Rimegepant (also known as BMS-927711), a highly potent and selective CGRP receptor antagonist, was discovered by Bristol-Myers Squibb and it is currently under development by Biohaven Pharmaceuticals. *In-vitro* Rimegepant demonstrated excellent properties with high binding affinity (Ki= 0.027nM), high potency on cAMP production inhibition (IC_{50} = 0.14nM) and good metabolic profile (good oral bioavailability and clearance) (Luo et al., 2012). In a randomized, double-blinded dose-ranging study Rimegepant was found to have excellent tolerability profile (no treatment related side effects) and to be superior at several doses (75, 150 and 300 mg) than the placebo in terms of the primary endpoint (pain freedom at 2h) (Marcus et al., 2014). A phase II multicenter clinical trial is currently in the recruitment stage aiming to further evaluate the safety and tolerability of the compound (ClinicalTrials.gov Identifier: NCT03266588).

Moreover, two more gepants are currently under development for the treatment of acute migraine (Ubrogepant) and for migraine prevention (Atogepant). Ubrogepant is chemically distinct compound from MK-3207 and Telcagepant. Early studies in humans have shown that Ubrogepant has excellent metabolic and pharmacokinetic profiles. More specifically, it was found to be rapidly absorbed (T_{max} = 0.7 - 1.5h) and to have half-life of ~ 3-7h (Voss et al., 2016). Furthermore, in a phase IIb, randomized, double-blinded, placebo-controlled clinical trial Ubrogepant (100mg) was found to be significantly more efficient than the placebo control for two-hour pain freedom. No treatment-related adverse effects were identified (Voss et al., 2016). Currently, one phase II (ClinicalTrials.gov Identifier: NCT01657370) and two phase III (ClinicalTrials.gov Identifier: NCT02867709, NCT02828020) clinical trials are undergoing to further characterized the pharmacokinetics of the compound and to establish its efficacy, tolerability and safety. Finally, a phase II clinical trial aiming to evaluate the efficacy and the safety profile of Atogepant is currently in the recruitment stage for the prevention of episodic migraine (ClinicalTrials.gov Identifier: NCT02848326). The chemical structures of Rimegepant, Ubrogepant and

Atogepant are shown in figure 4.6 below. The activity of CGRP small molecule antagonists was investigated using our cAMP cell-based assay (data shown in appendix chapter 8, Figure 8.1)

Rimegepant

Ubrogepant
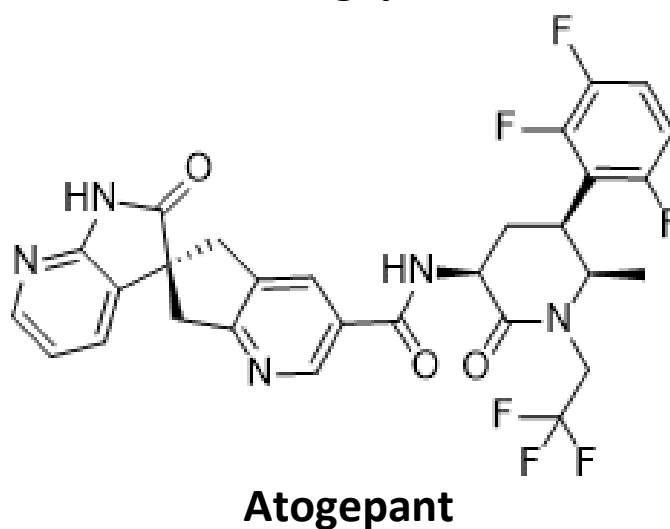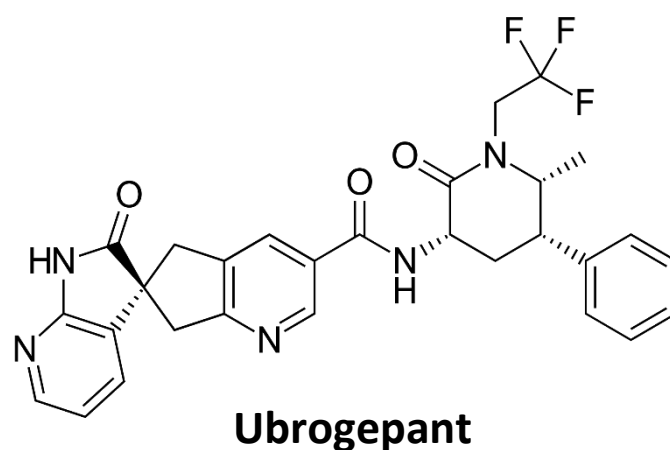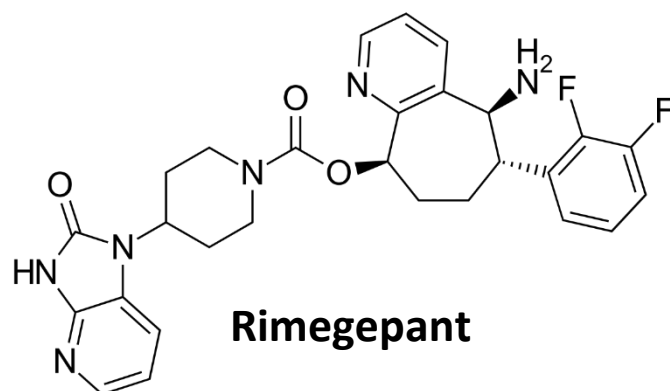
Atogepant

Figure 4.6: Chemical formula/structure CGRP receptor small molecule antagonists under development. Illustrating the chemical structures of Rimegepant, Ubrogepant and Atogepant.

Table 4.4: Pharmacological properties of CGRP antagonists

Antagonist	Receptor/ Species	Assay	Affinity (nM)	Reference
Olcegepant	CGRP/Human	cAMP	0.01 (K_B)	(Doods et al., 2000)
		Binding	0.01 (K_i)	
		cAMP	0.02 (A_2)	(Miller et al., 2010)
	CGRP/ Marmoset	Binding	0.06 (IC_{50})	(Schindler and Doods, 2002)
		cAMP	0.08 (K_D)	
	CGRP/ Rat	Binding	3.4 (K_i)	Doods et al., 2000
	AM_1/Human	cAMP	>10 000 (K_B)	(Hay et al., 2003a)
	AM_1/Rat	cAMP	>10 000 (A_2)	(Hay et al., 2002)
	AM_2/Human	cAMP	407 (K_B)	(Hay et al., 2006a)
	CTR/Human	cAMP	>10 000 (K_B)	
	AMY_1/Human	cAMP	36 (K_B)	
	AMY_3/Human	cAMP	≤10 000 (K_B)	
Telcagepant	CGRP/Human	cAMP	2.2 (IC_{50})	(Salvatore et al., 2008)
		Binding	0.8 (K_i)	
		cAMP	0.5 (IC_{50})	(Moore et al., 2010)
	CGRP/Rhesus	Binding	1.2 (K_i)	(Salvatore et al., 2008)
	CGRP/Rat	Binding	1192 (K_i)	
	CGRP/Dog	Binding	1204 (K_i)	
	AM_1/Human	Binding	>100 000 (K_i)	
	AM_2/Human	Binding	29 000 (K_i)	
	CTR/Human	Binding	>100 000 (K_i)	Salvatore (2009)
	AMY_1/Human	Binding	190 (K_i)	
	AMY_3/Human	Binding	>100 000 (K_i)	
MK-3207	CGRP/Human	cAMP	0.12 (IC_{50})	(Salvatore et al., 2010)
		Binding	0.02 (K_i)	
	CGRP/Rhesus	Binding	0.02 (K_i)	
	CGRP/Rat	Binding	10 (K_i)	
	CGRP/Dog	Binding	10 (K_i)	
	AM_1/Human	Binding	16 500 (K_i)	
	AM_2/Human	Binding	156 (K_i)	
	CTR/Human	Binding	1900 (K_i)	
	AMY_1/Human	Binding	0.8 (K_i)	
	AMY_3/Human	Binding	128 (K_i)	

4.1.4 CGRP antagonists' structural characteristics / receptor binding

A retrospective examination of the structural activity relationships (SARs) and structural alignments of Olcegepant and Telcagepant in the context of the CLR/RAMP1 structure, suggested the presence of three distinct regions (parts) in all CGRP antagonists (Archbold et al., 2011). As shown in figure 4.7 below CGRP receptor small molecule antagonists are divided three communication regions with the receptor: a CLR binding region, an interface (linker) region (at the CLR–RAMP1 interface) and a CLR/RAMP1 binding region. The crystal structures of the Olcegepant and Telcagepant bound CGRP receptor reported by ter Haar and coworkers, illustrated these communication regions as well as the specific residues responsible for these interactions. More specifically, it was shown that both compounds interact with the CLR T122 residue by hydrogen bonding with its backbone carbonyl and amide groups (CLR binding region). Furthermore, an interaction between the interface (linker) CLR/RAMP1 region of both compounds and the residue W72 (Try ''shelf'' or bulge region) of the CLR and the backbone of RAMP1 (residues W74 and W84) was also determined. Moreover, the CLR/RAMP1 binding region of the compounds was shown to interact with different residues of the CLR/RAMP1 hydrophobic pocket, depending on the compound's structure. Figure 4.8 below illustrates the important interacting residues of CLR and RAMP1 with the different small molecule antagonists (ter Haar et al., 2010, Archbold et al., 2011, Booe et al., 2015).
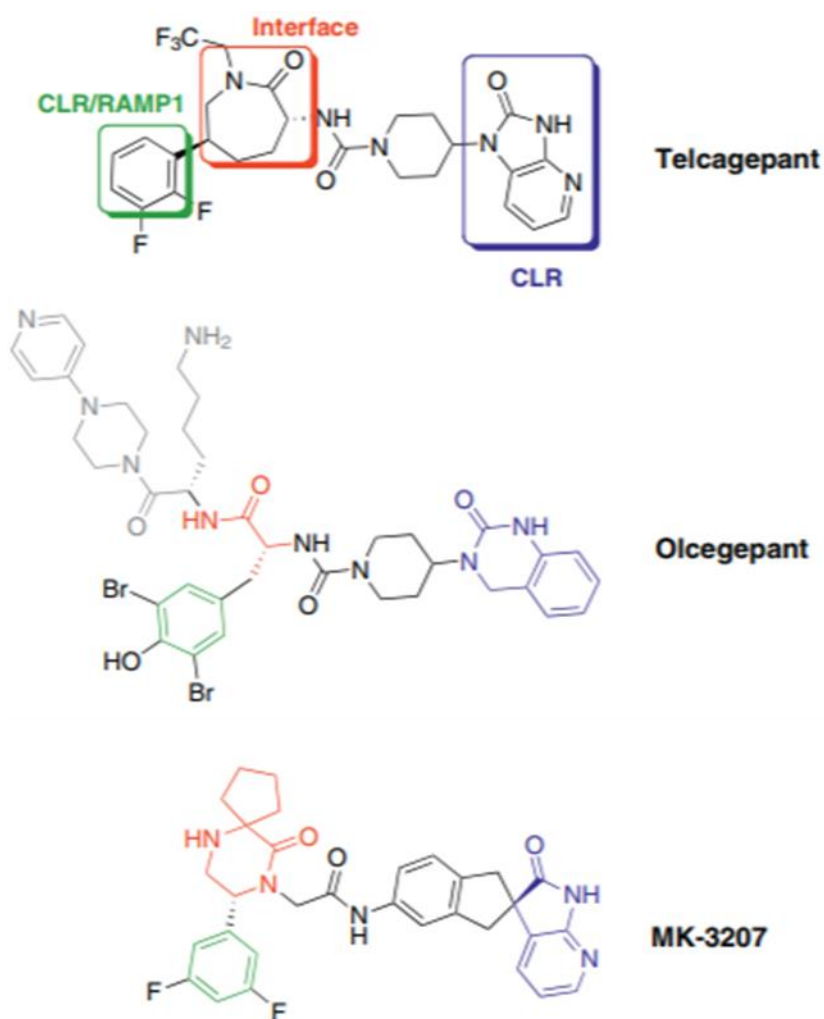
Figure 4.7: Main communication regions of CGRP antagonists with CLR/RAMP1 (CGRP) receptor. Schematic illustration of the structures of CGRP receptor small molecule antagonists, showing the three interactive regions of each compound with the CGRP receptor. The CLR binding region is highlighted in blue. The interface region between CLR and RAMP1 is highlighted in red and the CLR/RAMP1 binding is highlighted in green. Image from Archbold et al., 2011, reused with permission from Elsevier.
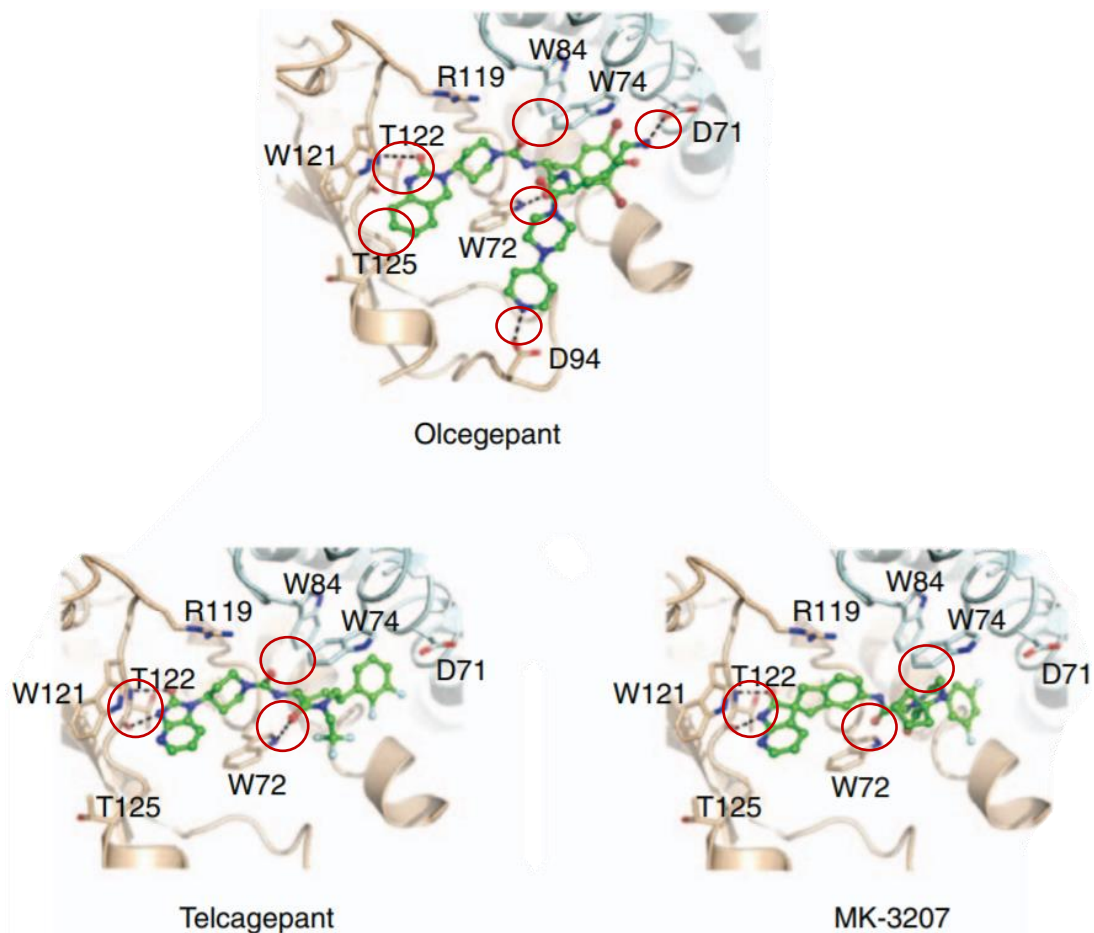
Figure 4.8: Important interactions between three CGRP receptor antagonists and CGRP receptor complex (CLR: light brown and RAMP1: light blue). Schematic illustration of the interaction between **A)** Olcegepant, **B)** Telcagepant and CGRP receptor based on ter Haar et al. and between **C)** MK-3207 based on its alignment with Telcagepant. Image from Archbold et al., 2011, reused with permission from Elsevier.

4.1.5 GPCRs as a target for development of cancer treatments

The standard interventions for cancer treatment and management are primarily surgery (if suitable), chemotherapy (single-agent or combination therapy), and radiation. Most chemotherapeutic agents are targeting dividing cancer cells, however, concomitantly they also affect normal cells with similar growth characteristics including cells of the digesting system, hair follicles and bone marrow causing severe side effects such as anaemia (Rodgers et al., 2012), alopecia (Paus et al., 2013), fatigue, nausea and vomiting (Gill et al., 2006). Similarly, radiotherapy which involves the use of ionizing radiation to eliminate malignant cells is often causing damage to surrounding normal cells and epithelial surfaces leading to undesirable severe side effects (Berkey, 2010). On the other hand, surgery is usually performed as a primary care for cancer management to prevent spreading to other organs and alleviate from discomfort and side effects cause by tissue inflammation. However, the removal of the malignant mass and the surrounding tissue can also cause side effects including bleeding, infection, pain and damage of nearby tissue or organs (The American Cancer Society, 2016). For these reasons and to avert the disadvantages of the traditional cancer treatment interventions, several efforts have been made to develop new therapies that will selectively eliminate cancer cells over the surrounding normal tissues by targeting specific molecular pathways involved in the development and progression of each cancer type.

A significant portion of research (70% of current drug targets) has been focused on the development of agents (monoclonal antibodies or small molecules) against several membrane proteins (such as cell surface receptors) that promote signals and activate downstream pathways which regulate development and progression of cancer (Lundstrom, 2009). One of the most prominent target family (~34% of all approved FDA drugs – 475 drugs (Hauser et al., 2017, Overington et al., 2006)) are GPCRs, a superfamily of seven transmembrane domain receptors that consists of more than 800 members (Pierce et al., 2002, Hauser et al., 2017). This superfamily is subdivided into seven distinct families/classes (A-F, however, D and E are not human) based on sequence similarity (members of each classes normally share ~ 25% homology) and the ligands to which they interact (Eglen and Reisine, 2009, Hauser

et al., 2017, Isberg et al., 2016). Calcitonin and calcitonin-like receptor families both belong to Class B subfamily alongside with parathyroid hormone and corticotropin-releasing hormone receptors (Pierce et al., 2002).

4.1.6 Drug discovery process

The identification and the development of new targeted therapies (in this chapter I will focused on small molecule antagonist) is a lengthy process that involves the efforts and expertise of several different scientific disciplines (chemistry, biology, pharmacology and medicine). This process is divided into four main stages: 1) target identification and validation, 2) Compound screening and library generation (Hit to lead), 3) Lead candidate selection and optimization and 4) Pre-clinical and clinical trials (Hoelder et al., 2012) (see figure 4.9 below).
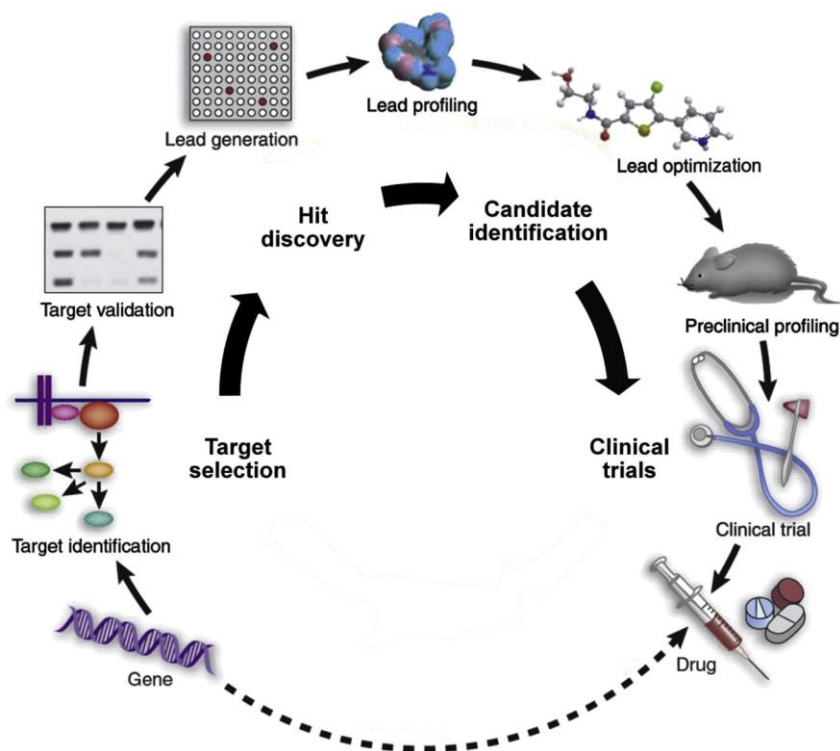
Figure 4.9: Stages of drug development. Illustration of the various stages of drug discovery and development. Image from (Hoelder et al., 2012), reused with permission from Elsevier (creative commons attribution license).

The target identification is the most crucial step in the process. Selecting the wrong or not biologically suitable target could lead to unnecessary waste of resources and research time. As was argued by Mark Bunnage in 2011 the significantly low survival

rates of drugs in phase 2 clinical trials (only 25% of drugs will progress to phase 3 clinical trials) are potentially affected by the selection of biological targets that influence the disease of interest (Bunnage, 2011). Moreover, target validation is as equally important since it is the process that determines if a promising target is suitable for the disease of interest or a specific group of patients (based on gene profiling/mutations) (Benson et al., 2006). Once a target is being identified a compound (chemical compounds and fragments) screening process is initiated for the discovery of hits that will developed into the lead compound series (Hoelder et al., 2012). The lead candidate compound then undergoes a multi-parameter optimization process that will ensure its good metabolic and pharmacokinetic properties (metabolic stability, bioavailability, tolerability, efficacy, potency and selectivity) (Ekins et al., 2010). The last step of the drug development process are the preclinical and clinical studies which is the most time and resource consuming aspect of the process. During this step the compound will undergo several safety preclinical trails followed by several clinical trials which will assess the faith of the compound depending on the hypothesis and the desirable outcomes (Yap and Workman, 2012, Hoelder et al., 2012).

4.1.7 Compound screening approaches

There are several approaches when it comes to the compound screening process including the conventional/HTS (chemical libraries), fragment screening, virtual screening, structure-based screening or a combination approach. The so-called conventional approach involves the HTS of large chemical libraries (few thousand compounds per day) of selected compounds either by using biochemical or cellular based assays to identify the most potent hits which will led to the candidate for preclinical and clinical studies (Macarron et al., 2011). On the other hand, in the fragment-based screening setting the efforts are made to identify weakly potent compounds which are then chemically modified to increase their potency. The libraries used in this approach are normally significantly smaller (few thousand-low molecular weight (<300) compounds), compared to the enormous libraries required in a conventional setting (Hajduk and Greer, 2007). Furthermore, virtual screening differs a lot from any other approach of drug discovery. This process is characterised

by the computational screening of large existing online libraries either to identify similar compounds to already existing antagonists or structures that will fit in the binding pocket of the molecular target of interest (the latter presupposes a solved crystal structure) (Cummings et al., 2003, Schneider, 2010). Lastly, an increasingly popular approach in the drug discovery world is the structure-based or also known as knowledge-based screening. In this setting the outcome of the screening process (i.e. the activities/potencies of each structure) is providing with valuable information that builds a SAR which helps in the further optimization of the compounds. Even though, as we seen above a substantial proportion of the existing drug targets are membrane receptors and a structure-based method will be beneficial for these targets, the limited publicly available high-resolution crystal structures is considered as one of the biggest drawbacks of this approach (Lundstrom, 2009).

There several methods that are used in these screening approaches depending on the target itself. When it comes to GPCRs, historically the most commonly methods used are assays that measure the binding of a ligand to a receptor and the ability of a drug to block that interaction (biochemical approach). However, the increase of our understanding on the different molecules (second messengers) and pathways activated upon receptor stimulation has led to the development of newer cell-based technologies. These technologies primarily measure the accumulation of second messenger levels in response to receptor activation. One of the most commonly measured second messenger is cAMP. cAMP production (activation or inhibition) is regulated by conformational changes of GPCRs on the cell surface that is triggered by several extracellular signals. cAMP regulates several biological processes under both physiological and pathophysiological condition making it valuable tool for the development of a robust screening assay. Some other cellular based assays include the measurement of inositol phosphate accumulation (Popiolek et al., 2016), the release of intracellular Ca^{2+} (Ma et al., 2017) and the translocation of β-arrestin (Luttrell and Lefkowitz, 2002, Zhu et al., 2014) upon GPCR activation.

4.2 Aim and objectives

Aim

The aim of these chapter was to determine the effects of novel small molecule antagonists on receptor activation using cAMP cell-based assay and investigate the changes that structural alterations could have on these activities.

Objectives

Objective 1: Determine the effects of different CLR regions on the activity of novel small molecule antagonists against AM2 receptor and other members of calcitonin receptor family.

Objective 2: Determine the effects of different CLR and RAMP linkers on the activity of novel small molecule antagonists against AM2 receptor and other members of calcitonin receptor family.

Objective 3: Investigate if changes on the RAMP region of the two primary families of antagonists will have a significant improvement on the activity and selectivity against AM2 receptor.

4.3 Material and methods

4.3.1 Structure-based drug design

In our attempt to develop novel small molecule antagonists against AM2 receptor we are using a structure/knowledge-based drug modelling program. The basis our program was the commercially available CGRP antagonists (details in introduction section 4.1.4) and their reported interactions with the receptor. More specifically, the crystal structure of Olcegepant (highly potent CGRPr small molecule antagonist) and CGRP receptor interaction, was previously described by (ter Haar et al., 2010), this information formed the initiation of our modelling. In order to understand better the interactions of the compounds with the different RAMP members and increase the efficiency of our modelling process, in collaboration with a group of medicinal chemists and molecular modellers, we used the recently discovered CGRP (CLR/RAMP1) (ter Haar et al., 2010) and AM1 (CLR/RAMP2) (Booe et al., 2015) receptor models as well as a homology model for AM2 (CLR/RAMP3) receptor that it was created based on these two crystal structures and information from the literature. Using this method, we were able to create virtual interactions between the compounds and the receptors, forming the basis of the design and modelling of new compounds.

4.3.2 Small molecule antagonist preparation

Small molecules were designed by Sandexis Molecular Design and provided by Peakdale Molecular and Wuxi Apptec. Considering their molecular weights and properties, small molecules were dissolved in DMSO to produce 20mM solution and sonicated at 37°C for 10 minutes to fully dissolve. The 20mM stocks were dissolved further in DMSO to produce 2mM solution and sonicated at 37°C for 10 minutes, to limit freeze-thaw cycles of the highest compound stocks. To be used in cAMP assays 2mM stocks were dissolved in stimulation buffer (details in chapter 2) to produce 400μM solution and sonicated at 37°C for 10 minutes. All small molecules stocks were stored at -20°C.

4.3.3 Semi-HTS (agonist/antagonist competition assays)

Using a high-speed liquid handling dispensation device (Freedom EVO 200, Tecan, Männedorf, Switzerland), we were able to develop a robust semi high-throughput LANCE TRFRET cAMP cell-based assay that was used as our primary screening tool. More details about the optimization and the quality control of the assay can be found in chapter 3. Small molecules, provided by Peakdale molecular and Wuxi AppTec, were screened for their potential to inhibit the production of cAMP by peptide agonist stimulated cells. The compounds were primarily screened against AM2r and CGRPr GPCR O/E cell lines. Selected compounds (based on potency and selectivity) were then tested for their activity against AM1r, AMY1r and AMY3r GPCR O/E cells. Similar experimental procedure as in agonist stimulation experiments (chapter 3) was followed with some modifications. Cells (6µl/well) were first pre-incubated with serial dilutions (3µl/well) of the different small molecules for 30 minutes at room temperature prior their stimulation with EC50 value (obtained from agonist dose response stimulations) of peptide agonist (3µl/well) for 15 minutes at room temperature. After stimulations the detection mix (12µl/well) was added and the results were obtained using Enspire multimode Plate reader (Perkin Elmer, Waltham, Massachusetts, United States), at; 320/340nm excitation and 615/665nm emission. Vehicle, Forskolin and peptide only controls were used for data normalization and experimental validation. Figure 4.10 below illustrates in detail the experimental procedure followed.
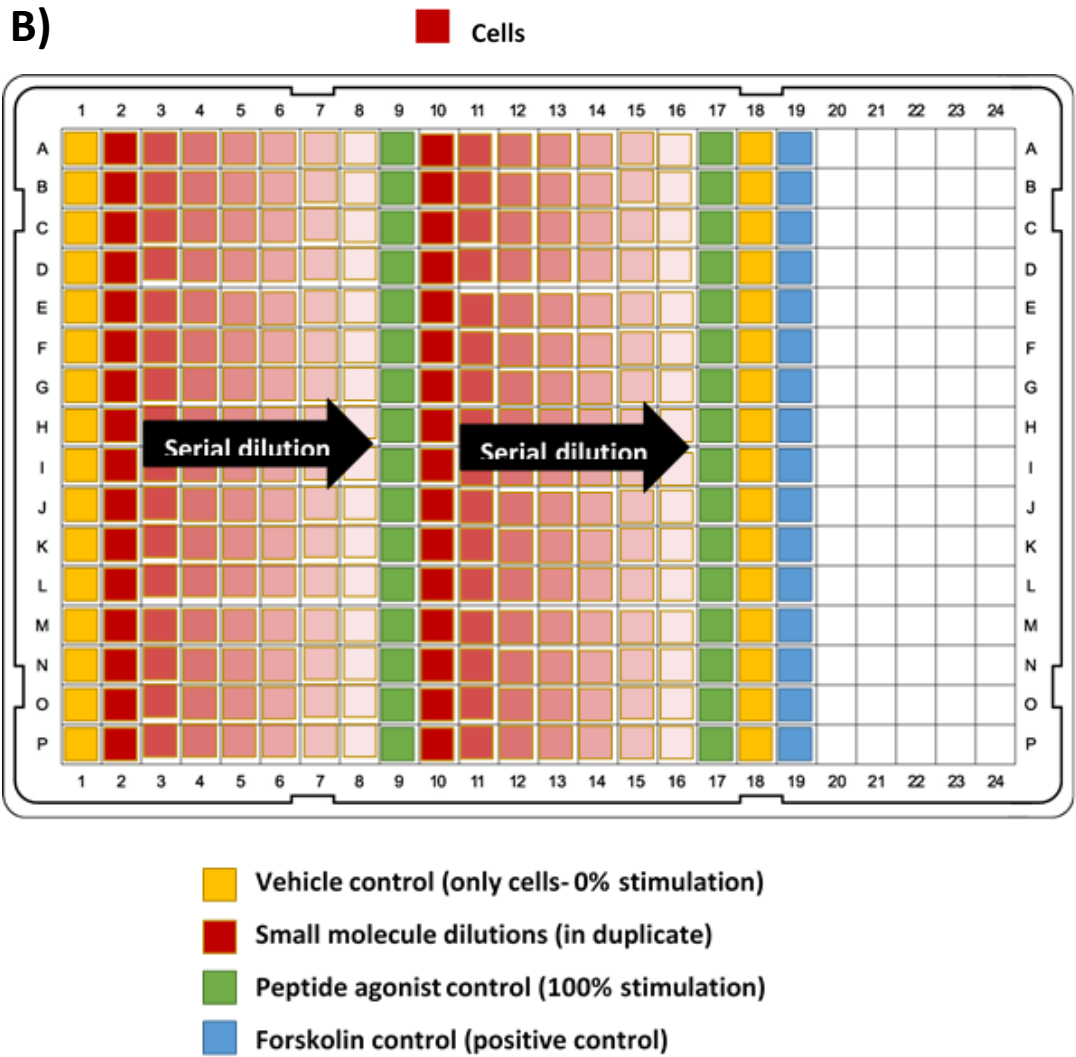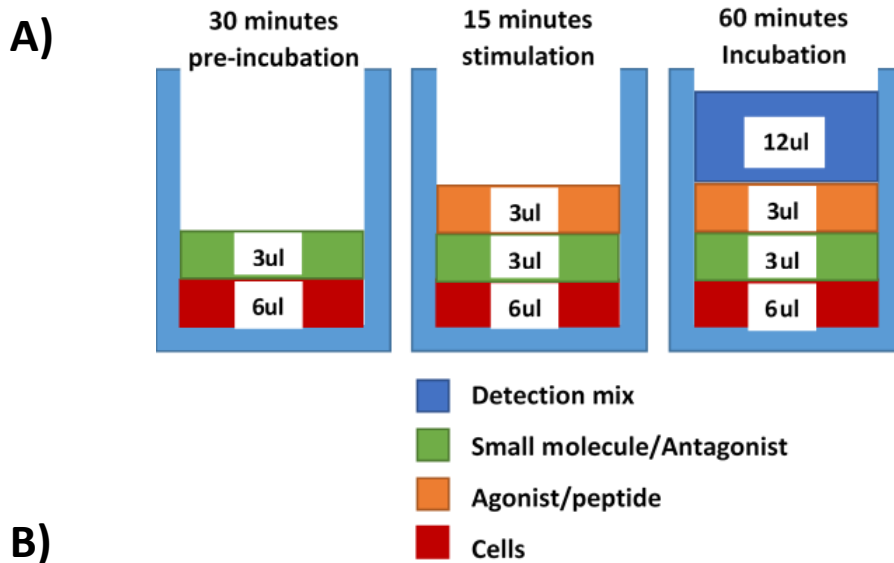
Figure 4.10: A) Illustrates the experimental procedure for measurement of cAMP that is produced after agonist/antagonist competition. **B)** Small molecules (antagonists) dilutions were plated in duplicates followed by peptide agonist, vehicle and Forskolin controls.

4.3.4 Single-point fragment screening

A single-point fragments screening was exploited in order to identify new compound components and expand our design to different families of receptors. The selection of the fragments was based on the CLR and RAMP components of our leading series of compounds. Fragments were purchased from ChemBridge Corporation (San Diego, USA) and Enamine Ltd (New Jersey, USA). Similar experimental procedure as in all cAMP assays described previously was followed with some modifications. Cells (6μl/well) were first pre-incubated with a single dose (in duplicates) of each fragment (3μl/well) for 30 minutes at room temperature prior their stimulation with EC50 value of peptide agonist (3μl/well) for 15 minutes at room temperature. After stimulations the detection mix (12μl/well) was added and the results were obtained using Enspire multimode Plate reader (Perkin Elmer, Waltham, Massachusetts, United States), at; 320/340nm excitation and 615/665nm emission. Vehicle, Forskolin and peptide EC50 dose controls were used for data normalization and experimental validation. Figure 4.11 below illustrates in detail the experimental procedure followed.

4.3.5 Data analysis

Data were analysed and plotted into graphs using Graphpad Prism Version 7.0 (Graphpad software, Inc). Data sets were normalised to the vehicle control as a 100% and the EC50 dose of each receptor as a 0% and presented as mean +/- SEM. A three-parameter logistic equation (for inhibition or stimulation) was used to obtain dose response curves for the data. Each curve consists of 3 experimental repeats (n=3).
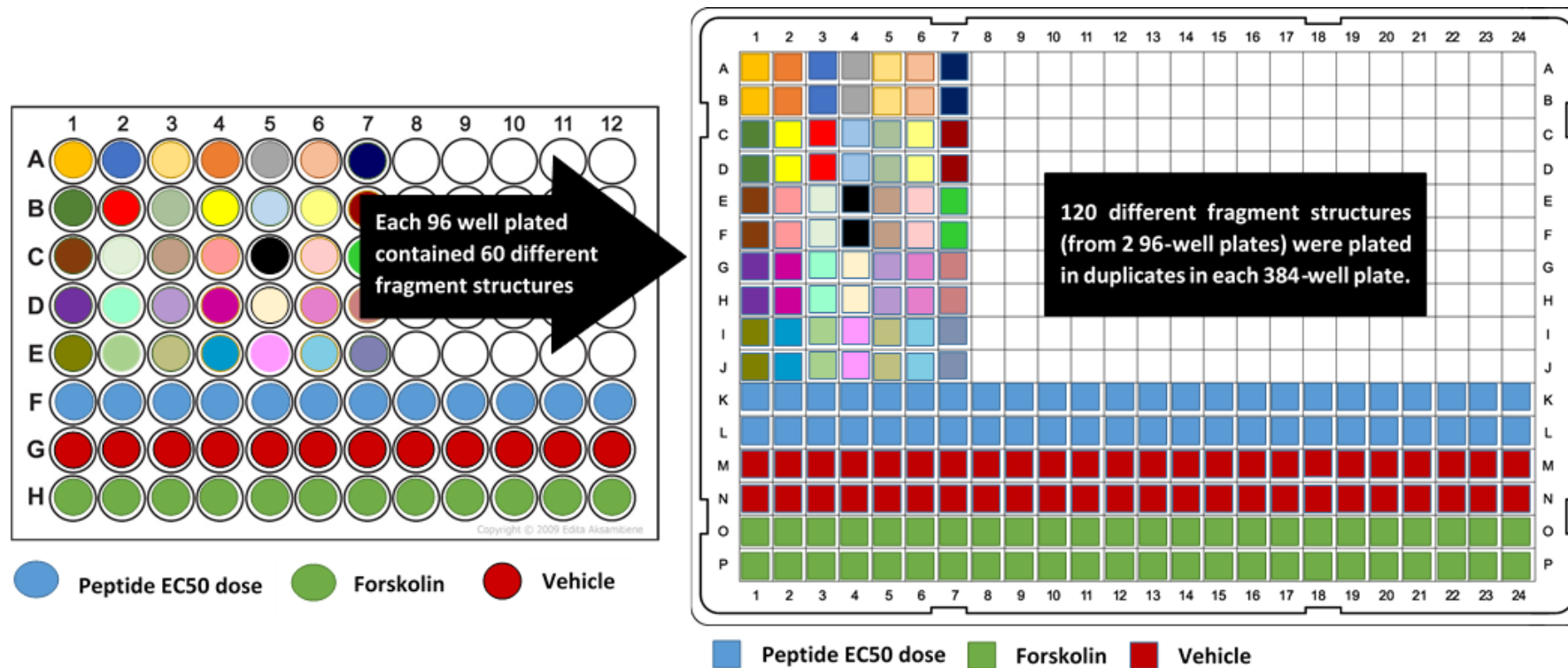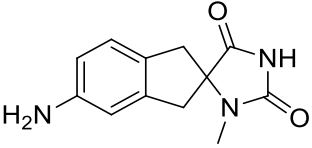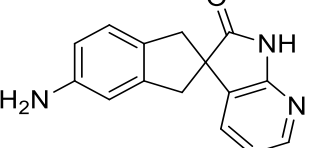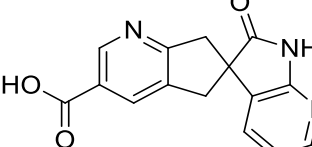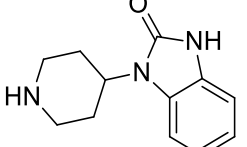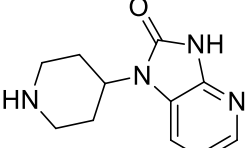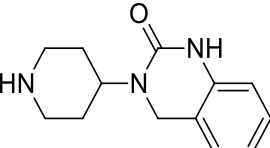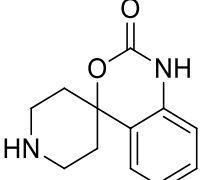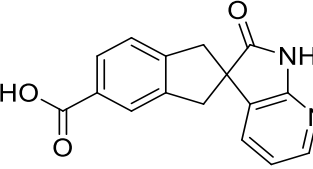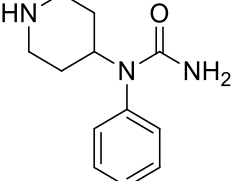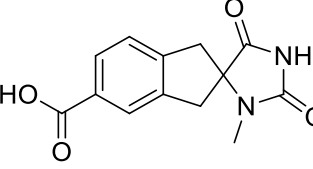
Figure 4.11: Single point fragment screening illustration. Single dose (100μM) of purchased fragments was plated in duplicate followed by peptide agonist (EC50), vehicle (buffer) and Forskolin controls.

4.4 Results

4.4.1 CLR fragment families

As mentioned in the material and methods section above, our compound design process was based on commercially available CGRP antagonists. More specifically, the CLR fragments (CLR binding region) of these compounds or structural variations of them, were used as building blocks for novel AM2 receptor antagonists. A list of the primary families of CLR fragments used can be found in table 4.5 below that shows both the name and the structure of each fragment. Moreover, the ability of each CLR fragment to inhibit the production of cAMP in both AM2r and CGRPr O/E cells can be seen in figure 4.12.

Table 4.5: Names and structures of CLR fragments used in compound synthesis

Name	Structure	Name	Structure
CLR A		CLR B	
CLR C		CLR D	
CLR E		CLR F	
CLR G		CLR H	
CLR I		CLR K	
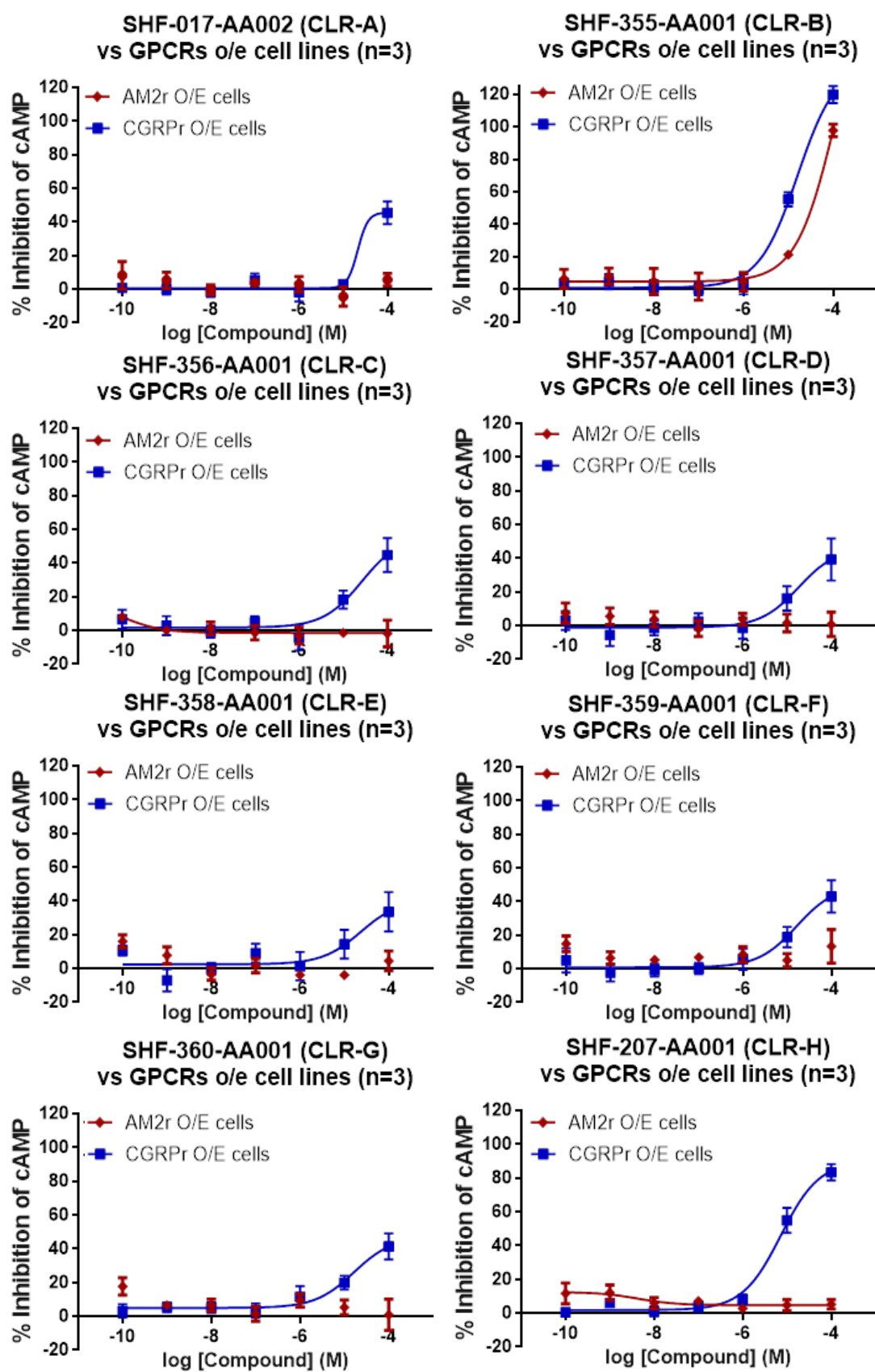
Figure 4.12: Dose-dependent inhibition of cAMP production by CLR fragments.

Inhibition was induced in dose-dependent manner by various CLR fragments, competing with the EC_{50} dose of AM and CGRP peptide ligands.

Whereas most of the CLR fragments have shown low to moderate activity over CGRP receptor, only CLR B (MK3207 CLR binding region fragment) was able to inhibit the production of cAMP in AM2r O/E cells (see table 4.6 below). Table 4.7 below shows the range of activity (potency) of compounds derived from each CLR family. The data suggest that compounds derived mainly from CLR-B and CLR-A fragments had significant effect in the production of cAMP by AM2r O/E cells. The use of the other CLR fragments had as a result the production of compounds with significantly lower or no activity. Moreover, as shown in figure 4.13 below, the activity of CLR B (SHF-355-AA001) was significantly lower over AM1r (32μM) and AMYr (AMY1r (27μM) and 3r (29μM)) receptor O/E cells when compared to AM2r and CGRPr O/E cells.

Table 4.6: Inhibitory effect (IC50 dose) of CLR fragments on the activation of cAMP by CGRPr and AM2r O/E cells.

Fragment name	Activity (IC50)	
	CGRPr	**AM2r**
CLR A	Low micromolar (ambiguous)	Inactive
CLR B	Low micromolar	Low micromolar
CLR C	Low micromolar (ambiguous)	Inactive
CLR D	Low micromolar (ambiguous)	Inactive
CLR E	Low micromolar (ambiguous)	Inactive
CLR F	Low micromolar (ambiguous)	Inactive
CLR G	Low micromolar (ambiguous)	Inactive
CLR H	Low micromolar	Inactive
CLR I	Low micromolar (ambiguous)	Inactive
CLR K	Inactive	Inactive
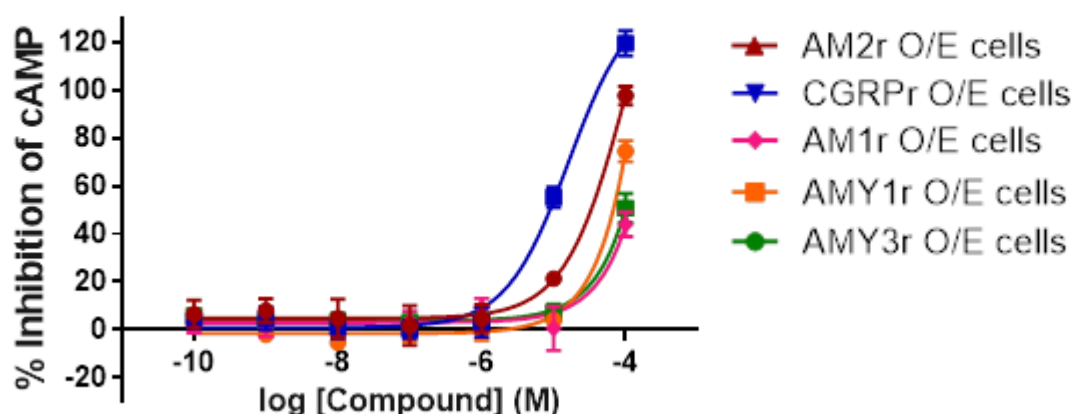
Figure 4.13: Dose-dependent inhibition of cAMP production by CLR-B. Inhibition of cAMP production induced by stimulation of AMY3r, AMY1r, CGRPr, AM1r and AM2r O/E cells by EC50 doses of AM, CGRP and AMY peptide ligands, by CLR-B (SHF-355-AA001).

Table 4.7: Number of compounds per CLR fragment family and their potency range for inhibition of cAMP production by AM2r and CGRPr O/E cells.

CLR Region	Number of compounds	Range of activity (IC50) – potency	
		CGRPr	AM2r
CLR A	75	Inactive - 55nM	Inactive - 45nM
CLR B	671	100µM-0.3nM	100µM-0.5nM
CLR C	1	Inactive	Inactive
CLR D	3	Inactive - 10µM	Inactive - 10µM
CLR E	10	10µM-0.2nM	Inactive - 2µM
CLR F	8	10µM-0.1nM	Inactive - 0.3µM
CLR G	6	Inactive	Inactive
CLR H	11	0.4µM-0.5nM	Inactive - 1µM
CLR I	1	Inactive	Inactive
CLR K	5	Inactive - 1µM	Inactive - 9µM

In an effort to identify new CLR fragment components and expand our design to different families of receptors a single point fragment screening process was exploited. Based on a computational (in-silico) screening, fragment compounds were purchased and screened at a single dose of 100µM for their ability of inhibit cAMP production by AM2r and CGRPr O/E cells. The outcome of this fragment screening can be found in figure 4.14(i) below. CLR-B and SHF-408-AA001 (CLR derived compound) were used as positive controls and DMSO as a negative control. As shown in the figure in both CGRP and AM2 O/E cells, CLR-B and SHF-408-AA001 have the highest percentage of inhibition. However, the data also suggested that several fragments were able to inhibit the production of cAMP at 100µM.

Fragments exceeded 20% of inhibition (DMSO levels of inhibition/background) were then selected and full dose response curves were used to determine the extent of their inhibitory activity. Some of these selected fragments are highlighted with different coloured dots in figure 4.14(i). The full dose response curves of these selected fragments can be found in figure 4.14(ii). Most fragments failed to produce a significant effect below 100µM with some exceptions showing low to moderate activity over the CGRP O/E cells. However, using this approach we were able to identify a structurally different fragment (SHF-856-AA002) with comparable activity to that of CLR B, in both CGRPr (11.4µM) and AM2r (8.7µM) O/E cells, providing us with the ability to broaden our design.
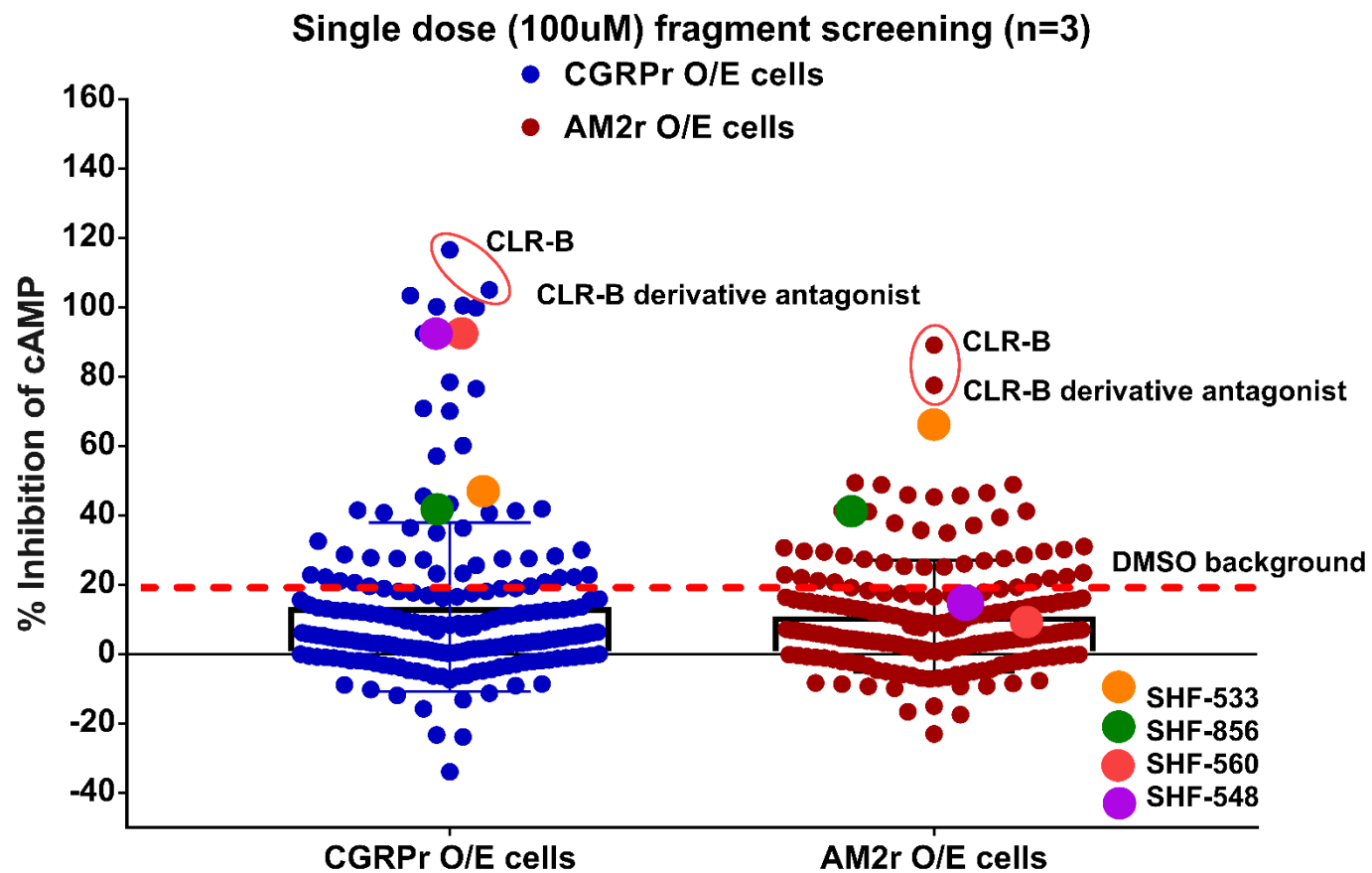
Figure 4.14(i): Single dose (100μM) screening. Percentage inhibition of cAMP production induced by stimulation of CGRPr and AM2r O/E cells by EC50 doses of AM, CGRP peptide ligands, by several fragment compounds as well as SHF-355 (CLR-B) and SHF-408 (CLR-B derived antagonist). Each dot represents a distinct fragment/compound.
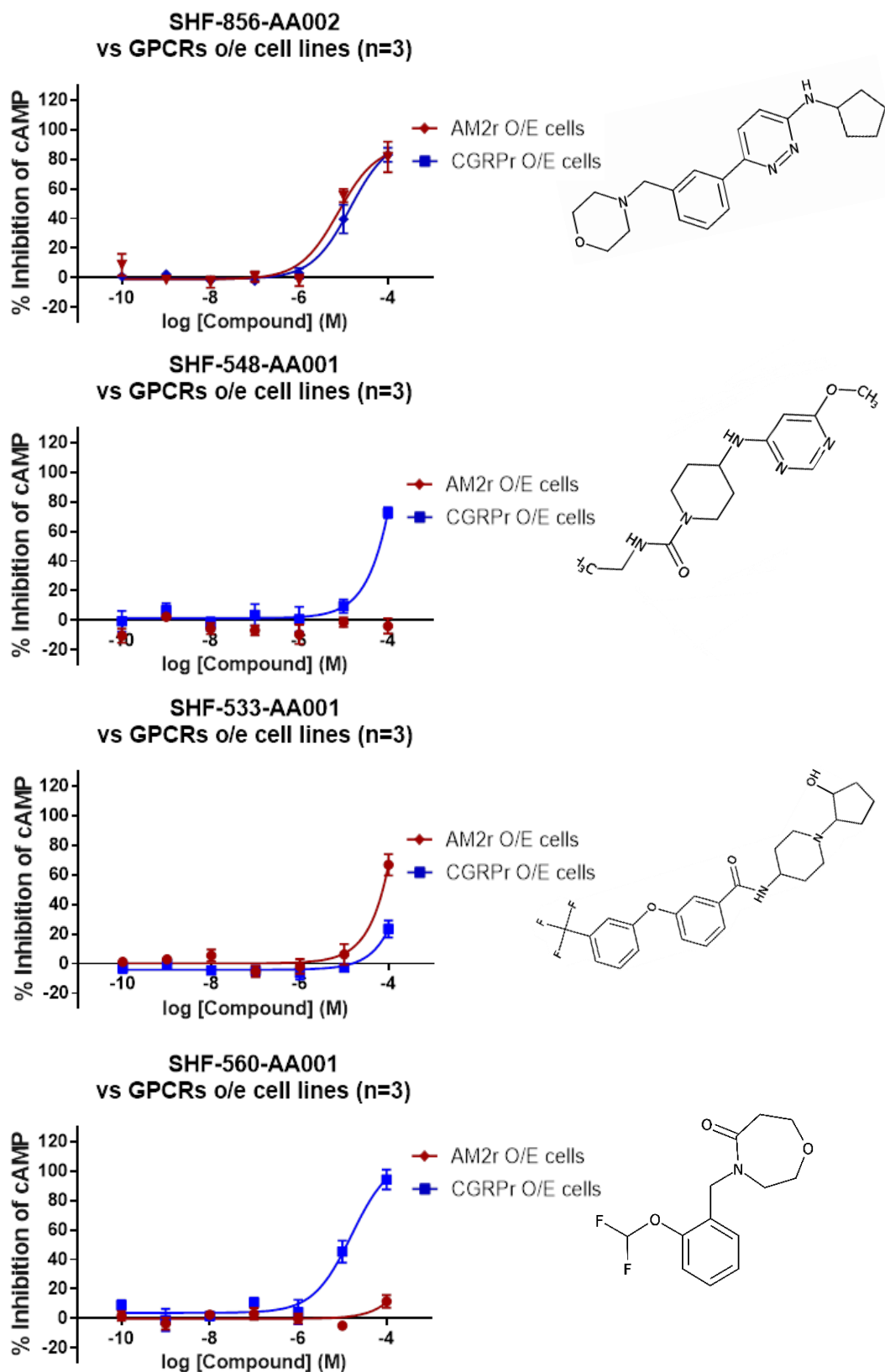
Figure 4.14(ii): Single dose (100µM) screening. Representative graphs of dose response inhibition curves of selected fragments (highlighted with different coloured circles in graph 4.12(i)).

4.4.2 CLR and RAMP region linker variations

After the identification of CLR-B as the primary CLR family for development of AM2 receptor antagonists, work was focused on the replacement of the linker between the CLR and RAMP regions of the compounds. Figures 4.15 and 4.16 below show the effects of linker variation on the activity and selectivity of SHF-082-AA001 and SHF-638-AA004; compounds that belong to the primary structure series of antagonists (see section 4.3.3 below).

As shown in figure 4.15 below replacement of amide linker of SHF-082 had as a result a significant decrease in activity (potency) in both AM2r and CGRPr O/E cells. More specifically, the use of alkyne linker (SHF-469), alkene linker (SHF-620) and amine (SHF-478) linker have shown no improvement in the activity of SHF-082 against AM2 receptor and had as a result the significant decrease of its activity against CGRP receptor. Furthermore, replacement of amide linker of SHF-638 by alkene (SHF-929) or alkane (SHF-932) linker significantly decrease the potency on both receptors. It is worth mentioning that the selectivity of SHF-638 over the AM2 receptor was also significantly decrease when the alkene linker was used (Figure 4.16). Table 4.8 below summarizes the activity of each compound against AM2r and CGRPr O/E cells.

Table 4.8: Effects of linker replacement on the activity of SHF-082-AA001 and SHF-638-AA004.

Compound name	Linker	Activity			
		CGRPr		AM2r	
		IC50	pIC50 +/- SEM	IC50	pIC50 +/- SEM
SHF-082-AA001	**Amide**	**4.9nM**	**8.31 +/- 0.09**	**280nM**	**6.55 +/- 0.09**
SHF-469-AA001	Alkyne	0.5µM	6.31 +/- 0.09	Ambiguous	-
SHF-620-AA001	Alkene	1.3µM	5.35 +/- 0.15	Ambiguous	-
SHF-478-AA001	Amine	1.1µM	5.95 +/- 0.10	1.4µM	5.86 +/- 0.23
SHF-638-AA004	**Amide**	**4.1nM**	**8.39 +/- 0.07**	**0.7nM**	**9.16 +/- 0.09**
SHF-929-AA001	Alkene	106nM	6.97 +/- 0.11	206nM	6.69 +/- 0.10
SHF-932-A001	Alkane	91nM	7.04 +/- 0.14	31nM	7.51 +/- 0.18
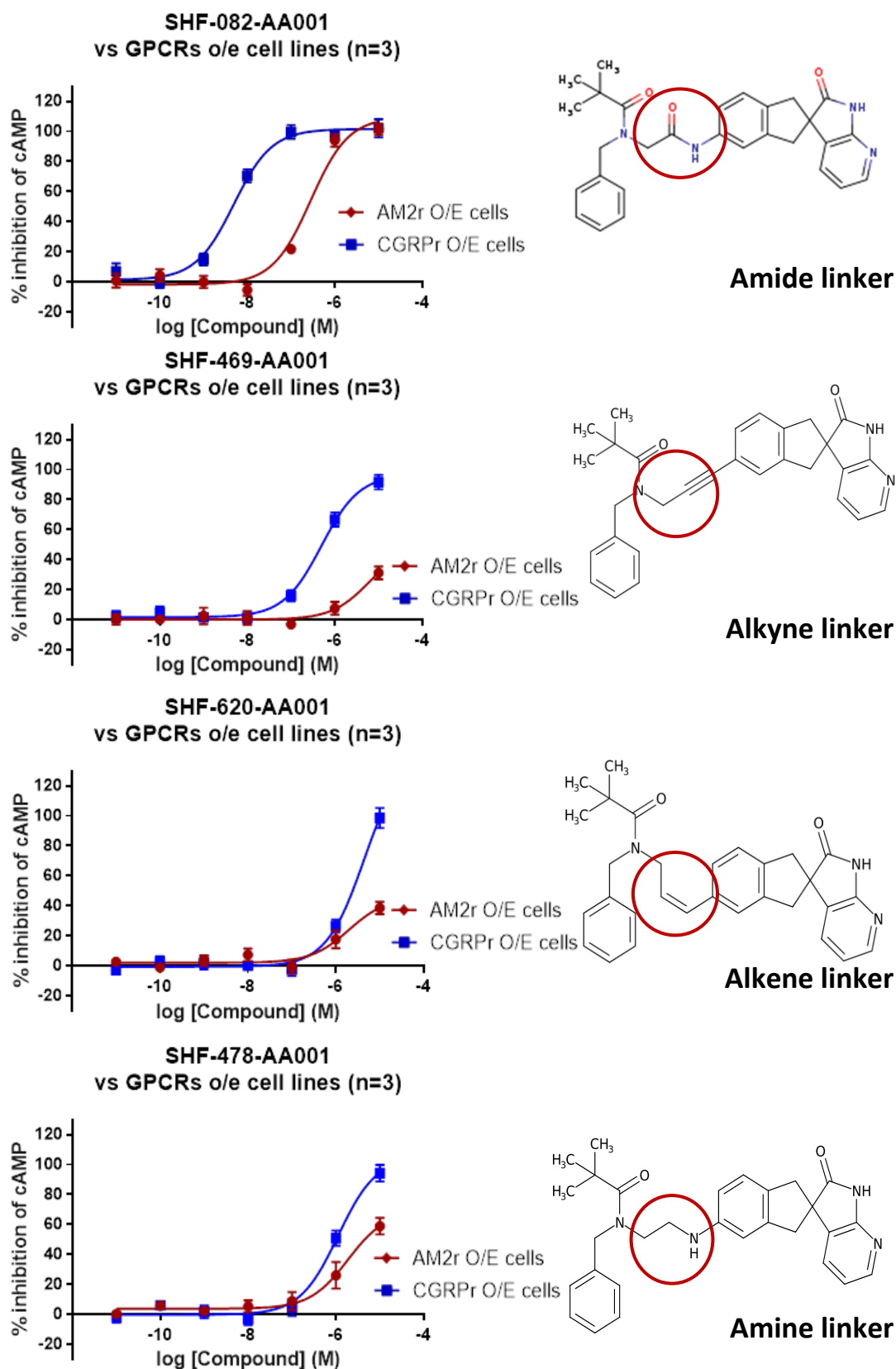
Figure 4.15: Effects of linker variation on activity of SHF-082-AA001. Shows the activity of SHF-082 and of the compounds synthesised by replacement of its amide linker.
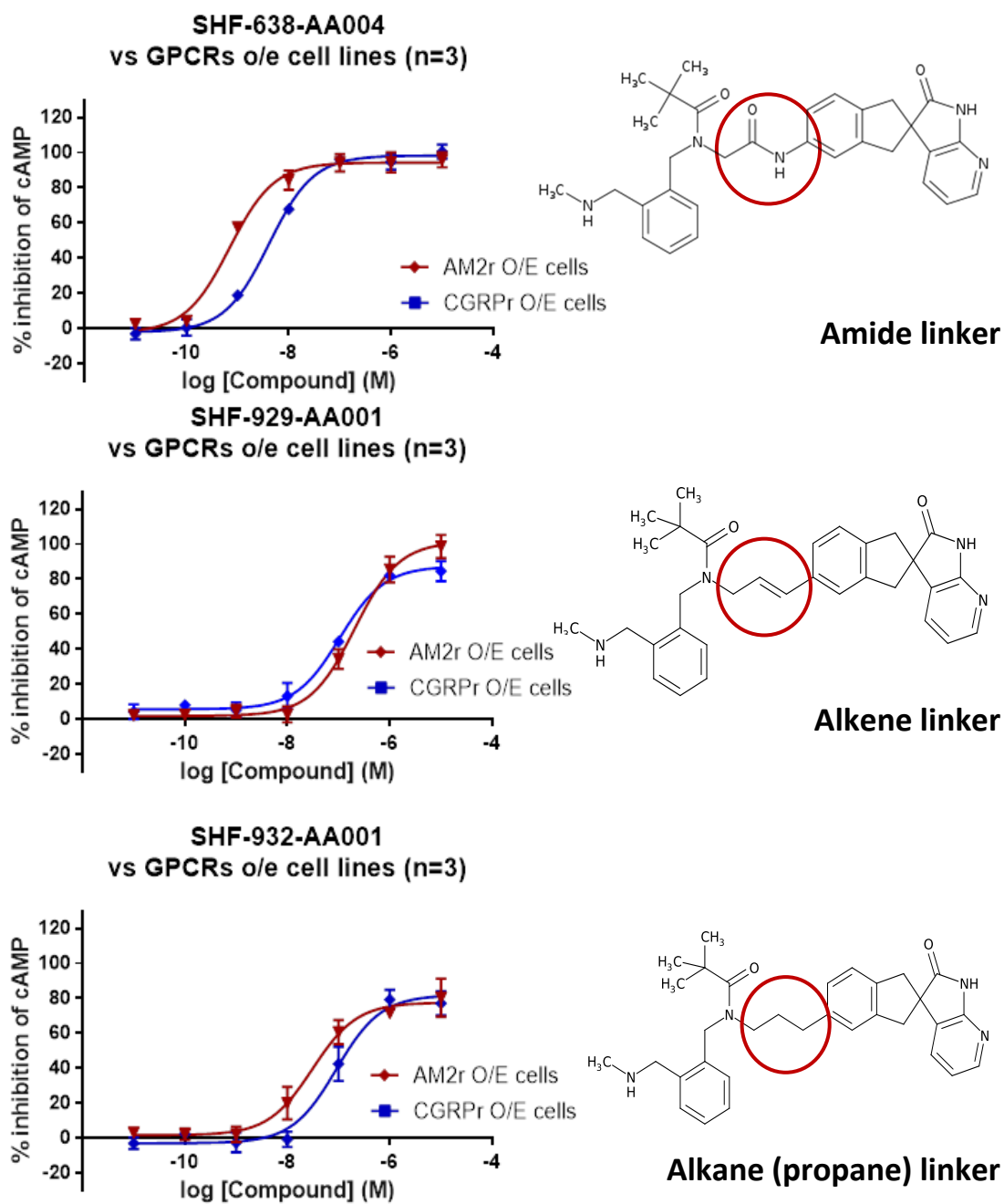
Figure 4.16: Effects of linker variation on activity and selectivity of SHF-638-AA004. Shows the activity and the selectivity of SHF-638 and of the compounds synthesised by replacement of its amide linker.

4.4.3 SHF-000408/SHF-000638 family (Primary structure series)

Small molecules designed by Sandexis Molecular Design were categorized into structurally different families, with the two main structure series been SHF-408/SHF-638 (primary) and SHF-491 (secondary). SHF-082-AA001 was the initial member of the family and the first compound to demonstrate robust pharmacology against AM2 receptor. Figure 4.17 illustrates the structural development of SHF-082 as well as the activity and selectivity of each compound. Data are presented as % inhibition on the Y-axis and compound concentration on X-axis. All data sets consist of three experimental repeats and are presented as Mean +/- SEM. Moreover, table 4.9 shows the inhibitory effect (IC_{50}) of each compound against different members of CTR and CLR families of receptors, obtained using a semi-high throughput cell-based cAMP assay as well as the best fit values and statistical significance obtained by comparison of fits analysis between the receptors.

SHF-082 showed high selective (p value: <0.0001) versus CGRPr O/E cells (4.9nM), however, reasonable potency (280nM) was observed against AM2r O/E cells as well. Initial efforts for the development of a more potent AM2 receptor antagonist were made by expansion of the RAMP region of the compound. More specifically, addition of methylamine (CH_3NH_2) on the benzyl group of the SHF-082, resulted in the development of SHF-408, the first equally potent (p value: 0.72) small molecule with IC50 of 7.7nM (CGRPr) and 4.9nM (AM2r). Furthermore, an addition of an extra methyl group (CH_3) on methylamine had as a result the development of a highly potent small molecule antagonist (SHF-638-AA004) against AM2r O/E cells (0.7nM) that showed moderate selectivity (p value: <0.0001) over the CGRP receptor (4.1nM).

Table 4.9: Activity of selected compounds that belong to primary structure series

Receptor	Best fit values				
	IC_{50}	pIC_{50} +/- SEM	Top	Bottom	P value
SHF-0082-AA001					
AM2r	280nM	6.55 +/- 0.09	109.6	-1.70	-
CGRPr	4.9nM	8.31 +/- 0.09	101.6	1.36	<0.0001
AM1r	Ambiguous	-	-	-	-
AMY1r	~16µM	4.78 +/- 0.92	115.8	8.70	<0.0001
AMY3r	700nM	6.16 +/- 0.10	76.2	-1.91	<0.0001
SHF-0408-AA001					
AM2r	4.9nM	8.31 +/- 0.16	96.8	1.09	-
CGRPr	7.7nM	8.12 +/- 0.12	96.8	7.76	0.72
AM1r	Ambiguous	-	-	-	-
AMY1r	~2.9µM	5.54 +/- 0.19	84.9	9.19	<0.0001
AMY3r	~1.1µM	5.99 +/- 0.11	102.1	3.40	<0.0001
SHF-0638-AA004					
AM2r	0.7nM	9.16 +/- 0.09	94.4	-2.51	-
CGRPr	4.1nM	8.39 +/- 0.07	98.4	-2.12	<0.0001
AM1r	Ambiguous	-	-	-	-
AMY1r	1.2µM	5.90 +/- 0.08	84.7	4.12	<0.0001
AMY3r	0.2µM	6.65 +/- 0.06	85.2	-3.19	<0.0001
SHF-1028-CN001					
AM2r	0.8nM	9.10 +/- 0.12	90.0	-3.19	-
CGRPr	5.3nM	8.27 +/- 0.10	92.9	1.96	<0.0001
AM1r	3.6µM	5.44 +/- 0.15	97.0	3.86	<0.0001
AMY1r	2.9µM	5.30 +/- 0.28	72.8	3.80	<0.0001
AMY3r	5.1µM	5.53 +/- 0.12	60.7	1.99	<0.0001
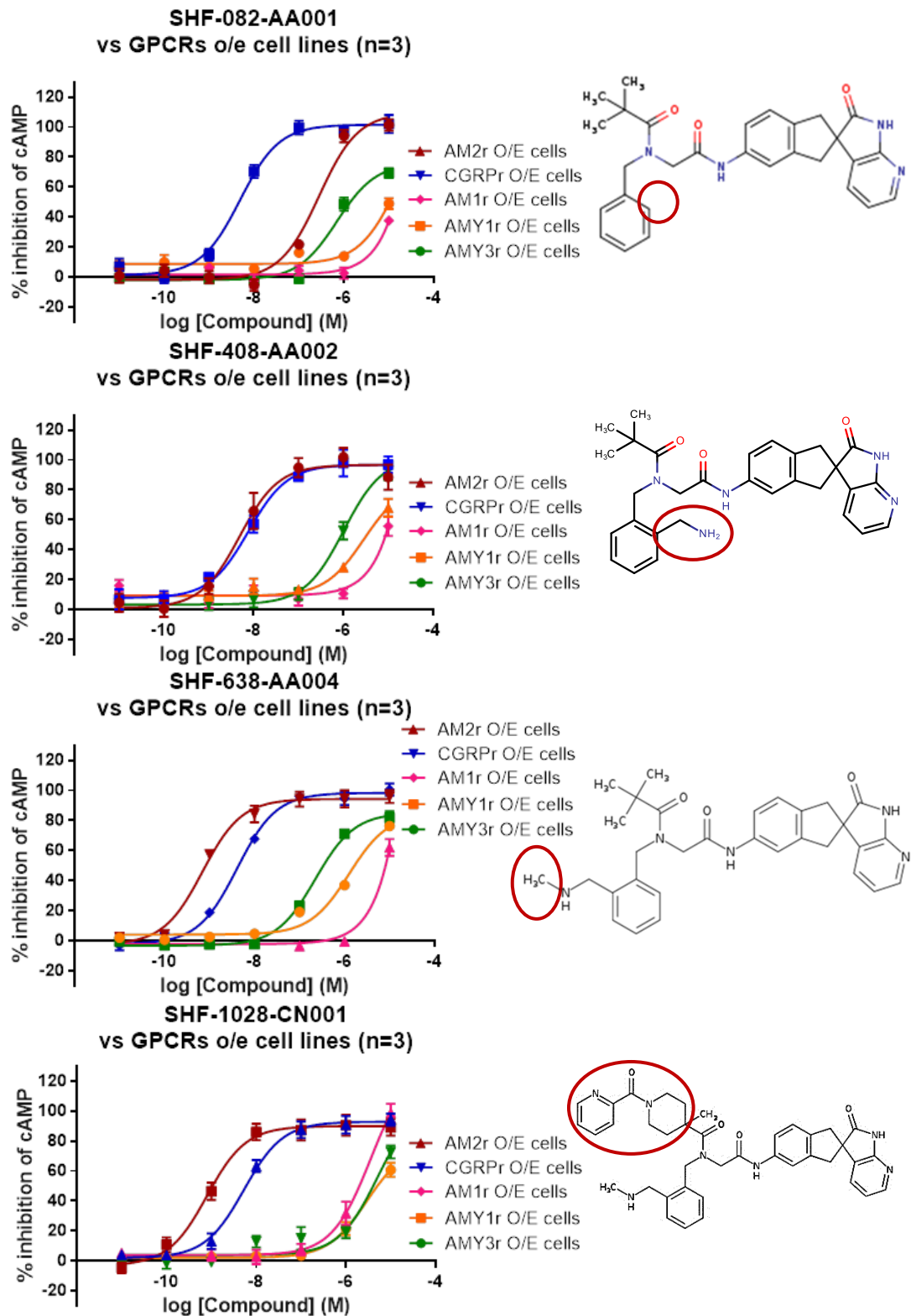
Figure 4.17: Activity and selectivity of primary structure series. Illustrates the structural development of SHF-082-AA001 as well as the activity and selectivity of each compound.

Further expansion on the butyl group (2-Methyl-2-propanol) of the SHF-638 structure resulted in the development of SHF-1028-CN001 which illustrated a significant increase in both potency and selectivity, with IC_{50} of 0.8nM and 5.3nM for AM2r and CGRPr respectively. It is worth mentioning that low potency was displayed when all compounds were screened against the other cell lines including AM1r, AMY1r and AMY3r O/E cells.

4.4.4 SHF-000491 family (Secondary structure series)

Compounds belonging to the secondary structure family had overall significantly lower potency than those in the primary family. Figure 4.18 illustrates the structural development the secondary structure family as well as the activity and selectivity of each compound. Data are presented as % inhibition on the Y-axis and compound concentration on X-axis. All data sets consist of three experimental repeats and are presented as Mean +/- SEM. Moreover, table 4.10 shows the inhibitory effect (IC50) of each compound against different members of CTR and CLR families of receptors, obtained using a semi-high throughput cell-based cAMP assay as well as the best fit values and statistical significance obtained by comparison of fits analysis between the receptors.

Table 4.10: Activity of selected compounds that belong to secondary structure series

Receptor	Best fit values				
	IC$_{50}$	pIC$_{50}$ +/- SEM	Top	Bottom	P value
SHF-0486-AA001					
AM2r	598nM	6.22 +/- 0.18	106.0	-1.43	-
CGRPr	181nM	6.74 +/- 0.10	101.4	-1.05	0.001
AM1r	Ambiguous	-	-	-	-
AMY1r	1.7µM	5.77 +/- 0.09	112.6	5.38	<0.0001
AMY3r	2.7µM	5.57 +/- 0.13	104.9	-7.81	0.07
SHF-0491-AA001					
AM2r	132nM	6.88 +/- 0.09	108.6	1.97	-
CGRPr	76nM	7.12 +/- 0.09	91.7	-2.77	0.03
AM1r	Ambiguous	-	-	-	-
AMY1r	4.2µM	5.37 +/- 0.19	98.7	3.17	<0.0001
AMY3r	0.64µM	6.19 +/- 0.08	97.7	-3.53	<0.0001
SHF-0658-AA001					
AM2r	54nM	7.27 +/- 0.06	95.0	2.17	-
CGRPr	370nM	6.43 +/- 0.08	96.0	3.00	<0.0001
AM1r	Inactive	-	-	-	-
AMY1r	2.3µM	5.64 +/- 0.09	114.2	0.59	<0.0001
AMY3r	260nM	6.58 +/- 0.09	101.8	4.65	<0.0001
SHF-0736-AA001					
AM2r	81.6nM	7.09 +/- 0.09	93.0	1.59	-
CGRPr	106nM	6.97 +/- 0.08	97.4	0.13	0.63
AM1r	Inactive	-	-	-	-
AMY1r	1.0µM	5.99 +/- 0.11	71.0	-0.15	<0.0001
AMY3r	0.4µM	6.45 +/- 0.10	98.7	0.14	<0.0001
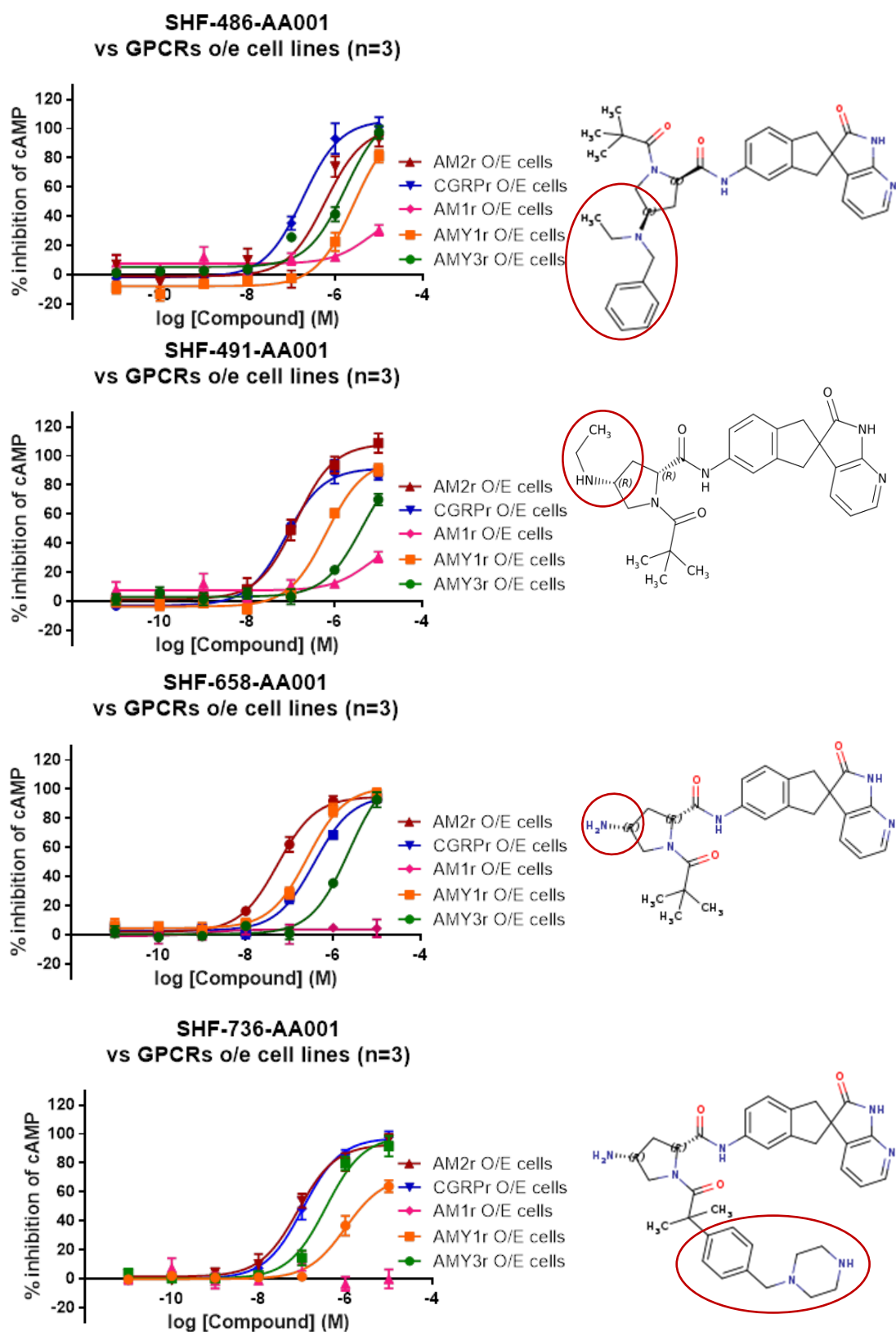
Figure 4.18: Activity and selectivity of secondary structure series. Illustrates the structural development of the secondary structure series as well as the activity and selectivity of each compound.

In contrast with the primary family of antagonists, where the expansion of the RAMP region resulted in a significant increase of potency and selectivity for AM2 receptor, improvements were observed when small groups were used. More specifically, removal of the benzyl group from the structure of SHF-486-AA001 had as a result the significant increase of SHF-491-AA001 potency against AM2 receptor from 598nM to 132nM. In addition, removal of the methyl group (CH_3), resulted in further increase of the potency over the AM2 receptor and a decrease in CGRP receptor potency, making SHF-658-AA001 selective over the AM2 receptor. It is worth mentioning that expansion on the butyl group (2-Methyl-2-propanol) of the SHF-658 structure, similar to that of SHF-1028 from the primary structure family (figure 4.17), did not have a significant effect on the potency of SHF-736-AA001 over AM2r O/E cells. Overall lower potency was displayed when all compounds were screened against the other cell lines including AM1r, AMY1r and AMY3r O/E cells.

4.5 Conclusion/Discussion

Due to the lack of effective therapies and the severe adverse effects that characterise the use of standard interventions for cancer treatment including chemotherapy, radiation and surgical resection, research has been focused on the development of targeted therapies (monoclonal antibodies or small molecule antagonists) against molecules and pathways that are directly or indirectly involved in the development and progression of cancer (Lundstrom, 2009). Drug discovery is a lengthy and costly process that involves the screening of large chemical libraries and the identification and optimization of the lead candidates before their use into pre-clinical and clinical trials (Macarron et al., 2011, Hoelder et al., 2012). A considerable proportion of this research is directed in the development of compounds that will block or inhibit the effects of several members of G-protein-coupled receptor superfamily (Hauser et al., 2017).

CGRP, a member of this family of receptors, has been the target of several drug discovery programs for the development of new therapies for the treatment of migraine. This led to the successful identification of several candidates including Olcegepant (Doods et al., 2000), Telcagepant (Salvatore et al., 2008) and MK-3207 Salvatore et al., 2010), some of which are currently into clinical trials. The structural

similarities between CGRP and AM2 receptors allowed us to successfully engineer the reported drug-like CGRP small molecule antagonists in potent levels of AM2 antagonism.

Using a structure/knowledge-based drug modelling program we were able to identify two major structure families with significant effects on the activity of AM2 receptor. Compounds were screened against various members of CLR and CTR family of receptors for their ability to inhibit cAMP production upon receptor activation by peptide ligands. More than 1100 compounds were screened using a semi-high throughput cell-based assay, optimization of which was described in Chapter 3. As described in the methods section 4.3.5, the antagonist responses were normalized to the EC50 value of the respective receptor that was present as a control on each plate. This allowed for a quick comparison of efficacy between the different O/E cell lines during the screening of active compounds. Similar approaches were previously used in several studies for the determination of agonists (Weston et al., 2016) or antagonists (Robinson et al., 2009) efficacy. Further analysis of the data could be done, using the raw values prior the normalization, to investigate for any partial agonism that might arise from the screening.

The design process was based on the structural similarities and differences between AM1, CGRP and AM2 receptors. Using the recently published crystal structures of the ECD of AM1 and CGRP receptors we were able to develop a homology model for AM2 receptor that was used to predict interactions and to establish structural SARs. Based on these models we were able to visualise and compared the binding pockets of CGRP and AM2 receptors (Figure 4.19). As mentioned previously, CGRP antagonists were found to interact with the receptor at three different regions: the CLR region, the interface (linker) region (at the CLR–RAMP1 interface) and the CLR/RAMP1 region (ter Haar et al., 2010, Archbold et al., 2011, Booe et al., 2015). Similarly, our novel compounds were design based on these assumptions and are consist of three distinct regions (CLR region, CLR - RAMP linker and RAMP region). Figure 4.19 below illustrates the binding pockets of the two receptors of interest and the different interaction regions between the receptor and the compounds. By comparing the two structures we were able to identify differences and similarities that aided our drug design. As shown in figure 4.19 the binding pocket of AM2

receptor is significantly smaller than that of CGRP receptor which is mainly due to structural differences between the RAMPs.
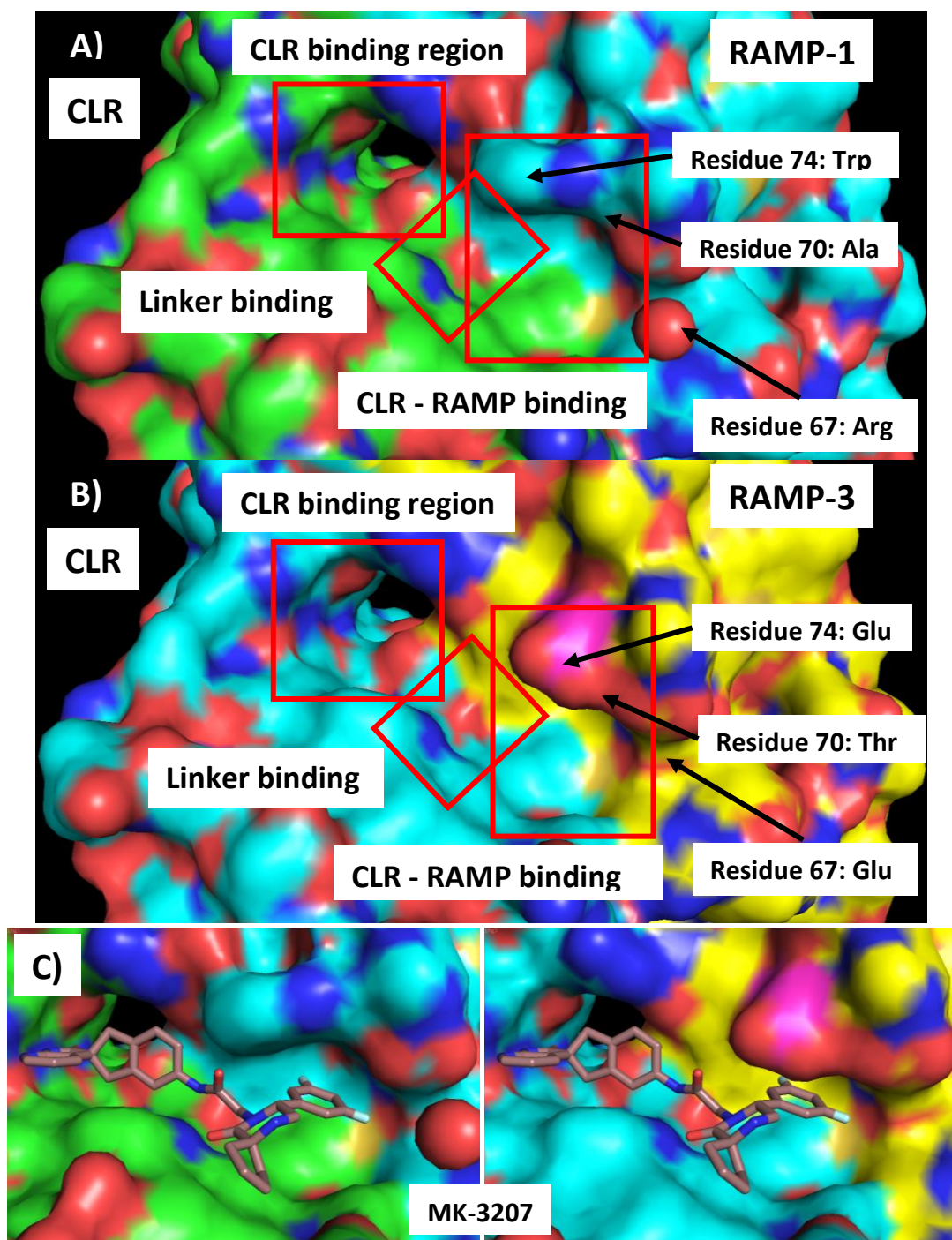
Figure 4.19: CGRP and AM2 receptor binding pocket. Illustrate the compound binding pockets of **A)** CGRP (CLR + RAMP-1) (based on recently published crystal structures of CGRP extracellular domain) and **B)** AM2 (CLR + RAMP-3) (based on a homology model design by our team) receptors. Binding pockets are divided into three regions: the CLR binding region, the linker binding region and the CLR-RAMP binding region. **C)** Molecular docking of MK-3207.

More specifically, the presence of glutamine (Glu) (tryptophan (Trp) on RAMP-1) at residue 74 and threonine (Thr) (alanine (Ala) on RAMP-1) at residue 70 of RAMP-3 significantly reduces the pocket size (Figure 4.19(B)), restricting interactions with the RAMP binding region and making the development of selective antagonists for AM2 receptor more challenging. This can be seen in figure 4.19(C) where molecular docking of MK-3207 in binding pockets of CGRP and AM2 receptor suggests a restricted binding of the MK-3207 with RAMP-3. Even though the threonine residue 70 of RAMP-3 reduces the pocket size it provides AM2 receptor (the CLR-RAMP region) with hydrogen bonding character compared with the alanine residue of RAMP-1. Moreover, Residue 67: Arginine (Arg) on RAMP-1 as shown on the figure 4.19(A) is directed outside of the pocket in contrast with the 67: glutamine (Glu) on RAMP-3 (figure 4.19(B)) which is directed on the inside of the pocket, providing with a scope of differentiation from CGRP receptor.

As mentioned previously, the starting point of our compound development were commercially available highly potent and selective drugs-like CGRP small molecule antagonists (see appendix figure 8.1) such as MK-3207. CLR fragments (CLR binding region) of the existing CGRP receptor antagonists and structural variations of them, were used as building blocks for novel AM2 receptor antagonists. During this process only one fragment (CLR-B), the CLR region of MK-3207, out of the twelve fragments initially tested was able to produce consistently highly potent AM2 and CGRP receptor antagonists, with selectivity over AM1 as well as AMY receptors (Figure 4.13). As expected most of the other CLR fragments used shown significantly higher selectivity over the CGRP receptor (Table 4.6). A single point screening was used to further expand our structural diversity and to identify novel CLR and RAMP region building blocks. This effort led to the identification of a structurally different fragment (SHF-856-AA002) with comparable activity to that of CLR-B, providing us with the tools to further expand our structural design (Figure 4.14). What is more, the presence of the amide linker between the CLR and the RAMP regions of the compounds was proven to be an essential determinant of the potency. Linker variation studies revealed that replacement of the amide linker has a significant effect on both activity and selectivity of the compounds (Figures 4.15 and 4.16).

Both CLR-B and the amide linker were present in the structure of SHF-82, the first compound to demonstrate robust pharmacology against AM2 receptor (IC50 of 200nM) (Figure 4.17). By keeping the CLR region and the linker and by expanding the RAMP region of SHF-82 we were able to develop a dual antagonist over AM2 and CGRP receptor with low nM potency (SHF-408), and a highly potent (1nM) and selective AM2 receptor antagonist (SHF-638) (Figure 4.17). Molecular docking of these three compounds, in the binding pockets of CGRP and AM2 receptors (shown in figure 4.20(A, B and C) below), suggest that the presence of the amine group (-NH_2) on the CLR – RAMP binding region of both SHF-408 and SHF-638 is essential for their interaction with RAMP-3. Moreover, the selectivity achieved by the expansion of that group (SHF-638) suggests its interaction with residues 67 (Glu) and 70 (Thr) (shown in figure 4.19) of RAMP-3 (Figure 4.20(C)) and their importance in differentiating from CGRP. Further modifications on the RAMP region resulted in an increase in both potency and selectivity (SHF-1028), indicating the possibility for the development of even more selective and potent compounds. Molecular docking of SHF-1028 (figure 4.20(D) indicates that by maintaining the interaction with RAMP-3 through binding with residues 67 and 70 and by expanding the CLR – RAMP region of the compounds towards CLR could be used to achieve higher selectivity over the CGRP receptor. These results indicate the importance of RAMPs on determination of receptor potency and binding and the possible use of differences in their structure to achieve higher potency and selectivity. Furthermore, compounds that belong to the secondary structure series had overall significantly lower potency than those in the primary family (Figure 4.18).

In conclusion, these data illustrate the development of a novel highly potent and selective AM2 receptor antagonist (SHF-638) that could potentially be used for the treatment of pancreatic cancer. Further pharmacological characterization and determination of its metabolic profiles are discussed in chapter 5.

CGRP receptor (CLR + RAMP-1) **AM2 receptor (CLR + RAMP-3)**

D) Amide linker

CLR-B

CLR - RAMP binding region SHF-082

B) SHF-408

C) SHF-638

A) SHF-1028
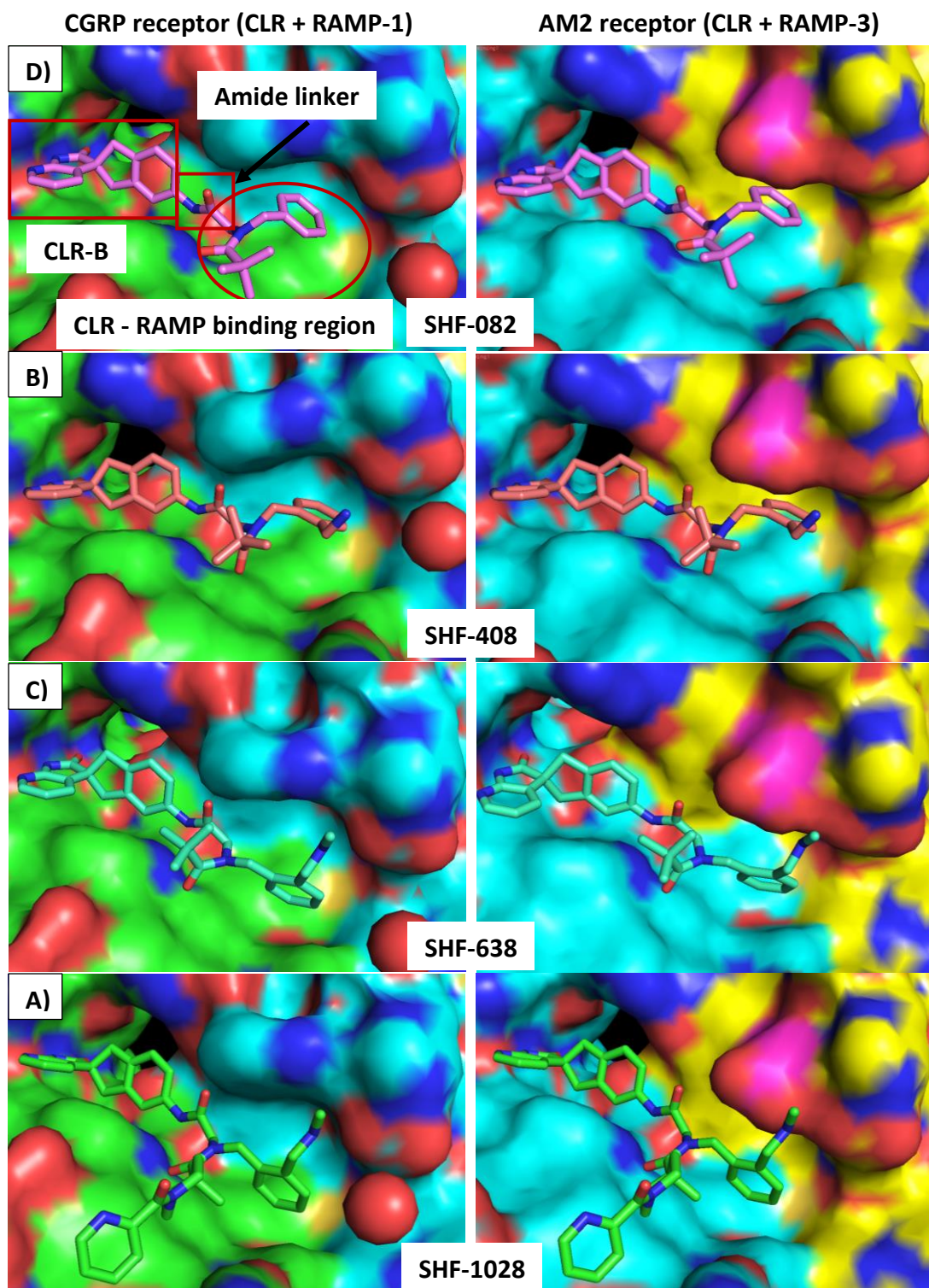
Figure 4.20: Molecular docking of lead compounds. Docking of compounds that belong to primary structural series (SHF-408/638 family) in the binding pockets of CGRP and AM2 receptor.

Chapter 5: *In-vitro* **pharmacological characterization of leading chemical candidate and metabolic profile**

Chapter 5: *In-vitro* pharmacological characterization of leading chemical candidate (SHF-638-AA004) and metabolic profile

5.1 Introduction

5.1.1 Ideal characteristics/properties of a drug candidate

During the lead optimisation stage of the drug discovery ADME and pharmacokinetics studies are routinely used to guide the selection of the lead drug candidate that will be used in preclinical and clinical studies. There several characteristics or properties that determine the druggability and the probability of success of such compounds.

Lipinski's rule of five (also known as Pfizer's rule of five), a set of chemical parameters developed by Lipinski and co-workers in 1997, are often used during the development of small molecule antagonists to access their "druglikeness" (Lipinski et al., 1997). These criteria were based on the observation that most clinically marketed orally administered drugs were relatively small (molecular weight less than 500) and had moderate lipophilicity (log P not greater than 5). Other than low molecular weight and moderate/high lipophilicity, candidate compounds must not have more than 5 hydrogen bond donors, and 10 hydrogen bond acceptors (Lipinski et al., 1997).

Establishing good activity (potency) and selectivity is an important aspect of lead optimization. High quality lead compounds will have high potency and selectivity for the target of interest. Avoiding interaction with other closely related targets (such as receptors belong to the same family) reduces the possibility of undesirable side effects in preclinical *in-vivo* studies (Hughes et al., 2011). Moreover, good solubility and permeability ensures that compounds will be able to access the circulation or absorbed by the digestive system depending on the route of administration (Hughes et al., 2011). The route of administration and the frequency of dosing is an important aspect when developing a new drug. An ideal compound will have good oral bioavailability that will allow less frequent dosing making it practical for human use

(Hefti, 2008). However, establishing the *in-vivo* pharmacokinetic characteristics (PK studies) of leading compounds using different routes of administration and varied species could be beneficial for the correct identification of the appropriate route and the accurate translation into preclinical (*in-vivo* mouse models) and clinical studies.

Furthermore, good safety and toxicity profiles are important characteristics of an ideal compound. Several *in-vitro* (ADME) and *in-vivo* (PK) studies are often used to determine the safety profiles of lead compounds and predict the possibility of causing any off-target toxicities upon administration (Hefti, 2008, Hughes et al., 2011). Unanticipated side effects are often encountered during preclinical evaluation of lead compounds.

In addition to good pharmacokinetic and metabolic profiles an ideal compound will be able to irreversibly bind to the target of interest. A non-competitive mode of antagonism will reduce the ability of the target to exert its effects.

The rest of this introduction will be focused on the role of Schild analysis on the determination the mode of inhibition and its use in the discovery of widely known receptor antagonists including CGRP receptor small molecule antagonists. Moreover, the use of ADME studies for the determination of the metabolic and safety profiles of lead compounds will be explained.

5.1.2 Investigating receptor antagonism / Schild analysis

Identification and classification of the mode of antagonism it is an important aspect of drug development and it is often used as an additional marker of receptor efficacy and potency. Moreover, it provides a more comprehensive analysis of the mode of interaction between a selective antagonist and the receptor of interest.

By definition, antagonists inhibit the effects of an agonist and therefore its ability activate the receptor. Depending on their mode of action (type of antagonism), antagonists are able to alter the effects of an agonist by either decreasing the potency of the agonist (i.e. EC_{50}) or its efficacy (maximal response) against the

receptor of interest (Kenakin et al., 2006, Lambert, 2004). There mainly two main categories of antagonists: the competitive antagonists, also known as reversible and the non-competitive which are also termed as irreversible (Lambert, 2004). In a system of competitive antagonism, both the agonist and the antagonist bind on the same binding site on the receptor and therefore by increasing the concentration of the agonist the effect of the antagonist is decreased. On the other hand, when the antagonist is non-competitive, its binding site differs than that of the agonist, therefore increasing the agonist concentration is unable to attenuate the actions of the antagonist (Lambert, 2004).

A more experimental approach on the classification of the receptor antagonism was taken by Sir John Gaddum in 1957, that categorized the antagonists into surmountable and insurmountable (Gaddum, 1957, Kenakin et al., 2006). Graphical illustration of surmountable antagonism is characterised by a right shift of the agonist dose response curve, changing therefore the potency (EC_{50}) of the agonist. In the case of insurmountable antagonism, the agonist dose response curve is shifted downwards with the maximal response (E_{max}, efficacy) of the agonist to be decreased. Figure 5.1 below illustrates the two main categories of receptor antagonists and their effects on agonist dose response curves.
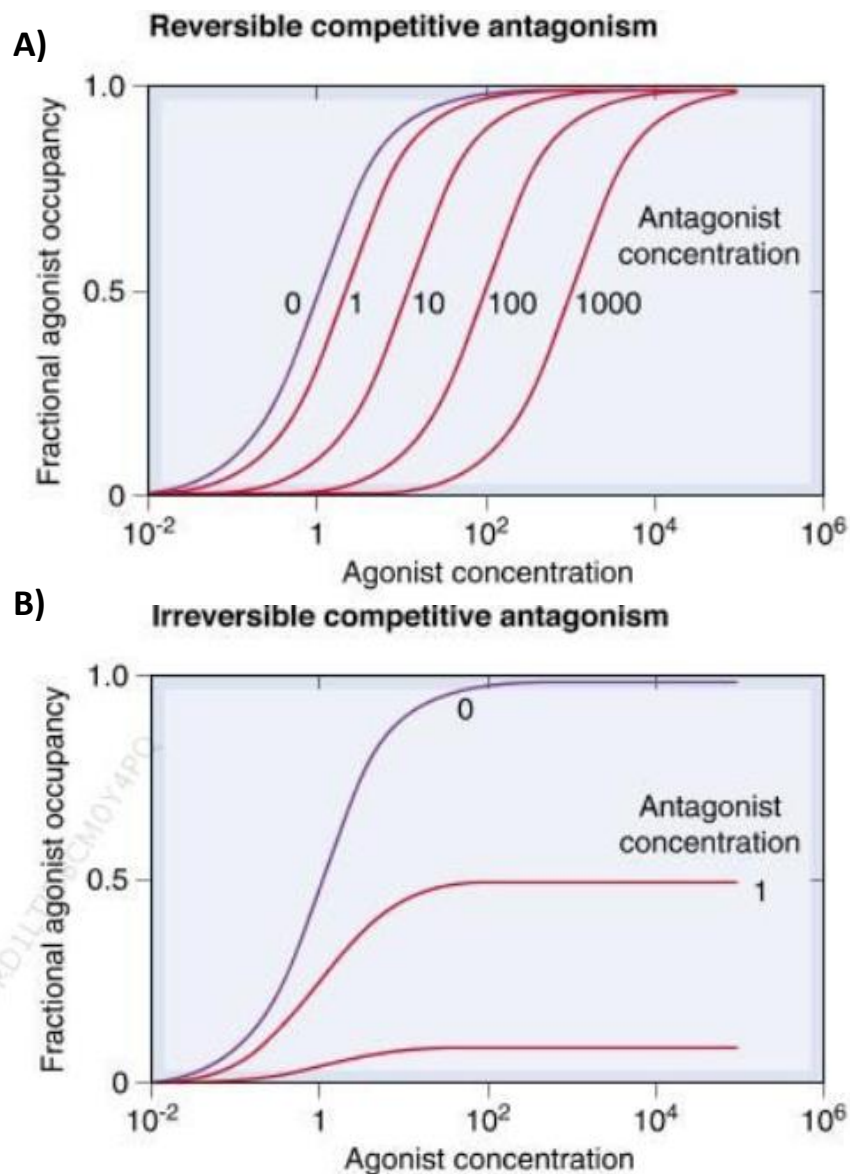
Figure 5.1: Competitive (reversible) and non-competitive (irreversible) antagonism. A) Graphical illustration of competitive (reversible, surmountable) antagonism. Increasing concentration of an antagonist causes a right shift on the agonist dose response curve (EC_{50} shift). **B)** Graphical illustration of non-competitive (irreversible, insurmountable) antagonism. The addition of antagonist is resulting in the inhibition of the agonist maximal response (E_{max} shift). Adapted from (Rang, 2014).

Schild analysis (Schild, 1949, Arunlakshana and Schild, 1959), a method that was first described almost 70 years ago, is often used to determine the potency of competitive antagonists in combination with antagonists dose response curves (used to determine IC_{50}). To perform a Schild analysis of a competitive antagonist, an agonist dose response curve without the presence of antagonist is first generated. This is followed by the generation of further agonist dose response curves in the presence of various concentrations of an antagonist. The dose ratio (dr), ratio between the EC_{50} concentration obtained in the presence and the EC_{50} concentration obtain in the absence of the antagonist, is then obtained for each concentration of the antagonist. See equation below.

$$DR = \frac{EC50\ [With\ antagonist]}{EC50\ [Without\ antagonist]}$$

A Schild plot (figure 5.2 below) is then generated by plotting the log (dose ratio - 1) against the log (antagonist concentration). A linear regression line is then fitted and the pA_2 (the concentration of the antagonist required to produce a two-fold shift in the agonist dose response curve) is calculated as the x-intercept of the fitted regression line. See equation below for mathematical determination of pA_2.

$$pA2 = -log[Antagonist] + log[DR - 1]$$

If the slope of the line is 1 then the antagonist is considered competitive and pA_2 equals to pK_B value (negative log of the concentration of the antagonist that will occupy 50% of the receptors at equilibrium). pK_B can then be used to calculate the association or affinity constant (K_B) of the antagonist (Wyllie and Chen, 2007). Figure 5.2 below shows a graphical illustration of Schild analysis.

If the slope of the Schild plot differs significantly from the theoretical value, a different mode of antagonism may be in place. A slope greater than one will give an underestimated pK_B value (K_B), whereas a slope significantly lower than 1 will give an overestimated pK_B value (K_B) (Kenakin et al., 2006). An assumption that can be made when the slope differs significantly from unity is the interaction of the agonist with more than one receptors or binding sites. Moreover, slow kinetics of an

antagonist might affect the equilibrium of the system leading to a slope lower or higher than the unity (Wyllie and Chen, 2007, Tallarida, 2007).
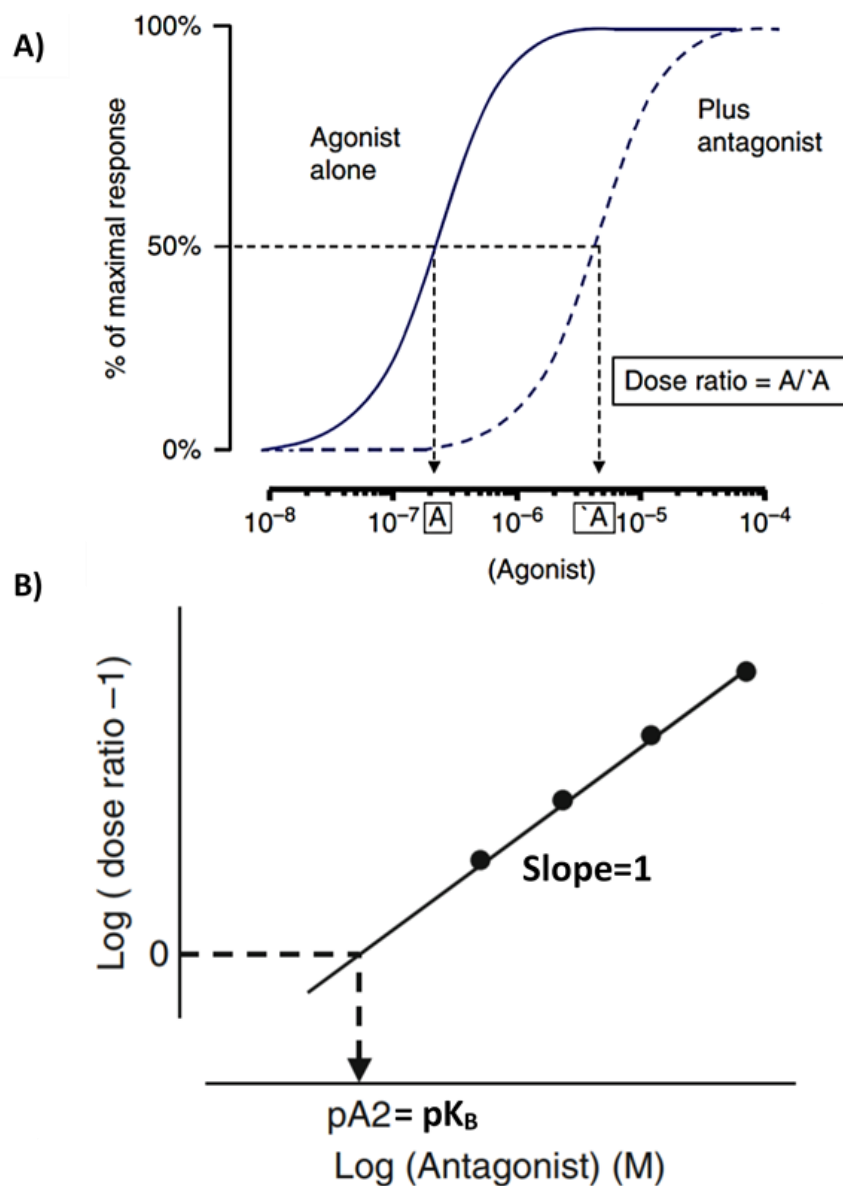
Figure 5.2: Schild plot analysis. A) Dose ratio is calculated between the EC_{50} concentration obtained in the presence and the EC_{50} concentration obtain in the absence of the antagonist. **B)** Schild plot is generated by plotting the log (dose ratio - 1) against the log (antagonist concentration). pA_2 is calculated as the x-intercept of the fitted regression line. The slope of a Schild curve should equal 1 if a true competitive antagonist is investigated. Using pA_2 which equals to pK_B value, the association or affinity constant (K_B) of the antagonist can be calculated. Adapted from (Hinder, 2011).

5.1.3 The use of Schild analysis in the pharmacological investigation of receptor antagonists (including examples of CGRP antagonists)

Schild analysis was successfully implicated in the pharmacological characterization of several clinically important drugs. Schild analysis was used to describe the mode of action of several well-known antagonists including: nicotinic acetylcholine receptor antagonists (Del Castillo and Katz, 1957), histamine H_2-receptor antagonists (Black et al., 1972), β_2-adrenergic receptors blockers (Black et al., 1965) and neuromuscular inhibitors (Bowman, 2006). In more recent studies, Schild analysis was utilised in the pharmacological characterization of a various types of receptor inhibitors including: GSK1004723 (histamine H_1 and $_3$-receptor antagonist) (Slack et al., 2011), novel β_2-adrenoceptor antagonists (Hothersall et al., 2011), PCS1055 (muscarinic M_4-receptor antagonist) (Croy et al., 2016) and novel opioid receptor antagonist (Naltrexone-14-O-sulfate) (Zador et al., 2017).

Schild plots were implicated in the pharmacological classification of Olcegepant (also known as BIBN4096BS), one of the most pharmacologically characterised novel CGRP antagonists, as well as many other members of CGRP inhibitors family. In the very first pharmacological report of Olcegepant after its discovery, the effect of a single dose of the antagonist (10 nM) against the activation of cAMP by human aCGRP in SK-N-MC (Human Neuroblastoma) cell line was used for the calculation of the pA_2, which was found to be at ~11 (Doods et al., 2000).

Using the same cell line, Edvinsson and co-workers investigated the effects of both Olcegepant and CGRP peptide antagonist ($CGRP_{8-37}$) on human aCGRP induced cAMP production. The data suggested the competitive antagonistic mode of both Olcegepant and $CGRP_{8-37}$, with pA_2 of 11.2 (slope: 1.1) and 7.8 (slope: 1.2) respectively. In the same study, Olcegepant showed an apparent competitive inhibition of both coronary (pA_2: 10.4) and cerebral (pA_2: 10.1) artery relaxation upon administration of human aCGRP (Edvinsson et al., 2002).

In another study, antagonism of CGRP mediated cAMP production by Olcegepant in both human SK-N-MC and L6 Rat myoblast cells resulted in pA_2 of 9.95 (slope: 1.37) and 9.25 (slope: 0.89) respectively, however, the slope of both Schild plots was

significantly different than the unity. These suggested a non-competitive mode of antagonism which was explained by the slow kinetic rates of the compound. When the slope of both Schild plots was constrained to 1, a pA_2 of 10.47 and 9.1 respectively was calculated (Hay et al., 2002). In the same study, on human Colony (Col) 29 cells Olcegepant showed a pA_2 of 9.98 with a slope of 0.86 that did not statistically differ from unity (Hay et al., 2002). What is more, Olcegepant showed a significantly lower potency when antagonizing the effects of adrenomedullin in both Rat2 fibroblasts (expressing rat CLR and RAMP2) and Cos-7 cells (expressing hAM1 and hAM2 receptors) showing selectivity over the CGRP receptor (Hay et al., 2002, Hay et al., 2003a).

Interestingly, a biphasic antagonism was suggested in a study of inhibition of CGRP-induced dilation of human brain cells. More specifically, in human pial vessels Schild analysis of the effects of Olcegepant CGRP-induced dilation produced biphasic Schild plot indicating interaction with more than one receptor. When the linear regression was fitted on the linear part of the plot this resulted a pA_2 of 14.5 with the a slope (0.73) still significantly lower than unity (Moreno et al., 2002). Table 5.1 below summarizes the pA_2 determinations for Olcegepant.

Table 5.1: Summary of pA_2 (potency) determinations for Olcegepant using Schild analysis

Tissue/Cell type	Expression	pA_2	Reference
Human SK-N-MC cells	CLR and RAMP1	11	(Doods et al., 2000)
		11.2	(Edvinsson et al., 2002)
		10.5	(Hay et al., 2002)
Human Col 29 cells	$CGRP_2$-like receptor	9.75	(Hay et al., 2002)
Rat L6 cells	CLR and RAMP1	9.1	(Hay et al., 2002)
Human coronary arteries	N/A	10.4	(Doods et al., 2000)
Human cerebral arteries	N/A	10.1	(Doods et al., 2000)
Human pial arteries	N/A	14.5	(Moreno et al., 2002)
Bovine cerebral arteries	N/A	7.9	(Moreno et al., 2002)

*N/A: not applicable

Similar studies were implicated for the pharmacological characterization of other members of the CGRP receptor antagonist family including telcagepant (MK-0974) and MK-3207. In CGRP receptor expressing cells (HEK-293), a telcagepant dose dependent rightward shift in the CGRP cAMP production dose response curve was observed with no apparent inhibition of the maximal response, indicating a competitive antagonism. Schild analysis plot showed a pA_2 of 8.9 and a slope of 1 (Salvatore et al., 2008). The same experiment was used to characterise MK-3207 antagonism showing a rightward shift competitive dose response manner with pA_2 of 10.3 and slope of 1.1 (Salvatore et al., 2010). The relaxant effects of human aCGRP on human coronary arteries (proximal and distal) and small coronary arterioles was also inhibited by telcagepant in competitive dose response manner. Schild analysis plot showed a pA_2 of 8.43 (distal coronary arteries), 7.78 (proximal coronary arteries) and 7.89 (coronary arterioles) (Chan et al., 2010).

5.1.4 *In-vitro* ADME/Safety studies in drug discovery

The disposition of a compound within an organism is characterised by various stages including Absorption, Distribution, Metabolism, and Excretion (ADME). Graphical illustration of the stages can be seen in figure 5.3 below. Absorption is the first stage and involves the movement of the drug from the site of administration into the bloodstream where it will be distributed to the rest of the body and the target of interest. This stage is an important aspect of drug distribution, especially after oral (Per os or P.O) and intraperitoneal (IP) administration, as it will determine the available drug concentration in the systemic circulation. The ability of a drug to permeate through the intestinal walls is often used as an initial indication of drug absorption. *In-vitro* assays are often used to determine and characterized this ability of the drugs. In these assays a cell monolayer of Caco-2 cell line (human colon carcinoma cells) is used and the rate of compound transport is measured (van Breemen and Li, 2005).

Distribution, the second phase of pharmacokinetics, refers to the transfer of a drug from the absorption site through the systemic circulation to various locations (tissues and organs) within the body. Similarly to the absorption phase, distribution is affected by various factors including vascular permeability, plasma protein binding,

regional blood flow and lipophilicity (lipid solubility) (Nishant et al., 2011). The most crucial factor is the plasma protein binding (PPB). PPB determines the amount (concentration) of free drug in the circulation that is available to act on the target and it is considered as a key factor for both drug distribution (drug efficacy) and metabolism.
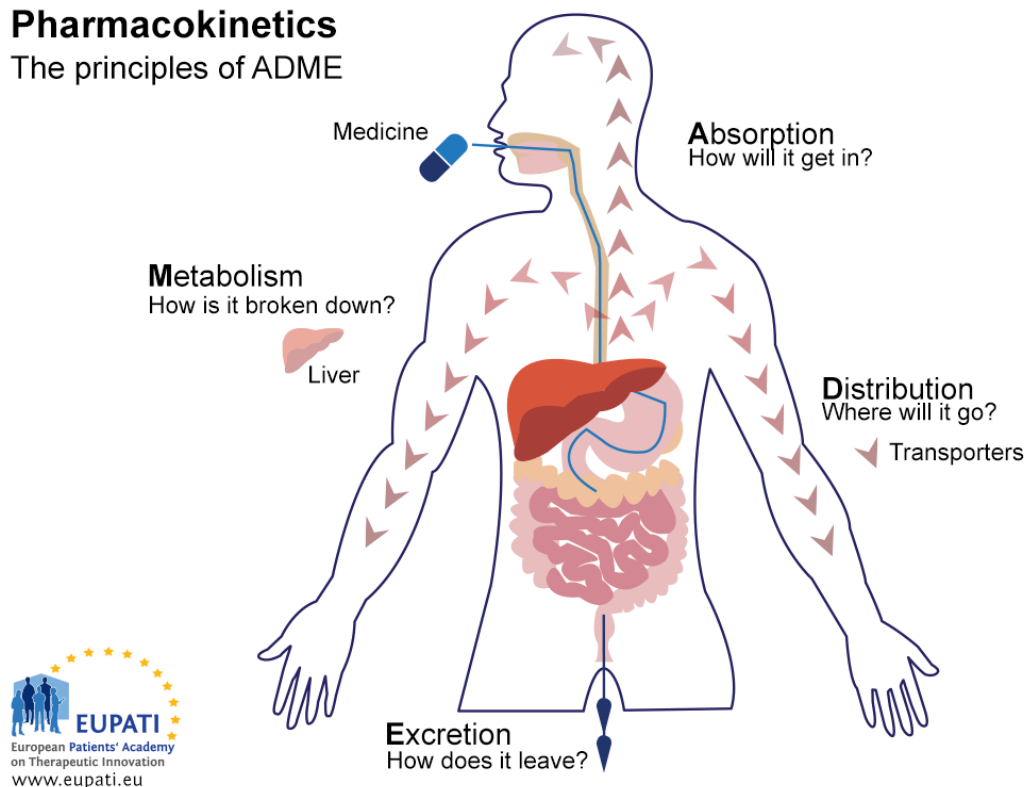
Figure 5.3: The key principles of Pharmacokinetics/Drug disposition – the study of the effect the body has on a drug/medicine– are represented in the acronym ADME. (Used under the Creative Commons Attribution-Non-Commercial-Share-Alike 4.0 International License)

The metabolic phase is an irreversible process that occurs mainly in the liver and it involves the breakdown/conversion of the parental compound into molar polar and therefore water-soluble daughter metabolites that could easily secreted by the body. The metabolism of a drug can affect its action (pro-drug is converted into the active analogue in the liver) as well as its action duration and intensity. In pharmacokinetics, several *in-vitro* assays including hepatic microsome stability (in the presence of liver microsomes: Cytochromes P450s), plasma stability (in the

presence of enzymes in plasma such as estarases) and cytotoxicity/hepatotoxicity assays (inhibition of Cytochromes P450s: 1A2, 2B6, 2C9, 2D6, 3A4) are used to predict the metabolic fade of a compound as well as to establish the possibility of side effects related to the site of metabolism (liver) (Chung et al., 2015).

Excretion or elimination phase is the process of which unbound molecules, toxic biproducts and metabolites are excreted from the kidney and through several pathways/routes (mainly urine) are cleared from the body.

5.2 Aim and objectives

Aim

The aim of these chapter was to determine the mode of antagonism of the leading compounds of the program (SHF-638) and its metabolic profiles prior its use *in-vivo*.

Objectives

Objective 1: Determine the mode of inhibition using Schild plot analysis.

Objective 2: Investigate the activity of leading compounds against cells with native expression.

Objective 3: Investigate the effects of serum in the functional activity of leading compounds.

Objective 4: Use ADME *in-vitro* studies to establish the metabolic profiles and suitability of SHF-638 and SHF-408 to be used *in-vivo*.

5.3 Material and methods

5.3.1 Schild plot analysis

Schild plot or Schild regression analysis is a pharmacological method of receptor classification and it is used to study the effects of an antagonist on a cellular response triggered by receptor activation. In such experiments, an antagonist (in various concentrations) is competing with the agonist (in the form of a constant dose response curve) for binding to the receptor. This competition is causing changes on the shape of the curves or causes its shift, aiding on the pharmacological characterization of the antagonist. Similar experimental procedure as in all cAMP assays described previously (chapter 3) was followed with some modifications. Cells (6μl/well) were first pre-incubated with different doses (3μl/well) of the different small molecules for 30 minutes at room temperature prior their stimulation with serial dilutions of peptide agonist (dose response curve) (3μl/well) for 15 minutes at room temperature. After stimulation, the detection mix (12μl/well) was added and the results were obtained after an hour, using Enspire multimode Plate reader (Perkin Elmer, Waltham, Massachusetts, United States), at; 320/340nm excitation and 615/665nm emission. Vehicle and peptide only controls were used for data normalization and experimental validation. Figure 5.4 below illustrates in detail the experimental procedure followed. Fitted dose response curves were plotted with and without the addition of the antagonist and were used to determine the potency (pA_2) of the antagonist.
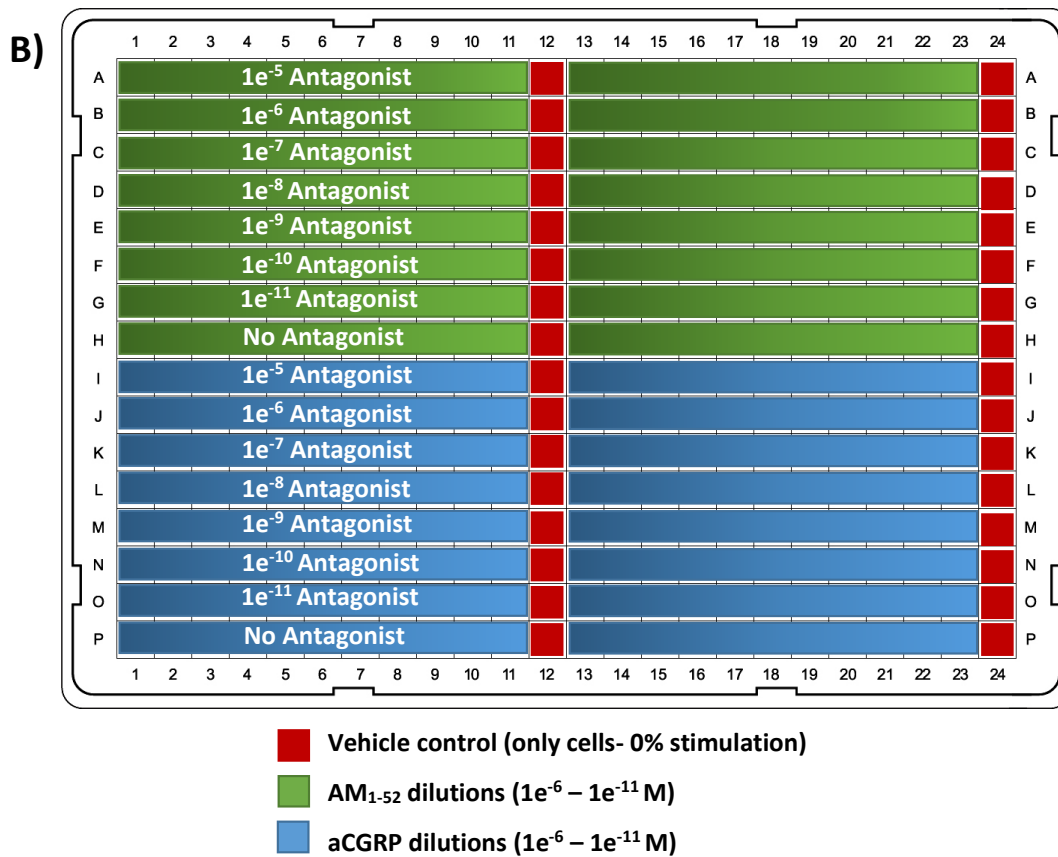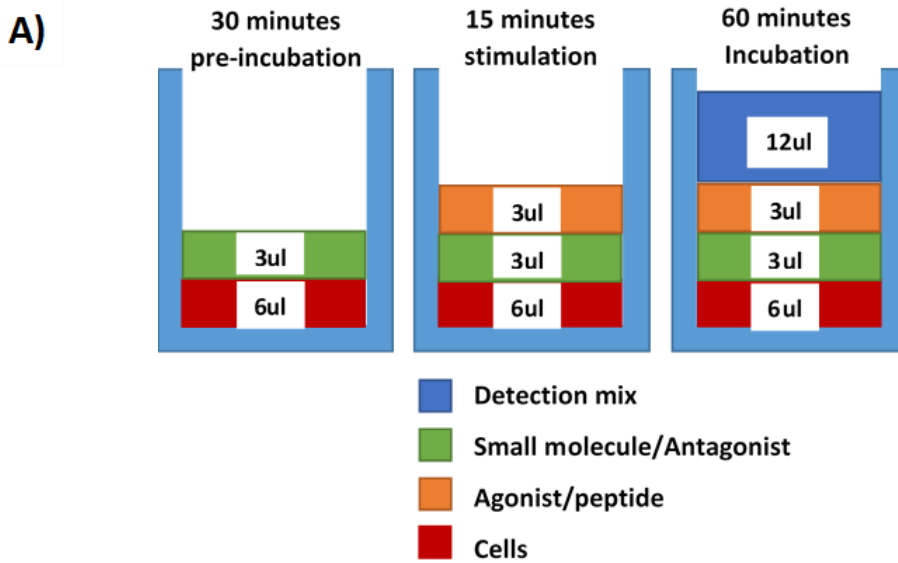
Figure 5.4: Experimental procedure for Schild plot analysis. A) Illustrates the experimental procedure for measurement of cAMP that is produced after agonist/antagonist competition. **B)** Increasing concentrations of the antagonists were plated as shown and incubated with the cells for 30 minutes. AM1-52 or aCGRP peptide dilutions were plated in duplicates followed by vehicle control and incubated for 15 minutes. Detection mix was then added, and data were obtained after 1 hour.

5.3.2 Potency evaluation on primary cancer cells

To evaluate the potency of leading compounds in different cancer cell lines, mouse prostate cancer cells 178-2 BMA and human pancreatic cancer cell line Panc 10.05 were used. To assess the ability of the antagonists of inhibiting the production of cAMP, after stimulation of primary cells with AM_{1-52} (peptide ligand agonist), the LANCE TR-FRET cAMP cell-based assay was used. The same experimental procedure that was previously explained in chapter 3 and 4 was used.

AM_{1-52} concentration response curves were first used to determine the EC_{50} dose of the ligand against each cell line (see chapter 3 for more details). Knowing the EC_{50} dose for each cell line, agonist/antagonist competition assays were used to establish the magnitude of cAMP production inhibition (potency) after treatment of each cell type with increasing concentration of an antagonist (see chapter 4 for more details).

5.3.3 Serum testing

To evaluate the effects of serum (protein-protein binding) on the activity of the compounds, competition assays were also performed in the presence of high concentration (50%) of both human and fetal calf serum (FCS). Serial dilutions of the compounds were made in the presence of either 50% human or fetal calf serum and incubated for 30 minutes (at RT) or overnight (at 4°C) before used.

5.3.4 *In-vitro* ADME studies

ADME studies of selected compounds were performed by WUXI Apptec (Shanghai, China) and Peakdale Molecular (Derbyshire, UK). The following methods are described based on information provided by the organizations that performed the studies.

5.3.4.1 Kinetic solubility

To determine the kinetic solubility, each compound (DMSO stock) was diluted in an aqueous buffer (50mM phosphate buffer pH 2 or 7.4) at a concentration of 200µM. This was followed by vigorous shaking for 24hours at room temperature. Any precipitated material was then removed by filtration and the remaining compound concentration was established using UV absorbance.

5.3.4.2 Microsomes stability assays

Microsome stability assays were performed in 96-well plates. The stability of the compounds was assessed in the presence of 0.5mg/mL of human, rat or mouse microsome solution. 10µL (10µM) of each test compound or positive controls (testosterone, diclofenac and propafenone) were added into the appropriate wells (a matrix blank was also included). Then 80µL of microsome solution was added to each well followed by incubation for 10 minutes at 37°C. 10µL/well of pre-warmed NADPH (β-Nicotinamide adenine dinucleotide phosphate) was added and plates were incubated at 37°C for different time durations (60, 30, 20, 10, 5 and 0 minutes). The reaction was then stopped by the addition of 300µL/well of cold (4°C) stop solution (100 ng/mL Tolbutamide and 100 ng/mL Labetalol). Sample plates were then shaken for 10 minutes followed by their centrifugation at 4000 rpm for 20 minutes under 4°C. Intrinsic microsome clearance ($CL_{int(mic)}$) and half-life ($t_{1/2}$) was then determined using LC-MS/MS.

5.3.4.3 Plasma stability assays

Similarly, to microsomal stability assays, a known concentration of a compound (0.1-1μM) was incubated in the presence of human, rat or mouse serum (80% in PBS, pH 7.4) for up to 120 minutes (0, 5, 15, 30, 60, 120 minutes). Positive control compounds such as Dextromethorphan, Midazolam, Diazepam and Phenacetin were also used for assay validation and quality control. At the end of each time point the % of the remaining compound concentration compared to time point 0 was calculated using LC-MS/MS.

5.3.4.4 Cytochrome P450 (CYP450) enzymes inhibition assays

Five different cytochrome P450 isoforms (CYP1A2, CYP2C9, CYP2C19, CYP2D6 and CYP3A4) are investigated with cytochrome P450 enzyme inhibition assays. Specific substrates (table 5.2) for each isoform were incubated with a range of test compound concentrations (0-50μM) in the presence of human liver microsomes. At the end of the incubation the formation of a known metabolite depending on the isoform is monitored using LC-MS/MS. The ability (IC_{50}) of each test compound to inhibit the formation of the metabolites was then measured compared to the vehicle control. Known positive inhibitors of each isoform were also used for assay validation (see Table 5.2 below).

Table 5.2: Isoform specific substrate reaction and positive control inhibitors

CYP450 Isoform	Isoform-specific Substrate Reaction	Positive Control Inhibitor
CYP1A2	Ethoxyresorufin *O*-deethylation	α-Naphthoflavone
CYP2C9	Tolbutamide 4-hydroxylation	Sulphaphenazole
CYP2C19	S-mephenytoin 4-hydroxylation	Tranylcypromine
CYP2D6	Dextromethorphan *O*-demethylation	Quinidine
CYP3A4	Midazolam 1-hydroxylation	Ketoconazole

5.3.4.5 Plasma Protein Binding (PPB) assays

To investigate the extent of binding of a compound to plasma proteins an equilibrium dialysis assay was used. In such assays a semi-permeable membrane that separates two compartments: 1) 100% plasma protein containing compartment (test compound is diluted in this solution) and 2) plasma protein free compartment is used. The system is then incubated at 37°C until equilibrium was reached. The % of the test compound in each compartment was then analysed using LC-MS/MS. The % of unbound compound was then calculated using the following equation. Known control compounds such as Verapamil and Warfarin were used for assay validation.

$$fu = 1 - \left(\frac{PC-PF}{PC}\right)$$

PC: Compound in protein-containing compartment.
PF: Compound in protein-free compartment.

5.4 Results

5.4.1 Pharmacological difference between the two enantiomers of SHF-638-AA004

Like many compounds in the market, SHF-638-AA004 was made as a racemate consisting of two enantiomers. To investigate the pharmacological differences of the two enantiomers, pure versions of both compounds were made (see figure 5.5 below) and their ability to inhibit cAMP production was investigated.

SHF-638-AA004 (racemate)

SHF-770-AA001 (S-enantiomer)   **SHF-771-CN001 (R-enantiomer)**
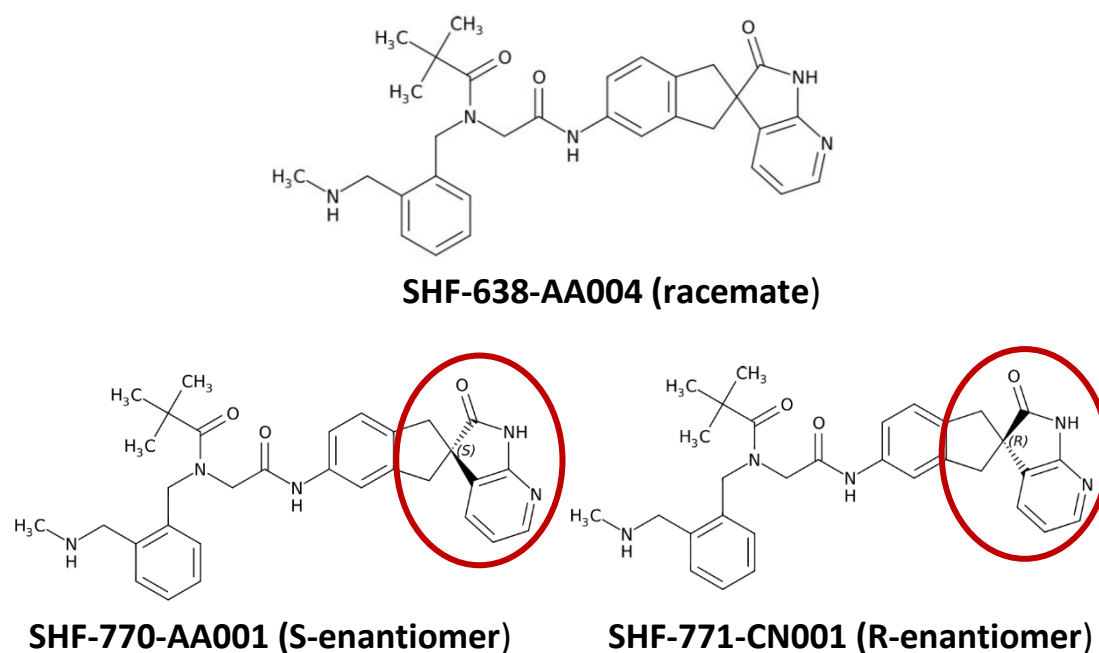
Figure 5.5: Racemate SHF-638-AA004 and pure enantiomers. Showing the chemical structure of the racemate compound SHF-638 and of its two enantiomers: SHF-770-AA001 ("Sinister" **(S)** or left) enantiomer and SHF-771-CN001 ("Rectus" **(R)** or right) enantiomer.

As shown in figure 5.6 and table 5.3 below significant difference was shown in the potency of the two enantiomers. More specifically, SHF-770 (left enantiomer), showed a significant lower IC_{50} when compared to both SHF-638 and SHF-771 (right enantiomer. Interestingly, SHF-771 was able to inhibit cAMP production in higher affinity than SHF-638 (racemate), increasing the potency in both cell lines. What is more, the selectivity over the AM2r O/E cells was retained in both enantiomers.
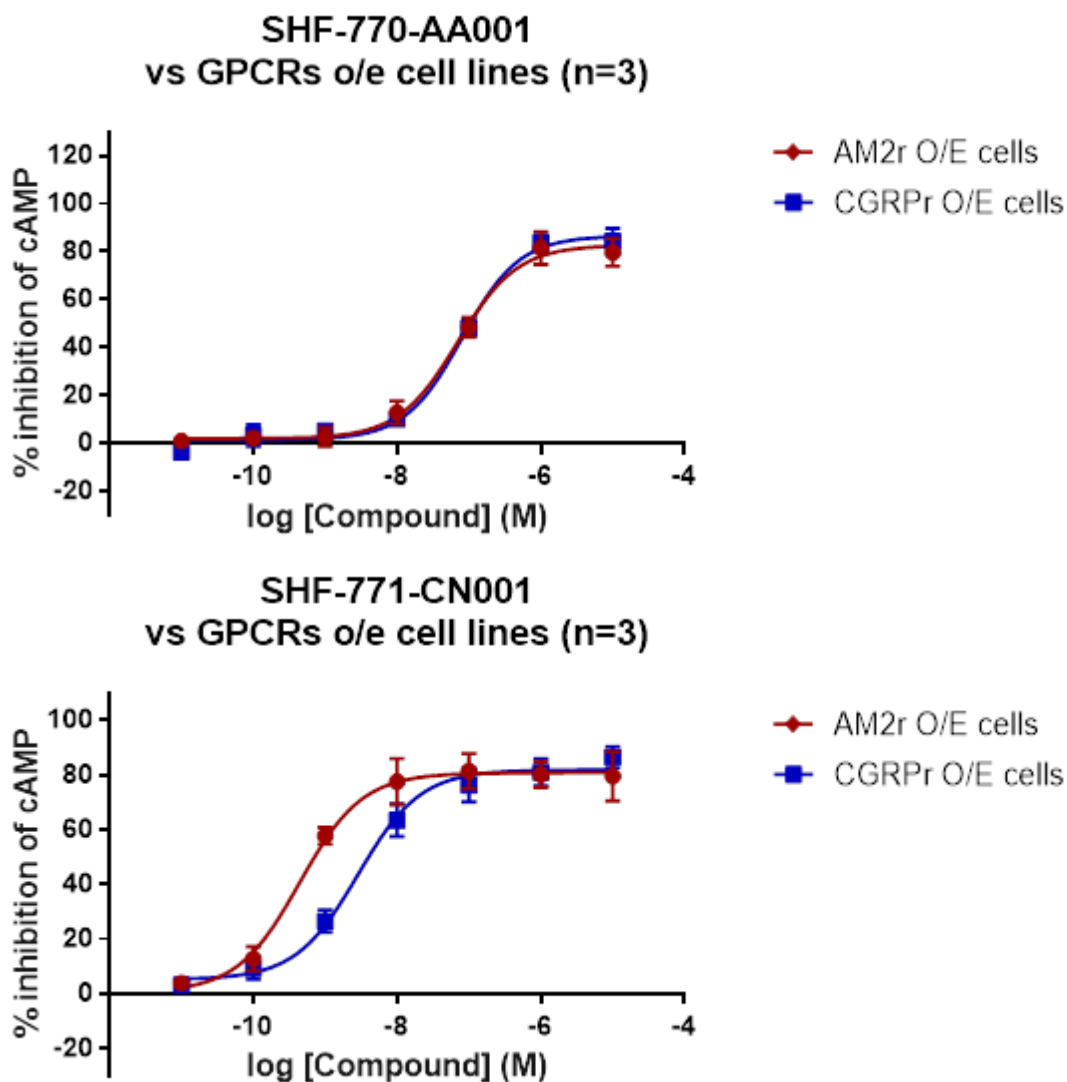
Figure 5.6: Potency of SHF-638 pure enantiomers. Illustrates the differences in the potency between the left (SHF-770) and the right (SHF-771) enantiomers of the racemate SHF-638.

Table 5.3: Potency of racemate SHF-638 and of its enantiomers.

Compound name	Racemate/ Enantiomer	Activity (IC50)	
		CGRPr	**AM2r**
SHF-638-AA004	Racemate	4.58nM	1.07nM
SHF-770-AA001	S-enantiomer	81nM	70nM
SHF-771-CN001	R-enantiomer	2.8nM	0.48nM

5.4.2 Effects of SHF-638-AA004 on cAMP production by 178-2 BMA and Panc 10.05 cancer cell lines

For a better disease representation and determination of the effects of SHF-638 under normal expression conditions, the production of cAMP upon stimulation of human pancreatic cells Panc 10.05 and mouse prostate cancer cells 178-2 BMA by AM_{1-52} was determined.

The EC_{50} dose of the AM_{1-52} against both cell lines, was first established using agonist dose response curves (see chapter 3 for method details). Figure 5.7 below shows the AM dose response curve for both cell lines as well as for AM2 receptor O/E cells. As shown the potency of AM was significantly lower in both cancer cell lines when compared to AM2r O/E cells. More specifically, stimulation of 178-2 BMA by peptide AM yielded an EC_{50} dose of 30.2nM, a ~5-fold change from AM2r cells EC_{50} (5.45nM). Moreover, the EC_{50} dose obtained from the stimulation of Panc 10.05 cells by AM was even lower than that of 178-2 BMA cells with a value of 310nM, more than 300-fold change from AM2r cells EC_{50}. Table 5.4 below illustrates data extracted from each dose response curve.

Using the obtained EC_{50} dose, the potency of SHF-638 for each cell line was then obtained using cAMP agonist vs antagonist competition assays as described in chapter 4. Interestingly, no significant difference (P = 0.246) was observed between the IC_{50} dose of AM2r O/E cells (0.72nM) and the IC_{50} dose obtained from the inhibition of cAMP production by Panc 10.05 cells (1.26nM). Moreover, the IC_{50} dose calculated from the antagonist dose response curve against the production of cAMP by 178-2 BMA cells was significantly (P = <0.0001) higher when compared with the AM2r cells IC_{50}. See figure 5.8 and table 5.5 below for more details.
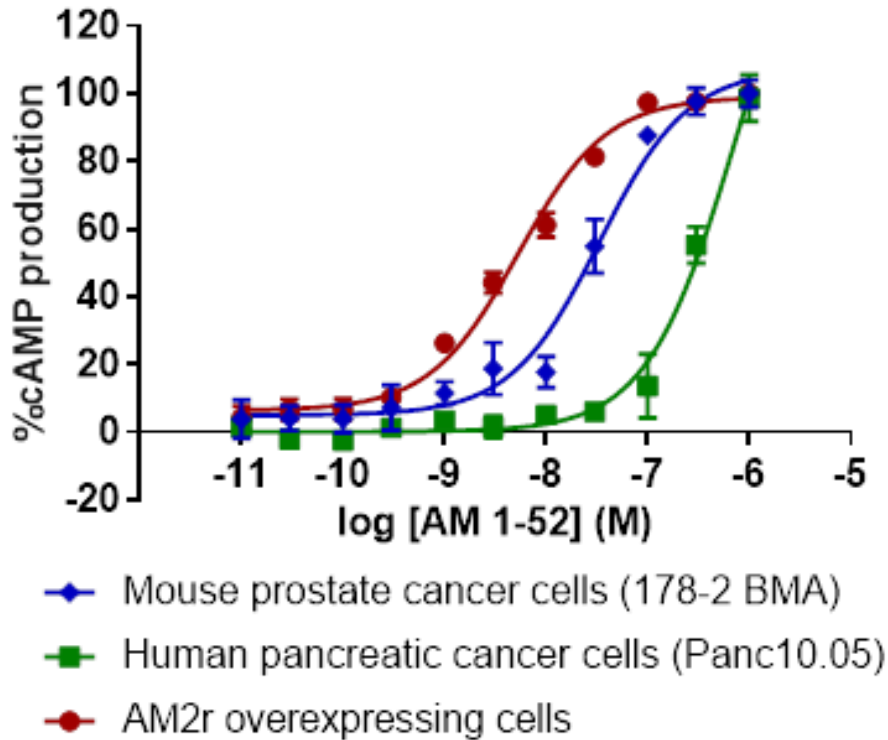
Figure 5.7: Agonist stimulation curves of AM2r O/E cells and primary cancer cell lines. Showing the % of cAMP production by AM2 receptor O/E cells, mouse prostate cancer cells (178-2 BMA) and human pancreatic cancer cells after stimulation with AM_{1-52} peptide ligand agonist.

Table 5.4: Best fit values for agonist stimulation of AM2r O/E cells and primary cancer cell lines.

Cell type	Parameters			
	EC$_{50}$	pEC$_{50}$ +/- SEM	Top	Bottom
AM2r O/E	5.45nM	8.26 +/- 0.053	103	3.24
178-2 BMA	30.2nM	7.52 +/- 0.068	100.7	6.98
Panc 10.05	310nM	6.51 +/- 0.081	111.2	1.34
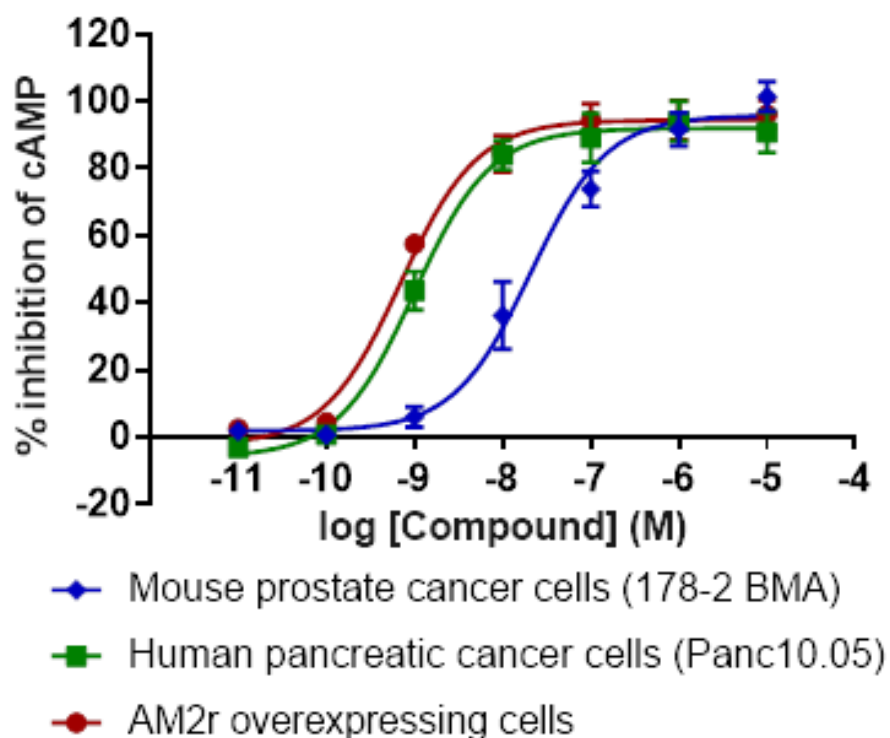
Figure 5.8: Dose response inhibition of cAMP production by AM2r O/E cells and primary cancer cell lines. Showing the % inhibition of cAMP production by AM2 receptor O/E cells, mouse prostate cancer cells (178-2 BMA) and human pancreatic cancer cells, upon treatment with SHF-638-AA004.

Table 5.5: Potency of SHF-638 against AM2r O/E cells and primary cancer cell lines.

Cell type	Parameters			
	IC_{50}	pIC_{50} +/- SEM	Top	Bottom
AM2r O/E	0.72nM	9.14 +/- 0.085	93.4	-0.272
178-2 BMA	24nM	7.62 +/- 0.140	100.6	-0.745
Panc 10.05	1.26nM	8.90 +/- 0.093	91.3	-4.667

5.4.3 Effects of serum on the potency of SHF-638

To investigate the effects of serum on the potency of SHF-638 antagonist dose response curves in the presence or not of both human and fetal calf serum were used. Results are illustrated in figure 5.9 and table 5.6 below. As described in the method section above, the compound was first incubated in the presence of serum (50%) for 30 minutes as well as overnight, followed by cAMP agonist vs antagonist competition assays.

As shown in the table 5.6, no difference in the potency was observed after a 30-minute incubation with both human (1.26nM, P = 0.087) and fetal calf (0.59nM, P = 0.616) serum, when compared to the control dose response curve (0.72nM). Similarly, no statistically significant difference was found after overnight incubation with human serum (0.74nM, P = 0.895) and fetal calf serum (1.48nM, P = 0.053).

5.4.4 Schild analysis of SHF-638-AA004

Schild plot analysis was used for the classification and characterization of the mode of antagonism of our leading compound (SHF-638). The effects of different concentrations (10μM to 10pM) of SHF-638 on aCGRP and AM_{1-52} induced cAMP production dose response curves upon stimulation of CGRPr and AM2r O/E cells respectively was examined.

Increasing concentration of SHF-638 had as a result the dose dependent rightward shift in both aCGRP (figure 5.8(A)) and AM_{1-52} (figure 5.11(A)) dose response curve with no apparent inhibition of the maximal response of both peptide agonists (See tables 5.7 and 5.8). Comparison of best fit values (using analysis tools of GraphPad Prism 7.03), between the dose response curves with and without antagonist, showed statistically (P= <0.05) significant difference between the EC_{50} dose of no antagonist dose response and almost all the concentrations of SHF-638 in both cell lines. However, no significant difference was observed when 0.1nM and 10pM of SHF-638 was used in CGRPr O/E cells and AM2r O/E cells respectively. Tables 5.7 and 5.8 below summarises these findings.

Effect of human and fetal calf serum on the potency of SHF-638-AA004

Legend:
- Control Buffer
- 50% Human serum
- 50% FCS
- 50% Human serum (O/N)
- 50% FCS (O/N)

O/N: Overnight
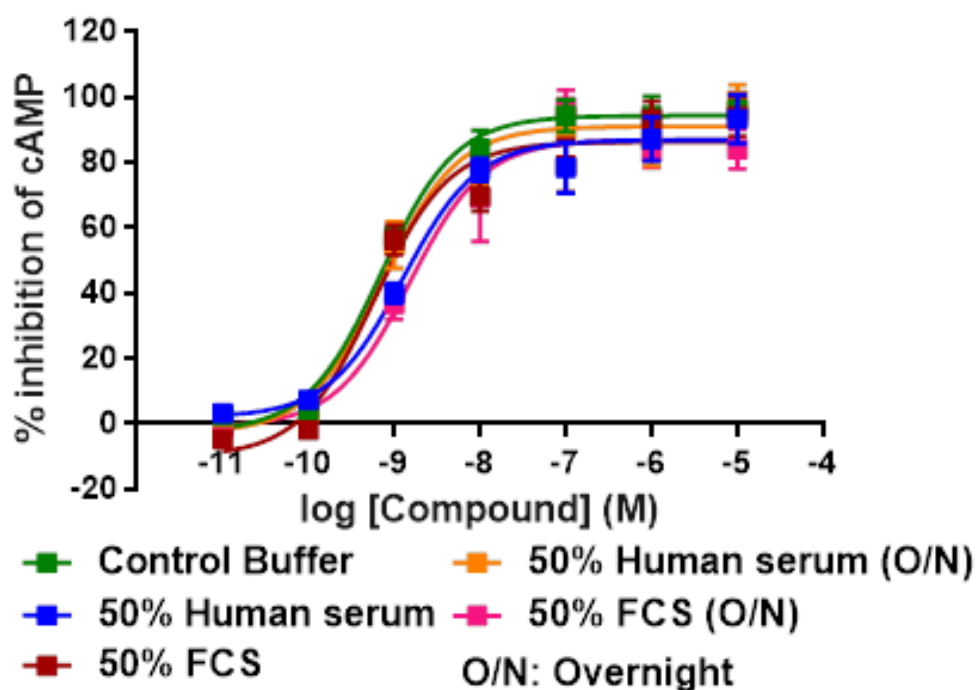
Figure 5.9: Effects on the inhibitory effects of SHF-638-AA004 by human and fetal calf serum. Showing the effects of human and fetal calf serum on the ability of SHF-638-AA004 to inhibit the production of cAMP by AM2r O/E cells. SHF-638 was incubated with 50% serum for 30 minutes as well as overnight.

Table 5.6: Effects of serum (human and fetal calf (FCS)) on SHF-638 potency.

Condition	Parameters				
	IC_{50}	pIC_{50} +/- SEM	Top	Bottom	P value
Control	0.72nM	9.14 +/- 0.085	93.4	-0.272	-
50% Human serum (HS)	1.26nM	8.90 +/- 0.135	87.3	1.322	0.087
50% Fetal calf serum (FCS)	0.59nM	9.23 +/- 0.154	87.1	-11.4	0.616
50% HS (O/N)	0.74nM	9.13 +/- 0.137	92.4	-0.040	0.895
50% FCS (O/N)	1.48nM	8.83 +/- 0.175	87.8	-2.508	0.053
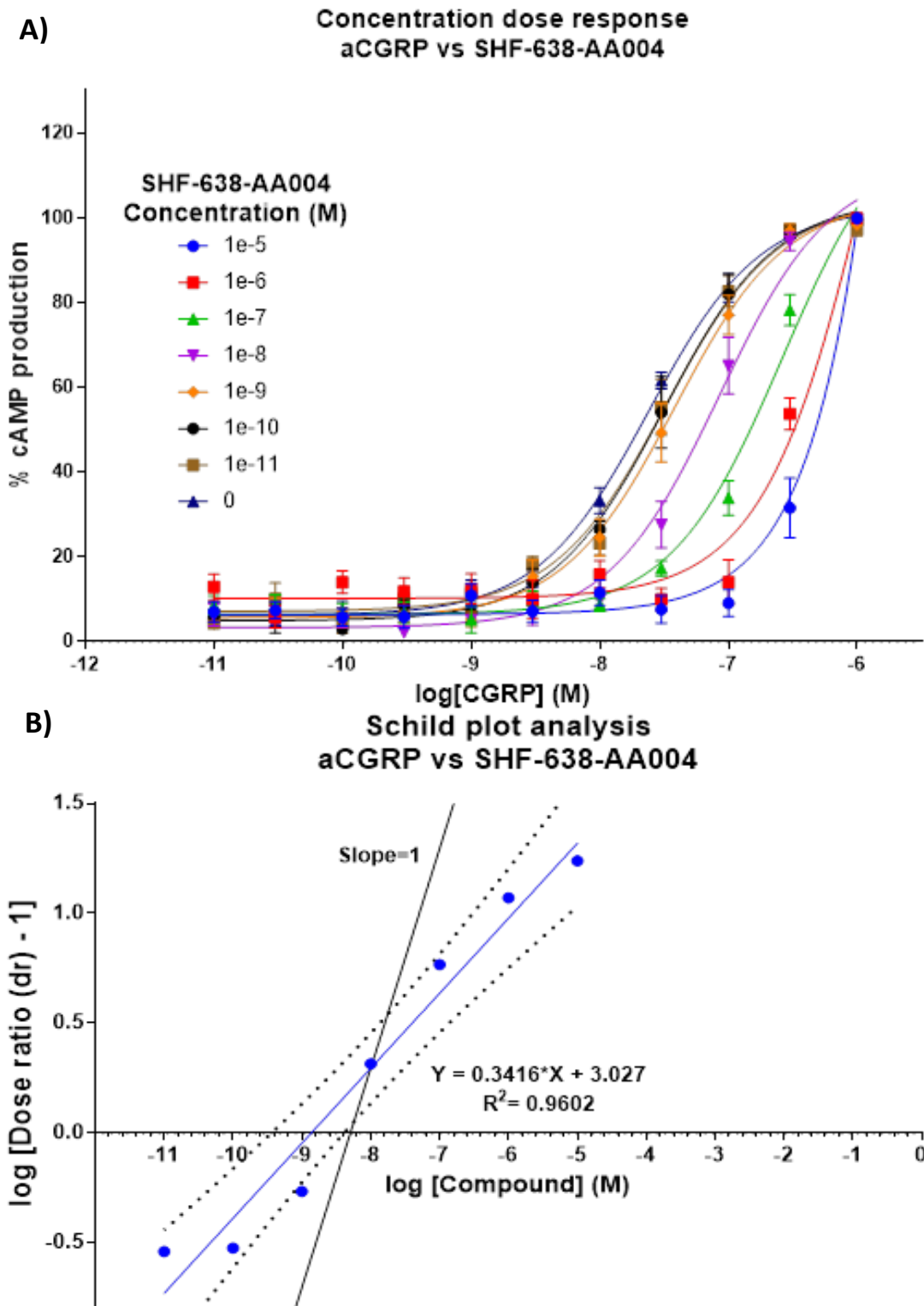
Figure 5.10: CGRP receptor antagonism by SHF-638-AA004. A) Concentration response curves for aCGRP in CGRPr O/E cells in the absence or presence of increasing concentrations of SHF-638. **B)** Schild plot analysis of the data presented in **(A).** Analysis yielded a pA_2 value of 8.862 (r=0.96, slope=0.3416, significantly different from unity, p<0.05) and a pA_2 value of 8.294 when the slope was constrained to 1.

Table 5.7: Effects of different concentrations of SHF-638 on the potency of aCGRP.

SHF-638 Conc.	Parameters			
	EC_{50}	pEC_{50} +/- SEM	Top	P value
No antagonist	23nM	7.63 +/- 0.038	101	-
10µM (1e-5 M)	446nM	6.35 +/- 0.215	108	<0.0001
1µM (1e-6 M)	313nM	6.50 +/- 0.032	102	<0.0001
0.1µM (1e-7 M)	176nM	6.75 +/- 0.042	106	<0.0001
10nM (1e-8 M)	70nM	7.16 +/- 0.042	103	<0.0001
1nM (1e-9 M)	36.7nM	7.44 +/- 0.061	103	0.0042
0.1nM (1e-10 M)	29.9nM	7.52 +/- 0.057	102	0.0874
10pM (1e-11 M)	30.1nM	7.52 +/- 0.049	100	**0.0471**

Table 5.8: Effects of different concentrations of SHF-638 on the potency of AM$_{1-52}$.

SHF-638 Conc.	Parameters			
	EC_{50}	pEC_{50} +/- SEM	Top	P value
No antagonist	19.7nM	7.71 +/- 0.048	101	-
10µM (1e-5 M)	313nM	6.50 +/- 0.032	106	<0.0001
1µM (1e-6 M)	176nM	6.75 +/- 0.042	103	<0.0001
0.1µM (1e-7 M)	69.9nM	7.16 +/- 0.042	103	<0.0001
10nM (1e-8 M)	36.6nM	7.44 +/- 0.061	103	0.0004
1nM (1e-9 M)	29nM	7.54 +/- 0.061	102	0.0296
0.1nM (1e-10 M)	28.3nM	7.55 +/- 0.062	101	0.0464
10pM (1e-11 M)	24.7nM	7.61 +/- 0.040	101	**0.0766**

Using the dose response curves obtained, Schild regression plots were generated following the method described in the introduction of this chapter (section 5.1.1). The pA_2 value from each plot was calculated as the x intercept. On CGRPr O/E cells, a pA_2 value of 8.862 was calculated with a slope of 0.3416 (see figure 5.10(B)). On AM2r O/E cells, Schild analysis yielded a pA_2 value of 8.402 with a slope of 0.3044 (see figure 5.11(B)). When the slope of both plots was constrained to 1 the pA_2 value on both cell lines was reduced to 8.294 (CGRPr) and 8.122 (AM2r). The slopes from both Schild plots were significantly different from unity, suggesting a non-competitive antagonism or an alternative (negative allosteric modulator) mode of action. Moreover, the biphasic Schild plots shown in the figures 5.10 and 5.11 (suggested from the sigmoidal shape of the plots) suggest the possible involvement of more than one receptor in the equilibrium. Therefore, the pA_2 values obtained by the Schild regression analysis could not be considered as relevant to the efficacy of the antagonist. These was further suggested by the presence of both AM2 and CGRP receptors on the parental cell line (1321N1 - Human brain astrocytoma cells) used for the generation of the O/E cells (see appendix figure 8.2 and table 8.1). Furthermore, as shown in section 5.3.1 above, the presence of two pharmacologically different enantiomers in SHF-638 (a highly potent enantiomer (SHF-771) and of one with a significant lower potency (SHF-770)) could affect the interaction of SHF-638 with the receptor (two phases: low and high affinity). These results did not support the competitive mode of antagonism suggested from the effects on the dose response curves (figure 5.10(A) and figure 5.11(A)).
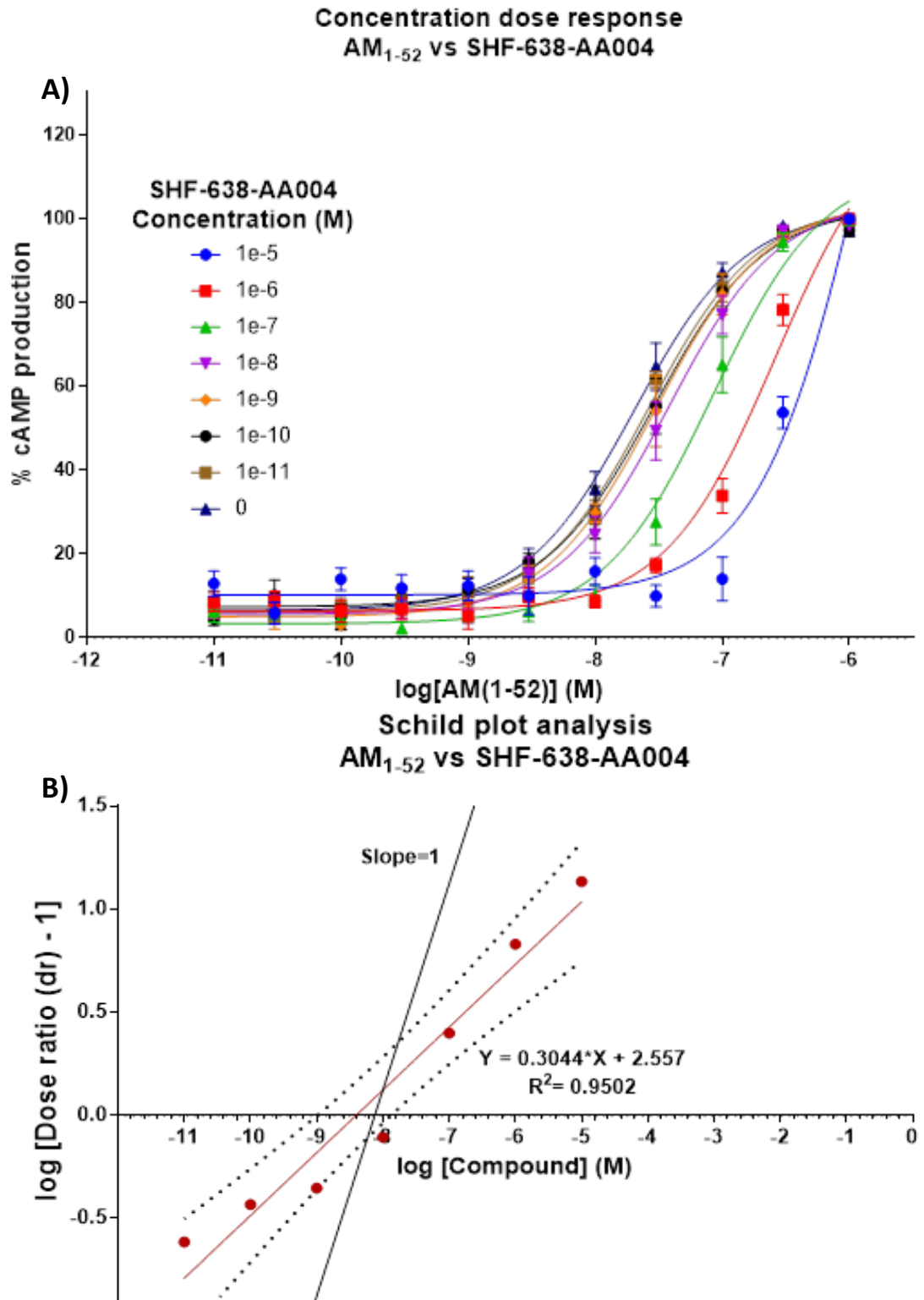
Figure 5.11: AM2 receptor antagonism by SHF-638-AA004. A) Concentration response curves for AM1-52 in AM2r O/E cells in the absence or presence of increasing concentrations of SHF-638. **B)** Schild plot analysis of the data presented in **(A).** Analysis yielded a pA$_2$ value of 8.402 (r=0.95, slope=0.3044, significantly different from unity, p<0.05) and a pA$_2$ value of 8.122 when the slope was constrained to 1.

5.4.5 Exploring the ADME properties of leading series of compounds

To investigate the ADME characteristics (solubility, plasma stability, permeability and toxicity) of the two leading compounds of our leading structural series, several *in-vitro* ADME studies were performed following the methodology explained in detail in the Materials and Methods section 5.2.4 above. The results from these studies are summarised in the tables 5.9 (SHF-408-AA002) and 5.10 (SHF-638-AA004) below. The tables are also including the potency on cAMP inhibition of the different compounds against various GPCR O/E cell lines (AM2r, CGRPr, AM1r, AMY1r and AMY3r).

5.4.5.1 Kinetic solubility

Compounds showed moderate to high kinetic solubility in both pH conditions tested. More specifically, SHF-638 has shown 83.9μM and 86.3μM solubility in pH 7.4 and 2 respectively. The kinetic solubility of SHF-408 was not determined under these conditions.

5.4.5.2 Microsome stability

The microsomal stability of the compounds was tested in three different species (human, rat and mouse) and is illustrated as the intrinsic clearance (CL_{int}) of the compounds as well as the elimination half-life ($T_{1/2}$). SHF-408 and SHF-638 shown moderate human microsomal intrinsic clearance with 21 μl/min/mg of protein. The half-life of the compounds in the presence of human microsomes *in-vitro* was 33 minutes (SHF-408) and 34 minutes (SHF-638). Moreover, both compounds showed low clearance in rat microsomes with values ranging between 12-14 μl/min/mg of protein. Similar was the elimination half-life of the compounds with 58 minutes for SHF-408 and 51 minutes for SHF-638. Moderate was the clearance of SHF-638 in the presence of mouse microsomes with 22 μl/min/mg of protein. A half-life of 31.5 minutes for SHF-638 was also observed. Mouse microsomal stability data for SHF-408 were not determined.

164

5.4.5.3 Plasma Stability and Plasma Protein Binding (PPB)

In-vitro plasma stability of our compounds was measured to establish the percentage of degradation of each compound in the presence of human and rat plasma. The assays were performed in two different time points (30 minutes and 120 minutes) in both species and data shown below as percentage (%) of parent compound remained at each time point. After 30 minutes in the human and rat plasma 84% and 95% of SHF-408 remained intact, values which were decreased to 56% and 70% respectively after 120 minutes. As shown in the table 5.9 below, parent SHF-638 was unaffected by the presence of human plasma in both time points as well as in the presence of rat plasma after 30 minutes (percentage of parent compound was decreased to 81% after 2hours).

To investigate the extend at which the compounds are bound to the plasma protein, PPB assays were performed. The data shown below are illustrated as percentage of bound compound to the plasma protein of rats. As shown all compounds had relatively high percentage binding to the plasma with 89% (SHF-408) and 90% (SHF-638).

5.4.5.4 Cytochrome P450 inhibition (potential toxicity indication)

The inhibition of various enzymes (1A2, 2C9, 2C19, 2D6 and 3A4) that belong to the cytochromes P450 family, by the compounds was tested to investigate the potential toxicity that could be caused by compound administration. Both compounds showed low to weak inhibition (> 10 µM) of most enzymes tested. However, both SHF-408 and SHF-638 showed moderate inhibition (1 and 10 µM) of enzymes CYP2D6 and CYP3A4.

It is worth mentioning, that as seen in the tables 5.9 and 5.10 below both compounds showed only one violation of the Lipinski rule of five with the molecular weight been marginally above the limit of 500 g/mol suggesting their possible use as orally active compounds in humans.

Table 5.9: ADME properties of SHF-408-AA002

cAMP Assay potency (pIC50)		Microsomes Stability		Plasma Stability and Interaction		Cyp P450s Inhibition (μM)		Lipinski Rule of Five
AM2r	8.1	Human CL_{int} (μl/min/mg)	21	Stability Human Plasma (30 min)	84%	1A2	>50	**MW:** 511.626 g/mol
CGRPr	8.3	Human $t_{1/2}$ (min)	33	Stability Human Plasma (120 min)	56%	2C9	15	**log P:** 3.74
AM1r	5.0	Rat CL_{int} (μl/min/mg)	12	Stability Rat Plasma (30 min)	95%	2C19	19	**H-bond donors:** 3
AMY3r	6.0	Rat $t_{1/2}$ (min)	58	Stability Rat Plasma (120 min)	70%	2D6	4	**H-bond acceptors:** 5
AMY1r	5.4	Mouse CL_{int} (μl/min/mg)	16	PPB Rat (bound)	89%	3A4	2.5	
*ND: Not Determined		Mouse $t_{1/2}$ (min)	43	Kinetic Solubility (μM) pH7.4/pH2	ND			

Table 5.10: ADME properties of SHF-638-AA004

cAMP Assay potency (pIC50)		Microsomes Stability		Plasma Stability and Interaction		Cyp P450s Inhibition (µM)		Lipinski Rule of Five
AM2r	9.1	**Human CL$_{int}$ (µl/min/mg)**	21	**Stability Human Plasma (30 min)**	100%	**1A2**	>50	**MW:** 525.653 g/mol
CGRPr	8.5	**Human t$_{1/2}$ (min)**	34	**Stability Human Plasma (120 min)**	100%	**2C9**	34	**log P:** 4.17
AM1r	5.1	**Rat CL$_{int}$ (µl/min/mg)**	14	**Stability Rat Plasma (30 min)**	100%	**2C19**	26	**H-bond donors:** 3
AMY3r	6.5	**Rat t$_{1/2}$ (min)**	51	**Stability Rat Plasma (120 min)**	81%	**2D6**	4	**H-bond acceptors:** 5
AMY1r	5.4	**Mouse CL$_{int}$ (µl/min/mg)**	22	**PPB Rat (bound)**	90%	**3A4**	2	
*ND: Not Determined		**Mouse t$_{1/2}$ (min)**	31.5	**Kinetic Solubility (µM) pH7.4/pH2**	83.9/ 86.3			

5.5 Conclusion/Discussion

This chapter was focused on the pharmacological characterization of SHF-638 and the determination of its metabolic profile *in-vitro*. Schild analysis is an important and commonly used method in drug discovery, utilised for the pharmacological mode of action (antagonism) of a candidate compound (Schild, 1949, Arunlakshana and Schild, 1959). In addition, generation of Schild curves can also be used as a marker of potency as well as receptor affinity due to its relationship with the association constant (K_B) (Wyllie and Chen, 2007). Schild analysis was previously used for the pharmacological classification of several clinically important compounds including: neuromuscular inhibitors (Bowman, 2006) and histamine receptor antagonists (Black et al., 1972, Slack et al., 2011) as well as recently developed novel CGRP receptor small molecule antagonists including Olcegepant (Doods et al., 2000, Edvinsson et al., 2002, Hay et al., 2002, Moreno et al., 2002).

Using peptide ligand induced cAMP production dose response curves we were able to investigate the effects of different concentrations of SHF-638 on the potency of AM_{1-52} and aCGRP on AM2r (Figure 5.11) and CGRPr (Figure 5.10) O/E cells respectively. The resulted dose response curves from each SHF-638 concentration were then compared with the no antagonist dose response curve in order to establish the mode of antagonism of SHF-638. On both cell lines, treatment with SHF-638 has as a result the dose dependent rightward shift of the peptide ligand induced dose response curve with no apparent inhibition of the maximal response suggesting a competitive mode of inhibition. As was previously described, a competitive inhibitor (also known as reversible or surmountable antagonist) is able to cause a right shift of the agonist dose response curve, changing the potency (EC_{50}) of the agonist but not its efficacy (E_{max}). On the other hand, a non-competitive antagonist (irreversible or insurmountable) will cause a dose dependent inhibition (downwards shift) of the maximal response, while not affecting the EC50 significantly (Gaddum, 1957, Kenakin et al., 2006). The competitive nature of our antagonist was also supported by the changes observed in the potency of the agonist dose response curve, showing a statistically ($P = <0.05$) significant dose dependent inhibition of EC_{50}

dose of no antagonist dose response when compared with the different concentrations of SHF-638 in both cell lines (Tables 5.7 and 5.8).

However, generation of Schild regression plots did not support the competitive mode of antagonism that was suggested from the effects on the dose response curves. More specifically, the slopes calculated from both Schild regression plots were significantly different from unity (1), suggesting a non-competitive antagonism or an alternative (negative allosteric modulator) mode of action (Figures 5.10 and 5.11). Moreover, the biphasic Schild plots shown in the figures 5.10 and 5.11 (suggested from the sigmoidal shape of the plots) suggest the possible involvement of more than one receptor in the equilibrium. Data obtained by our group have shown that the parental cell line (1321N1 - Human brain astrocytoma cells) used for the generation of the O/E cells, responded to stimulation by both AM_{1-52} and aCGRP resulting in the production of cAMP, suggesting the expression of both receptors (see appendix figure 8.2 and table 8.1). A biphasic manner of interaction of Olcegepant and CGRP receptor was previously shown, suggesting the presence of two receptors with different affinities (low and high) for the antagonist (Moreno et al., 2002). Although highly selective to CGRP receptor, lower affinity (200-fold less) for human AMY1 receptor (CTR + RAMP1) was previously reported suggesting the possible involvement of AMY1 receptor in this biphasic manner of interaction (Hay et al., 2006a).

Another possible explanation for these results could be the presence of two pharmacologically different enantiomers in SHF-638. Data shown in the result section 5.3.1 suggested the presence of a highly potent enantiomer (SHF-771) and of one with a significant lower potency (SHF-770) suggesting that interaction of SHF-638 with the receptor occurs in two phases (low and high affinity).

For a better disease representation and in order to determine the effects of SHF-638 under conditions of native expression, human pancreatic cancer cells Panc 10.05 and mouse prostate cancer cells 178-2 BMA were used. Whereas identifying the activity of the compound in human pancreatic cancer cells is used as a prediction of its ability to alter the function of such cells *in-vitro* and *in-vivo,* the use of mouse cancer cells will help predict the effects of the compound in the tumour microenvironment in

169

mouse models. Interestingly, SHF-638 was able to inhibit the AM_{1-52} induced production of cAMP in both cell lines. However, significantly lower potency was observed in the mouse cancer cells suggesting a lower affinity for the mouse receptor (Figure 5.8). Related results were observed previously with CGRP receptor antagonists. More specifically, in binding studies of Olcegepant (Doods et al., 2000), Telcagepant (Salvatore et al., 2008) and MK-3207 (Salvatore et al., 2010), significantly lower binding affinities (Ki) were observed against rat CGRP when compared with human CGRP. Previous studies have suggested the important role of RAMP-1 in the determination of species selectivity. More specifically, recombinant expression of human/rat CGRP receptor components (CLR + RAMP-1) in HEK293-EBNA cells showed that RAMP-1 was able to determine both receptor pharmacology as well as antagonist binding affinities (Mallee et al., 2002).

To access the effects of serum in the pharmacological activity and function of SHF-638 *in-vitro*, its potency was determined in the presence of human and fetal calf serum. 30minute and overnight incubation of SHF-638 with both human and fetal calf serum, showed no notable change in the potency (IC_{50}) of the compound on inhibiting cAMP production (Figure 5.9). The plasma stability of SHF-638 was further investigated in ADME pharmacokinetic studies that aimed to establish the metabolic profiles of our compounds prior their use *in-vivo* (data summarised in table 5.10). A good plasma stability was suggested, since SHF-638 was unaffected by the presence of human and rat plasma, after 30 and 120 minutes (in rat plasma the percentage of parent compound was decreased to 81% after 2hours). However, high PPB was observed in PPB assays with bound SHF-638 to be at 90% suggesting that only 10% of the concentration is able to produce a pharmacological response (Smith et al., 2010).

Determining the metabolism of new compounds *in-vitro* is a crucial step in drug development since it can be used as a prediction of its fate *in-vivo* (Jia and Liu, 2007). Since liver is the primary site of drug metabolism in the body, with more than 60% of marketed drugs to be cleared by hepatic cytochrome P450-mediated metabolism (McGinnity et al., 2004), *in-vitro* liver microsomal stability studies are often used to determine the hepatic compound clearance. Low to moderate metabolic clearance

of SHF-638 was suggested after investigating the microsomal stability of the compound in three different species (human, rat and mouse) *in-vitro*. Moderate intrinsic clearance was shown in the presence of human and mouse microsomes, however, low clearance was observed in rat microsomes. These results are suggesting a good stability profile of SHF-638 that could potentially result in prolong exposure and therefore a reduction in dose.

A commonly used marker for possible drug adverse effects is the inhibition of cytochrome P450 (CYP450) enzymes, enzymes important for the metabolism of most drugs (Lynch and Price, 2007). Inhibition of such enzymes could possible result in drug-drug interactions that could potential cause unanticipated side effects or decrease the effects of the drugs (Lynch and Price, 2007). SHF-638 shown no significant inhibition of any of the cytochrome P450 enzymes used suggesting good metabolic profile.

In conclusion, pharmacological characterization of SHF-638 suggested competitive manner of antagonism, however, further studies are required to fully understand the mode of interaction and binding with the receptor. Good metabolic profiles were established using *in-vitro* ADME studies supporting the use of SHF-638 *in-vivo* to establish its efficacy. The pharmacokinetic characteristics of SHF-638 will be discussed in chapter 6.

Chapter 6:
Pharmacokinetic (PK)
studies and *In-vivo* efficacy

Chapter 6: Pharmacokinetic (PK) studies and *In-vivo* efficacy

6.1 Introduction

6.1.1 AM and pancreatic cancer

The role of AM in several aspects of cancer development and progression was previously described in Chapter 1. However, an increased amount of evidence in the last few years suggests a significant role of AM and its receptors in the development and progression of pancreatic cancer. Immunohistochemical staining of 30 pancreatic cancer resection specimens revealed the overexpression of AM when compared with histologically normal pancreatic specimens. AM was only found to be expressed in periphery of the normal pancreatic islets whereas high expression of AM was found in both cancer cells and neighbouring ducts, acini and islets of the pancreatic cancer resection specimens (Aggarwal et al., 2012). In the same study, plasma AM levels were significantly higher in pancreatic cancer patients when compared with normal individuals or patients with diabetes and even higher in pancreatic cancer (Aggarwal et al., 2012). Elevated levels of AM were reported in plasma samples of 12 pancreatic cancer patients when compared to healthy individuals regardless of the tumour stage (D'Angelo et al., 2016). Similarly, in another study, AM serum levels were significantly increased in patients with pancreatic adenocarcinoma when compared to healthy controls and chronic pancreatitis patients (Keleg et al., 2007). Expression of AM was found in pancreatic adenocarcinomas (Ishikawa et al., 2003, Ramachandran et al., 2007) as well as pancreatic insulinomas (Letizia et al., 2001). As was reported by Ishikawa and co-workers in 2003, administration of AM_{22-52}, a peptide antagonist for AM, inhibited significantly the growth of pancreatic tumours *in-vivo* by affecting their vascularization (smaller blood vessels) (Ishikawa et al., 2003). Furthermore, treatment of three different pancreatic cancer cell lines (Panc-1 (epithelioid carcinoma), BxPC3 (adenocarcinoma) and MPanc96 (metastatic derived adenocarcinoma)) with the same antagonists showed a significant decrease in cell proliferation as well as the in the activity of Nuclear factor-κB (NF-κB), a protein which is often mutated by cancer cells to promote their development. The same

effect was observed *in-vivo* whereas small hairpin (sh)RNA silencing of AM had as a result significant decrease in tumour growth and metastasis of MPanc96 cells (Ramachandran et al., 2007). Similarly, a study contacted by the same group have shown that administration of AM antagonist *in-vitro* had inhibitory effects on BxPC3 cell growth. What is more, knockdown (using shRNA) of AM receptor in BxPC3 cells injected orthotopically into mice, had a significant decrease in the tumour development and metastasis to distant sites including liver and lung when compared with the control cells. It is worth mentioning that silencing (using small interfering (si)RNA) of AM receptor in both human cancer cells injected (BxPC-3) and of the mouse tumour stromal cells had the same effects (Ramachandran et al., 2009). In a study of tissue microarrays derived from 116 patients with pancreatic cancer, AM2/Intermedin (a closely related peptide that utilises the same receptors as AM) was found to be correlated with poor prognosis and lower survival rates (Hollander et al., 2015). In a recent study, sequencing data of pancreatic cancer cells O/E the proto-oncogene MYB showed a significant increase of AM and Sonic-hedgehog (SHH) genes when compared to silenced cells. Moreover, AM was able to influence the growth of pancreatic cancer cells and pancreatic stellate cells, indicating a possible role of AM in the desmoplastic nature (formation of dense fibrous and connective tissue) of pancreatic cancer as well as in the crosstalk between the tumour and the microenvironment (Bhardwaj et al., 2016). The expression of AM was found in pancreatic cancer exosomes that were associated with paraneoplastic β-cell dysfunction, a common characteristic of several pancreatic tumours (Javeed et al., 2015). AM exosomes are also believed to be involved in the early onset weight loss of pancreatic cancer by mediating lipolysis in subcutaneous adipose tissue (Sagar et al., 2016). This growing body of evidence suggests the possible use of AM as a predictive biomarker for the diagnosis of pancreatic cancer (Antolino et al., 2017). A novel function of AM in pancreatic cancer progression was revealed in a recent study. More specifically, AM was found to promote pancreatic cancer progression by the recruitment and regulation of myelomonocytes. AM was able to increase the adhesion, invasion and migration of myelomonocytes (monocyte-macrophage that associated with inflammation and poor diagnosis) by activating PI3K/Akt, eNOS and MAPK signalling pathways as well as by increasing the expression of MMP-2.

Moreover, both administration of AM antagonist or knockdown of AM in tumour-bearing mice had as a result a significant decrease in the tumour angiogenesis and the recruitment of myelomonocytes. Interestingly, depletion of myelomonocytes themselves *in-vivo* had as a result the significant decrease in tumour development (Xu et al., 2016).

As noted in the introduction chapter, AM exerts its actions through two cell-surface receptors (AM1 and AM2) with distinct roles (Poyner et al., 2002). Even though this was clearly illustrated under physiological conditions where the deletion of RAMP-2 but not RAMP-3 was related with embryonic lethality (Shindo et al., 2001, Dackor et al., 2006, Dackor et al., 2007), under pathophysiological conditions the role of each receptors is not completely understood mainly due to the lack of evidence. The expression of all receptor components (CLR, RAMP-2 and RAMP-3) was found in several cancer types including breast, pancreatic, prostate, pheochromocytoma and aldosteronoma (reviewed by (Hay et al., 2011)). However, some studies have shown the expression of only some of the components. More specifically, in a study of clear cell renal carcinoma, expression of RAMP-2 was found in the cancer cells whereas RAMP-3 was only found to be expressed in the inflammatory cells surrounding the tumour suggesting a role of RAMP-3 in the cross-talk between the tumour and the host microenvironment (Deville et al., 2009). Moreover, in a study of adrenocortical carcinoma RAMP-3 was the only RAMP subtype expressed in SW-13 cells compared to all three RAMPs in normal cells suggesting a AM tumour promoting effect through AM2 receptor (Albertin et al., 2005). Furthermore, inhibition of RAMP-3 in breast cancer cells was related with reduced tumour development *in-vivo* (Brekhman et al., 2011). The lack of selective antagonists or antibodies is making the determination of the specific role of each receptor subtype under different conditions challenging. However, considering the physiological role of AM1 receptor described in detail above and the evidence suggesting a possible role of AM2r in tumour progression and development targeting AM2r could be beneficial and without the RAMP-2 associated side effects.

6.1.2 Pharmacokinetics (PK) in drug development

Understanding the pharmacokinetics and the metabolic profiles of a compound is an essential component of any drug development program, particularly when it comes to the selection of leading candidates for pre-clinical and clinical studies. Knowing the efficacy and safety characteristics of a new candidate during all the stages of its development can significantly maximise the possibility of a success. The use of such approaches is becoming essential in the initial stages of drug development such as the compound discovery and lead candidate optimization phases (Chien et al., 2005). PK and ADME studies of existing or leading compounds are often used as benchmarks to evaluate new chemical entities (NCE) during lead optimization.

Pharmacokinetics is the study that provides a better understanding of the fade of a drug after it is administrated into the body (i.e. pharmacological and metabolic properties) and during the separate phases of its life. Such phases include the Absorption, Distribution, Metabolism, and Excretion (ADME) of the drug (described in more detail in chapter 5/*in-vitro* ADME studies).

Absorption is the process of drug movement from the site of administration (absorption site) to the circulation. An important subcategory of the absorption phase is bioavailability (also known as BA or F) which is described as a fraction/concentration of the drug in the systemic circulation (plasma or urine) during a duration of time (rate and extent of unchanged drug). The bioavailability of the drug is influenced by the route of administration. More specifically, when a drug is introduced into the body via routes such as P.O, intramuscularly (IM), subcutaneously (SB) and IP its absorption will be affected by several factors including first-pass metabolism, intestinal permeability, vascularity, surface area of absorption and Gastrointestinal (GI) tract mobility. On the other hand, when the compound is injected IV its absorption is not affected, and it is considered as 100% (Ahmed, 2015). The difference in bioavailability depending on the route of administration is illustrated in the figure 6.1 below, showing the drug concentration in the plasma over time. The absorption and the bioavailability of a drug is also influenced by its solubility. For example, a poorly soluble compound would not be able to be

formulated as an orally available drug since its absorption from the GI tract will be limited.
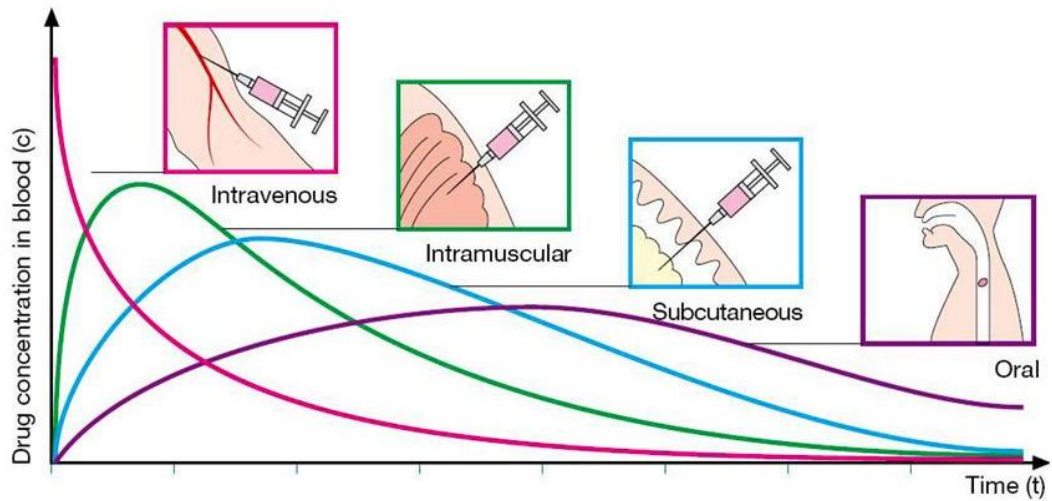
Figure 6.1: Routes of administration and bioavailability.

6.1.3 Pharmacokinetics and safety during the development of CGRP antagonists

Safety and PK studies are commonly used during the preclinical evaluation of a new candidate antagonist as well as early clinical studies, to identify the metabolic profiles and the tolerability of the compounds. Such studies were used during the development of several CGRP antagonists.

In a safety and pharmacokinetic clinical trial, Olcegepant was found well tolerated (at all doses) and with no clinically relevant adverse effects, following a single IV dose in healthy individuals. The plasma clearance (CL) of the compound was ~12L/h and the terminal half-life (t1/2) ~2.5h (Iovino et al., 2004). Similarly, in a double-blinded placebo-controlled crossover study, no adverse effects linked with the cerebral or systemic circulation (such as blood pressure and heart rate) were reported (Petersen et al., 2005).

Moreover, during the development of telcagepant pharmacokinetic studies using several routes of administration and species were used for the pharmacological characterization and lead optimization of leading candidates. In early studies, telcagepant have shown good oral bioavailability both in rats (20%) and dogs (35%). Furthermore, further pharmacokinetic studies revealed low clearance in both rats (9.4 ml/min/kg) and rhesus monkeys (7 ml/min/kg) and moderate clearance in dogs (17 ml/min/kg). Moreover, moderate and good half-life was shown in rats (1.6h) and monkeys (2.8h) respectively, following IV administration. Short oral T_{max} (0.67h) was also observed in rats (Paone et al., 2007).

The preclinical pharmacokinetic data of MK-3207 showed promising results supporting its advancement into clinical trials. More specifically, the compound showed low plasma clearance levels in both rat and dog and moderate clearance in monkey. Moreover, the oral bioavailability was good in both rat and dog but lower in monkeys (this was improved with higher dose) (Bell et al., 2010). The oral bioavailability of the compound was similar in humans with T_{max} of ~ 1–2 h and a half-life of ~ 9–18 h (Li et al., 2015a).

6.1.4 *In-vivo* efficacy studies

In addition to cell-based assays and pharmacokinetics, *in-vivo* efficacy preclinical studies are often used for leading compound optimization and selection for early clinical trials. There several models (shown in figure 6.2 below) that are widely used, each one with its advantages and disadvantages. The most frequently used species for such studies are mice due to its relative physiological resemblances to humans and the high efficiency of breeding and housing mice.
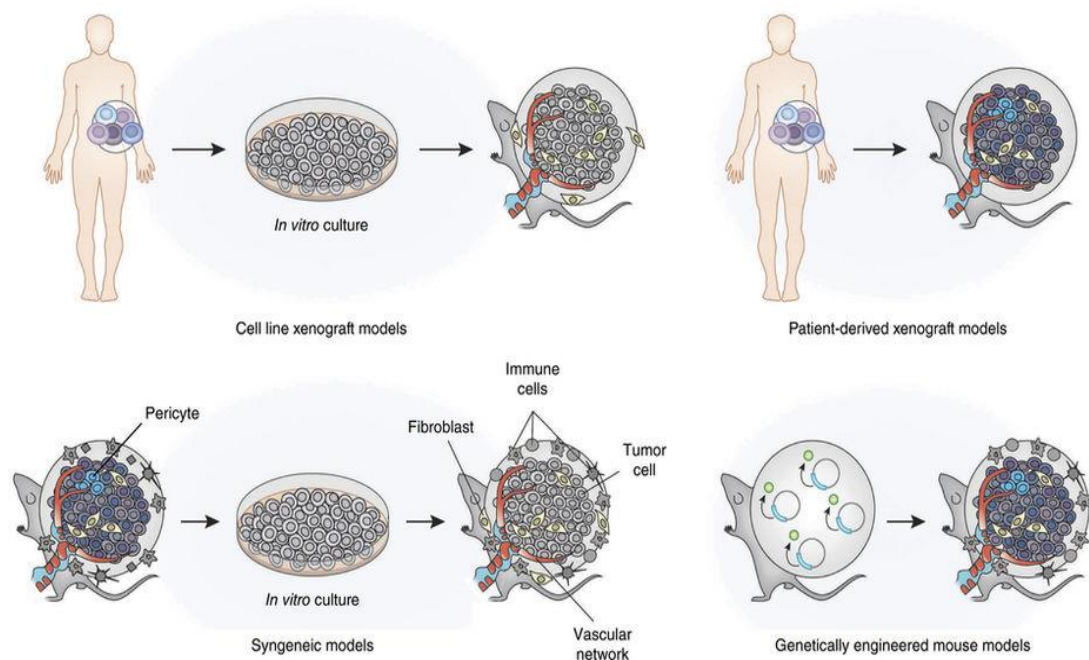
Figure 6.2: Mouse models used in tumour biology *in-vivo.* Schematic illustration of four mouse models that are commonly used in tumour biology studies. Image from (Gould et al., 2015) reused with permission from Elsevier.

6.1.4.1 Cell line xenograft models for drug development

The development of the athymic nude mice in 1968 (Pantelouris, 1968) meant that tissue cultured human tumour cells were able to grow in mice without been rejected by the host. The subcutaneous xenograft model is considered as the standard model for validating and assessing the efficacy and activity of anti-cancer agents. It is a tractable and reproducible model, is relatively fast (short duration) as well as easy to control and monitor (Jung, 2014, Gould et al., 2015). In these models changes in

tumour progression is assessed by tumour size comparing a treated to a control group. In 2005, Qu and colleagues using several pancreatic cancer xenograft models (CFPAC-1, CAPAN-1 and PANC-1 cancer cell lines) were able to show that treatment with alpha-immunoconjugate (AIC) had significantly inhibit tumour growth *in-vivo* (Qu et al., 2005). One of the main limitations of subcutaneous models is that the site of injection (tumour growth) does not represent the actual tumour (not the case for soft tissue sarcomas) and its microenvironment making the assessment of invasion and metastasis limited.

For these reasons, alternative models that represent better the site of tumour growth and the role of the microenvironment have been developed including the orthotopic xenograft model. In this model, tissue cultured human tumour cells are injected directly into their origin site. Even though this model is more clinically relevant to the progression process (i.e. invasion and angiogenesis) and in some cases, could be used as a metastatic model (mammary fat pad tumour implant model (Nozaki et al., 2003)), it possesses several limitations. More specifically, the inoculation of the cells requires good surgical skills to ensure reproducibility. Moreover, visualizing the tumours requires either the labelling of the cells and use of expensive imaging equipment or the sacrifice of the animals which limits the monitoring over time (Jung, 2014).

Other more complex models such as patient derived xenografts (tumour cells are implanted directly into athymic mice), immune-competent also known as syngeneic models (mouse tumour cells or tissue are transplanted into immune-competent mice) and genetically engineered mice (mouse genome is engineered/manipulated resulted in spontaneous tumours in mice) are often used (reviewed by (Gould et al., 2015)). However, these models are more complex and time consuming.

6.2 Aim and objectives

Aim

The aim of these chapter was to establish the pharmacokinetic (PK) characteristics of leading compounds and their efficacy in vivo.

Objectives

Objective 1: Establish the PK characteristics of compounds using *in-vivo* PK studies and different routes of administration.

Objective 2: Use subcutaneous xenograft models in immune compromised mice to determine the ability of our compounds to decrease/inhibit tumour growth.

Objective 3: Use immunohistochemistry to further evaluate the effects of the compounds on the tumour cells and tumour microenvironment.

6.3 Materials and methods

6.3.1 *In-vivo* efficacy studies

All *in-vivo* experiments were performed following the regulations of the Animals (Scientific Procedures) Act 1986 (ASPA) and after the approval of Home Office and local research ethics committees.

In these studies, we use Balb-c nude mice. Animals were provided by Envigo Corporation (Cambridgeshire, UK) or Charles River Laboratories (Massachusetts, USA) depending on the availability. The animals were housed in individually ventilated cages (IVCs) (with the appropriate bedding and flooring conditions) in environmentally controlled conditions with a 12hr light/dark cycles at ~26°C. Mice had access to adequate amount of water and 2018 Teklad Global 18% Protein Rodent Diet containing 1.01% Calcium (Harlan Laboratories, UK). The day-to-day care of the animals was carried out by the technicians in the Biological Services (The University of Sheffield, UK). All scientific procedures on animals were carried under the Home Office Project license (40/3499) and Personal license (I0EF31741).

6.3.1.1 Cell preparation and tumour inoculation

General tissue culture methods (Chapter 2) were followed with some variation. Cell lines used in the *in vivo* studies were purchased from ATCC (Virginia, USA). The cells were cultured in complete growth medium (see table 6.1 below), according to the manufacturer's instruction, in in T500 Triple Layer Flasks (Thermo Fisher, Cat #: 132913) until reach 80-90% confluency. When the confluency was reached the cells were then detached from the flasks using TrypLE Express Enzyme dissociation reagent (Thermo Fisher, Cat #: 12605). The cell suspension was counted (see chapter 2 for more details) using Countess II Automated Cell Counter (Thermo Fisher, Massachusetts, USA) prior its centrifugation at 110 x g for 5 mins. The cell pellet was re-suspended in the appropriate volume of ice cold PBS and ice cold matrigel (Corning, Cat #: 354234) (50:50 solution) depending to the cell number obtained by the count. Matrigel was used to ensure accuracy and consistency during tumour inoculation. During the cell preparation with the matrigel all reagents (PBS and

matrigel) and materials (tubes, pipette tips) used were kept on ice to ensure that the matrigel will not solidify.

Matrigel/cell suspension and syringes were transferred to the animal house on ice before injected into mice. 100ul of cell suspension (5×10^6) was injected SB into the back of twenty 6-7 weeks old female immunodeficient Nude athymic mice (Balb/c nude) for each study (10 mice in each group: treatment and vehicle control).

Table 6.1: Cell lines and corresponding complete growth media

Cell Line	Complete Growth Media	Supplements
MDA-MB-231	RPMI + 10% FBS (Sigma)	Pen/Strep + 1 mM NaPyr
CFPAC-1	DMEM + 10% FBS (Gibco)	Pen/Strep

6.3.1.2 Treatment

The treatment started a day after the injection of tumour cells into the mice and lasted for ~4weeks. Mice were treated daily IP with 100ul of the compound of interest (SHF-638) at concentration of 20mg/kg or 100ul of vehicle control. Tumour size and mouse weights were measured once a week.

Compound Preparation

A powder stock of a compound was diluted in 100% DMSO (Sigma Aldrich, Cat #: D4540) according to the following formula: $Volume\ of\ DMSO = 0.06 \times \frac{Mass\ of\ compound\ (mg)}{8mg/mL}$. The compound was then sonicated at 37°C for 10 mins. Appropriate volume of solvent (see table 6.2 below for solvent formulation) was then added to yield a 6% DMSO/94% solvent solution according to the following formula: $Volume\ of\ solvent = 0.94 \times \frac{Mass\ of\ compound\ (mg)}{8mg/mL}$. The compounds were then sonicated at 37°C for 10 mins. Following this protocol, a working stock concentration of 40mg/kg or 8mg/mL was achieved which was then aliquoted and stored at -20°C. When needed for treatments equal amounts of the compound and the solvent were mixed together resulting in 20mg/kg or 4mg/mL concentration (3% DMSO/97% solvent). A vehicle control with the same formulation (3% DMSO/97%

solvent) was used for the control group. Both vehicle control and compound were sonicated at 37°C for 10 mins prior their IP injection into the mice. Figure 6.3 below shows a schematic illustration of the experimental procedure followed.

Table 6.2: Compound solvent formulation

Reagent	Ratio
Kolliphor HS15	1 (weight in g)
Kollisolv PCGE400	3 (volume in mL)
PBS	6 (volume in mL)

At the end of each study the animals were euthanized following the appropriated procedures listed in the Animals (Scientific Procedures) Act 1986 (ASPA). The organs, bones and tumours were stored in 10% formalin for further analysis (histological studies)
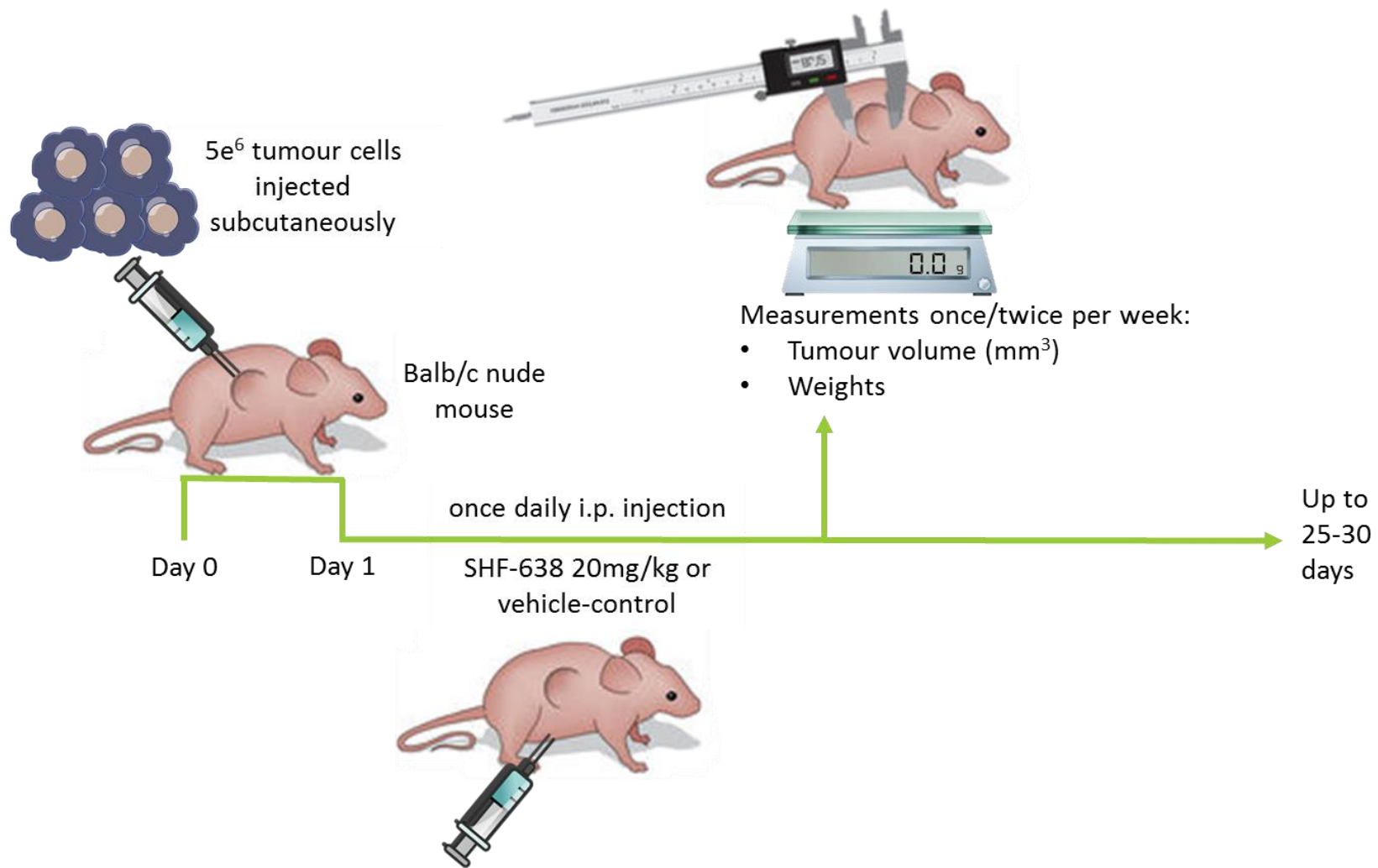
Figure 6.3: Schematic illustration of *in-vivo* experimental procedure.

6.3.2 *In-vivo* Pharmacokinetics studies.

PK studies of selected compounds were performed by WUXI Apptec (Shanghai, China) and Peakdale Molecular (Derbyshire, UK) prior their potential use in *in-vivo* studies. The following methods are described based on information provided by the organizations that performed the studies.

6.3.2.1 PK studies

Plasma PK studies were performed in two species (mice and rats) and by using different routes of administration (IV, PO and IP dosing). Depending on the species, the route of administration and the concentration selected for each study, the appropriate amount of the compound was accurately measured and dissolved with the appropriate volume of vehicle (30%PEG400:70%H_2O). The solution was then sonicated in a water bath (until clear solution was obtained), pH was adjusted if needed and sterile filtered prior dosing the animals. Appropriate volume (determined by the body weight) of the dose formulation was then administrated to the animals using the selected route.

After administration ~0.25mL of blood was collected (via jugular or another suitable vein) from each animal at different time points. All samples were transferred into ice cold microcentrifuge tubes containing 5ul of anti-coagulant (EDTA-K2 0.5M) until they been processed. Samples were then centrifuged at 3000g (4°C) for 15minutes. Plasma samples were then collected and stored in polypropylene tubes at -80°C until been examined by LC-MS/MS analysis. Schematic illustration of the procedure is shown in the figure 6.4 below. For each study the appropriate internal controls (standards) were used for data validation.

Compound administration   **LC-MS/MS analysis**

Blood serum collection   **Plasma precipitation**

Figure 6.4: Plasma *in-vivo* pharmacokinetic studies schematic illustration

6.3.3 Immunohistochemistry

At the end of each *in-vivo* study tumours were stored in 10% formalin for further histological analysis. After adequate fixation in formalin (at least 48 hours at RT), the tumour tissues were embedded in paraffin wax cassettes, forming blocks. Tissue blocks were then sectioned into 5μM paraffin ribbons using a microtome (set at a 5º angle) and fixed/bonded on clean glass microscope slides by incubating in a 65°C oven for ~20 minutes. The slides were stored at RT overnight and then transferred in the fridge (4°C) for long storage. All histological processing was performed by Mark Kinch from the Skeletal Analysis Laboratory (University of Sheffield). Prior to any specific staining procedure, slides were stained for haematoxylin and eosin by Mark Kinch.

Before any staining procedure tissue slides were labelled with date, initials, antibody and concentration using a pencil. All stained slides were scanned using Panoramic 250 Flash III slide scanner (3DHISTECH) and analysed using either ImageJ or QuPath software.

The table 6.3 and table 6.4 below list the buffers, antibodies, reagents and equipment used during the various Immunohistochemical procedures explained in more details below.

Table 6.3: Antibodies and reagents used for immunohistochemical protocols

Reagent/Amount	Source	Catalogue number
Antibodies		
Rabbit monoclonal anti-alpha smooth muscle Actin (α-SMA)	Abcam (Cambridge, UK)	ab124964
Rabbit polyclonal anti-Ki67	Abcam (Cambridge, UK)	Ab15580
Rat monoclonal anti-CD31	Dianova (Hamburg, DE)	DIA-310
Staining kits/ Reagents/Equipment		
ABC VECTASTAIN Peroxidase, Rabbit IgG Kit	Vector Laboratories (Peterborough, UK)	PK-4001
ABC VECTASTAIN Peroxidase, Rat IgG Kit	Vector Laboratories (Peterborough, UK)	PK-4004
ImmPACT DAB EqV Peroxidase (HRP) Substrate	Vector Laboratories (Peterborough, UK)	SK-4103
Hydrogen Peroxide Solution 30% (w/w)	Sigma Aldrich (Dorset, UK)	31642-1L-M
Antigen Retrieval Buffer: 100X Citrate Buffer (pH 6.0)	Abcam (Cambridge, UK)	ab93678
Gill's haematoxylin solution	Merck (Darmstadt, DE)	105174
DPX mounting medium	Sigma Aldrich (Dorset, UK)	06522
ImmEdge Hydrophobic Barrier PAP Pen	Vector Laboratories (Peterborough, UK)	H-4000
Lab Vision™ PT Module	Thermo Fisher scientific (Loughborough, UK)	A80400012
Food Steamer	Tesco PLC	2TS08
Slide staining system, StainTray™ M920	VWR (Pennsylvania, USA)	631-1923

Table 6.4: Preparation of all buffers required for Immunohistochemical protocols

Reagent/Amount	Source	Catalogue number
PBS Buffer/PBS-Tween Buffer (pH 7.4) – 2L		
20 Oxoid Phosphate Buffered Saline Tablets	Thermo Fisher scientific (Loughborough, UK)	BR0014G
2L Distilled water	N/A	N/A
2mL Tween-20 (0.05%)	Fisher Scientific (Loughborough, UK)	BP337-500
TBS Buffer/TBS-Tween Buffer (pH 7.6) – 1L		
6.05 g Tris base (Final: 50mM)	Fisher Scientific (Loughborough, UK)	BP152-1
8.76 g NaCl (Final: 150 mM)	Fisher Scientific (Loughborough, UK)	5/3120/63
Distilled water (Final: 1L)	N/A	N/A
2mL Tween-20 (0.05%)	Fisher Scientific (Loughborough, UK)	BP337-500
Adjust the pH with 1M HCl		
1M Tris-Cl (pH 8.0) – 1L		
121.1 g Tris base	Fisher Scientific (Loughborough, UK)	BP152-1
Distilled water (Final: 1L)	N/A	N/A
Adjust the pH with concentrated HCl (12.1M)		
Tris-EDTA (TE) Buffer (pH 8.0) – 500mL		
5mL 1M Tris-Cl (pH 8.0)	Refer to 1M Tris-Cl (pH 8.0) – 1L recipe	
UltraPure EDTA (0.5 M, pH 8.0)	Thermo Fisher scientific (Loughborough, UK)	15575020
494mL Distilled water	N/A	N/A

6.3.3.1 Alpha smooth muscle Actin (α-SMA) Immunohistochemical staining

Slides were first dewaxed by immersing in xylene (twice for 5 minutes each) and rehydrated for 2 minutes through decreasing alcohol concentrations (100%-75%). The slides were left to rest in distilled H_2O for ~5 minutes and then transferred in a preheated (65°C) PT module (Thermo Scientific) containing 1x citrate buffer (pH 6) (Abcam). This process (antigen retrieval) aims to eliminate any chemical modifications (methylene bridges) occurred during the fixation process that could mask the antigenic sites. Slides were incubated in the citrate buffer for 25 minutes at 95°C and cooled down to 65°C before transferred and rested in distilled H_2O for ~5 minutes. Endogenous peroxidase was then blocked by incubating slides in 3%H_2O_2 (Sigma-Aldrich) in distilled H_2O for 30 minutes at RT, to eliminate background staining. Slides were then washed twice with PBS-Tween for 5 minutes on an orbital shaker at 550-600 rpm. The regions of interest were outlined by a hydrophobic circle using PAP pen (Vector Laboratories) to reduce the usage and the waste of the reagents. Slides were then blocked with 1.5% blocking serum (part of ABC VECTASTAIN Rabbit IgG Kit) in PBS-Tween for 30 minutes at RT in an immunostaining incubation tray. Diluted (1:1000 in blocking buffer) primary antibody (Rabbit monoclonal anti-αSMA) was then added on the slides, after the removal of the blocking serum, and slides were incubated overnight at 4°C in an immunostaining incubation tray.

The next day, slides were washed twice on an orbital shaker at 550-600 rpm in PBS-Tween. This was followed by incubation with a biotinylated anti-rabbit secondary antibody (part of ABC VECTASTAIN Rabbit IgG Kit) diluted 1:200 in blocking serum, for 30 minutes at RT in an immunostaining incubation tray. After incubation with the secondary antibody slides were washed twice on an orbital shaker at 550-600 rpm in PBS-Tween and incubated in Avidin biotinylated enzyme complex (ABC Reagent) (part of ABC VECTASTAIN Rabbit IgG Kit) for 30 minutes at RT in an immunostaining incubation tray. Slides were then washed twice for 5 minutes on an orbital shaker at 550-600 rpm in PBS-Tween. Secondary antibody detection was carried out by

incubation with 3, 3'-Diaminobenzidine (DAB) (ImmPACT™ DAB EqV) for 1.5-2 minutes in the dark (positive staining was indicated by brown colour). Slides were then washed under running tap water for 5 minutes before they were counterstained with Gill's haematoxylin for 20 seconds (Merck) and rinsed with distilled water. This was followed by the dehydration of the slides through increasing concentrations of alcohol (70%-100%) for 2 minutes each and incubation in xylene twice for 5 minutes. Slides were then mounted with coverslips using DPX (distyrene, plasticiser and xylene mixture) mounting medium (Sigma-Aldrich) and left to dry for at least 30 minutes before visualised and at least overnight before scanning.

6.3.3.2 Ki67 Immunohistochemical staining

Slides were first dewaxed by immersing in xylene (twice for 5 minutes each) and rehydrated for 2 minutes through decreasing alcohol concentrations (100%-75%), before rested in distilled H_20 for 5 minutes. Antigen retrieval was achieved by incubating the slides in Tris-EDTA (TE) buffer with 0.05% Tween-20 (Fisher Scientific), for 20 minutes using a conventional food steamer. After steaming, slides were set aside to cool down for 20 minutes at RT. Slides were rinsed quickly with TE buffer and then washed twice for 5 minutes on an orbital shaker at 550-600 rpm in the same buffer. This was followed by the outlining of the regions of interest on the slides with hydrophobic circle using PAP pen (Vector Laboratories) to reduce the usage and minimise the waste of valuable reagents. Slides were then blocked with 1.5% blocking serum (part of ABC VECTASTAIN Rabbit IgG Kit) in TBS (Tris-buffered saline)-Tween buffer for 1 hour at RT in an immunostaining incubation tray. The blocking buffer was then tipped off the slides and diluted (1:250 in blocking buffer) primary antibody (Rabbit polyclonal anti-Ki67) was added followed by 1-hour incubation at RT. Slides were then washed twice with TBS buffer for 5 minutes on an orbital shaker at 550-600 rpm.

The slides were then incubated with a biotinylated anti-rabbit secondary antibody (part of ABC VECTASTAIN Rabbit IgG Kit) diluted 1:400 in blocking serum, for 30 minutes at RT in an immunostaining incubation tray. After incubation with the secondary antibody slides were washed twice on an orbital shaker at 550-600 rpm

in TBS and incubated in ABC Reagent (part of ABC VECTASTAIN Rabbit IgG Kit) for 30 minutes at RT in an immunostaining incubation tray. Slides were then washed twice for 5 minutes on an orbital shaker at 550-600 rpm in TBS. Secondary antibody detection was carried out by incubation with DAB (ImmPACT™ DAB EqV) for ~2 minutes in the dark. Slides were then washed under running tap water for 5 minutes before they were counterstained with Gill's haematoxylin for 20 seconds (Merck) and rinsed with distilled water. This was followed by the dehydration of the slides through increasing concentrations of alcohol (70%-100%) for 2 minutes each and incubation in xylene twice for 5 minutes. Slides were then mounted with coverslips using DPX mounting medium (Sigma-Aldrich) and left to dry for at least 30 minutes before visualised and at least overnight before scanning.

6.3.3.3 CD31 Immunohistochemical staining

Slides were first dewaxed by immersing in xylene (twice for 5 minutes each) and rehydrated for 2 minutes through decreasing alcohol concentrations (100%-75%), before rested in distilled H_2O for 5 minutes. Antigen retrieval was performed using a PT module (Thermo Scientific). Slides were immersed in preheated (80°C) 1x citrate buffer (pH 6) (Abcam) and incubated at 95°C for 25 minutes. Slides were then cooled down to 65°C before transferred and rested in distilled H_2O for ~5 minutes. This was followed by the immersion and incubation of the slides in 3%H_2O_2 (Sigma-Aldrich) in distilled H_2O for 30 minutes at RT to block endogenous peroxidase. Slides were then washed with tap water for 5 minutes on an orbital shaker at 550-600 rpm. Excess liquid was removed, and the regions of interest were outlined by a hydrophobic circle using PAP pen (Vector Laboratories). Slides were then blocked with 1.5% blocking serum (part of ABC VECTASTAIN Rat IgG Kit) in TBS-Tween for 30 minutes at RT in an immunostaining incubation tray. Slides were then incubated in diluted (1:50 in blocking buffer) primary antibody (Rat monoclonal anti-CD31) overnight at 4°C in an immunostaining incubation tray.

The next day, slides were washed three times on an orbital shaker at 550-600 rpm in TBS-Tween and incubated with a biotinylated anti-rat secondary antibody (part of ABC VECTASTAIN Rat IgG Kit) diluted 1:200 in blocking serum, for 30 minutes at RT

in an immunostaining incubation tray. After incubation with the secondary antibody slides were washed once for 10 minutes on an orbital shaker at 550-600 rpm in PBS buffer. Slides were then incubated in ABC Reagent (part of ABC VECTASTAIN Rat IgG Kit) for 30 minutes at RT in an immunostaining incubation tray. Slides were then washed once for 5 minutes an orbital shaker at 550-600 rpm in PBS buffer. Secondary antibody detection was carried out by incubation with DAB (ImmPACT™ DAB EqV) for ~10 minutes in the dark. Slides were then washed twice for 5 minutes on an orbital shaker at 550-600 rpm in PBS buffer before they were counterstained with Gill's haematoxylin for 20 seconds (Merck) and rinsed with distilled water. This was followed by the dehydration of the slides through increasing concentrations of alcohol (70%-100%) for 2 minutes each and incubation in xylene twice for 5 minutes. Slides were then mounted with coverslips using DPX mounting medium (Sigma-Aldrich) and left to dry for at least 30 minutes before visualised and at least overnight before scanning.

6.3.3.4 Ki67 staining analysis using QuPath Software

QuPath v0.1.2, an open source digital pathology software funded by Invest Northern Ireland and Cancer Research UK, was used to identify and count the positive (brown) Ki67 staining. Slide images obtained using Panoramic 250 Flash III slide scanner (3DHISTECH) were opened in QuPath software and using the drawing tools the whole tumour sections were selected as regions of interest (ROIs)/annotations. This allowed the quantify a whole tumour section rather than some selected regions. Then the command positive cell detection (path: Analyse → Cell analysis → Positive cell detection command) was performed, using the single threshold option, to distinguish and quantify the brown stained (positive) cells from the negative haematoxylin (blue) stained cells. Positive cells were defined based on the average DAB (brown) nuclear staining (Score compartment value of Nucleus: DAB OD mean). The same settings (see figure 6.5 below) were used for all images and data (percentage positive cells) were plotted using GraphPad Prism 7.03. Plotted data were presented as mean +/- SD and significance was calculated using an unpaired nonparametric Mann-Whitney t test, due to the small group numbers. Statistical

significance was defined as P<0.05. A more graphical illustration of the analysis can be found in figure 6.6 below.
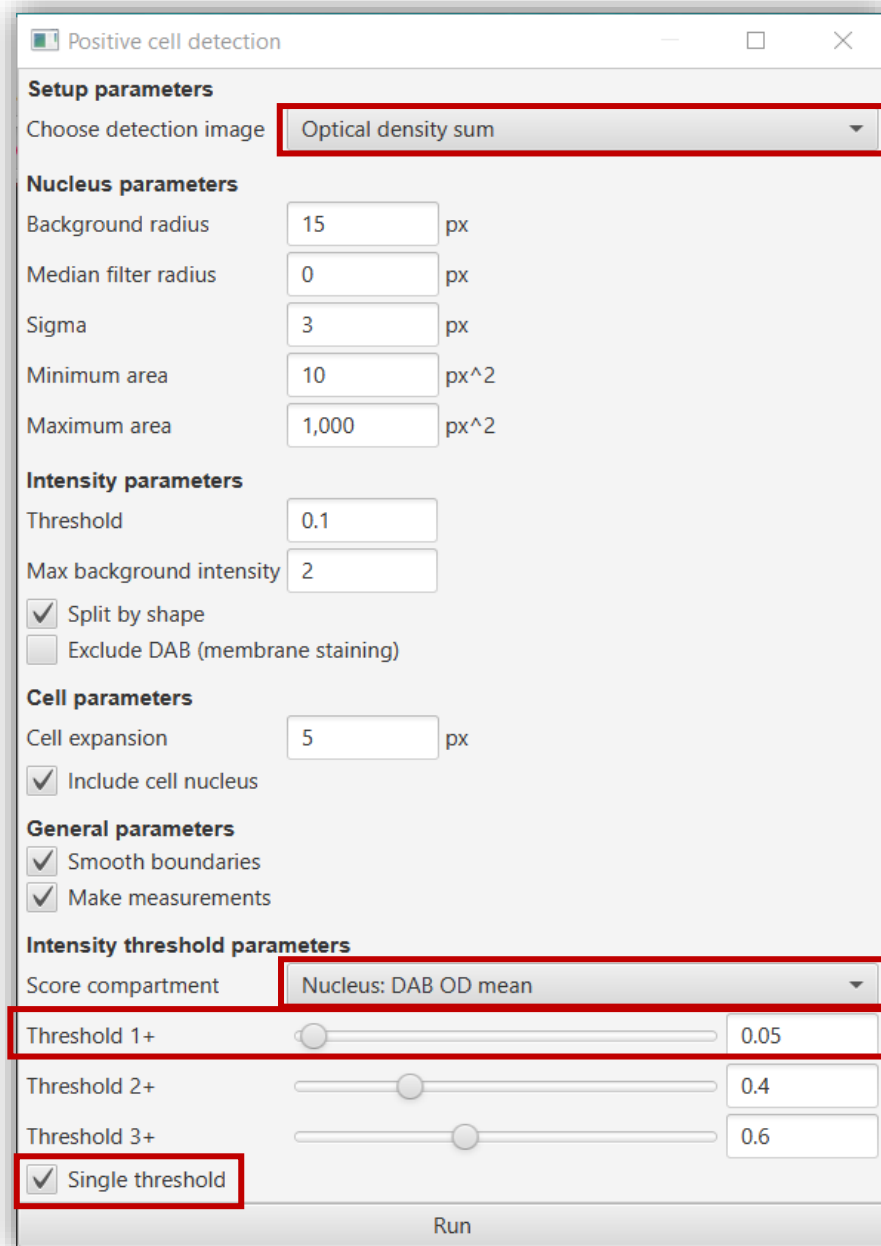
Figure 6.5: QuPath Positive cell detection command settings. Screenshot obtained from QuPath software showing the settings used to analyse DAB positive Ki67 cells. Detection image was set to optimal density sum, score compartment was set to Nucleus: DAB OD mean and a single threshold of 0.05 was used.
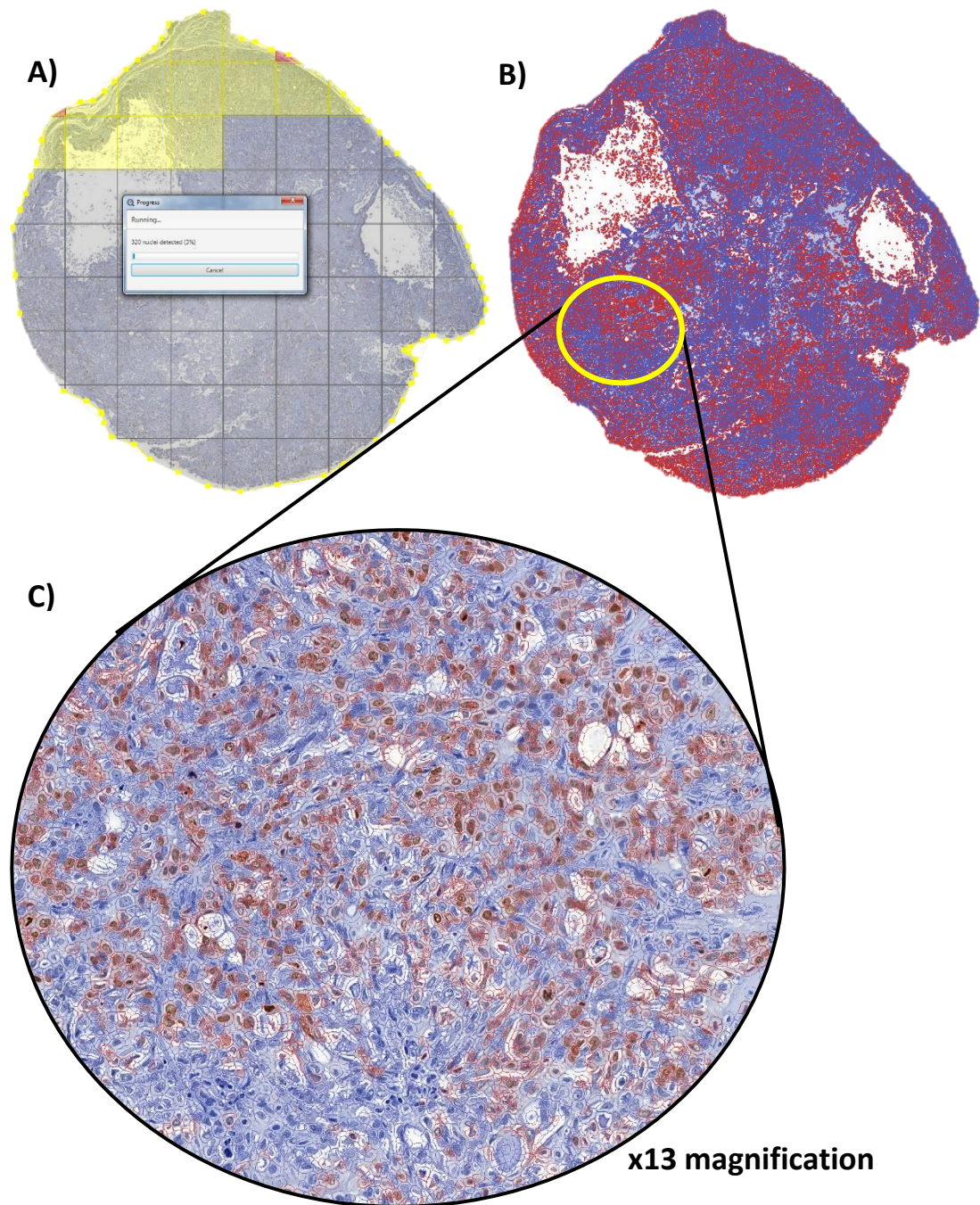
Figure 6.6: Illustration of Ki67 staining analysis procedure. A) Showing the selection of the region of interest (yellow outline) and the processing of the slide image (using QuPath v0.1.2). **B)** Showing the positively (red) and negatively (blue) DAB stained cells after the processing of the image using the positive cell detection command of the QuPath software. **C)** A magnified (x13) image of a post-processed region of the slide image, showing the accurate detection and distinction of positive and negative cells.

6.3.3.5 α-SMA staining analysis using ImageJ Software

Slide images were first opened with ImageJ v1.49 and the regions of interest (ROI) was selected using the freehand selection tool. Similarly, to the Ki67 analysis the whole tumour section was selected to ensure accuracy and avoid biased selection of regions. Using the colour threshold tool (path: Image → Adjust → Colour threshold), brown DAB (positive) staining was highlighted while all blue haematoxylin (negative) stained sections were excluded. Any background staining was excluded using the brightness section of the tool. This was followed by conversion of the images to 8-bit (path: Image → Type → 8-bit) and readjustment of the threshold (path: Image → Adjust → Threshold) to ensure correct selection of the positive regions. The analyse particles tool (path: Analyse → Analyse particles) was then used to generate "masks" of the stained regions. Area fraction measurement was selected using the set measurements tool (path: Analyse → Set measurements). The area fraction of these mask images was then measured (path: Analyse → Measure), and the percentage area of positive staining was recorded. The same settings were used for all images analysed. Data (percentage positive cells) were plotted using GraphPad Prism 7.03. Plotted data were presented as mean +/- SD and significance was calculated using an unpaired nonparametric Mann-Whitney t test, due to the small group numbers. Statistical significance was defined as $P<0.05$. Figure 6.7 below shows an illustration of the analysis using ImageJ software.

6.3.3.5 CD31 staining analysis using ImageJ Software

The same procedure described above was used to analyse the CD31 stained slides. Due to the low intensity of the CD31 staining the analysis of the whole slide was not possible. Representative regions of interest (ROIs) (four snapshots per slide) were obtained using QuPath software and analysed using ImageJ software. Plotted data were presented as mean +/- SD and significance was calculated using an unpaired nonparametric Mann-Whitney t test, due to the small group numbers. Statistical significance was defined as $P<0.05$.
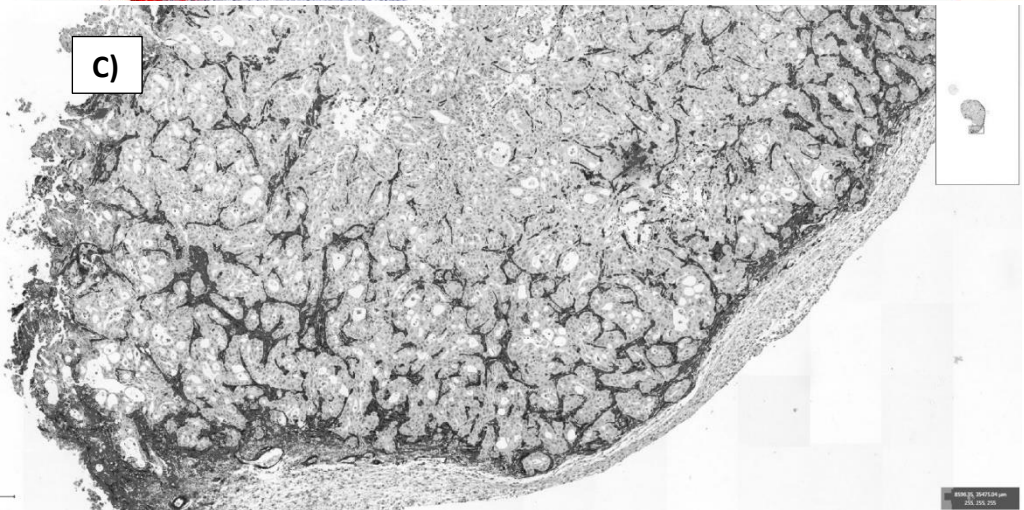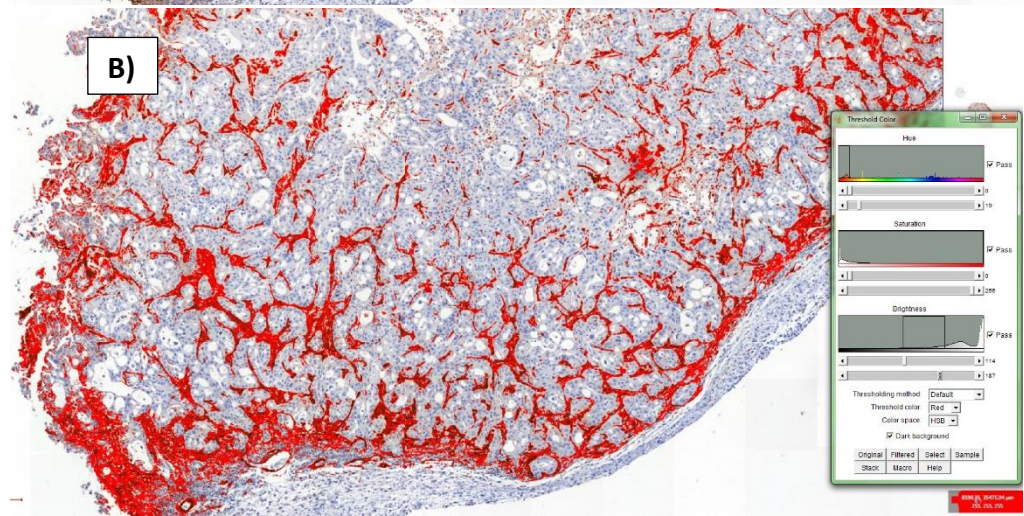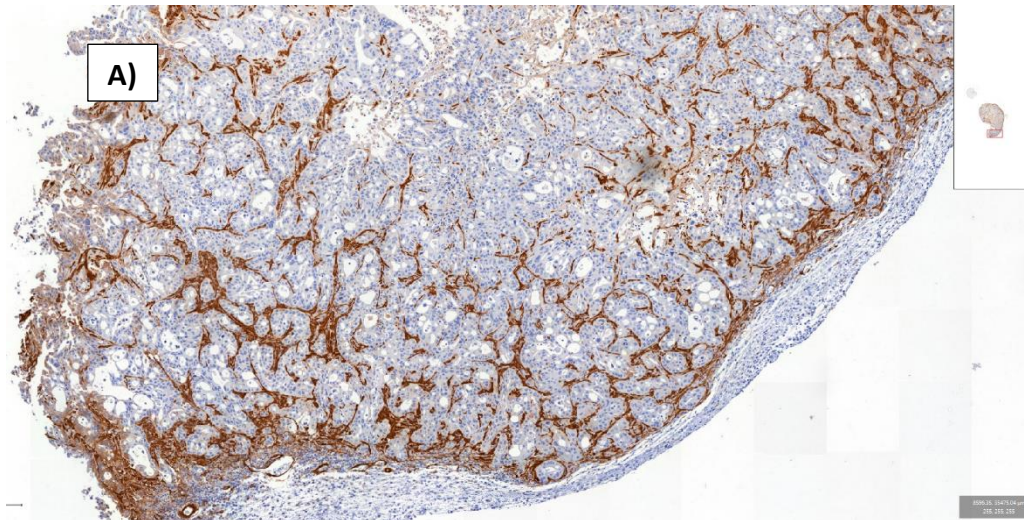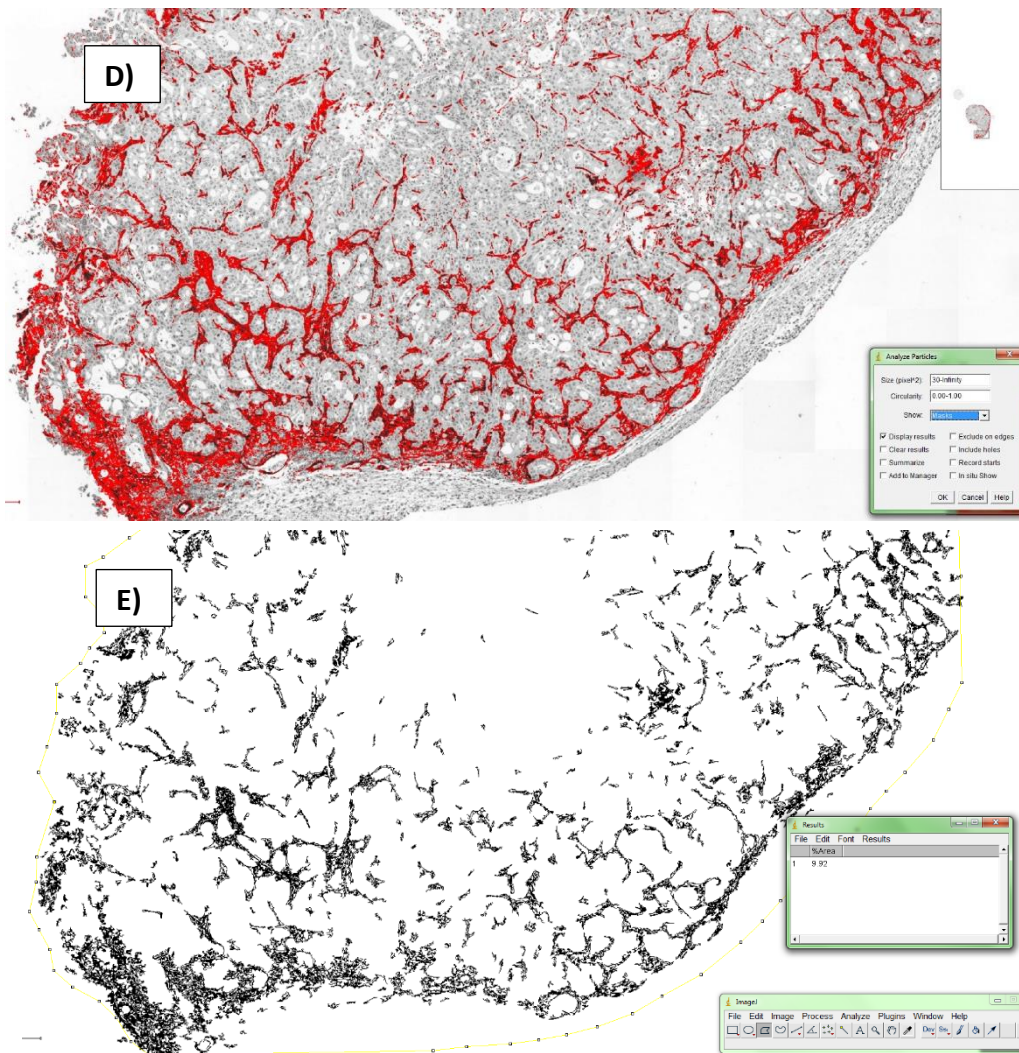
Figure 6.7: Illustration of α-SMA staining analysis procedure. A) The original image that was obtained by scanning the slide using Panoramic 250 Flash III slide scanner (3DHISTECH). **B)** Positive DAB (brown) staining was highlighted while negative haematoxylin (blue) staining was excluded using the colour threshold tool. **C)** The image was converted to 8-bit. **D)** Using the threshold tool, the highlighted areas were selected again. **E)** A mask of the highlighted region was generated, and the area of positive staining was measured.

6.4 Results

6.4.1 Identification of compound bioavailability using various routes of administration

To establish the oral bioavailability and pharmacokinetic characteristics of our compounds plasma PK studies were performed. Compounds from the two main structural groups of our screening cascade were selected based on their potency and selectivity over the AM2r O/E cells. All compounds shown below were tested using two different routes of administration (IV and IP) in different species including mouse and rat. No adverse effects were observed from the administration of any of the compounds via all the routes.

The first compound to be tested was SHF-408-AA002 (first compound of primary structural series), a breakthrough compound that showed as described in chapter 4 similar potency over CGRPr and AM2r O/E cells. SHF-408 was administrated intravenously into 3 male Sprague Dawley (SD) fasted rats, blood samples were collected at different time points (T_{last}: 24hours) and analysed using LC-MS/MS. Pharmacokinetic parameters such as C_0, $T_{1/2}$, Cl, V_{dss}, and AUC_{0-inf} were determined from the plasma concentration – time data obtained from LC-MS/MS analysis (data shown in Figure 6.8 below). SHF-408 had a peak concentration (C_0) of 1665 ng/mL, half-life ($T_{1/2}$) of 6.01 hours, clearance rate (Cl) of 66.8 mL/min/kg and distribution rate (V_{dss}) of 15.8 L/kg. The overall exposure AUC_{0-last} and AUC_{0-inf} to the drug were 488 and 502 ng.h/mL respectively. Following IP administration (in 3 male CD-1 fasted mice) of SHF-408, the maximum concertation (1330 ng/mL) was observed after 25 minutes (T_{max}). The half-life of the compound after IP injection was 1.12 hours and the overall exposure (AUC_{0-last}) after 8 hours (T_{last}) was 1955 ng.h/mL (more details in Figure 6.9 below).

Similar experimental procedures were followed when investigating the PK characteristics of our lead compound SHF-638-AA004. The plasma concentration of the compound after IV administration was tested both in male Sprague Dawley (SD) fasted rats and in male CD-1 fasted mice. After administration in mice (n=3) a peak mean concentration of 1366 ng/mL was observed. The mean elimination half-life

($T_{1/2}$) of the compound was 1.33 hours and the clearance rate 37.8 mL/min/kg. The overall exposure $AUC_{0\text{-}last}$ and $AUC_{0\text{-}inf}$ to the drug were 901 and 914 ng.h/mL respectively. More details can be found at Figure 6.10 below. Moreover, following IV administration in rats (n=3) SHF-638 showed higher maximum concentration of 2631 ng/mL and higher elimination half-life of 3.01 hours. The distribution rate and clearance rate were 8.04 L/kg and 77.0 mL/min/kg respectively. More details such as $AUC_{0\text{-}last}$ and $AUC_{0\text{-}inf}$ can be found in Figure 6.11 below). Furthermore, after an IP injection of SHF-638 into rats (n=3), a C_{max} of 1290 ng/mL was observed within 25 minutes. The elimination half-life of the compound was 5.9 hours. It is worth mentioning that the last observed concentration was after 24hours which gave a total exposure $AUC_{0\text{-}last}$ of 3311 ng.h/mL. More details can be found at Figure 6.12 below.

The PK characteristics after oral (PO) administration of SHF-638 was determined showing significantly low bioavailability (see appendix figure 8.3).

A) Plasma Concentration of SHF-408-AA002 after Intravenous (IV) Dosing at 2 mg/kg (Rat n=3)

B)
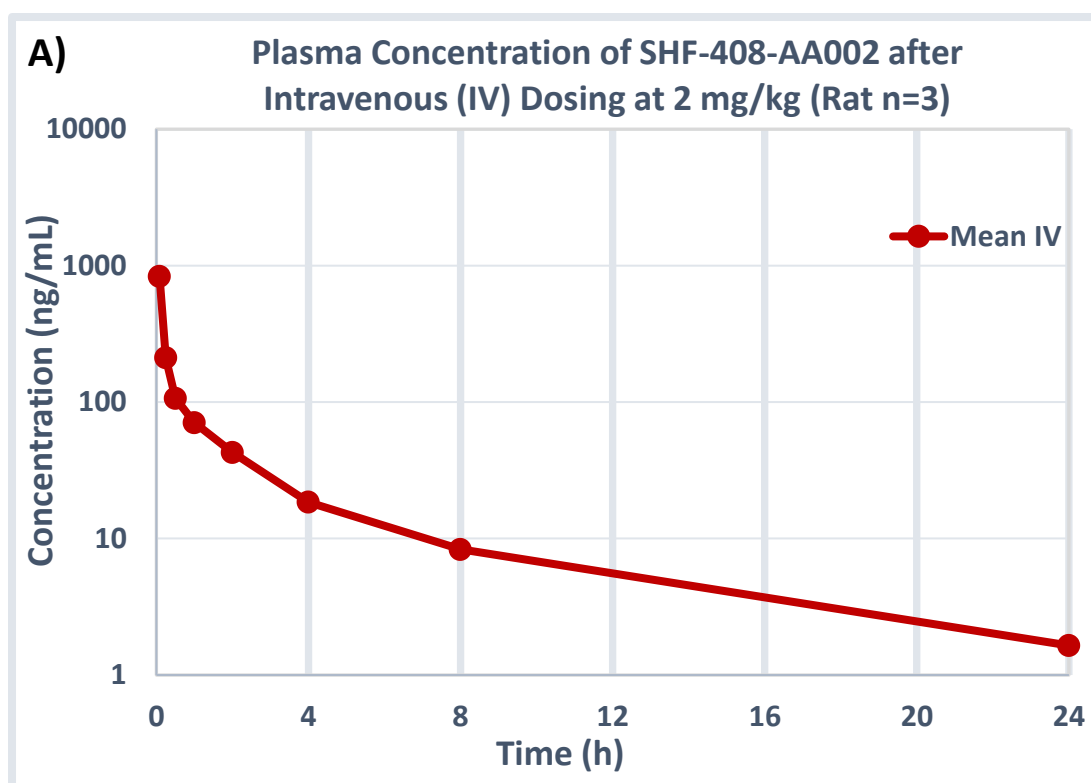
PK Parameters	Mean		SD	CV (%)
SHF-408-AA002 (2mg/kg IV dosing)				
Points used for $T_{1/2}$	3.00	±	--	--
C_0 (ng/mL)	1665	±	303	18.2
$T_{1/2}$ (h)	6.01	±	0.613	10.2
Vd_{ss} (L/kg)	15.8	±	1.17	7.43
Cl (mL/min/kg)	66.8	±	6.15	9.20
T_{last} (h)	24.0	±	--	--
AUC_{0-last} (ng.h/mL)	488	±	45.7	9.37
AUC_{0-inf} (ng.h/mL)	502	±	48.8	9.72

C_0: Maximum conc. observed

AUC: Area under the conc. – time curve

AUC_{0-last}: Drug exposure until the last observed conc.

AUC_{0-inf}: Total drug exposure over time

$T_{1/2}$: Terminal phase half-life

T_{last}: Time at which the final conc. is observed

Vd_{ss}: Volume of distribution

Figure 6.8: SHF-408-AA002 PK Characteristics after IV administration. **A)** Rat plasma concentration of SHF-408-AA002 after Intravenous (IV) dosing (2mg/kg). **B)** PK characteristics obtained after IV administration of SHF-408 in rats.

A) Plasma Concentration of SHF-408-AA002 after Intraperitoneal (IP) Dosing at 10 mg/kg (Mouse n=6)

B)
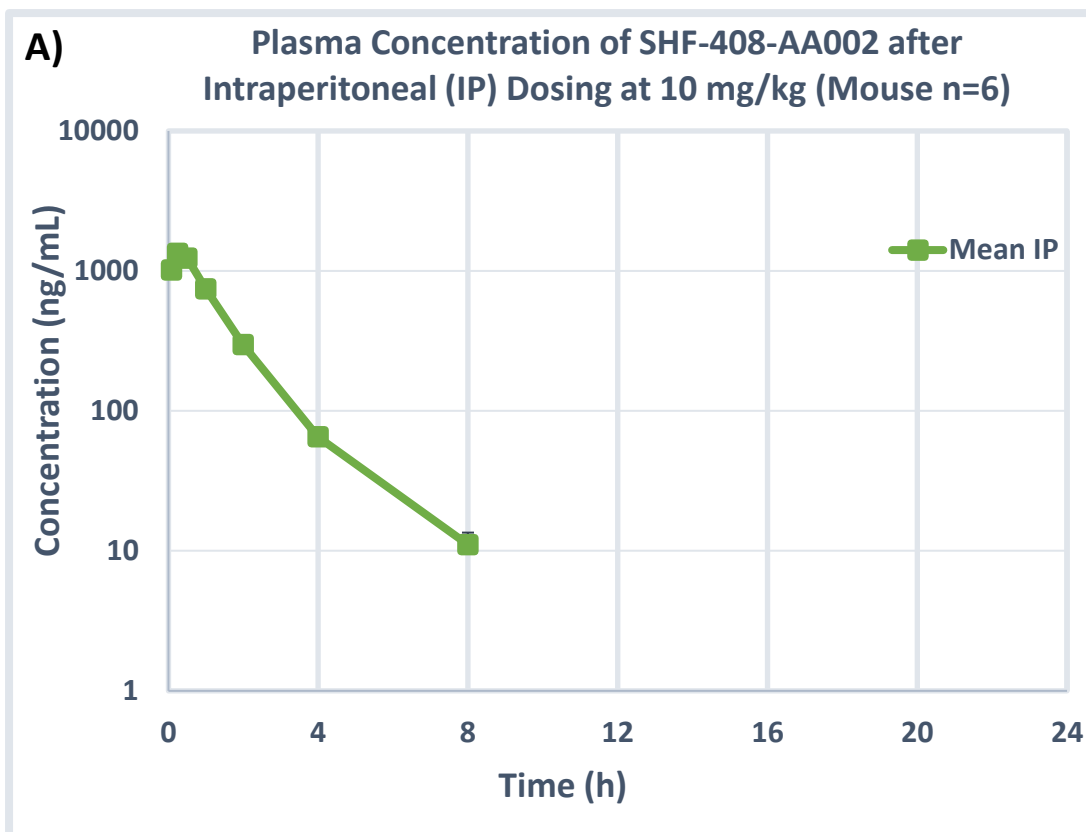
PK Parameters	
SHF-408-AA002 (10mg/kg IP dosing)	
Points used for $T_{1/2}$	**5.00**
C_{max} (ng/mL)	**1330**
T_{max} (h)	**0.250**
$T_{1/2}$ (h)	**1.12**
T_{last} (h)	**8.00**
AUC_{0-last} (ng·h/mL)	**1955**
AUC_{0-inf} (ng.h/mL)	**1973**

C_{max}: Maximum conc. observed

AUC: Area under the conc. – time curve

AUC_{0-last}: Drug exposure until the last observed conc.

AUC_{0-inf}: Total drug exposure over time

T_{max}: Time at which the maximum conc (C_{max}) is observed

$T_{1/2}$: Terminal phase half-life

T_{last}: Time at which the final conc. is observed

Figure 6.9: SHF-408-AA002 PK Characteristics after IP administration. **A)** Mouse plasma concentration of SHF-408-AA001 after Intraperitoneal (IP) dosing (10mg/kg). **B)** PK characteristics obtained after IV administration of SHF-408 in mice.

A)

Plasma Concentration of SHF-638-AA004 after Intravenous (IV) Dosing at 2 mg/kg (Mouse n=3)

B)
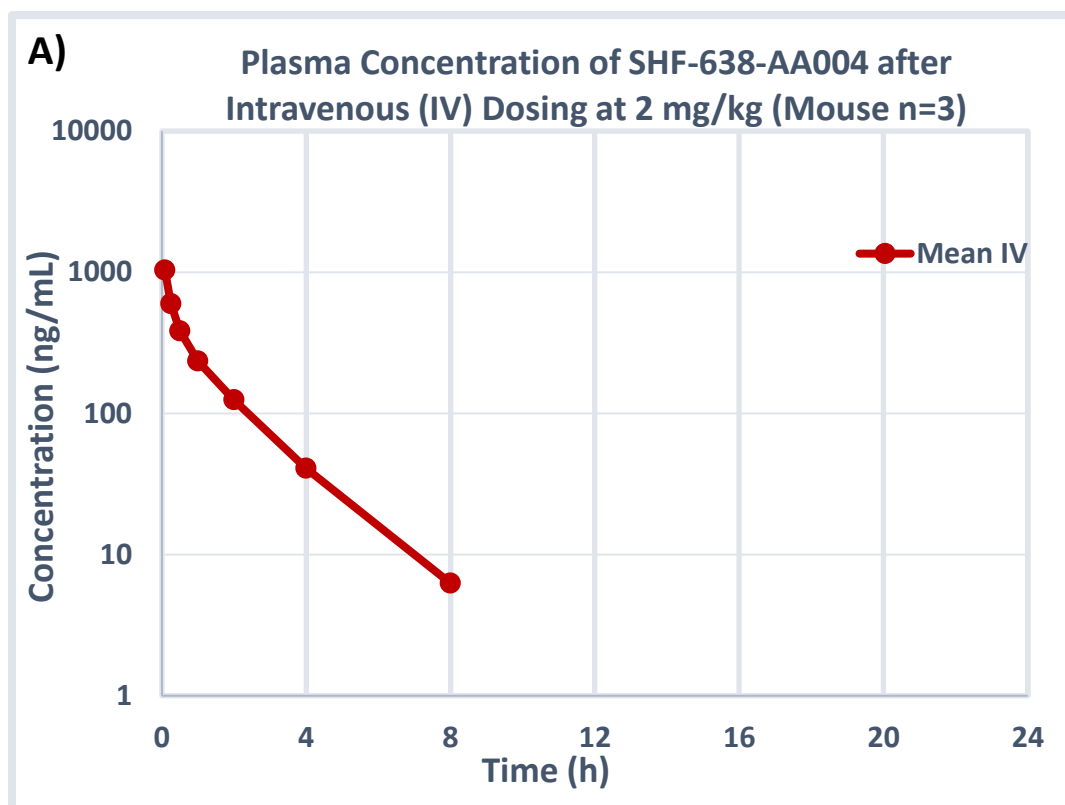
PK Parameters	Mean		SD	CV (%)
SHF-638-AA004 (2mg/kg IV dosing) - Mouse				
Points used for $T_{1/2}$	ND	±	--	--
C_0 (ng/mL)	1366	±	172	12.6
$T_{1/2}$ (h)	1.33	±	0.231	17.4
Vd_{ss} (L/kg)	3.18	±	0.041	1.29
Cl (mL/min/kg)	37.8	±	8.92	23.6
T_{last} (h)	8.00	±	--	--
AUC_{0-last} (ng.h/mL)	901	±	201	22.3
AUC_{0-inf} (ng.h/mL)	914	±	213	23.2

*ND: Not Determined

C_0: Maximum conc. observed
AUC: Area under the conc. – time curve
AUC_{0-last}: Drug exposure until the last observed conc.
AUC_{0-inf}: Total drug exposure over time
$T_{1/2}$: Terminal phase half-life
T_{last}: Time at which the final conc. is observed
Vd_{ss}: Volume of distribution at steady state
CL: Clearance of Drug

Figure 6.10: SHF-638-AA004 PK Characteristics after IV administration. **A)** Mouse plasma concentration of SHF-638-AA004 after Intravenous (IV) dosing (2mg/kg). **B)** PK characteristics obtained after IV administration of SHF-638 in mice.

A) Plasma Concentration of SHF-638-AA004 after Intravenous (IV) Dosing at 2 mg/kg (Rat n=3)

B)
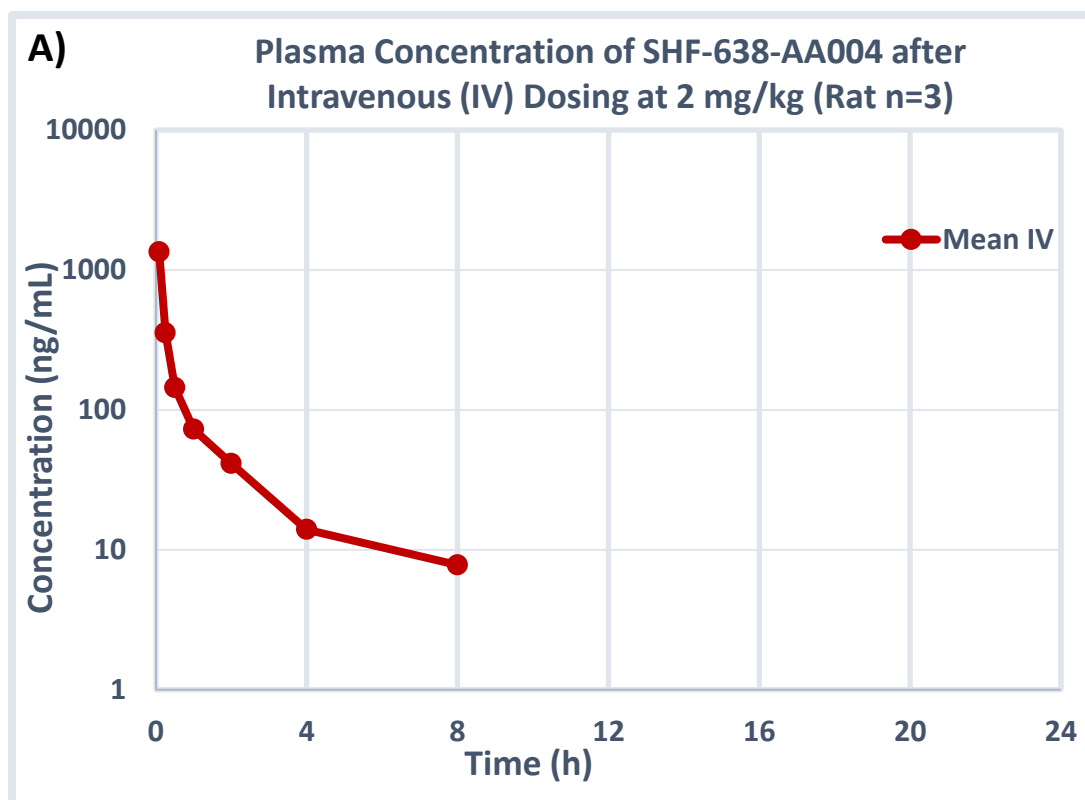
PK Parameters	Mean		SD	CV (%)
SHF-638-AA004 (2mg/kg IV dosing) - Rat				
Points used for $T_{1/2}$	ND	±	--	--
C_0 (ng/mL)	2631	±	325	12.3
$T_{1/2}$ (h)	3.01	±	2.04	67.7
Vd_{ss} (L/kg)	8.04	±	2.70	33.6
Cl (mL/min/kg)	77.0	±	5.10	6.62
T_{last} (h)	ND	±	--	--
AUC_{0-last} (ng.h/mL)	562	±	45.6	8.11
AUC_{0-inf} (ng.h/mL)	577	±	39.7	6.87

*ND: Not Determined

C_0: Maximum conc. observed
AUC: Area under the conc. – time curve
AUC_{0-last}: Drug exposure until the last observed conc.
AUC_{0-inf}: Total drug exposure over time
$T_{1/2}$: Terminal phase half-life
T_{last}: Time at which the final conc. is observed
Vd_{ss}: Volume of distribution at steady state
CL: Clearance of Drug

Figure 6.11: SHF-638-AA004 PK Characteristics after IV administration. **A)** Rat plasma concentration of SHF-638-AA004 after Intravenous (IV) dosing (2mg/kg). **B)** PK characteristics obtained after IV administration of SHF-638 in rats.

204

A)

Plasma Concentration of SHF-638-AA004 after Intraperitoneal (IP) Dosing at 10 mg/kg (Mouse n=3)

B)
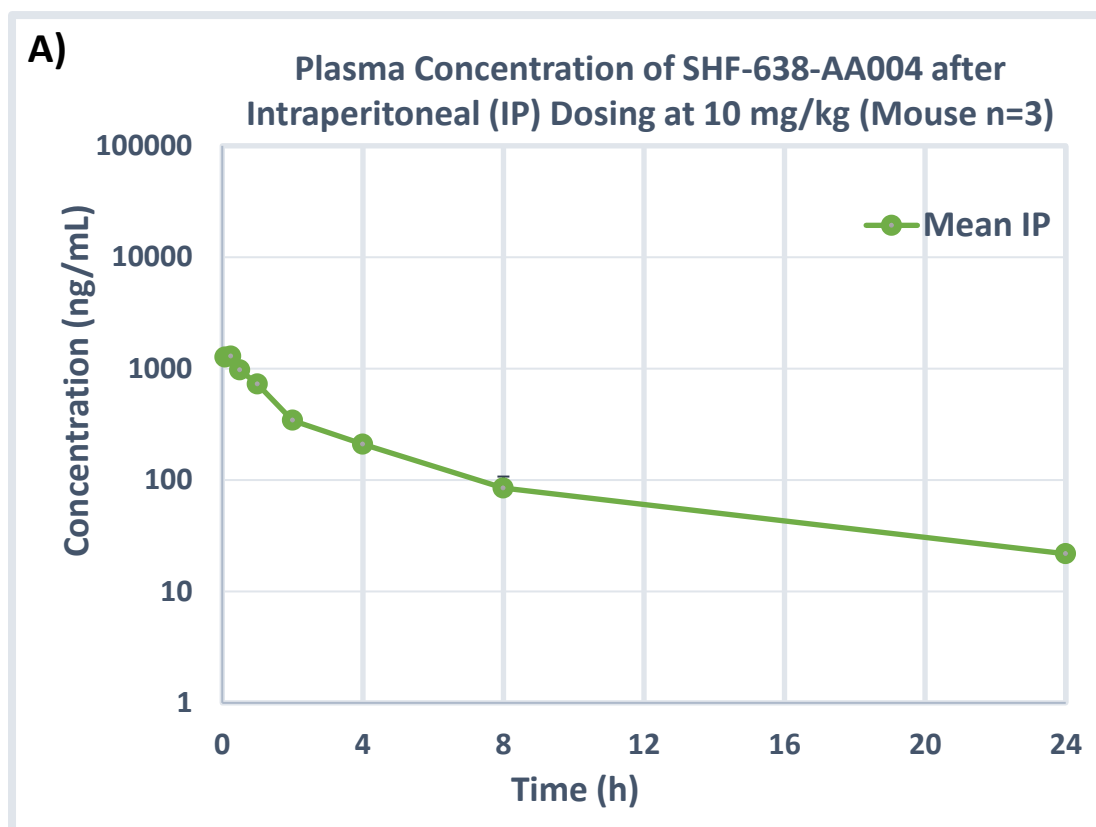
PK Parameters	
SHF-0000638-AA004 (10mg/kg IP dosing)	
Points used for $T_{1/2}$	4.00
C_{max} (ng/mL)	1290
T_{max} (hr)	0.250
$T_{1/2}$ (hr)	5.90
T_{last} (hr)	24.0
AUC_{0-last} (ng.h/mL)	3311
AUC_{0-inf} (ng.h/mL)	3497

C_{max}: Maximum conc. observed

AUC: Area under the conc. – time curve

AUC_{0-last}: Drug exposure until the last observed conc.

AUC_{0-inf}: Total drug exposure over time

T_{max}: Time at which the maximum conc (C_{max}) is observed

$T_{1/2}$: Terminal phase half-life

T_{last}: Time at which the final conc. is observed

Figure 6.12: SHF-638-AA004 PK Characteristics after IP administration. **A)** Mouse plasma concentration of SHF-638-AA004 after Intraperitoneal (IP) dosing (10mg/kg). **B)** PK characteristics obtained after IV administration of SHF-638 in mice.

6.4.2 *In-vivo* activity/efficacy of SHF-638-AA004

The *in-vivo* efficacy of the lead compound was established using subcutaneous xenografts models with pancreatic (CFPAC-1) and breast (MDA-MB-231) cancer cell lines. As described in the material and methods section above, SHF-638-AA004 (at a 20mg/kg dose) or a vehicle control was administrated once daily by intraperitoneal injection (IP) following the inoculation of tumour cells subcutaneously into the back of Balb-c nude mice. Tumour volume (mm^3) and mice weights were measured once or twice a week to monitor the tumour growth and ensure the wellbeing of the mice.

The compound was very well tolerated as no adverse effects were observed from the administration of SHF-638 or the vehicle control. Administration of SHF-638 in MDA-MB-231 xenograft mice had a significant inhibition of tumour growth as early as week one (~29%, P<0.02) with the biggest reduction of ~55% (P<0.03) shown at week 4. Moreover, no significant different was observed in liver and kidney mass between control and treatment group mice. More details can be found in figure 6.13 below. Interestingly, administration of SHF-408-AA002 twice daily at a dose of 20mg/kg (i.e.40mg/kg/day), had no significant effect on the tumour volume when compared to the vehicle control, even though the tumours in the treatment group grew in a lower rate compared to the control group (Figure 6.14).

Furthermore, similarly to the MDA-MB-231 model, treatment of SHF-638 had tumour growth inhibitory effects in the CFPAC-1 xenograft model when compared with the control mice. More specifically, significant inhibition in tumour growth was observed as soon as day 5 (~21%, P<0.03) with the biggest reduction of ~56% (P<0.0001) shown at week 3. Significant reduction up to 50% was maintained up to week 4 (Day 31, P=0.005). Moreover, significant difference (18% decrease) in liver mass was found between the treatment and the control group after the completion of the study (P=0.005). No significant difference was observed in kidney mass. More details can be found in figure 6.15 below.

M D A - M B - 2 3 1 c e l l s +
S H F - 6 3 8 - A A 0 0 1 2 0 m g / k g (o n c e d a i l y)
T u m o u r v o l u m e
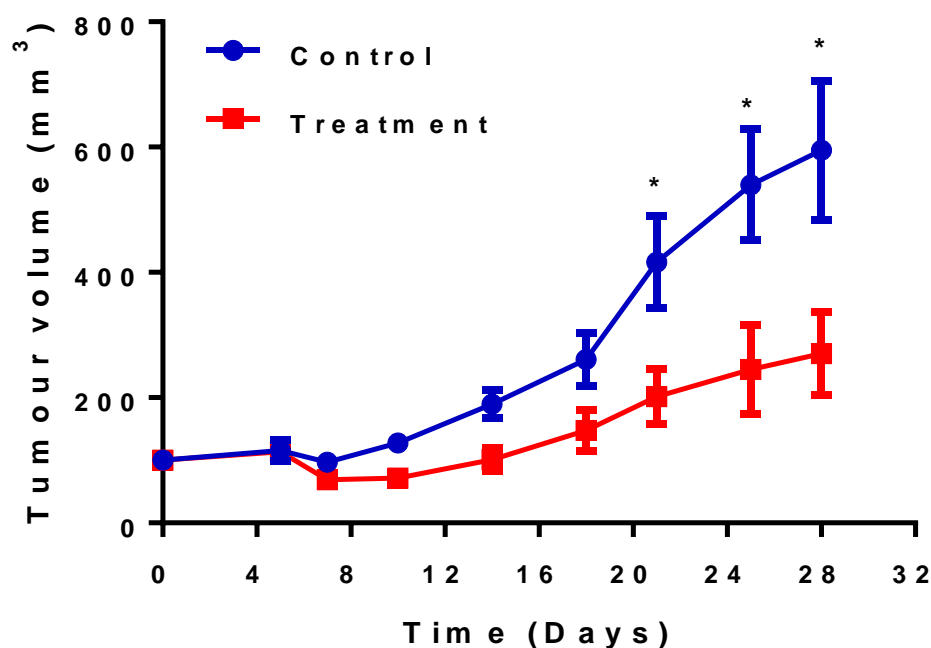
Time (Days)	Percentage decrease (%)	P value
7	29.2	0.0183
10	43.9	0.0050
14	46.6	0.0087
18	43.3	0.0532
21	51.6	0.0256
24	54.6	0.0215
28	54.5	0.0247

Figure 6.13(i): *In-vivo* **efficacy of SHF-638-AA004 on MDA-MB-231 subcutaneous xenografts.** Once daily IP administration of SHF-638 (20mg/kg) had a significant inhibition of tumour growth as early as week one when compared to the vehicle control. The biggest reduction of ~55% was observed at week 4. Data are presented as Mean +/- SD.

A)
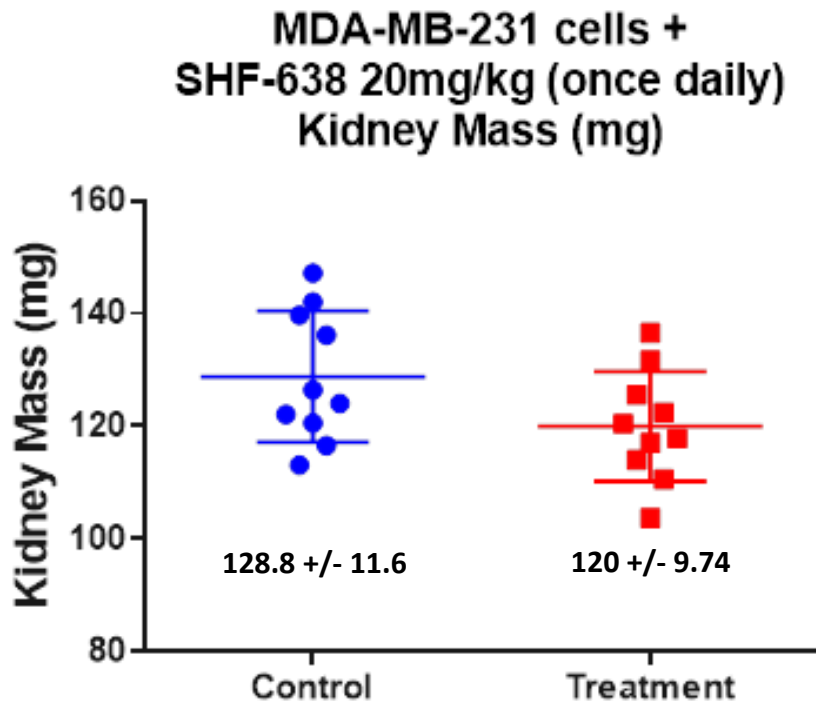
B)
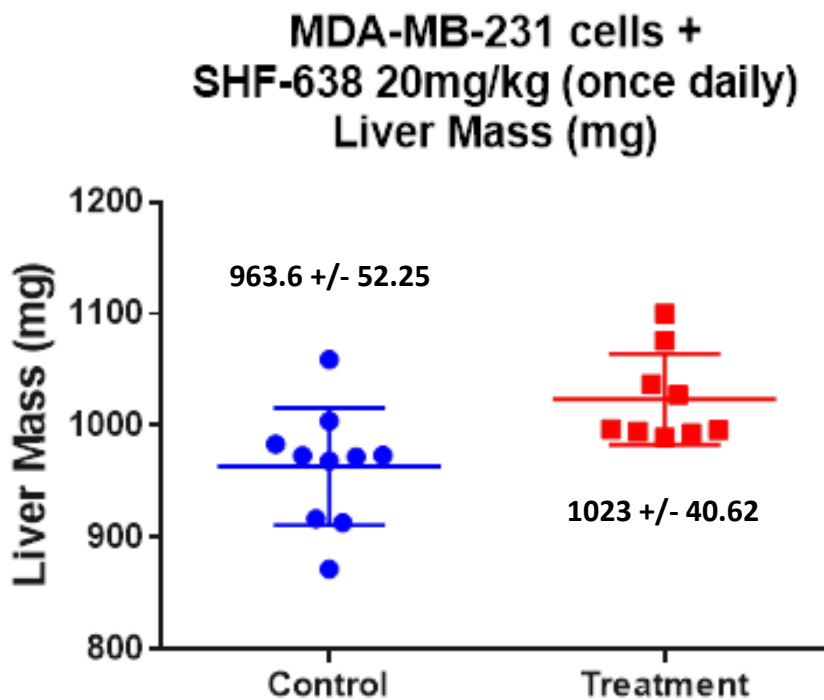
Figure 6.13(ii): *In-vivo* **efficacy of SHF-638-AA004 on MDA-MB-231 subcutaneous xenografts.** Daily administration of SHF-638 had no significant effect on kidney **(A)** and liver **(B)** mass when compared to vehicle control group. Data are presented as Mean +/- SD. In the liver data, an outlier in the treatment group was identified using ROUT outlier test and the point was excluded from the calculation.
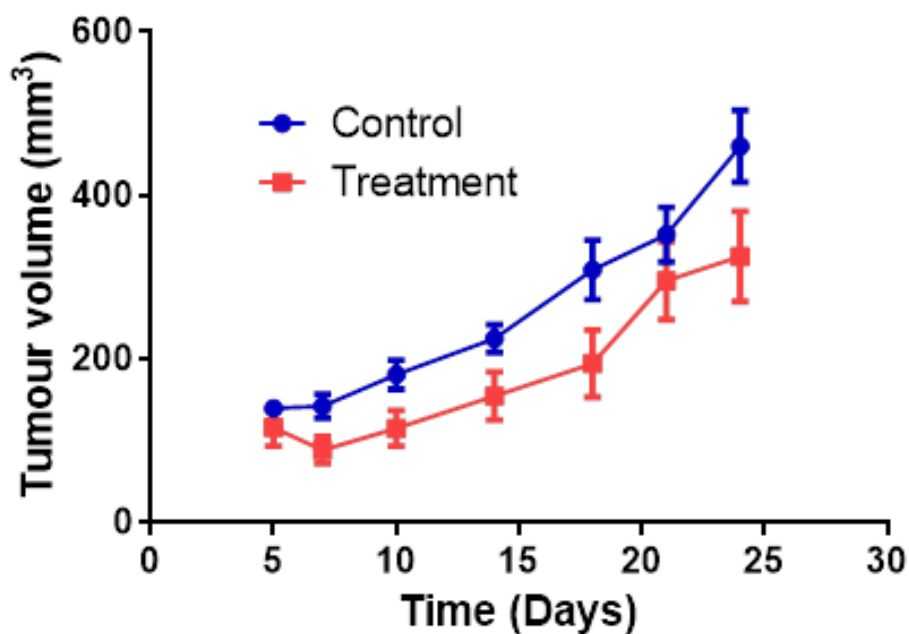
Figure 6.14: *In-vivo* **efficacy of SHF-408-AA002 on MDA-MB-231 subcutaneous xenografts.** Twice daily administration of SHF-408 (20mg.kg) had no significant effect the tumour volume when compared with the control group. Data are presented as Mean +/- SD.

CFPAC-1 cells +
SHF-638-AA001 20mg/kg (once daily)
Tumour volume
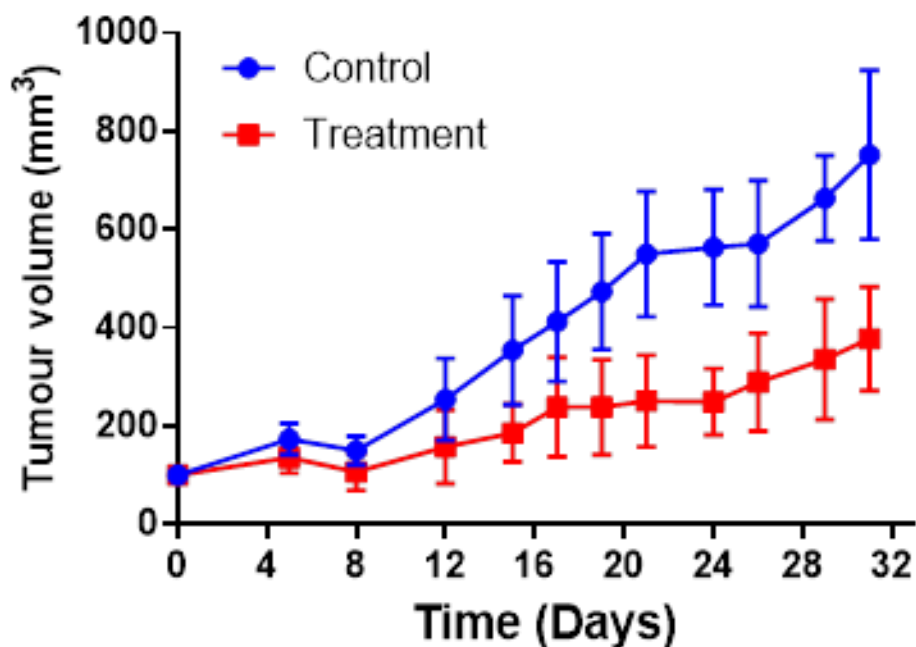
Time (Days)	Percentage decrease (%)	P value
5	21.5	0.0234
12	38.1	0.0202
17	42.2	0.0043
19	49.6	0.0003
21	54.4	<0.0001
24	55.8	<0.0001
26	49.3	0.0008
31	49.7	0.0005

Figure 6.15(i): *In-vivo* **efficacy of SHF-638-AA004 on CFPAC-1 subcutaneous xenografts.** Once daily IP administration of SHF-638 (20mg/kg) had a significant inhibition in tumour volume as soon as day 5 with the biggest reduction of ~56% to be observed at week 3. Data are presented as Mean +/- SD.

A)

CFPAC-1 cells +
SHF-638-AA001 20mg/kg (once daily)
Kidney mass (mg)

139.8 +/- 11.6

133.5 +/- 18.6

B)

CFPAC-1 cells +
SHF-638-AA001 20mg/kg (once daily)
Liver mass (mg)

** 18% decrease

1109 +/- 64.5

904.6 +/- 196.4
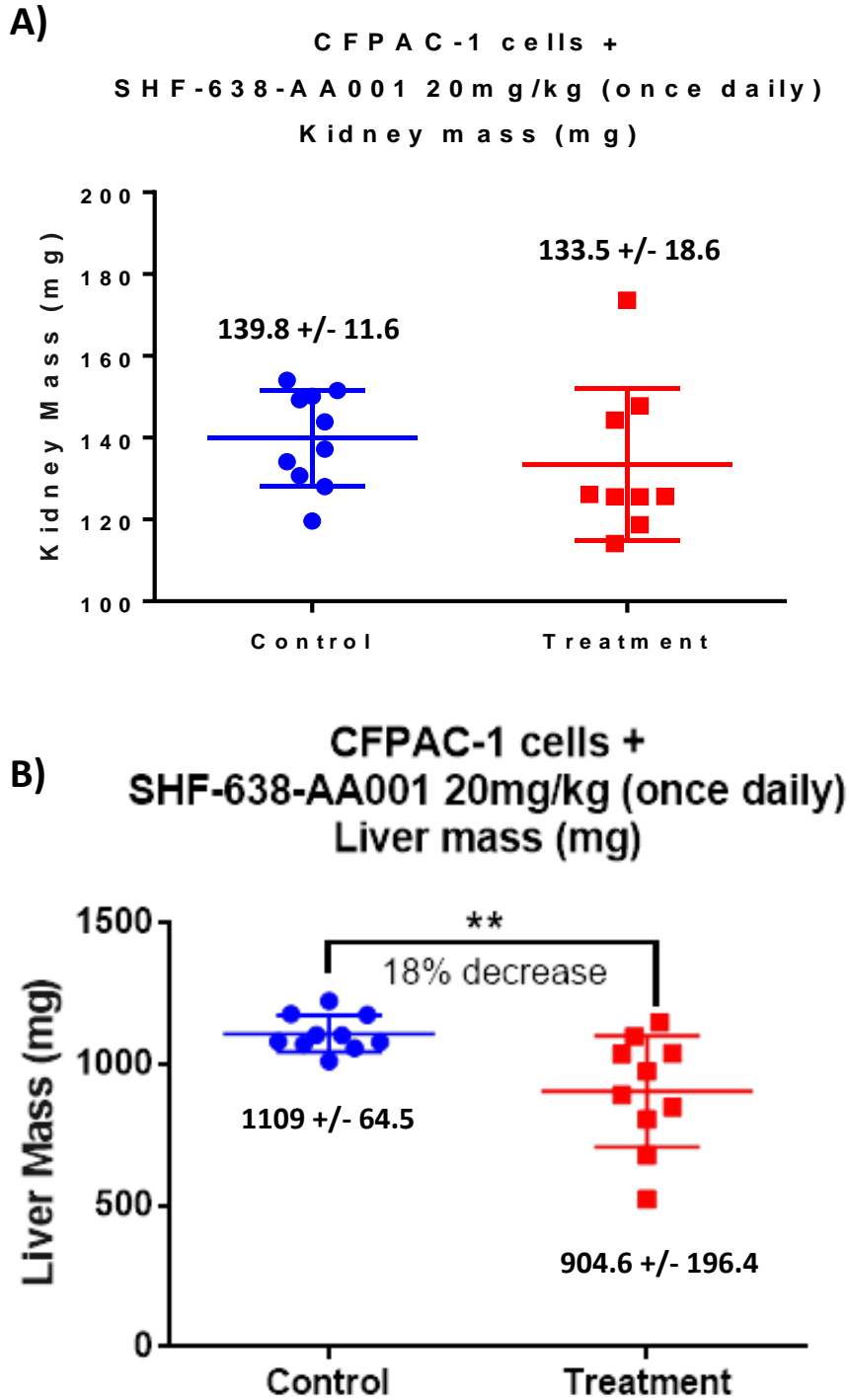
Figure 6.15(ii): *In-vivo* **efficacy of SHF-638-AA004 on CFPAC-1 subcutaneous xenografts.** Daily administration of SHF-638 had no significant effect on kidney **(A)** mass when compared to vehicle control group. Liver **(B)** mass was significant lower when compared to the vehicle control (P=0.005). Data are presented as Mean +/- SD.

6.4.3 Histological analysis of CFPAC-1 subcutaneous tumours

6.4.3.1 Quantification of necrotic areas

Haematoxylin and eosin (H&E) staining of the tumour sections was used to identify and quantify any necrotic areas in vehicle control and treatment groups. The analysis was performed using QuPath software where necrotic areas were highlighted using the selection tools and the percentage area was calculated in relation to the whole section area. A significant increase (40.7%, p=0.03) in the % of necrotic area was observed in the treatment group (20mg/Kg SHF-638) when compared with the vehicle control group (see Figure 6.16 below). Representative images of each group can be found in figure 6.17 below. An outlier in the treatment group was identified using ROUT outlier test and the point was excluded from the calculation.

CFPAC-1 cells + SHF-638-AA001 20mg/kg (once daily) Immunohistochemical analysis
% necrotic area
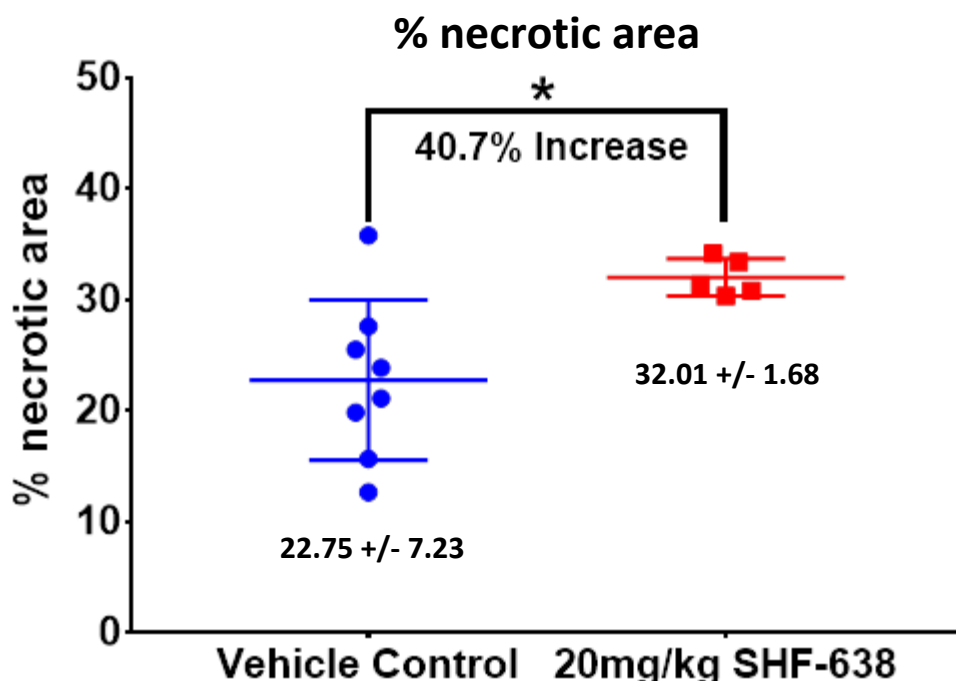
Figure 6.16: Percentage of necrotic area. Quantification the necrotic areas was achieved using QuPath software. A significant decrease of 40.7% in the percentage necrotic areas was observed in the treatment group (20mg/Kg SHF-638) when compared with the vehicle control.

Data are presented as Mean +/- SD, p=0.03 (*).
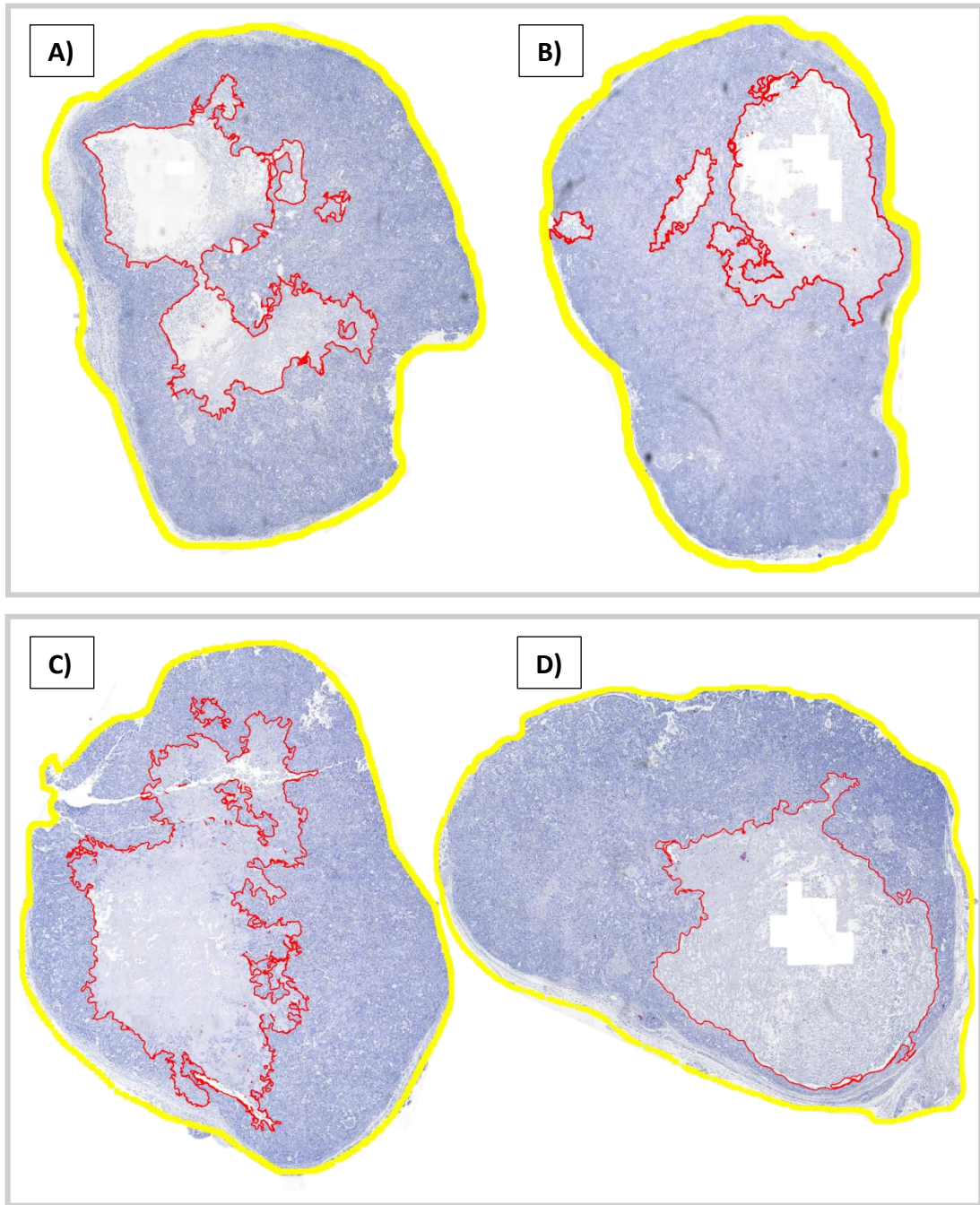
Figure 6.17: Images of H&E staining for vehicle control and treatment group tumours. H&E staining of vehicle control group (A & B) and 20mg/kg SHF-638 treatment group (C & D) tumour sections. Necrotic areas (red) and the whole tumour sections (yellow) were selected using QuPath software. The size of the necrotic areas in the treatment group were significant larger compared with the control group.

6.4.3.2 Determination of cell proliferation *in-vivo*

To determine the anti-proliferative effect of SHF-638 *in-vivo*, tumour sections were stained with anti-Ki67 antibody. Ki67 protein is a widely known cell proliferation marker. A significant decrease (39%, p=0.02) in the presence of Ki67 positive cells was observed in the treatment group (20mg/Kg SHF-638) when compared with the vehicle control group (see Figure 6.18 below). Representative images of each group pre and post-analysis can be found in figure 6.19 below.
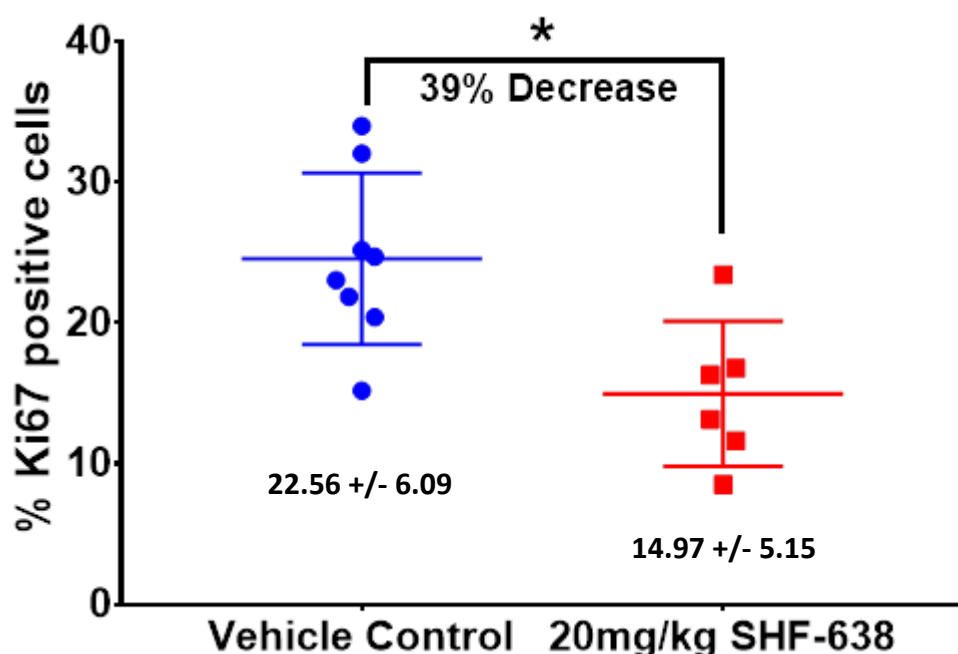
Figure 6.18: Percentage of Ki67 positive cells. Quantification of Ki67 staining was achieved using QuPath software. A significant decrease of 48.5% in the percentage of Ki67 positive cells was observed in the treatment group (20mg/Kg SHF-638) when compared with the vehicle control.

Data are presented as Mean +/- SD, p=0.02 (*).
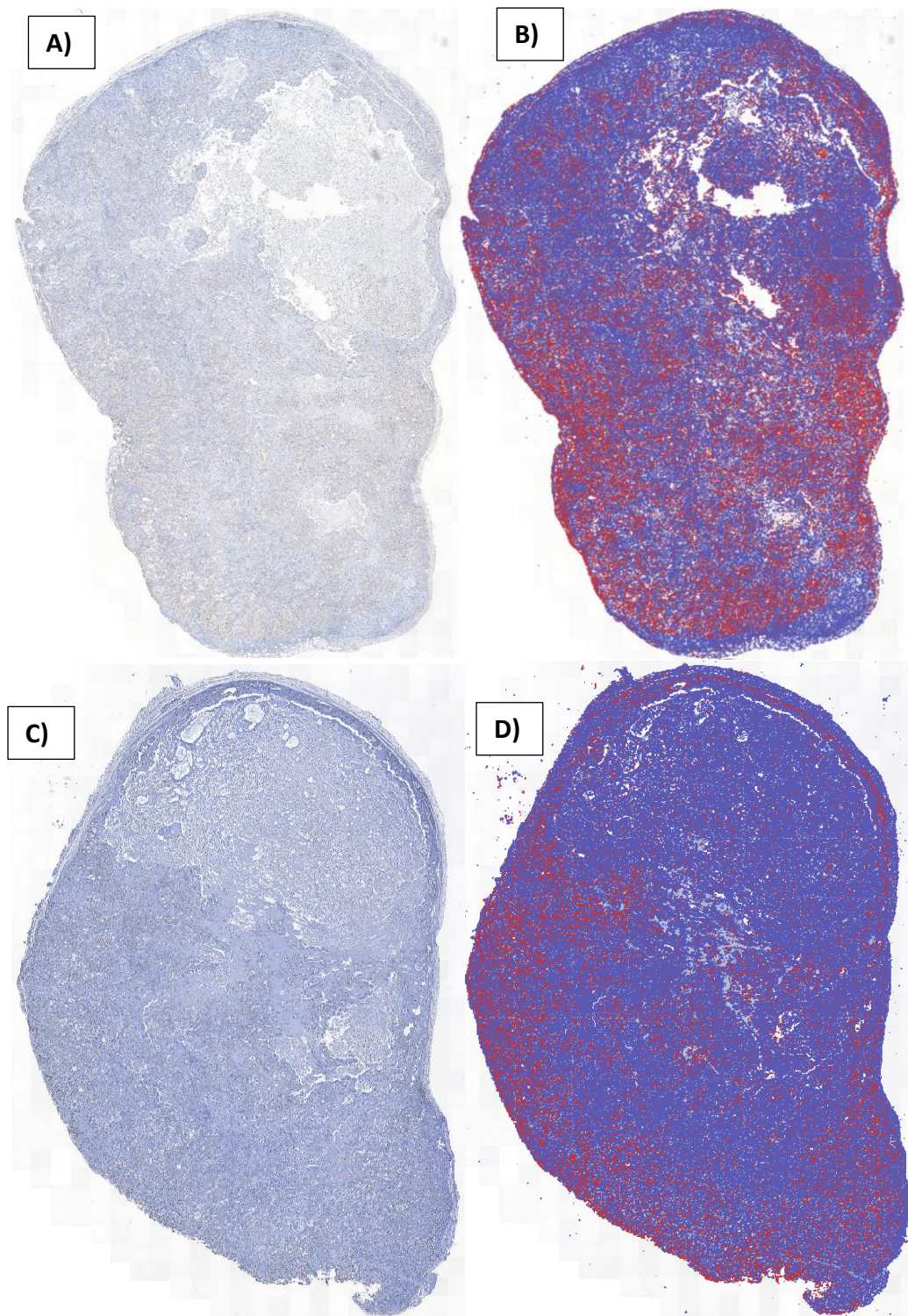
Figure 6.1*9*: Images of Ki67 staining for vehicle control and treatment group tumours. Immunohistochemical staining for Ki67 in vehicle control group (A & B) and 20mg/kg SHF-638 treatment group (C & D) tumour sections. Differences in the intensity of the staining and the number of positive cells, in both the original images (left) and the post-analysis images (right), can be observed between the two groups.

6.4.3.3 Effects of SHF-638 on stroma cells *in-vivo*

α-SMA antibody was used to identify the effects of the treatment on the tumour stroma cells. α-SMA is known to be highly expressed by CAFs also known as myofibroblasts. The area of α-SMA positive cells was determined using ImageJ software as described in the methods section above. As illustrated in figure 6.20 below, a significant decrease (35%, P=0.005) in the percentage of α-SMA positive cells (% area) was observed in the treatment group (20mg/Kg SHF-638) when compared with the vehicle control group. Representative images of each group pre and post-analysis can be found in figure 6.21 below.
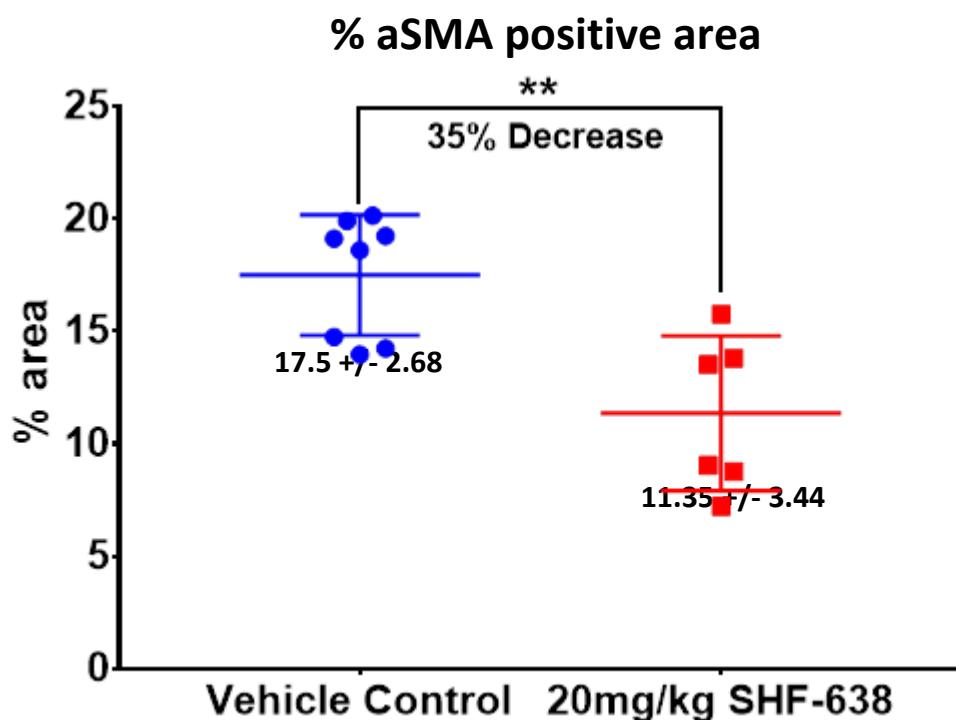
Figure 6.20: Percentage of α-SMA positive area. Quantification of α-SMA staining was achieved using ImageJ software. A significant decrease of 35% in the percentage of α-SMA positive cells (% area) was observed in the treatment group (20mg/Kg SHF-638) when compared with the vehicle control.

Data are presented as Mean +/- SD, p=0.005 (**).
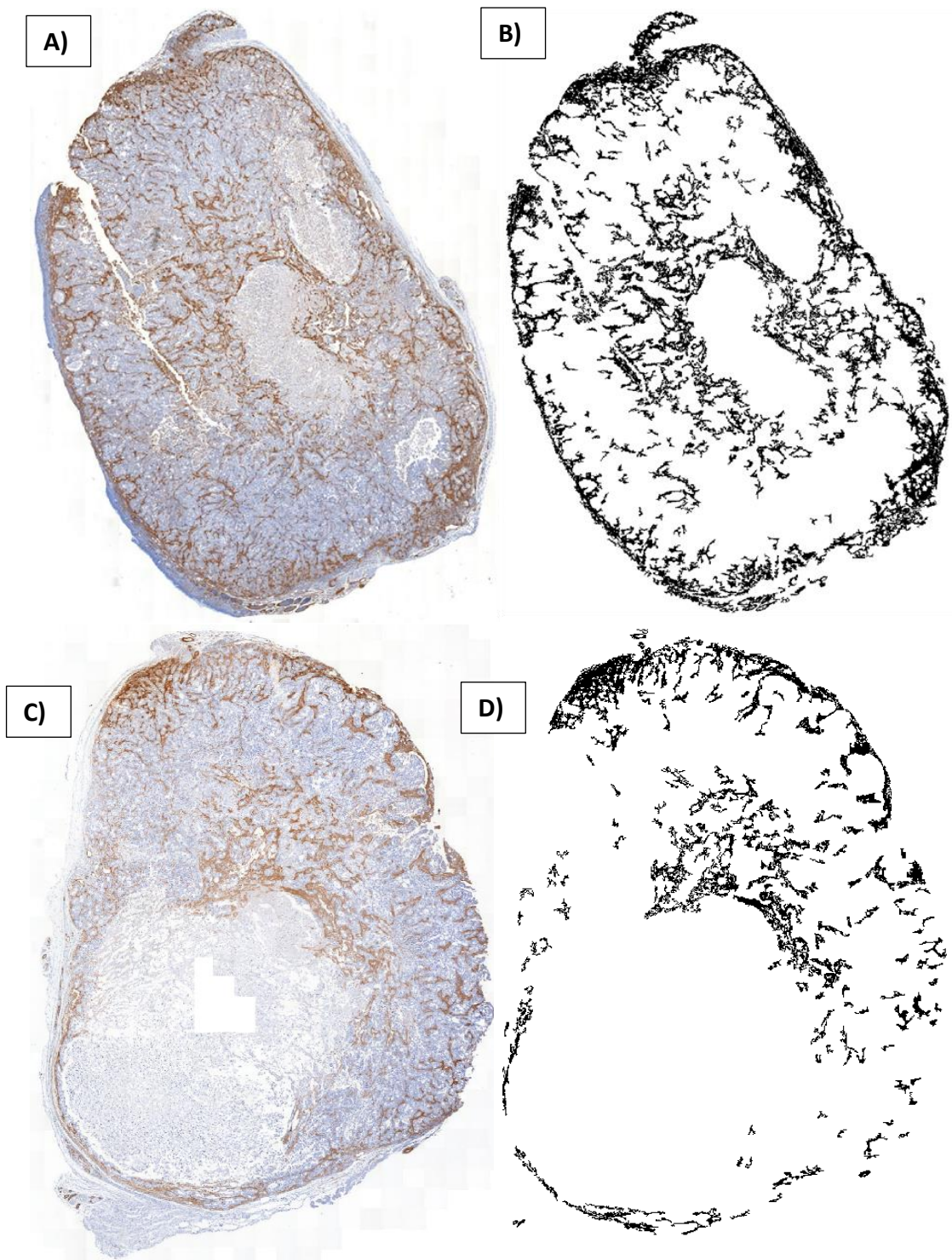
Figure 6.2*1*: Images of α-SMA staining for vehicle control and treatment group tumours. Immunohistochemical staining for α-SMA in vehicle control group (A & B) and 20mg/kg SHF-638 treatment group (C & D) tumour sections. Differences in positive staining (area), in both the original images (left) and the post-analysis images (right), can be observed between the two groups.

6.4.3.4 Effects on endothelial cells/vessel development *in-vivo*

CD31, a marker of endothelial cells was used to assess the effects of the treatment on the vessel development and therefore angiogenesis. The area of CD31 positive area was determined using ImageJ software as described in the methods section above. As illustrated in figure 6.22 below, a non-significant decrease (23%, P=0.08) in was observed in the treatment group (20mg/Kg SHF-638) when compared with the vehicle control group. Representative images of each group pre and post-analysis can be found in figure 6.23 below.

CFPAC-1 cells + SHF-638-AA001 20mg/kg (once daily)
Immunohistochemical analysis
% CD31 positive area
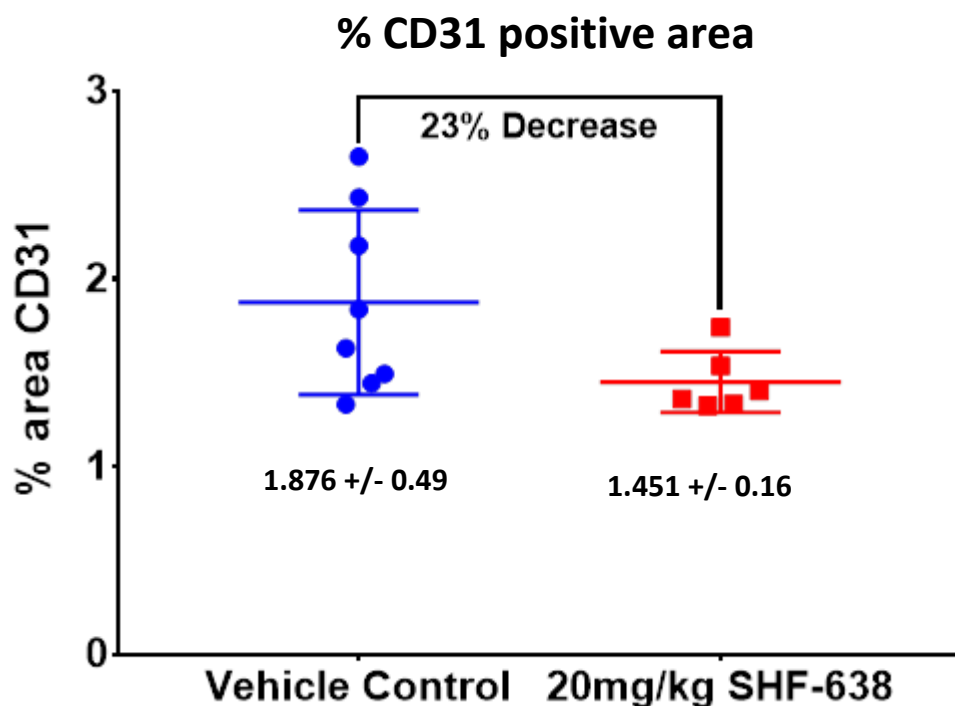
Figure 6.22: Percentage of CD31 positive area. Quantification of CD31 staining was achieved using ImageJ software. A non-significant decrease of 23% in the percentage of CD31 area was observed in the treatment group (20mg/Kg SHF-638) when compared with the vehicle control.

Data are presented as Mean +/- SD, p=0.08.
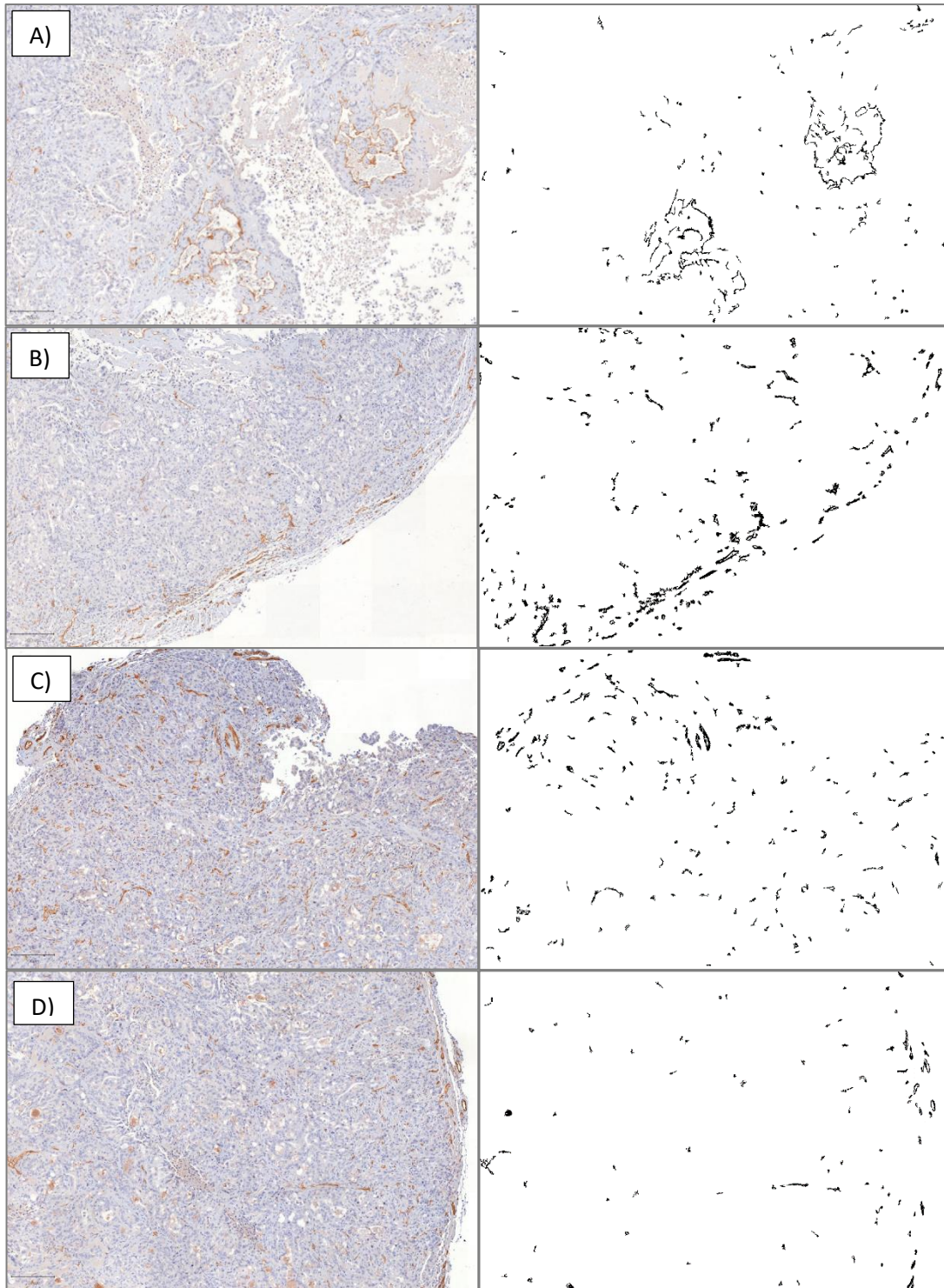
Figure 6.23: Images of CD31 staining for vehicle control and treatment group tumours. Immunohistochemical staining for CD31 in vehicle control group (A & B) and 20mg/kg SHF-638 treatment group (C & D) tumour sections. Snap shots (ROIs) of the original stained slide images scanned using Panoramic 250 Flash III slide scanner are shown on the right-hand side. The post analysis masks obtained using ImageJ software are shown on the left-hand side.

6.5 Conclusion/Discussion

When it comes to the selection of the lead candidate for pre-clinical and clinical studies, good pharmacokinetic profiles are essential in addition to the high efficacy over the target of interest (Chien et al., 2005). Studying pharmacokinetics is providing valuable information about the fate of a drug after it is administrated into the body. *In-vitro* pharmacokinetic and drug metabolism studies are often used during the initial stages of the drug discovery and lead optimization. These studies provide with essential information about the metabolic profiles of the drugs and can be used as a prediction of possible human clinical outcomes (i.e. human hepatocytes cultures and CYP enzyme inhibition) that cannot always be successfully determined with *in-vivo* species (Zhang et al., 2012a). However, these studies are only providing information about an aspect of the drug metabolism. A more holistic approach that allows for the measurement of a combination of parameters (i.e. pharmacological and pharmacokinetic properties as well as safety data) is the use of *in-vivo* pharmacokinetic studies (Zhang et al., 2012a). The most commonly used animal species in such studies are rats and mice mainly due to their inexpensiveness, the low amount of compound requirements and the fact that they easy to operate and handle (McIntyre et al., 2008, Zhang et al., 2012a).

In-vivo determination of the intravenous (IV) and intraperitoneal (IP) PK characteristics of both SHF-408 and SHF-638 were determined. High clearance of both compounds was suggested from the data after IV administration in rats (Figure 6.8 and 6.11). However, IV administration in mice showed moderate clearance of SHF-638 suggesting possible differences in rodent species (Figure 6.10). Interestingly, a large systematic review of historic data from 40 lead optimization programmes, have shown that out of 498 compounds compared, only 278 compounds showed similar clearance values in rats and mice. Moreover, out of 225 compounds that showed high clearance in rats, almost 45% (99 compounds) have shown low to moderate clearance in mice (McIntyre et al., 2008). Moreover, 43% of compounds with high clearance in both rats and mice, had low to moderate clearance in higher species such as dogs and monkeys (McIntyre et al., 2008). This indicates the importance of using multiple species when investigating the

pharmacokinetic properties of leading candidates to decrease the possibilities of a false negative or positive result.

Furthermore, SHF-638 have shown excellent *in-vivo* exposure, with detectable levels to be well above the AM2 receptor functional Ki, 24 hours (T_{last}) after an IP injection into mice (Figure 6.12). This resulted in a total exposure (AUC_{0-last}) of 3311 ng.h/mL, almost double than that of SHF-408 which showed significantly lower exposure (1955 ng.h/mL) and T_{last} of 8 hours, indicating faster clearance (Figure 6.9). This was confirmed by our preliminary *in-vivo* efficacy studies. More specifically, single daily IP injection of SHF-638 (20mg/kg) caused a significant decrease in the formation of breast cancer (MDA-231-MB) subcutaneous tumours in Balb/c nude mice, with the biggest reduction of ~55% (P<0.03) shown at week 4 (Figure 6.13(i)). This was not the case with SHF-408, that was unable to significantly inhibit the growth of the same tumours even with twice daily doing (total of 40mg/kg) (Figure 6.14).

Moreover, SHF-638 was also able to inhibit the growth of pancreatic cancer (CFPAC-1) subcutaneous tumours after a daily administration of 20mg/kg, with the biggest reduction of ~56% (P<0.0001) shown at week 3 and significant decrease of up to 50% to be maintained up to week 4 (Figure 6.15(i)). These results are consistent with previous studies showing that inhibition of AM *in-vivo* have a significant effect in the formation of subcutaneous pancreatic tumours (Ishikawa et al., 2003, Xu et al., 2016) as well as other types tumour xenografts including glioblastomas (Ouafik et al., 2002, Kaafarani et al., 2009), lung and colorectal (Kaafarani et al., 2009). A significant decrease (18%) in the liver mass of the treatment group was observed when compared to the controls (Figure 6.15(ii)). However, the mean value of the livers (~900mg) in the treatment group was considered normal and difference was explained by inconsistencies during the dissection of the mice at the end of the study (two livers were well below the average mass). No significant differences in mice or organ weights or any other adverse effects were observed in any of the other *in-vivo* studies.

Histological sections from the pancreatic cancer subcutaneous model were used to further characterise the effects of SHF-638 in the development and progression of cancer. The anti-proliferative effect of SHF-638 *in-vivo* was determine using an anti-

Ki67 antibody, a widely known cell proliferation marker. A significant decrease (39%) in the presence of Ki67 positive cells was observed in the treatment group when compared with the vehicle control group suggesting a direct effect on cell proliferation by inhibiting the actions of AM2 receptor *in-vivo* (Figure 6.18). Decrease in pancreatic cancer cells proliferation *in-vitro* was previously shown after inhibition (by peptide antagonists) or knockdown (small hairpin RNA silencing) of AM (Ramachandran et al., 2007, Ramachandran et al., 2009, Bhardwaj et al., 2016, Xu et al., 2016). However, in another study, knockdown of AM was not able to cause any significant difference in colon cancer cell proliferation both *in-vitro* and *in-vivo* suggesting an indirect effect on tumour growth by suppression of angiogenesis and stimulation of apoptosis (Wang et al., 2014).

Using CD31, a well-known marker of endothelial cells and vessel development, we assess the effects of AM inhibition on angiogenesis. A 23% decrease, even though not significant, was found in the treatment group (20mg/Kg SHF-638) when compared with the vehicle control, suggesting a possible role of AM in vessel development (Figure 6.22). Several studies have previously shown this role of AM. Increased vascular density was observed after the overexpression of AM in T47D breast cancer cell line both in-vitro (aortic ring assay) and *in-vivo* (Martinez et al., 2002). *In-vivo* treatment of pancreatic cancer cell line (PCI-43) xenografts with AM antagonist (AM_{22-52}) had as a result the significant decrease blood vessel formation (Ishikawa et al., 2003). A more recent study has suggested the role of AM in the regulation of HIF-1α and VEGF. Administration of either AM or AM_{22-52} on epithelial ovarian cancer cells (CAOV3) resulted in the upregulation or downregulation of HIF-1a and VEGF, respectively (Zhang et al., 2017).

Inhibiting angiogenesis could potentially lead to starvation of tumour cells leading to cell death and formation of necrotic areas. Analysis of H&E sections shown a significant increase in the necrotic areas of the treatment group when compared to the control group (Figure 6.16), suggesting an increase in cell death due to the lack of nutrients and oxygen (hypoxia). However, studies have previously associate excessive necrotic areas with poor prognosis and aggressive phenotype in several

types of cancer including osteosarcoma (Li et al., 2011), endometrial (Bredholt et al., 2015) and pancreatic (Hiraoka et al., 2010).

One of the unique characteristics of pancreatic cancer is desmoplasia. It is characterized by the formation of dense fibrous and connective tissue around the tumours that consists of α-SMA positive CAFs or activated PSCs, immune cells and ECM proteins (Pandol et al., 2009).

α-SMA antibody was used to identify the effects of AM receptor inhibition on the tumour stroma cells. α-SMA is well known marker of CAFs also known as myofibroblasts as well as activated PSCs. Analysis has shown a significant decrease (35%) in the percentage of α-SMA positive cells (% area) in the treatment group (when compared with the vehicle controls, suggesting a lower number of CAFs and PSCs in the treatment tumours (Figure 6.20). There are increasing evidence suggesting the role of PSCs in the promotion of pancreatic cancer development. Conditioned media from PSCs cultures promote invasion, colony formation and increase proliferation in pancreatic cancer cells. Moreover, the same media was found to have protective effects against hypoxia, gemcitabine induced apoptosis and radiation (Vonlaufen et al., 2008, Hwang et al., 2008a). Furthermore, studies have shown the role of stellate cells in the formation of desmoplastic structures that characterise pancreatic cancer that provides support and growth factors for tumour cells to grow (Apte et al., 2004, Masamune et al., 2009). These findings indicate the importance of stroma cells such as CAFs and PSCs in the formation and survival of pancreatic tumours. A recent study, has shown that AM (regulated by MYB oncogene) was able to directly promote the growth of pancreatic cancer cells as well as pancreatic stellate cells *in-vitro* (Bhardwaj et al., 2016). What is more, the expression of AM receptor was previously reported in pancreatic stellate cells, suggesting the role of AM on both pancreatic cells as well as on the cells of the tumour microenvironment in a paracrine manner (Ramachandran et al., 2007).

Overall, the findings of this chapter demonstrate that inhibition of AM2 receptor by small molecule antagonist SHF-638-AA004 have a significant reduction in the growth and development of tumours *in-vivo*. Also, it suggests the role of AM in the proliferation of cancer cells as well as its effects on tumour microenvironment. Its

role on tumour angiogenesis is not clear due to the known significance in the analysis of the tumour sections.

Chapter 7: General discussion

Chapter 7: General discussion

This study has successfully used a structure/knowledge-based drug modelling, with its basis on commercially available CGRP antagonists and their reported interactions with the CGRP receptor, to develop the first highly potent and selective AM2 receptor antagonist (SHF-638) when compared to the other members of calcitonin family of receptors. The compound showed a competitive mode of inhibition and good metabolic profile *in-vitro* enabling its use *in-vivo*. When its pharmacokinetic profile was established *in-vivo,* SHF-638 proved to be an excellent compound for *in-vivo* efficacy studies, showing high total exposure after IP administration in mice. Inhibition of AM2 receptor *in-vivo* had as a result the significant decrease of pancreatic subcutaneous tumour growth. *Ex-vivo* analysis of subcutaneous tumours showed that inhibition of AM2 receptor not only causes a direct effect on the proliferation of cancer cells *in-vivo* but also affects the tumour microenvironment. These findings provide compelling evidence that AM2 receptor plays a significant role in the development and progression of pancreatic cancer.

Both incidence (Cancer research UK, 2014c) and mortality (Cancer Research UK, 2014) rates of pancreatic cancer have dramatically increased during the last few decades and are predicted to increase even more in the next few years (Rahib et al., 2014). Current best treatment option for pancreatic cancer involves the surgical removal of the tumour, however, more than 80% of patients present with non-resectable tumours, locally advanced tumours or metastatic disease leaving palliative care as the only option (Pierantoni et al., 2008). Moreover, the use of cytotoxic chemotherapeutic cocktails is one of the most common treatment options following surgery or for non-resectable tumours, however, this is shown to be only mildly beneficial. These data illustrate the unmet need for development of novel targets and new therapies which will be more effective than the existing approaches.

Studies have shown the involvement of AM in several aspects of tumour development including cancer cell growth (proliferation), tumour angiogenesis and cancer cell survival (Martinez et al., 2002, Zudaire et al., 2003). Moreover, AM was found to be an important regulator of the crosstalk between tumour cells and host microenvironment (Zudaire et al., 2006, Bhardwaj et al., 2016). Increased plasma AM

levels were observed in patients with pancreatic cancer, suggesting the use of AM as a prognostic marker (Letizia et al., 2001, Ishikawa et al., 2003, Keleg et al., 2007, Ramachandran et al., 2007, Aggarwal et al., 2012, D'Angelo et al., 2016). Furthermore, inhibition or silencing of AM significantly decreased the growth of pancreatic cancer cells *in-vitro* and tumour development *in-vivo* (Ishikawa et al., 2003, Ramachandran et al., 2007, Ramachandran et al., 2009, Hollander et al., 2015, Bhardwaj et al., 2016).

The aim of this study was the development of novel small molecule antagonists against adrenomedullin 2 receptor (AM2r) for the treatment of pancreatic cancer, while not targeting the other members of calcitonin family of receptors and especially AM1 receptor (AM1r). AM1r was found to be an important regulator of blood pressure in several *in-vivo* studies. Embryonic lethality was observed due to cardiovascular defects upon the deletion of functional AM or its receptor components (CLR and RAMP2 but not RAMP3) (Shindo et al., 2001, Dackor et al., 2006, Ichikawa-Shindo et al., 2008) indicating a significant difference in the physiological role of AM1 and AM2 receptors.

7.1 Establishing a robust cell-based assay suitable for HTS

Using Lance TR-FRET cell-based cAMP production assay kit we were able to develop a highly consistent assay, with the ability to produced excellent quality, reproducible data. The assay showed significantly high sensitivity (detection of IC_{50} values in the low nM range) and large detection window (dynamic range) (Figure 3.5). Moreover, a screening window coefficient (Z-factor) of 0.74 was determined indicating an extremely robust and consistent assay, suitable for identifying active compounds ("hits") with high fidelity (Figure 3.8). Furthermore, cells used in the screening process showed high transfection stability (Figure 3.9) and extreme tolerance to DMSO (Figure 3.12).

cAMP assays are widely used in drug discovery programs due to its importance in the regulation of several intracellular signal transductions upon GPCR activation (Norskov-Lauritsen et al., 2014). Like most of GPCRs, activation of both AM and CGRP receptors results in the activation of adenylate cyclase (AC) that subsequently

increases the levels of cAMP and activates cAMP-dependent pathways ($G\alpha_s/G\alpha_{i/o}$) (Hay et al., 2003b, Beltowski and Jamroz, 2004). This indicates that using cAMP as a marker of cellular response upon receptor stimulation is a valuable tool for characterization of such receptors (Evans et al., 2000, Hay et al., 2003a, Hay et al., 2006). However, studies have shown that activation of AM and CGRP receptor could also lead to the stimulation of cAMP-independent pathways ($G\alpha_q$, $G\beta\gamma$ or β-arrestins). Activation of both receptors resulted in the significant increase of intracellular Ca^{2+} in several studies (Shimekake et al., 1995, Uezono et al., 1998, Drissi et al., 1999, Kuwasako et al., 2000). Moreover, activation of MAPK signalling pathways including ERK1/2 and p38MAPK have been observed in several studies (Fritz-Six et al., 2008, Wang et al., 2009, Potes et al., 2012). These findings illustrate the possible use of other markers as indicators of AM and CGRP receptor activation that could also give more information on the signalling pathways responsible for a specific response both *in-vitro* and *in-vivo*.

One of the main limitations of using only functional assays for drug screening, and therefore of this study, is that they do not provide any details about the kinetics (association and dissociation constants) of the compounds tested and the mode of their action. A combination of binding and functional assays is a common approach during the lead optimization stages of drug discovery and candidate selection for pre-clinical and clinical trials. Such approaches were used in the recent discoveries of Olcegepant, Telcagepant and MK-3207 with remarkable results (Doods et al., 2000, Salvatore et al., 2008, Salvatore et al., 2010).

Since the development of the first radioligand binding assay in 1970, that was used for the kinetic characterization of adrenocorticotropic hormone receptor (Lefkowitz et al., 1970), several assays have been developed using ^{3}H- or ^{125}I-labeled ligands for the characterization of various GPCR compounds (reviewed by (Zhang and Xie, 2012)). The use of expensive radioligands which could be difficult and dangerous to be disposed as well as the difficulty of scaling these assays to a HTS setting (i.e. 384 well plates) are some of the limitations of such approaches. Moreover, even though binding assays provide kinetic characteristics they are not able to distinguish if a candidate compound is an agonist, a partial agonist or an antagonist. During the last

few years several innovative technologies (such as scintillation proximity assay (SPA) and homogeneous time-resolved fluorescence (HTRF)) (reviewed by (Zhang and Xie, 2012)), as well as label free technologies such as dynamic mass redistribution (DMR) and Surface plasmon resonance (SPR) (Fang, 2016) have been developed trying to solve some of those issues and making the use of binding assays in HTS more feasible. Label free binding assays such as SPR and DMR are currently been developed in our lab to resolve some of the limitations of using functional assays and to provide us with the valuable information about the interaction of the antagonists with the different calcitonin receptors.

7.2 Novel compound development – design program

Utilizing the developed cell-based cAMP assay, we were able to screen more than 1100 compounds for their activity (efficacy) to inhibit peptide ligand induced cAMP production in AM2r and CGRPr O/E cells, as a primary screening process. Selected compounds were screened against AM1 and AMY receptor- O/E cell lines to establish selectivity. The overexpression of the target of interest in a low expression naïve cell line is a common feature of cell-based assays in drug discovery. The use of these highly expressed cell lines, yields a high detection window and a sufficient signal output, ensuring data reproducibility and efficiency (having comparable expression levels between the cell batches). Using these O/E cells, we were able to establish the functional characteristics (potency) of each compound and investigate their selectivity over the different members of calcitonin family of receptors with high accuracy (data will be discussed in the next sections). However, one of the main disadvantages of using such cell lines is the difficulty of translating the pharmacological data obtained using such highly artificial model to a meaningful physiological response. For this reason, the response or the activity of the candidates is often investigated under normal expression conditions in naïve cells, as well as, by using animal models for a better representation of the disease of interest (see section 7.3 and 7.5).

Structural similarities and differences between CGRP and AM2 receptors (homology model developed in our lab) aid the design and development of novel compounds, aiming to increase selectivity and potency for AM2 receptor over CGRP receptor as

well as the other members of the family. Existing highly potent and selective drugs-like CGRP small molecule antagonists (see appendix figure 8.1) such as MK-3207 were used as a starting point of this structure/knowledge-based drug modelling program. Compounds were design based on previous studies that suggested the presence of three distinct interaction (binding) regions in the structure of most CGRP small molecule antagonists, using SARs and structural alignments (Archbold et al., 2011). More specifically, CGRP antagonists were found to interact with the receptor at three different regions: the CLR region, the interface (linker) region (at the CLR–RAMP1 interface) and the CLR/RAMP1 region (ter Haar et al., 2010, Archbold et al., 2011, Booe et al., 2015). Similarly, our novel antagonists consist of three distinct regions (CLR region, CLR - RAMP linker and RAMP region). In this study efforts have been made to increase the potency and selectivity of small molecule antagonists for AM2 receptor by modifying the structure of each of these binding regions. Sections 7.2.1-3 below will focused on the discussion of these regions.

7.2.1 CLR binding region

During the initial stages of the study efforts were made to identify the appropriate CLR binding region that would produce the most potent AM2 antagonists. Several commercially available fragments were selected (table 4.5), based on their structural similarity with CGRP antagonists CLR regions, and tested for their ability to inhibit the production of cAMP in AM2 and CGRP receptor O/E cells (figure 4.12). Interestingly, only one fragment, the CLR region of MK-3207 (CLR-B), was able to significantly decrease the production of cAMP with equal potency over AM2 and CGRP receptor O/E cells (figure 4.13). Moreover, when this fragment was used as a building block for the design of more complex structures, it resulted in the development of consistently highly potent AM2 and CGRP receptor antagonists, with selectivity over AM1 as well as AMY receptors (table 4.7). Compounds derived from the other CLR fragments, with the exception of CLR-A which produced relatively high AM2 and CGRP antagonists, showed low to no activity for AM2 receptor. This indicates the importance of CLR-B in the potency of small molecule antagonists against AM2 receptor.

7.2.2 CLR – RAMP linker variations (importance of amide linker)

Another essential factor of the high potency achieved against AM2 receptor was the presence of an amide linker between the CLR and the RAMP regions of the compounds. Replacement of the amide linker with several linker variations including double and triple bond, as well as, aniline and alkane linkers resulted in a significant decrease on both potency and selectivity of the compounds. Interestingly, the presence of the same linker was observed in the structure of most recently developed CGRP small molecule antagonists (Doods et al., 2000, Salvatore et al., 2008, Salvatore et al., 2010).

7.2.3 RAMP end modifications and primary structure series

By using CLR-B and CLR – RAMP amide linkers as the main building blocks of the design and by engineering the RAMP region of CGRP antagonists we were able to not only increase the potency of the compounds against AM2 receptor but also achieve selectivity over CGRP receptor. The screening process led to the identification of two major structure families with significant effects on the activity of AM2 receptor. The primary structure family, SHF-408/SHF-638, showed significantly higher efficacy for AM2 receptor than the secondary structure series (SHF-491 family). Figures 7.1 and 7.2 illustrate the activities of compounds that belong to SHF-408/SHF-638 family against CGRP and AM2 receptors.

As shown in the figure 7.1 significant improvement in both the potency and the selectivity for AM2 receptor was achieved by modifying the RAMP region of the compounds (see compounds highlighted red rings). The addition of methylamine (CH_3NH_2) on the benzyl group of the SHF-082 highly selective CGRP antagonist, with reasonable potency against AM2r O/E cells, significantly increased the potency against AM2 receptor resulting in the development of an equally potent antagonist (SHF-408). Further expansion of the RAMP region by the addition of an extra methyl group (CH_3) resulted in the first selective and highly potent AM2 receptor antagonist (SHF-638). The presence of threonine on residue 70 and glutamine on residue 67 in the structure of RAMP-3 were found to be of significant importance in determining the potency of these compounds (Figure 4.19 and 4.20). These data indicate the significant role of RAMPs in receptor interactions. The role of RAMPs in the

pharmacology and functionality of calcitonin family of receptors was previously described in numerous studies (reviewed by Hay and Pioszak, 2016).

As shown in figure 7.1 below, a wide range of activity was observed in both AM2 and CGRP receptor O/E cells. Activity is divided into two main sections: compounds with higher than 100nM potency for both receptors and compounds with lower than 100nM potency for both receptors. As illustrated in figure 7.2, the vast majority of the compounds have shown pIC_{50} less than 100nM (~175 compounds in CGRPr cells and ~140 compounds in AM2r cells). Not surprisingly, lower peak potency (pIC_{50}) was observed in CGRP receptor O/E cells with 58 compounds been in the region of 20-6nM. On the other hand, peak potency for AM2 receptor O/E cells was shown in the region of 20μM-70nM (48 compounds). However, a similar number of compounds (~20) was found in the low nM (2-0.5nM) region in both cell lines. It is worth mentioning that high selectivity over the other members of CLR and CTR family was observed in all compounds tested.

Even though our design program succeeded in increasing significantly the potency of small molecule antagonists against AM2 receptor, the data indicate that the majority of the compounds have cross-selectivity for both CGRP and AM2 receptors. Studies have previously shown the involvement of CGRP in the regulation of cancer related pain (Mantyh et al., 2002, Jimenez-Andrade et al., 2010). Moreover, CGRP was found as an important regulator of prostate (Logan et al., 2013) and lung (Toda et al., 2008) cancer development by increasing proliferation, migration and angiogenesis. These data suggest that possible inhibition of CGRP could be beneficial for the treatment of cancer and its symptoms. However, its role in several physiological process of the nervous and cardiovascular system indicate that this could possible lead to undesirable side effects. Moreover, molecular modelling of the two receptors showed a significantly smaller receptor binding pocket in AM2 receptor when compared to CGRP (Figure 4.19) indicating that developing selective and potent AM2 receptor antagonists could be challenging.
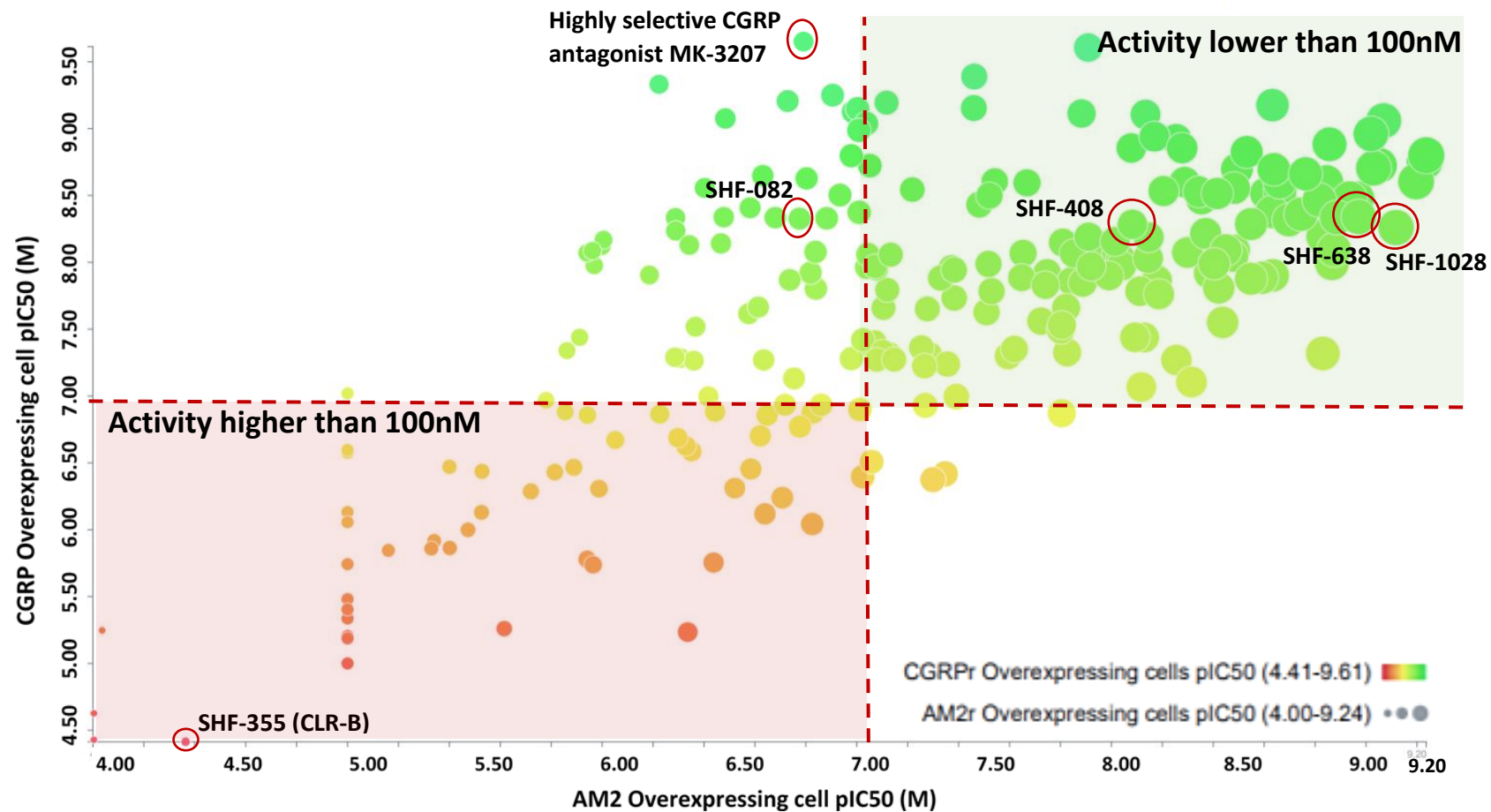
Figure 7.1: Graphical illustration of the activity of SHF-408/SHF-638 family compounds. Activity over the CGRP receptor (Y-axis) is illustrated as a colour range, with red being the least potent and green being the most potent. On the other hand, activity over AM2 receptor (X-axis) is illustrated as a change in size, with the biggest object being the most potent AM2 antagonist.
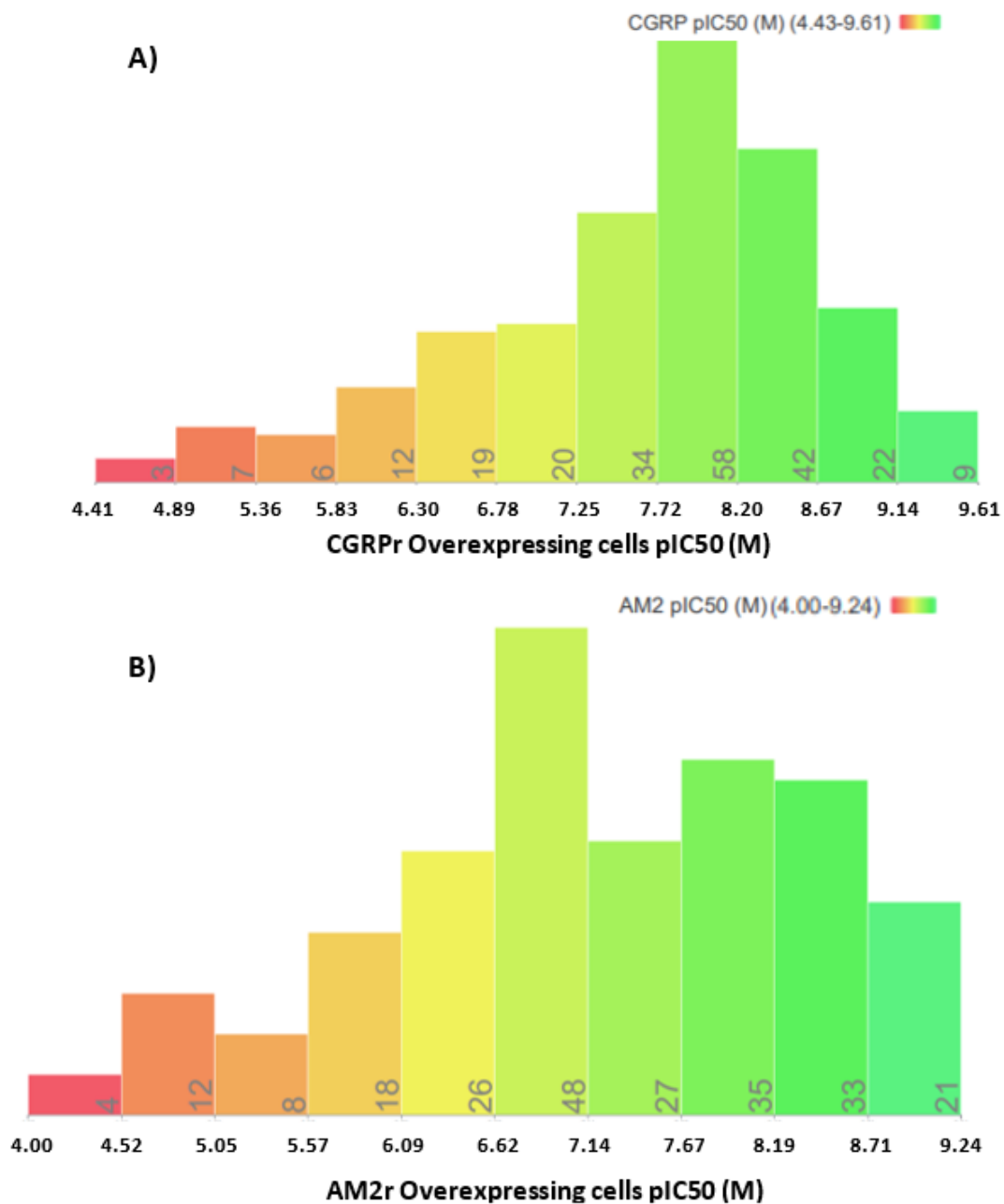
Figure 7.2: Activity of SHF-408/SHF-638 compounds against AM2 or CGRP receptor. Compounds are divided into separate groups according to their activity (pIC$_{50}$) against CGRP **(A)** and AM2 **(B)** receptors. The number of compounds per group is shown on each bar.

7.3 A complicated mode of inhibition was suggested *in-vitro*

As the first selective small molecule antagonist for AM2 receptor, SHF-638 was selected for further pharmacological characterization and determination of its metabolic profile *in-vitro*. The pharmacological characterization of SHF-638 (mode of antagonism) was achieved using the Schild analysis, a method that is commonly used in drug discovery (Schild, 1949, Arunlakshana and Schild, 1959). This approach was previously used for the pharmacological classification of several clinically important compounds including: neuromuscular inhibitors (Bowman, 2006) and histamine receptor antagonists (Black et al., 1972, Slack et al., 2011) as well as recently developed novel CGRP receptor small molecule antagonists including Olcegepant (Doods et al., 2000, Edvinsson et al., 2002, Hay et al., 2002, Moreno et al., 2002).

A competitive (reversible) mode of antagonism was suggested when SHF-638 was used in a competition assay with AM_{1-52} and aCGRP ligands. Increasing concentration of SHF-638 had as a result the rightward shift of the peptide ligand induced cAMP production dose response curve in both AM2r and CGRPr O/E cells (Figures 5.10 and 5.11). What is more, no apparent inhibition of the maximal response (Efficacy - E_{max}), a common feature of non-competitive (irreversible) antagonism, was observed (Gaddum, 1957, Kenakin et al., 2006).

This was not supported however by the Schild analysis plot that suggested a more complicate mode of antagonism. More specifically, the calculated slope values obtained from the Schild regression plots in both cell lines, showed a significant decrease from unity (1) (Figures 5.10 and 5.11). Moreover, the shape of the regression plots (S shape) suggested a biphasic binding with the involvement of more than one receptor. This can be explained by the presence of both CGRP and AM2 receptor on the parental cell line (1321N1 - Human brain astrocytoma cells) used for the stable transfection of the receptors. Data obtained by our group have shown that stimulation of 1321N1 parental cell line by AM_{1-52} and aCGRP resulted in a significant increase in production of cAMP suggesting the presence of both receptors (Appendix figure 8.2). Moreover, the higher potency of aCGRP shown in the same experiment suggests higher expression of CGRP receptor. Further pharmacological characterization of SHF-638 provided another possible explanation for the biphasic

Schild plot. More specifically, functional analysis of the two enantiomers present in SHF-638 suggested the presence of a highly potent enantiomer (SHF-771) and of one with a significant lower potency (SHF-770) (Figure 5.6 and table 5.3). This suggests that binding of SHF-638 with the receptor occurs in two phases due to the presence of a low and a high affinity enantiomer. This indicates the need for further pharmacological analysis of racemate SHF-638 and its enantiomers to establish its mode of antagonism.

A biphasic manner of interaction of Olcegepant and CGRP receptor was previously shown, suggesting the presence of two receptors with different affinities (low and high) for the antagonist (Moreno et al., 2002). This was also explained by the slow kinetics (on-rate) of Olcegepant, previously shown in human brain epithelial cells (SK-N-MC) (Schindler and Doods, 2002), suggesting that longer incubation time might be required to reach equilibrium. No kinetic rates of SHF-638 were obtained, however, determination of its binding profile could aid its pharmacological classification.

To establish the effects of SHF-638 under native receptor expression, human pancreatic cancer cells Panc 10.05 and mouse prostate cancer cells 178-2 BMA were used. The ability of SHF-638 to block the activation of AM2 receptor in human pancreatic cancer cells is used as a prediction of its ability to alter the function of such cells in *in-vitro* and *in-vivo* studies. Moreover, the use of mouse cells provides a better representation of the mouse models used *in-vivo* and specifically the effects of SHF-638 on mouse tumour microenvironment. A lower potency over the mouse receptor when compared to the human receptor was observed. More specifically, SHF-638 was able to inhibit cAMP production by human pancreatic cells Panc 10.05 with a significantly higher potency when compared with mouse prostate cancer cells 178-2 BMA (Figure 5.8). Lower binding affinities for rat CGRP receptor when compared with the human receptor were previously observed with several CGRP antagonists including Olcegepant (Doods et al., 2000), Telcagepant (Salvatore et al., 2008) and MK-3207 (Salvatore et al., 2010). The important role of RAMP-1 in the determination of species selectivity was suggested previously. Recombinant expression of human/rat CGRP receptor components (CLR + RAMP-1) in HEK293-

EBNA cells showed that RAMP-1 was able to determine both receptor pharmacology as well as antagonist binding affinities (Mallee et al., 2002).

7.4 Good metabolic profiles were obtained *in-vitro*

The metabolic profile and the stability of SHF-638 was then obtained using various *in-vitro* studies (results are summarised on table 5.10). The effects of fetal calf and human serum on the functionality of SHF-638 was first investigated showing no significant decrease (Figure 5.9). It was previously shown that serum albumin can potentially decrease the bioavailability as well as the potency of chemical entities *in-vitro* through a protein-protein interaction (Seibert et al., 2002). Both plasma stability and PPB were investigated using *in-vitro* ADME studies. ADME (Absorption, Distribution, Metabolism, and Excretion) studies are considered as a useful tool in drug discovery due to their ability to determine important characteristics (solubility, plasma stability, permeability and toxicity) of the compounds aiding the optimization of lead candidates prior to their use *in-vivo*. SHF-638 remained unaffected by the presence of both human and rat plasma supporting the results obtained in the cAMP assays. However, in PPB assay, 90% of SHF-638 was found to be bound suggesting that only 10% of the concentration is able to produce a pharmacological response (Smith et al., 2010). Furthermore, SHF-638 was found to be relatively stable (low to moderate) in the presence of microsomes from different species (human, rat and mouse). Good metabolic profile (intrinsic clearance) was also observed in the presence of human (moderate), mouse (moderate) and rat (low) microsomes. These results are suggesting a good stability and metabolic profile of SHF-638 that could potentially result in prolong exposure and therefore a reduction in dose. Furthermore, possible liver toxicity was investigated by the ability of SHF-638 to inhibit commonly used cytochrome P450 (CYP450) enzymes; proteins important for the metabolism of most drugs (Lynch and Price, 2007). SHF-638 showed no significant inhibition of any of the cytochrome P450 enzymes used suggesting good metabolic profile.

Inhibition of such enzymes could possibly result in drug-drug interactions that could potential cause unanticipated side effects or decrease the effects of the drugs (reviewed by Lynch and Price, 2007). More specifically, results from two phase I

clinical trials suggested that co-administration of a MAPK kinase inhibitor Selumetinib, currently used in the treatment of several types of cancer, with commonly known CYP3A4 or CYP2C19 inhibitors (itraconazole and fluconazole) resulted in an increased drug exposure. On the other hand, the use of CYP3A4 inducer (rifampicin) had the opposite effects on Selumetinib exposure time (Dymond et al., 2017). In another study, co-administration of tamoxifen (a hormone therapy used for the treatment of breast cancer) with CYP2D6 (one of the main metabolic enzymes of tamoxifen) inhibitors had a significant impact in the prognosis and recurrence of the disease (Goetz et al., 2007). Finally, administration of erythromycin (antibiotic that prolongs the cardiac repolarization) in combination with inhibitors of CYP3A isozymes was correlated with sudden death due to cardiac conditions (Ray et al., 2004). These findings indicate the importance of metabolic characterisation of novel compounds during the early stages of drug discovery to avoid any adverse side effects and/or to recognise the possibility of anticipated effects on drug activities.

7.5 *In-vivo* pharmacokinetics of SHF-638

The *in-vivo* IV and IP pharmacokinetics of SHF-638 were determined. PK studies are an essential part of drug discovery as they provide valuable information about the fate of a drug after it is administrated into the body. *In-vivo* pharmacokinetic studies allow the determination of several parameters including pharmacokinetic properties and safety (Zhang et al., 2012). Interestingly, differences in the clearance of SHF-638 were observed between the species used. Even though SHF-638 clearance was relatively high after IV administration in rats (Figure 6.11), significantly lower clearance was observed in mice (Figure 6.10). This was previously shown in several studies indicating the importance of using multiple species when establishing pharmacokinetics. In a large systematic review of 498 compounds, significant differences were observed in the clearance values between species with 45% of the compounds showing high clearance in rats while showing moderate to low clearance in mice. Differences were also observed between rodent (high clearance) and other species including monkeys and dogs (moderate to low clearance) (McIntyre et al., 2008). Low IV clearance was previously shown in both rats and monkeys after administration of Olcegepant (Paone et al., 2007). Moreover, IP PK studies were used

as an indication of the compound exposure *in-vivo* as well as for the correct determination of the compound dose. SHF-638 was determined as an excellent tool for further *in-vivo* efficacy studies with detectable levels to be well above the AM2 receptor functional Ki for up to 24 hours (T_{last}) after an IP injection into mice (total exposure 3311 ng.h/mL) (Figure 6.12). This was significantly higher than SHF-408, that showed only 8 hours (T_{last}) of *in-vivo* exposure and total exposure of only 1955 ng.h/mL (Figure 6.9). Not surprisingly, this was directly reflected in the ability of the compounds to inhibit the growth of cancer cells *in-vivo*. However, low oral bioavailability was observed after PO administration in rats indicating that oral dosing of SHF-638 is limited (appendix figure 8.3), making its use in clinical trials challenging.

7.6 SHF-638 significantly decrease the growth of subcutaneous tumour *in-vivo*

The *in-vivo* efficacy of SHF-638 was investigated in subcutaneous xenografts in Balb/c nude mice. The development of athymic nude mice (genetically mutated mice with significantly lower T cells – reduce immune system) in 1968 is of significant importance since it meant that human cells were able to grow and establish in mice (most often subcutaneously) without been rejected by the host (Pantelouris, 1968). Since then several subcutaneous xenograft models have been developed and utilised for the validation and discovery of several anti-cancer agents. The ability to easily monitor and measure the effects of treatment on cancer progression and tumour growth (tumours are readily visible from the outside) as well as the tractability, reproducibility and short duration of such models are some of the reasons why this model is considered one of the standard approaches in cancer research (Jung, 2014, Gould et al., 2015).

The IP PK characteristics significantly modulate their ability of the two compounds (SHF-408 and SHF-638) to inhibit the growth of subcutaneous tumours. More specifically, a single IP administration of SHF-638 (20mg/kg/day) was able to significantly decrease the growth of breast cancer tumours in Balb/c nude female mice by up to 55% when compared to the control group. However, even though SHF-

408, that showed a significantly lower IP exposure than SHF-638, was given in a higher dose than SHF-638 (40mg/kg/day), this was not able to produce the same effect when compared to the control group, with no significant decrease in the overall tumour growth. These data illustrate the importance of utilizing pharmacokinetic studies during the development and optimization of new compounds, as it can be used as a marker of exposure and even efficacy *in-vivo*. SHF-638 had similar effects in the development of pancreatic cancer (CFPAC-1) subcutaneously. A daily administration of 20mg/kg was able to significantly decrease the growth by up to ~56% when compared with the control group. These results are in agreement with several studies suggesting that inhibition of AM *in-vivo* has a significant effect in the formation of subcutaneous pancreatic tumours (Ishikawa et al., 2003, Xu et al., 2016) as well as other types of tumour xenografts including glioblastomas (Ouafik et al., 2002, Kaafarani et al., 2009), lung and colorectal (Kaafarani et al., 2009). These results indicate the important role of AM and its receptor in the growth of pancreatic and breast cancer cells *in-vivo*.

Even though subcutaneous xenograft models are widely used with high success in cancer research, one of the main limitations is the actual site of injection that fails to represent and replicate the real environment of tumour growth *in-situ*. Such models do not facilitate the study of the role of tumour microenvironment and the effects of treatment in tumour invasion and metastatic processes. Alternative models that represent better the site of tumour growth and the role of the microenvironment have been developed including the orthotopic xenograft model. These models allow the inoculation of the cancer cells directly into their origin site, providing a more clinically relevant model for the study of the entire process of tumour development and progression including invasion, angiogenesis and metastasis (Nozaki et al., 2003). Pancreatic orthotopic models (Qiu and Su, 2013) are often used to evaluate the drug effects on human pancreatic cancer cells. In a recent study, orthotopic SUIT-2 pancreatic cancer mouse model was successfully used for the investigation of the metastatic process of pancreatic cancer and the effects of gemcitabine on the development of pancreatic cancer *in-vivo* (Higuchi et al., 2018).

7.7 Ex-vivo analysis of the effects of SHF-638

Immunohistological analysis of tumour sections obtained from the pancreatic cancer subcutaneous model were used to further characterise the effects of SHF-638 in the development and progression of cancer.

7.7.1 AM2 receptor inhibition decreased cancer cell proliferation *in-vivo*

The analysis suggested the inhibitory effect of SHF-638 on the proliferation of tumour cells *in-vivo,* showing a significant decrease in the presence of Ki67 (a widely known cell proliferation marker) positive cells when compared with the untreated control group (Figure 6.18). Studies have previously supported the role of AM in cancer cell proliferation *in-vitro*, showing a significant decrease in the proliferation of pancreatic cancer cells upon inhibition or silencing of AM (Ramachandran et al., 2007, Ramachandran et al., 2009, Bhardwaj et al., 2016, Xu et al., 2016). However, an indirect effect (suppression of angiogenesis and stimulation of apoptosis) of AM inhibition on tumour growth was previously shown *in-vitro* and *in-vivo* (Wang et al., 2014). Moreover, data from our group have shown a significant decrease of up to 50% in the proliferation of several pancreatic cancer cells (including CFPAC-1) *in-vitro,* supporting the effects of the compound *in-vivo* (Ameera Jailani).

7.7.2 Data suggested involvement of AM2 receptor in tumour angiogenesis

The importance of AM and its receptor on tumour angiogenesis is well documented. Overexpression of AM in T47D breast cancer cell line both *in-vitro* and *in-vivo* resulted in a significantly increased vascular density (Martinez et al., 2002). Moreover, administration of AM peptide antagonist (AM_{22-52}) *in-vivo* had as a result the significant decrease in blood vessel formation in pancreatic cancer cell line (PCI-43) xenografts (Ishikawa et al., 2003). Downregulation of VEGF and upregulation of HIF-1α was observed after administration of the same antagonist on epithelial ovarian cancer cells (CAOV3) (Zhang et al., 2017).

Using CD31, a well-known marker of endothelial cells and vessel development, we investigated the effects of SHF-638 treatment in the formation of vessels *in-vivo*.

Data from the analysis suggested the possible role of AM in angiogenesis, showing a 23% decrease in the presence of CD31 positive vessels when compared with the vehicle control (Figure 6.22). However, this difference was not significant and further investigations are needed to establish this effect *in-vivo*. Administration of SHF-638 *in-vitro* had a significant effect in the formation of vessels by Human Umbilical Vein Endothelial Cells (HUVEC), showing possible effects in the maturation of the vessels (Ameera Jailani). A significant increase in the necrotic area of the treatment tumours when compared to the control group was found after analysis of H&E sections (Figure 6.16). This further supports the role of AM in vessel development suggesting that inhibition of angiogenesis by SHF-638 could potentially lead to starvation of tumour cells resulting in cell death and formation of necrotic areas. Nevertheless, studies have previously shown that excessive necrotic areas are associated with poor prognosis and aggressive phenotype in several types of cancer including osteosarcoma (Li et al., 2011), endometrial (Bredholt et al., 2015) and pancreatic cancer (Hiraoka et al., 2010).

7.7.3 Effects on tumour microenvironment

Moreover, the effects of SHF-638 and therefore of AM inhibition in tumour microenvironment were evaluated using α-SMA antibody (a well-known marker of CAFs and activated PSCs). Treatment with SHF-638 resulted in a significant decrease (35%) of α-SMA positive areas when compared to the control group (Figure 6.20), suggesting a lower number of CAFs and PSCs, as well as, connective tissue in the treatment tumours. The role of pancreatic stellate cells in the progression of pancreatic cancer was suggested in several studies. An increase in proliferation of pancreatic cancer cells as well as their ability to invade and form colonies was shown when cultured in the presence of PSCs conditioned media. In addition, the same media were able to protect the cells against hypoxia and gemcitabine induced apoptosis (Vonlaufen et al., 2008, Hwang et al., 2008). Furthermore, studies have shown the presence of stellate cells in pancreatic desmoplasia, a dense fibrous and connective tissue that surrounds the tumours (consists of alpha α-SMA positive CAFs or PSCs, immune cells and ECM proteins) (Apte et al., 2004, Pandol et al., 2009, Masamune et al., 2009). Desmoplastic structures are commonly found in pancreatic

tumours and they are believed to provide support and growth factors for tumour cells to grow. Expression of AM was previously found in pancreatic stellate cells, suggesting the role of AM on both pancreatic cells, as well as, on the cells of the tumour microenvironment in a paracrine manner (Ramachandran et al., 2007). In a recent study, AM was found to be a key growth factor of pancreatic cancer cells as well as pancreatic stellate cells *in-vitro* (Bhardwaj et al., 2016).

7.8 Conclusion

These data indicate a possible role of AM in the communication between the cancer cells and the tumour microenvironment, as well as, the development of desmoplastic structure characterized pancreatic tumours. It was shown that the formation of such dense structures could potentially affect the delivery of anticancer agents to the site of the primary tumour (pancreas) causing drug resistance (Schober et al., 2014). This indicates a possible use of AM antagonists in combination with chemotherapeutic agents in an effort to increase the delivery of the drug and therefore its efficacy. Orthotopic *in-vivo* studies investigating the effects of SHF-638 alone and in combination with gemcitabine are currently on-going in our lab with promising preliminary results.

7.9 Future work

This study was a part of a large multidisciplinary Wellcome Trust funded drug discovery program that aims the development of AM2 antagonists for the treatment of pancreatic cancer. The program is currently at the early stages of lead compound optimization with the objective of developing a suitable candidate that could be used in clinical trials alone or in combination with current treatment, with the ultimate goal of providing more treatment options and improving the quality of life of patients with pancreatic cancer.

The data above illustrate that by engineering commercially available highly selective and potent CGRP antagonist (MK3207) we were able to increase the potency against AM2 receptor and achieve a moderate selectivity over CGRP receptor and high selectivity over the other members of calcitonin family (SHF-638). However, the cross-selectivity over AM2r and CGRPr that characterised the majority of the

compounds developed indicates that further optimisation and refinement of the structure is required to avoid cross activity. Moreover, the good IV pharmacokinetic characteristics showed in this study suggested that intravenous infusion is the most feasible route of administration due to the low oral bioavailability shown (see appendix figure 8.3). This could be considered as a limitation due to the fact that patients will have to be regularly treated in hospital as opposed to taking the compound in the comfort of their home. Preliminary data from our group suggested that the use of a prodrug could potentially increase the oral bioavailability, however, this is not yet achieved with further studies ongoing. Moreover, differences in the pharmacokinetic properties between the different species used demonstrate the need for more extensive characterisation using more species including primates and dogs (studies are currently ongoing and likely to be completed during the next months). In addition, future studies using DMR and SPR analysis will be focused on investigating the binding kinetics of leading compounds that will provide more information on the mode and extent of receptor binding. Finally, ongoing studies are aiming to investigate the possible pathways and molecules involved on AM2 receptor mechanism of action and the effects of its inhibition on cancer cells and the tumour microenvironment.

Chapter 8: Appendix

Chapter 8: Appendix

MK-3207
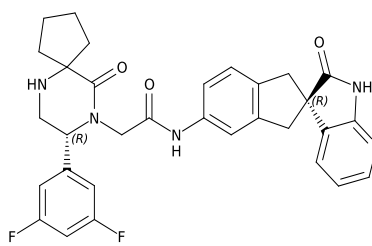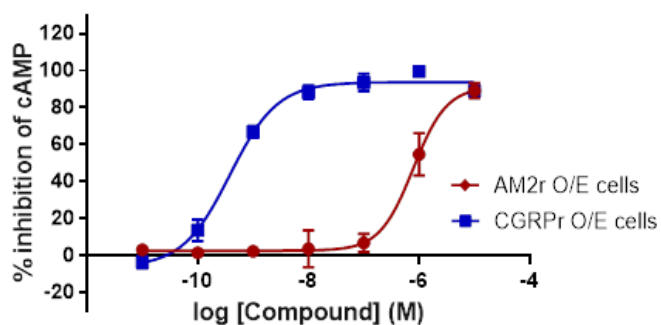
Olcegepant
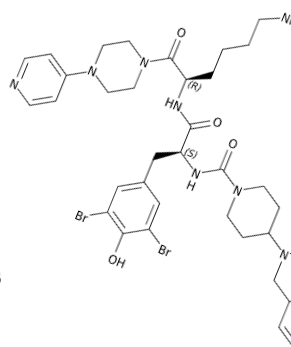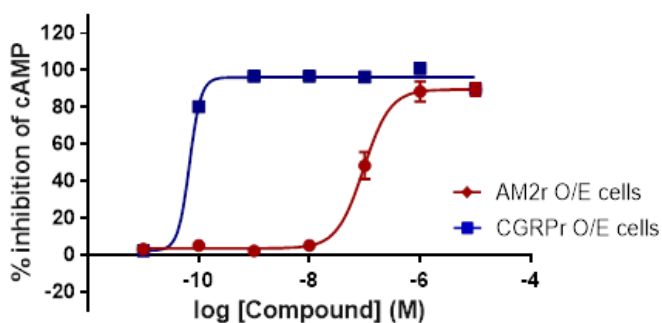
Telcagepant
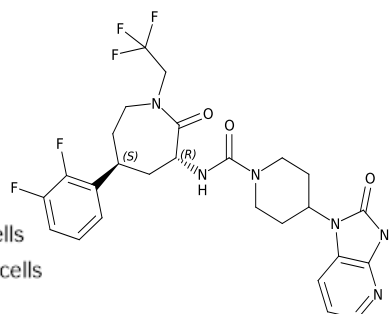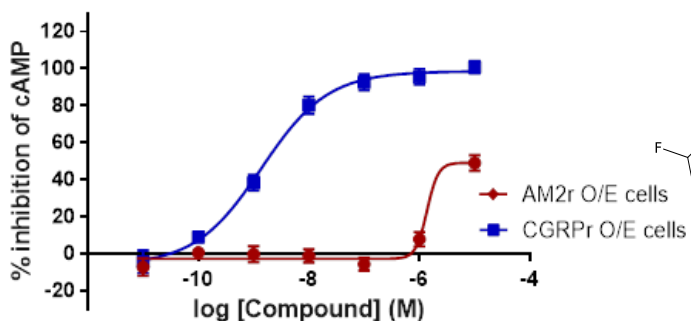
Ubrogepant
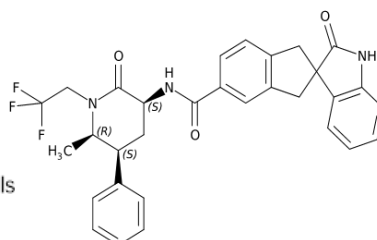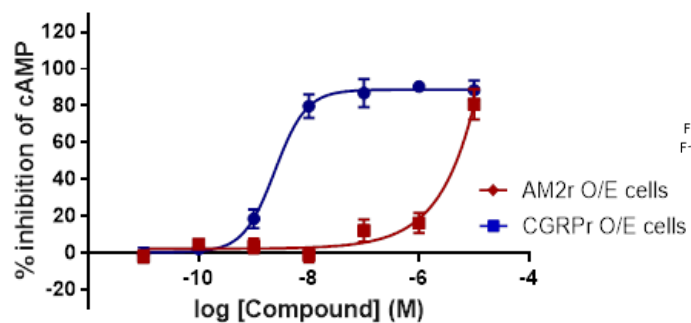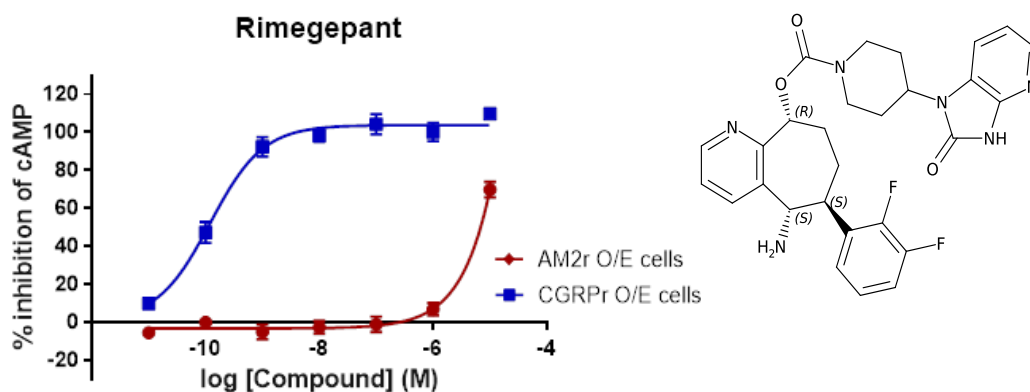
Figure 8.1: Activity of CGRP small molecule antagonists against AM2 and CGRP receptor O/E cells. Commercially available CGRP antagonists were tested for their ability to block the peptide ligand induced cAMP production in AM2 and CGRP receptor O/E cells. As expected, all compounds were highly potent and selective for CGRP receptor compared to AM2 receptor.
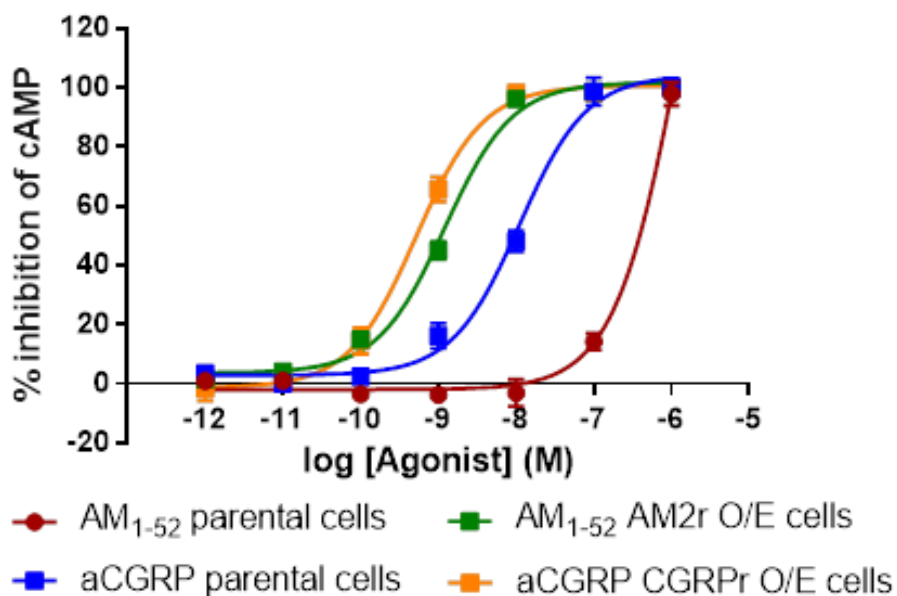
Figure 8.2: Agonist stimulation of 1321N1 parental cells and O/E cells. Showing the potency of AM1-52 and aCGRP for AM2r and CGRPr O/E cells respectively. The same activity was investigated their parental cell line 1321N1 cells.

Table 8.1: Differences in the activity of parental cells and O/E cells

Condition	Parameters			
	IC_{50}	pIC_{50}	Top	Bottom
AM1-52 stimulation				
Parental cells	145nM	-6.84	97.8	-1.76
AM2r O/E cells	1.2nM	-8.91	101	4.43
aCGRP stimulation				
Parental cells	11nM	-7.96	104	2.75
CGRPr O/E cells	0.53nM	-9.27	100	-0.79

Plasma Concentration of SHF-638-AA001 after Oral (PO) Dosing at 10 mg/kg (Rat n=3)
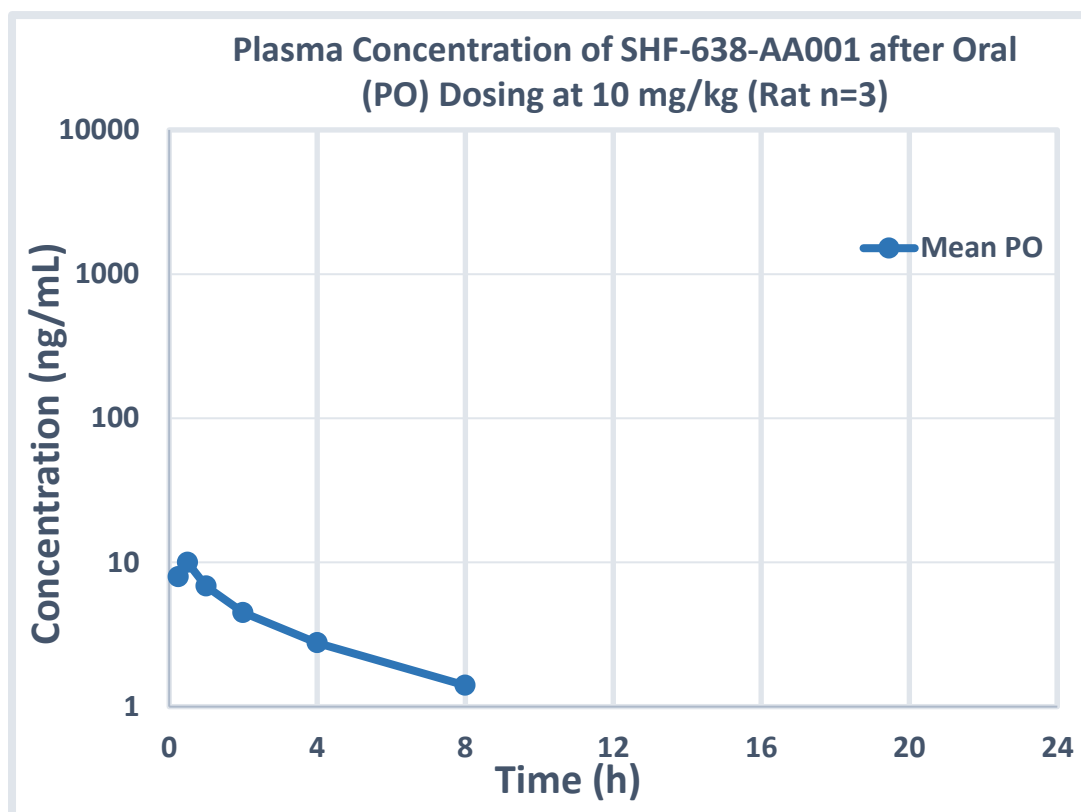
PK Parameters	Mean		SD	CV (%)
SHF-638-AA001 (10mg/kg PO dosing)				
Points used for $T_{1/2}$	ND	±	--	--
C_{max} (ng/mL)	9.99	±	0.889	8.90
T_{max} (h)	0.500	±	0.000	0.0
$T_{1/2}$ (h)	3.56	±	0.813	22.8
T_{last} (h)	8.00	±	--	--
AUC_{0-last} (ng·h/mL)	28.1	±	1.18	4.19
AUC_{0-inf} (ng.h/mL)	35.4	±	3.37	9.53
Bioavailability (%)[a]	0.999	±	--	--

*ND: Not Determined

C_{max}: Maximum conc. observed

AUC: Area under the conc. – time curve

AUC_{0-last}: Drug exposure until the last observed conc.

AUC_{0-inf}: Total drug exposure over time

$T_{1/2}$: Terminal phase half-life

T_{last}: Time at which the final conc. is observed

T_{max}: Time at which the maximum conc (C_{max}) is observed

Figure 8.3: Rat plasma concentration of SHF-638-AA001 after Oral (PO) dosing (10mg/kg).

Chapter 9: Bibliography

Chapter 9: Bibliography

ABASOLO, I., MONTUENGA, L. M. & CALVO, A. 2006. Adremomedullin prevents apoptosis in prostate cancer cells. *Regulatory Peptides,* 133**,** 115-122.

ABE, K., MINEGISHI, T., IBUKI, Y., KOJIMA, M. & KANGAWA, K. 2000. Expression of adrenomedullin in the human corpus luteum. *Fertility and Sterility,* 74**,** 141-145.

ABOU-ALFA, G. K., LETOURNEAU, R., HARKER, G., MODIANO, M., HURWITZ, H., TCHEKMEDYIAN, N. S., FEIT, K., ACKERMAN, J., DE JAGER, R. L., ECKHARDT, S. G. & O'REILLY, E. M. 2006. Randomized phase III study of exatecan and gemcitabine compared with gemcitabine alone in untreated advanced pancreatic cancer. *Journal of Clinical Oncology,* 24**,** 4441-4447.

ADAMCZYK, M., MOORE, J. A. & SHREDER, K. 2002. Dual analyte detection using tandem flash luminescence. *Bioorganic & Medicinal Chemistry Letters,* 12**,** 395-398.

AGGARWAL, G., RAMACHANDRAN, V., JAVEED, N., ARUMUGAM, T., DUTTA, S., KLEE, G. G., KLEE, E. W., SMYRK, T. C., BAMLET, W., HAN, J. J., VITTAR, N. B. R., DE ANDRADE, M., MUKHOPADHYAY, D., PETERSEN, G. M., FERNANDEZ-ZAPICO, M. E., LOGSDON, C. D. & CHARI, S. T. 2012. Adrenomedullin is Up-regulated in Patients With Pancreatic Cancer and Causes Insulin Resistance in beta Cells and Mice. *Gastroenterology,* 143**,** 1510-+.

AHMED, T. A. 2015. Pharmacokinetics of Drugs Following IV Bolus, IV Infusion, and Oral Administration. *In:* AHMED, D. T. A. (ed.) *Basic Pharmacokinetic Concepts and Some Clinical Applications.* InTech.

AIYAR, N., RAND, K., ELSHOURBAGY, N. A., ZENG, Z. Z., ADAMOU, J. E., BERGSMA, D. J. & LI, Y. 1996. A cDNA encoding the calcitonin gene-related peptide type 1 receptor. *Journal of Biological Chemistry,* 271**,** 11325-11329.

AKERMAN, S., WILLIAMSON, D. J., KAUBE, H. & GOADSBY, P. J. 2002. Nitric oxide synthase inhibitors can antagonize neurogenic and calcitonin gene-related peptide induced dilation of dural meningeal vessels. *British Journal of Pharmacology,* 137**,** 62-68.

AL-SABAH, S. & DONNELLY, D. 2003. A model for receptor-peptide binding at the glucagon-like peptide-1 (GLP-1) receptor through the analysis of truncated ligands and receptors. *British Journal of Pharmacology,* 140**,** 339-346.

ALBERTIN, G., CARRARO, G., PETRELLI, L., GUIDOLIN, D., NERI, G. & NUSSDORFER, G. G. 2005. Endothelin-1 and adrenomedullin enhance the growth of human adrenocortical carcinoma-derived SW-13 cell line by stimulating proliferation and inhibiting apoptosis. *International Journal of Molecular Medicine,* 15**,** 469-474.

ALLEN, M., HALL, D., COLLINS, B. & MOORE, K. 2002. A homogeneous high throughput nonradioactive method for measurement of functional activity of G(s)-coupled receptors in membranes. *Journal of Biomolecular Screening,* 7**,** 35-44.

AMARA, S. G., ARRIZA, J. L., LEFF, S. E., SWANSON, L. W., EVANS, R. M. & ROSENFELD, M. G. 1985. EXPRESSION BRAIN OF A MESSENGER-RNA ENCODING A NOVEL NEUROPEPTIDE HOMOLOGOUS TO CALCITONIN GENE-RELATED PEPTIDE. *Science,* 229**,** 1094-1097.

AMARA, S. G., JONAS, V., ROSENFELD, M. G., ONG, E. S. & EVANS, R. M. 1982. ALTERNATIVE RNA PROCESSING IN CALCITONIN GENE-EXPRESSION GENERATES MESSENGER-RNAS ENCODING DIFFERENT POLYPEPTIDE PRODUCTS. *Nature,* 298**,** 240-244.

ANDO, K., PEGRAM, B. L. & FROHLICH, E. D. 1990. HEMODYNAMIC-EFFECTS OF CALCITONIN GENE-RELATED PEPTIDE IN SPONTANEOUSLY HYPERTENSIVE RATS. *American Journal of Physiology,* 258**,** R425-R429.

ANTOLINO, L., LA ROCCA, M., TODDE, F., CATARINOZZI, E., AURELLO, P., BOLLANTI, L., RAMACCIATO, G. & D'ANGELO, F. 2017. Can pancreatic cancer be detected by adrenomedullin in patients with new-onset diabetes? The PaCANOD cohort study protocol. *Tumori*, 0.

APTE, M. V., PARK, S., PHILLIPS, P. A., SANTUCCI, N., GOLDSTEIN, D., KUMAR, R. K., RAMM, G. A., BUCHLER, M., FRIESS, H., MCCARROLL, J. A., KEOGH, G., MERRETT, N., PIROLA, R. & WILSON, J. S. 2004. Desmoplastic reaction in pancreatic cancer - Role of pancreatic stellate cells. *Pancreas,* 29**,** 179-187.

ARCHBOLD, J. K., FLANAGAN, J. U., WATKINS, H. A., GINGELL, J. J. & HAY, D. L. 2011. Structural insights into RAMP modification of secretin family G protein-coupled receptors: implications for drug development. *Trends in Pharmacological Sciences,* 32**,** 591-600.

ARULMANI, U., SCHUIJT, M. P., HEILIGERS, J. R. C., WILLEMS, E. W., VILLALON, C. M. & SAXENA, P. R. 2004. Effects of the calcitonin gene-related peptide (CGRP) receptor antagonist BIBN4096BS on alpha-CGRP-Induced regional haemodynamic changes in anaesthetised rats. *Basic & Clinical Pharmacology & Toxicology,* 94**,** 291-297.

ARUNLAKSHANA, O. & SCHILD, H. O. 1959. SOME QUANTITATIVE USES OF DRUG ANTAGONISTS. *British Journal of Pharmacology and Chemotherapy,* 14**,** 48-58.

ASADA, Y., HARA, S., MARUTSUKA, K., KITAMURA, K., TSUJI, T., SAKATA, J., SATO, Y., KISANUKI, A., ETO, T. & SUMIYOSHI, A. 1999. Novel distribution of adrenomedullin-immunoreactive cells in human tissues. *Histochemistry and Cell Biology,* 112**,** 185-191.

BARWELL, J., CONNER, A. & POYNER, D. R. 2011. Extracellular loops 1 and 3 and their associated transmembrane regions of the calcitonin receptor-like receptor are needed for CGRP receptor function. *Biochimica Et Biophysica Acta-Molecular Cell Research,* 1813**,** 1906-1916.

BARWELL, J., GINGELL, J. J., WATKINS, H. A., ARCHBOLD, J. K., POYNER, D. R. & HAY, D. L. 2012. Calcitonin and calcitonin receptor-like receptors: common themes with family B GPCRs? *British Journal of Pharmacology,* 166**,** 51-65.

BAZIN, H., PREAUDAT, M., TRINQUET, E. & MATHIS, G. 2001. Homogeneous time resolved fluorescence resonance energy transfer using rare earth cryptates as a tool for probing molecular interactions in biology. *Spectrochimica Acta Part a-Molecular and Biomolecular Spectroscopy,* 57**,** 2197-2211.

BELL, D. & MCDERMOTT, B. J. 2008. Intermedin (adrenomedullin-2): a novel counter-regulatory peptide in the cardiovascular and renal systems. *British Journal of Pharmacology,* 153**,** S247-S262.

BELL, I. M., GALLICCHIO, S. N., WOOD, M. R., QUIGLEY, A. G., STUMP, C. A., ZARTMAN, C. B., FAY, J. F., LI, C. C., LYNCH, J. J., MOORE, E. L., MOSSER, S. D., PRUEKSARITANONT, T., REGAN, C. P., ROLLER, S., SALVATORE, C. A., KANE, S. A., VACCA, J. P. & SELNICK, H. G. 2010. Discovery of MK-3207: A Highly Potent, Orally Bioavailable CGRP Receptor Antagonist. *Acs Medicinal Chemistry Letters,* 1**,** 24-29.

BELTOWSKI, J. & JAMROZ, A. 2004. Adrenomedullin - What do we know 10 years since its discovery? *Polish Journal of Pharmacology,* 56**,** 5-27.

BENSON, J. D., CHEN, Y. N. P., CORNELL-KENNON, S. A., DORSCH, M., KIM, S., LESZCZYNIECKA, M., SELLERS, W. R. & LENGAUER, C. 2006. Validating cancer drug targets. *Nature,* 441**,** 451-456.

BERENGUER, C., BOUDOURESQUE, F., DUSSERT, C., DANIEL, L., MURACCIOLE, X., GRINO, M., ROSSI, D., MABROUK, K., FIGARELLA-BRANGER, D., MARTIN, P. M. & OUAFIK, L. 2008. Adrenomedullin, an autocrine/paracrine factor induced by androgen withdrawal, stimulates 'neuroendocrine phenotype' in LNCaP prostate tumor cells. *Oncogene,* 27**,** 506-518.

BERGWITZ, C., GARDELLA, T. J., FLANNERY, M. R., POTTS, J. T., KRONENBERG, H. M., GOLDRING, S. R. & JUPPNER, H. 1996. Full activation of chimeric receptors by hybrids between parathyroid hormone and calcitonin - Evidence for a common pattern of ligand-receptor interaction. *Journal of Biological Chemistry,* 271**,** 26469-26472.

BERKEY, F. J. 2010. Managing the Adverse Effects of Radiation Therapy. *American Family Physician,* 82**,** 381-388.

BHARDWAJ, A., SRIVASTAVA, S. K., SINGH, S., TYAGI, N., ARORA, S., CARTER, J. E., KHUSHMAN, M. & SINGH, A. P. 2016. MYB Promotes Desmoplasia in Pancreatic Cancer through Direct Transcriptional Up-regulation and Cooperative Action of Sonic Hedgehog and Adrenomedullin. *Journal of Biological Chemistry,* 291**,** 16263-16270.

BLACK, J. W., DUNCAN, W. A. M. & SHANKS, R. G. 1965. COMPARISON OF SOME PROPERTIES OF PRONETHALOL AND PROPRANOLOL. *British Journal of Pharmacology and Chemotherapy,* 25**,** 577-&.

BLACK, J. W., PARSONS, E. M., DURANT, C. J., DUNCAN, W. A. M. & GANELLIN, C. R. 1972. DEFINITION AND ANTAGONISM OF HISTAMINE H2-RECEPTORS. *Nature,* 236**,** 385-&.

BOMBERGER, J. M., PARAMESWARAN, N., HALL, C. S., AIYAR, N. & SPIELMAN, W. S. 2005. Novel function for receptor activity-modifying proteins (RAMPs) in post-endocytic receptor trafficking. *Journal of Biological Chemistry,* 280**,** 9297-9307.

BOND-SMITH, G., BANGA, N., HAMMOND, T. M. & IMBER, C. J. 2012. Pancreatic adenocarcinoma. *British Medical Journal,* 344.

BOOE, J. M., WALKER, C. S., BARWELL, J., KUTEYI, G., SIMMS, J., JAMALUDDIN, M. A., WARNER, M. L., BILL, R. M., HARRIS, P. W., BRIMBLE, M. A., POYNER, D. R., HAY, D. L. & PIOSZAK, A. A. 2015. Structural Basis for Receptor Activity-Modifying Protein-Dependent Selective Peptide Recognition by a G Protein-Coupled Receptor. *Molecular Cell,* 58**,** 1040-1052.

BORNMAN, P. C. & BECKINGHAM, I. J. 2001. ABC of diseases of liver, pancreas, and biliary, system - Pancreatic tumours. *British Medical Journal,* 322**,** 721-723.

BOWMAN, W. C. 2006. Neuromuscular block. *British Journal of Pharmacology,* 147**,** S277-S286.

BRAIN, S. D., TIPPINS, J. R., MORRIS, H. R., MACINTYRE, I. & WILLIAMS, T. J. 1986. POTENT VASODILATOR ACTIVITY OF CALCITONIN GENE-RELATED PEPTIDE IN HUMAN-SKIN. *Journal of Investigative Dermatology,* 87**,** 533-536.

BRAIN, S. D., WILLIAMS, T. J., TIPPINS, J. R., MORRIS, H. R. & MACINTYRE, I. 1985. CALCITONIN GENE-RELATED PEPTIDE IS A POTENT VASODILATOR. *Nature,* 313**,** 54-56.

BREDHOLT, G., MANNELQVIST, M., STEFANSSON, I. M., BIRKELAND, E., BO, T. H., OYAN, A. M., TROVIK, J., KALLAND, K. H., JONASSEN, I., SALVESEN, H. B., WIK, E. & AKSLEN, L. A. 2015. Tumor necrosis is an important hallmark of aggressive endometrial cancer and associates with hypoxia, angiogenesis and inflammation responses. *Oncotarget,* 6**,** 39676-39691.

BREKHMAN, V., LUGASSIE, J., ZAFFRYAR-EILOT, S., SABO, E., KESSLER, O., SMITH, V., GOLDING, H. & NEUFELD, G. 2011. Receptor activity modifying protein-3 mediates the protumorigenic activity of lysyl oxidase-like protein-2. *Faseb Journal,* 25**,** 55-65.

BUHLMANN, N., LEUTHAUSER, K., MUFF, R., FISCHER, J. A. & BORN, W. 1999. A receptor activity modifying protein (RAMP)2-dependent adrenomedullin receptor is a calcitonin gene-related peptide receptor when coexpressed with human RAMP1. *Endocrinology,* 140**,** 2883-2890.

BUNNAGE, M. E. 2011. Getting pharmaceutical R&D back on target. *Nature Chemical Biology,* 7**,** 335-339.

BUSCH, M., THOMA, H. B. & KOBER, I. 2013. Does Your Lab Coat Fit to Your Assay? *Journal of Biomolecular Screening,* 18**,** 744-747.

CALVO, A., ABASOLO, I., JIMENEZ, N., WANG, Z. & MONTUENGA, L. 2002. Adrenomedullin and proadrenomedullin N-terminal 20 peptide in the normal prostate and in prostate carcinoma. *Microscopy Research and Technique,* 57**,** 98-104.

CANCER RESEARCH UK. 2014a. *Cancer incidence for common cancers* [Online]. Available: http://www.cancerresearchuk.org/health-professional/cancer-statistics/incidence/common-cancers-compared#heading-Zero [Accessed 21 December 2017].

CANCER RESEARCH UK. 2014b. *Cancer survival for common cancers* [Online]. Available: http://www.cancerresearchuk.org/health-professional/cancer-statistics/survival/common-cancers-compared [Accessed 21 December 2017].

CANCER RESEARCH UK. 2014c. *Pancreatic cancer statistics* [Online]. Available: http://www.cancerresearchuk.org/health-professional/cancer-statistics/statistics-by-cancer-type/pancreatic-cancer#heading-Two [Accessed 20 December 2017].

CANCER RESEARCH UK. 2014. *Pancreatic cancer statistics* [Online]. Available: http://www.cancerresearchuk.org/health-professional/cancer-statistics/statistics-by-cancer-type/pancreatic-cancer#heading-Zero [Accessed 21 December 2017].

CANO, D. A., HEBROK, M. & ZENKER, M. 2007. Pancreatic development and disease. *Gastroenterology,* 132**,** 745-762.

CARON, K. M. & SMITHIES, O. 2001. Extreme hydrops fetalis and cardiovascular abnormalities in mice lacking a functional Adrenomedullin gene. *Proceedings of the National Academy of Sciences of the United States of America,* 98**,** 615-619.

CHAI, W. X., MEHROTRA, S., DANSER, A. H. J. & SCHOEMAKER, R. G. 2006. The role of calcitonin gene-related peptide (CGRP) in ischemic preconditioning in isolated rat hearts. *European Journal of Pharmacology,* 531**,** 246-253.

CHAN, K. Y., EDVINSSON, L., EFTEKHARI, S., KIMBLAD, P. O., KANE, S. A., LYNCH, J., HARGREAVES, R. J., DE VRIES, R., GARRELDS, I. M., VAN DEN BOGAERDT, A. J., DANSER, A. H. J. & MAASSENVANDENBRINK, A. 2010. Characterization of the Calcitonin Gene-Related Peptide Receptor Antagonist Telcagepant (MK-0974) in Human Isolated Coronary Arteries. *Journal of Pharmacology and Experimental Therapeutics,* 334**,** 746-752.

CHANG, C. P., PEARSE, R. V., OCONNELL, S. & ROSENFELD, M. G. 1993. IDENTIFICATION OF A 7 TRANSMEMBRANE HELIX RECEPTOR FOR CORTICOTROPIN-RELEASING FACTOR AND SAUVAGINE IN MAMMALIAN BRAIN. *Neuron,* 11**,** 1187-1195.

CHEN, J., LAKE, M. R., SABET, R. S., NIFORATOS, W., PRATT, S. D., CASSAR, S. C., XU, J., GOPALAKRISHNAN, S., PEREDA-LOPEZ, A., GOPALAKRISHNAN, M., HOLZMAN, T. F., MORELAND, R. B., WALTER, K. A., FALTYNEK, C. R., WARRIOR, U. & SCOTT, V. E. 2007. Utility of large-scale transiently transfected cells for cell-based high-throughput screens to identify transient receptor potential channel A1 (TRPA1) antagonists. *Journal of Biomolecular Screening,* 12**,** 61-69.

CHEUNG, B. M. Y. & TANG, F. 2012. Adrenomedullin: exciting new horizons. *Recent patents on endocrine, metabolic & immune drug discovery,* 6**,** 4-17.

CHIEN, J. Y., FRIEDRICH, S., HEATHMAN, M. A., DE ALWIS, D. P. & SINHA, V. 2005. Pharmacokinetics/pharmacodynamics and the stages of drug development: Role of modeling and simulation. *Aaps Journal,* 7**,** E544-E559.

CHRISTOPOULOS, A., CHRISTOPOULOS, G., MORFIS, M., UDAWELA, M., LABURTHE, M., COUVINEAU, A., KUWASAKO, K., TILAKARATNE, N. & SEXTON, P. M. 2003. Novel

receptor partners and function of receptor activity-modifying proteins. *Journal of Biological Chemistry,* 278**,** 3293-3297.

CHUNG, T., TERRY, D. & SMITH, L. 2015. In Vitro and In Vivo Assessment of ADME and PK Properties During Lead Selection and Lead Optimization – Guidelines, Benchmarks and Rules of Thumb. *In:* SITTAMPALAM, G., COUSSENS, N. & BRIMACOMBE, K. (eds.) *Assay Guidance Manual.* Eli Lilly & Company and the National Center for Advancing Translational Sciences.

CRAIG, R. K., HALL, L., EDBROOKE, M. R., ALLISON, J. & MACINTYRE, I. 1982. PARTIAL NUCLEOTIDE-SEQUENCE OF HUMAN CALCITONIN PRECURSOR MESSENGER-RNA IDENTIFIES FLANKING CRYPTIC PEPTIDES. *Nature,* 295**,** 345-347.

CROY, C. H., CHAN, W. Y., CASTETTER, A. M., WATT, M. L., QUETS, A. T. & FELDER, C. C. 2016. Characterization of PCS1055, a novel muscarinic M-4 receptor antagonist. *European Journal of Pharmacology,* 782**,** 70-76.

CUMMINGS, M. D., DESJARLAIS, R. L., GIBBS, A. C., MOHAN, V. & JAEGER, E. P. 2003. Comparison of virtual screening programs. *Abstracts of Papers of the American Chemical Society,* 226**,** U456-U456.

CUNNINGHAM, D., CHAU, I., STOCKEN, D. D., VALLE, J. W., SMITH, D., STEWARD, W., HARPER, P. G., DUNN, J., TUDUR-SMITH, C., WEST, J., FALK, S., CRELLIN, A., ADAB, F., THOMPSON, J., LEONARD, P., OSTROWSKI, J., EATOCK, M., SCHEITHAUER, W., HERRMANN, R. & NEOPTOLEMOS, J. P. 2009. Phase III Randomized Comparison of Gemcitabine Versus Gemcitabine Plus Capecitabine in Patients With Advanced Pancreatic Cancer. *Journal of Clinical Oncology,* 27**,** 5513-5518.

D'ANGELO, F., LETIZIA, C., ANTOLINO, L., LA ROCCA, M., AURELLO, P., RAMACCIATO, G., DEPARTMENT OF SURGERY AND TRANSLATIONAL MEDICINE, F. O. M. A. P., SAPIENZA UNIVERSITY OF ROME, ROME, ITALY AURELLO PAOLO & DEPARTMENT OF SURGERY AND TRANSLATIONAL MEDICINE, F. O. M. A. P., SAPIENZA UNIVERSITY OF ROME, ROME, ITAL RAMACCIATO GIOVANNI AURELLO PAOLO. 2016. Adrenomedullin in pancreatic carcinoma: A case-control study of 22 patients.

DACKOR, R., FRITZ-SIX, K., SMITHIES, O. & CARON, K. 2007. Receptor activity-modifying proteins 2 and 3 have distinct physiological functions from embryogenesis to old age. *Journal of Biological Chemistry,* 282**,** 18094-18099.

DACKOR, R. T., FRITZ-SIX, K., DUNWORTH, W. P., GIBBONS, C. L., SMITHIES, O. & CARON, K. M. 2006. Hydrops fetalis, cardiovascular defects, and embryonic lethality in mice lacking the Calcitonin receptor-like receptor gene. *Molecular and Cellular Biology,* 26**,** 2511-2518.

DAL MASO, E., ZHU, Y., PHAM, V., REYNOLDS, C. A., DEGANUTTI, G., HICK, C. A., YANG, D., CHRISTOPOULOS, A., HAY, D. L., WANG, M.-W., SEXTON, P. M., FURNESS, S. G. B. & WOOTTEN, D. 2018. Extracellular loops 2 and 3 of the calcitonin receptor selectively modify agonist binding and efficacy. *Biochemical Pharmacology,* 150**,** 214-244.

DE LA CRUZ, M. S. D., YOUNG, A. R. & RUFFIN, M. T. 2014. Diagnosis and Management of Pancreatic Cancer. *American Family Physician,* 89**,** 626-632.

DEL CASTILLO, J. & KATZ, B. 1957. Interaction at end-plate receptors between different choline derivatives. *Proc R Soc Lond B Biol Sci,* 146**,** 369-81.

DEVILLE, J. L., BARTOLI, C., BERENGUER, C., FERNANDEZ-SAUZE, S., KAAFARANI, I., DELFINO, C., FINA, F., SALAS, S., MURACCIOLE, X., MANCINI, J., LECHEVALLIER, E., MARTIN, P. M., FIGARELLA-BRANGER, D., OUAFIK, L. & DANIEL, L. 2009. Expression and role of adrenomedullin in renal tumors and value of its mRNA levels as prognostic factor in clear-cell renal carcinoma. *International Journal of Cancer,* 125**,** 2307-2315.

DIIORIO, R., MARINONI, E., SCAVO, D., LETIZIA, C. & COSMI, E. V. 1997. Adrenomedullin in pregnancy. *Lancet,* 349**,** 328-328.

DOODS, H., HALLERMAYER, G., WU, D. M., ENTZEROTH, M., RUDOLF, K., ENGEL, W. & EBERLEIN, W. 2000. Pharmacological profile of BIBN4096BS, the first selective small molecule CGRP antagonist. *British Journal of Pharmacology,* 129**,** 420-423.

DRISSI, H., LIEBERHERR, M., HOTT, M., MARIE, P. J. & LASMOLES, F. 1999. Calcitonin gene-related peptide (CGRP) increases intracellular free Ca2+ concentrations but not cyclic AMP formation in CGRP receptor-positive osteosarcoma cells (OHS-4). *Cytokine,* 11**,** 200-207.

DYMOND, A. W., SO, K. R., MARTIN, P., HUANG, Y. F., SEVERIN, P., MATHEWS, D., LISBON, E. & MARIANI, G. 2017. Effects of cytochrome P450 (CYP3A4 and CYP2C19) inhibition and induction on the exposure of selumetinib, a MEK1/2 inhibitor, in healthy subjects: results from two clinical trials. *European Journal of Clinical Pharmacology,* 73**,** 175-184.

EDVINSSON, L. 2004. Blockade of CGRP receptors in the intracranial vasculature: a new target in the treatment of headache. *Cephalalgia,* 24**,** 611-622.

EDVINSSON, L., ALM, R., SHAW, D., RUTLEDGE, R. Z., KOBLAN, K. S., LONGMORE, J. & KANE, S. A. 2002. Effect of the CGRP receptor antagonist BIBN4096BS in human cerebral, coronary and omental arteries and in SK-N-MC cells. *European Journal of Pharmacology,* 434**,** 49-53.

EGLEN, R. M. & REISINE, T. 2008. Photoproteins: Important New Tools in Drug Discovery. *Assay and Drug Development Technologies,* 6**,** 659-671.

EGLEN, R. M. & REISINE, T. 2009. New Insights into GPCR Function: Implications for HTS. *G Protein-Coupled Receptors in Drug Discovery,* 552**,** 1-13.

EKINS, S., HONEYCUTT, J. D. & METZ, J. T. 2010. Evolving molecules using multi-objective optimization: applying to ADME/Tox. *Drug Discovery Today,* 15**,** 451-460.

ETO, T., KATO, J. & KITAMURA, K. 2003. Regulation of production and secretion of adrenomedullin in the cardiovascular system. *Regulatory Peptides,* 112**,** 61-69.

EVANS, B. N., ROSENBLATT, M. I., MNAYER, L. O., OLIVER, K. R. & DICKERSON, I. M. 2000. CGRP-RCP, a novel protein required for signal transduction at calcitonin gene-related peptide and adrenomedullin receptors. *Journal of Biological Chemistry,* 275**,** 31438-31443.

FANG, Y. 2016. Label-free technologies and pharmacology. *Pharmacological Research,* 108**,** 88-89.

FENG, C. J., KANG, B., KAYE, A. D., KADOWITZ, P. J. & NOSSAMAN, B. D. 1994. L-NAME MODULATES RESPONSES TO ADRENOMEDULLIN IN THE HINDQUARTERS VASCULAR BED OF THE RAT. *Life Sciences,* 55**,** PL433-PL438.

FERNANDES, E. S., SCHMIDHUBER, S. M. & BRAIN, S. D. 2009. Sensory-nerve-derived neuropeptides: possible therapeutic targets. *Handbook of experimental pharmacology***,** 393-416.

FERNANDEZ-SAUZE, S., DELFINO, C., MABROUK, K., DUSSERT, C., CHINOT, O., MARTIN, P. M., GRISOLI, F., OUAFIK, L. & BOUDOURESQUE, F. 2004. Effects of adrenomedullin on endothelial cells in the multistep process of angiogenesis: Involvement of CRLR/RAMP2 and CRLR/RAMP3 receptors. *International Journal of Cancer,* 108**,** 797-804.

FLUHMANN, B., MUFF, R., HUNZIKER, W., FISCHER, J. A. & BORN, W. 1995. A HUMAN ORPHAN CALCITONIN RECEPTOR-LIKE STRUCTURE. *Biochemical and Biophysical Research Communications,* 206**,** 341-347.

FOLIAS, A. E. & HEBROK, M. 2013. Anatomy and Physiology of the Pancreas. *In:* LAMMERT, E. & ZEEB, M. (eds.) *Metabolism of Human Diseases.* Springer.

FOX, S., FARR-JONES, S., SOPCHAK, L., BOGGS, A., NICELY, H. W., KHOURY, R. & BIROS, M. 2006. High-throughput screening: Update on practices and success. *Journal of Biomolecular Screening,* 11**,** 864-869.

FRASER, N. J., WISE, A., BROWN, J., MCLATCHIE, L. M., MAIN, M. J. & FOORD, S. M. 1999. The amino terminus of receptor activity modifying proteins is a critical determinant of glycosylation state and ligand binding of calcitonin receptor-like receptor. *Molecular Pharmacology,* 55**,** 1054-1059.

FRITZ-SIX, K. L., DUNWORTH, W. P., LI, M. & CARON, K. M. 2008. Adrenomedullin signaling is necessary for murine lymphatic vascular development. *Journal of Clinical Investigation,* 118**,** 40-50.

FURSOV, N., CONG, M., FEDERICI, M., PLATCHEK, M., HAYTKO, P., TACKE, R., LIVELLI, T. & ZHONG, Z. 2005. Improving consistency of cell-based assays by using division-arrested cells. *Assay and Drug Development Technologies,* 3**,** 7-15.

GADDUM, J. H. 1957. THEORIES OF DRUG ANTAGONISM. *Pharmacological Reviews,* 9**,** 211-218.

GALLAI, V., SARCHIELLI, P., FLORIDI, A., FRANCESCHINI, M., CODINI, M., GLIOTI, G., TREQUATTRINI, A. & PALUMBO, R. 1995. VASOACTIVE PEPTIDE LEVELS IN THE PLASMA OF YOUNG MIGRAINE PATIENTS WITH AND WITHOUT AURA ASSESSED BOTH INTERICTALLY AND ICTALLY. *Cephalalgia,* 15**,** 384-390.

GANGULA, P. R. R., ZHAO, H., SUPOWIT, S., WIMALAWANSA, S., DIPETTE, D. & YALLAMPALLI, C. 1999. Pregnancy and steroid hormones enhance the vasodilation responses to CGRP in rats. *American Journal of Physiology-Heart and Circulatory Physiology,* 276**,** H284-H288.

GILL, P., GROTHEY, A. & LOPRINZI, C. 2006. Nausea and vomiting in the cancer patient . *Oncology: An Evidence-Based Approach.*: Springer New York.

GINGELL, J. J., SIMMS, J., BARWELL, J., POYNER, D. R., WATKINS, H. A., PIOSZAK, A. A., SEXTON, P. M. & HAY, D. L. 2016. An allosteric role for receptor activity-modifying proteins in defining GPCR pharmacology. *Cell Discovery,* 2.

GOADSBY, P. J. & EDVINSSON, L. 1994. HUMAN IN-VIVO EVIDENCE FOR TRIGEMINOVASCULAR ACTIVATION IN CLUSTER HEADACHE - NEUROPEPTIDE CHANGES AND EFFECTS OF ACUTE ATTACKS THERAPIES. *Brain,* 117**,** 427-434.

GOADSBY, P. J., EDVINSSON, L. & EKMAN, R. 1988. RELEASE OF VASOACTIVE PEPTIDES IN THE EXTRACEREBRAL CIRCULATION OF HUMANS AND THE CAT DURING ACTIVATION OF THE TRIGEMINOVASCULAR SYSTEM. *Annals of Neurology,* 23**,** 193-196.

GOADSBY, P. J., EDVINSSON, L. & EKMAN, R. 1990. VASOACTIVE PEPTIDE RELEASE IN THE EXTRACEREBRAL CIRCULATION OF HUMANS DURING MIGRAINE HEADACHE. *Annals of Neurology,* 28**,** 183-187.

GOADSBY, P. J., LIPTON, R. B. & FERRARI, M. D. 2002. Drug therapy: Migraine - Current understanding and treatment. *New England Journal of Medicine,* 346**,** 257-270.

GOETZ, M. P., KNOX, S. K., SUMAN, V. J., RAE, J. M., SAFGREN, S. L., AMES, M. M., VISSCHER, D. W., REYNOLDS, C., COUCH, F. J., LINGLE, W. L., WEINSHILBOUM, R. M., FRITCHER, E. G. B., NIBBE, A. M., DESTA, Z., NGUYEN, A., FLOCKHART, D. A., PEREZ, E. A. & INGLE, J. N. 2007. The impact of cytochrome P450 2D6 metabolism in women receiving adjuvant tamoxifen. *Breast Cancer Research and Treatment,* 101**,** 113-121.

GOLLA, R. & SEETHALA, R. 2002. A homogeneous enzyme fragment complementation cyclic AMP screen for GPCR agonists. *Journal of Biomolecular Screening,* 7**,** 515-525.

GOULD, S. E., JUNTTILA, M. R. & DE SAUVAGE, F. J. 2015. Translational value of mouse models in oncology drug development. *Nature Medicine,* 21**,** 431.

GUNTER, B., BRIDEAU, C., PIKOUNIS, B. & LIAW, A. 2003. Statistical and graphical methods for quality control determination of high-throughput screening data. *Journal of Biomolecular Screening,* 8**,** 624-633.

HAGUE, S., ZHANG, L., OEHLER, M. K., MANEK, S., MACKENZIE, I. Z., BICKNELL, R. & REES, M. C. P. 2000. Expression of the hypoxically regulated angiogenic factor adrenomedullin correlates with uterine leiomyoma vascular density. *Clinical Cancer Research,* 6**,** 2808-2814.

HAJDUK, P. J. & GREER, J. 2007. A decade of fragment-based drug design: strategic advances and lessons learned. *Nature Reviews Drug Discovery,* 6**,** 211-219.

HAMID, S. A. & BAXTER, G. F. 2006. A critical cytoprotective role of endogenous adrenomedullin in acute myocardial infarction. *Journal of Molecular and Cellular Cardiology,* 41**,** 360-363.

HAO, S. L., YU, Z. H., QI, B. S., LUO, J. Z. & WANG, W. P. 2011. The antifibrosis effect of adrenomedullin in human lung fibroblasts. *Experimental Lung Research,* 37**,** 615-626.

HARADA, K., YAMAHARA, K., OHNISHI, S., OTANI, K., KANOH, H., ISHIBASHI-UEDA, H., MINAMINO, N., KANGAWA, K., NAGAYA, N. & IKEDA, T. 2011. Sustained-release adrenomedullin ointment accelerates wound healing of pressure ulcers. *Regulatory Peptides,* 168**,** 21-26.

HARIKUMAR, K. G., SIMMS, J., CHRISTOPOULOS, G., SEXTON, P. M. & MILLER, L. J. 2009. Molecular Basis of Association of Receptor Activity-Modifying Protein 3 with the Family B G Protein-Coupled Secretin Receptor. *Biochemistry,* 48**,** 11773-11785.

HARRIS, A. L. 2002. Hypoxia - A key regulatory factor in tumour growth. *Nature Reviews Cancer,* 2**,** 38-47.

HAUSER, A. S., ATTWOOD, M. M., RASK-ANDERSEN, M., SCHIÖTH, H. B. & GLORIAM, D. E. 2017. Trends in GPCR drug discovery: new agents, targets and indications. *Nature Reviews Drug Discovery*.

HAY, D. L., CHEN, S., LUTZ, T. A., PARKES, D. G. & ROTH, J. D. 2015. Amylin: Pharmacology, Physiology, and Clinical Potential. *Pharmacological Reviews,* 67**,** 564-600.

HAY, D. L., CHRISTOPOULOS, G., CHRISTOPOULOS, A., POYNER, D. R. & SEXTON, P. M. 2005. Pharmacological discrimination of calcitonin receptor: receptor activity-modifying protein complexes. *Molecular Pharmacology,* 67**,** 1655-1665.

HAY, D. L., CHRISTOPOULOS, G., CHRISTOPOULOS, A. & SEXTON, P. M. 2004. Amylin receptors: molecular composition and pharmacology. *Biochemical Society Transactions,* 32**,** 865-867.

HAY, D. L., CHRISTOPOULOS, G., CHRISTOPOULOS, A. & SEXTON, P. M. 2006a. Determinants of 1-piperidinecarboxamide, N- 2- 5-amino-l- 4(4-pyridinyl)-l-piperazinyl carbonyl pentyl amino -1 - (3,5-dibromo-4-hydroxyphenyl)methyl -2-oxoethyl -4-(1,4-dihydro-2-oxo- 3(2H)-quinazolinyl) (BIBN4096BS) affinity for calcitonin gene-related peptide and amylin receptors - The role of receptor activity modifying protein 1. *Molecular Pharmacology,* 70**,** 1984-1991.

HAY, D. L., HOWITT, S. G., CONNER, A. C., DOODS, H., SCHINDLER, M. & POYNER, D. R. 2002. A comparison of the actions of BIBN4096BS and CGRP(8-37) on CGRP and adrenomedullin receptors expressed on SK-N-MC, L6, Col 29 and Rat 2 cells. *British Journal of Pharmacology,* 137**,** 80-86.

HAY, D. L., HOWITT, S. G., CONNER, A. C., SCHINDLER, M., SMITH, D. M. & POYNER, D. R. 2003a. CL/RAMP2 and CL/RAMP3 produce pharmacologically distinct adrenomedullin receptors: a comparison of effects of adrenomedullin(22-52), CGRP(8-37) and BIBN4096BS. *British Journal of Pharmacology,* 140**,** 477-486.

HAY, D. L. & PIOSZAK, A. A. 2016. Receptor Activity-Modifying Proteins (RAMPs): New Insights and Roles. *Annual Review of Pharmacology and Toxicology,* 56**,** null.

HAY, D. L., POYNER, D. R. & SEXTON, P. M. 2006b. GPCR modulation by RAMPS. *Pharmacology & Therapeutics,* 109**,** 173-197.

HAY, D. L., POYNER, D. R. & SMITH, D. M. 2003b. Desensitisation of adrenomedullin and CGRP receptors. *Regulatory Peptides,* 112**,** 139-145.

HAY, D. L., WALKER, C. S., GINGELL, J. J., LADDS, G., REYNOLDS, C. A. & POYNER, D. R. 2016. Receptor activity-modifying proteins; multifunctional G protein-coupled receptor accessory proteins. *Biochemical Society Transactions,* 44**,** 568-573.

HAY, D. L., WALKER, C. S. & POYNER, D. R. 2011. Adrenomedullin and calcitonin gene-related peptide receptors in endocrine-related cancers: opportunities and challenges. *Endocrine-Related Cancer,* 18**,** C1-C14.

HAZELL, G. G. J., HINDMARCH, C. C., POPE, G. R., ROPER, J. A., LIGHTMAN, S. L., MURPHY, D., O'CARROLL, A. M. & LOLAIT, S. J. 2012. G protein-coupled receptors in the hypothalamic paraventricular and supraoptic nuclei - serpentine gateways to neuroendocrine homeostasis. *Frontiers in Neuroendocrinology,* 33**,** 45-66.

HE, Y. L., DING, G. F., WANG, X., ZHU, T. J. & FAN, S. G. 2000. Calcitonin gene-related peptide in Langerhans cells in psoriatic plaque lesions. *Chinese Medical Journal,* 113**,** 747-751.

HEFTI, F. F. 2008. Requirements for a lead compound to become a clinical candidate. *Bmc Neuroscience,* 9.

HEINEMANN, V., QUIETZSCH, D., GIESELER, F., GONNERMANN, M., SCHONEKAES, H., ROST, A., NEUHAUS, H., HAAG, C., CLEMENS, M., HEINRICH, B., VEHLING-KAISER, U., FUCHS, M., FLECKENSTEIN, D., GESIERICH, W., UTHGENANNT, D., EINSELE, H., HOLSTEGE, A., HINKE, A., SCHALHORN, A. & WILKOWSKI, R. 2006. Randomized phase III trial of gemcitabine plus cisplatin compared with gemcitabine alone in advanced pancreatic cancer. *Journal of Clinical Oncology,* 24**,** 3946-3952.

HEROUX, M., BRETON, B., HOGUE, M. & BOUVIER, M. 2007. Assembly and signaling of CRLR and RAMP1 complexes assessed by BRET. *Biochemistry,* 46**,** 7022-7033.

HEWITT, D. J., AURORA, S. K., DODICK, D. W., GOADSBY, P. J., GE, Y., BACHMAN, R., TARABORELLI, D., FAN, X. Y., ASSAID, C., LINES, C. & HO, T. W. 2011. Randomized controlled trial of the CGRP receptor antagonist MK-3207 in the acute treatment of migraine. *Cephalalgia,* 31**,** 712-722.

HIGUCHI, T., YOKOBORI, T., NAITO, T., KAKINUMA, C., HAGIWARA, S., NISHIYAMA, M. & ASAO, T. 2018. Investigation into metastatic processes and the therapeutic effects of gemcitabine on human pancreatic cancer using an orthotopic SUIT-2 pancreatic cancer mouse model. *Oncology Letters,* 15**,** 3091-3099.

HINDER, M. 2011. Pharmacodynamic Drug–Drug Interactions. *In:* VOGEL, H. G., MAAS, J. & GEBAUER, A. (eds.) *Drug Discovery and Evaluation: Methods in Clinical Pharmacology.* Berlin, Heidelberg: Springer Berlin Heidelberg.

HINSON, J. P., KAPAS, S. & SMITH, D. M. 2000. Adrenomedullin, a multifunctional regulatory peptide. *Endocrine Reviews,* 21**,** 138-167.

HIRAOKA, N., INO, Y., SEKINE, S., TSUDA, H., SHIMADA, K., KOSUGE, T., ZAVADA, J., YOSHIDA, M., YAMADA, K., KOYAMA, T. & KANAI, Y. 2010. Tumour necrosis is a postoperative prognostic marker for pancreatic cancer patients with a high interobserver reproducibility in histological evaluation. *British Journal of Cancer,* 103**,** 1057-1065.

HO, T. W., CONNOR, K. M., ZHANG, Y., PEARLMAN, E., KOPPENHAVER, J., FAN, X. Y., LINES, C., EDVINSSON, L., GOADSBY, P. J. & MICHELSON, D. 2014. Randomized controlled trial of the CGRP receptor antagonist telcagepant for migraine prevention. *Neurology,* 83**,** 958-966.

HO, T. W., FERRARI, M. D., DODICK, D. W., GALET, V., KOST, J., FAN, X. Y., LEIBENSPERGER, H., FROMAN, S., ASSAID, C., LINES, C., KOPPEN, H. & WINNER, P. K. 2008a. Efficacy

and tolerability of MK-0974 (telcagepant), a new oral antagonist of calcitonin gene-related peptide receptor, compared with zolmitriptan for acute migraine: a randomised, placebo-controlled, parallel-treatment trial. *Lancet,* 372**,** 2115-2123.

HO, T. W., HO, A. P., GE, Y., ASSAID, C., GOTTWALD, R., MACGREGOR, E. A., MANNIX, L. K., VAN OOSTERHOUT, W. P. J., KOPPENHAVER, J., LINES, C., FERRARI, M. D. & MICHELSON, D. 2016. Randomized controlled trial of the CGRP receptor antagonist telcagepant for prevention of headache in women with perimenstrual migraine. *Cephalalgia,* 36**,** 148-161.

HO, T. W., MANNIX, L. K., FAN, X., ASSAID, C., FURTEK, C., JONES, C. J., LINES, C. R., RAPOPORT, A. M. & MK- PROTOCOL 004 STUDY, G. 2008b. Randomized controlled trial of an oral CGRP receptor antagonist, MK-0974, in acute treatment of migraine. *Neurology,* 70**,** 1304-1312.

HOARE, S. R. J. 2005. Mechanisms of peptide and nonpeptide ligand binding to class B G-protein coupled receptors. *Drug Discovery Today,* 10**,** 417-427.

HOELDER, S., CLARKE, P. A. & WORKMAN, P. 2012. Discovery of small molecule cancer drugs: Successes, challenges and opportunities. *Molecular Oncology,* 6**,** 155-176.

HOLLANDER, L. L., GUO, X. J., SALEM, R. R. & CHA, C. H. 2015. The novel tumor angiogenic factor, adrenomedullin-2, predicts survival in pancreatic adenocarcinoma. *Journal of Surgical Research,* 197**,** 219-224.

HOTHERSALL, J. D., BLACK, J., CADDICK, S., VINTER, J. G., TINKER, A. & BAKER, J. R. 2011. The design, synthesis and pharmacological characterization of novel beta(2)-adrenoceptor antagonists. *British Journal of Pharmacology,* 164**,** 317-331.

HU, D. & CROSS, J. C. 2010. Development and function of trophoblast giant cells in the rodent placenta. *International Journal of Developmental Biology,* 54**,** 341-354.

HUGHES, J. P., REES, S., KALINDJIAN, S. B. & PHILPOTT, K. L. 2011. Principles of early drug discovery. *British Journal of Pharmacology,* 162**,** 1239-1249.

HURTADO, O., SERRANO, J., SOBRADO, M., FERNANDEZ, A. P., LIZASOAIN, I., MARTINEZ-MURILLO, R., MORO, M. A. & MARTINEZ, A. 2010. LACK OF ADRENOMEDULLIN, BUT NOT COMPLEMENT FACTOR H, RESULTS IN LARGER INFARCT SIZE AND MORE EXTENSIVE BRAIN DAMAGE IN A FOCAL ISCHEMIA MODEL. *Neuroscience,* 171**,** 885-892.

HWANG, I. S. S., AUTELITANO, D. J., WONG, P. Y. D., LEUNG, G. P. H. & TANG, F. 2003. Co-expression of adrenomedullin and adrenomedullin receptors in rat epididymis: Distinct physiological actions on anion transport. *Biology of Reproduction,* 68**,** 2005-2012.

HWANG, R. F., MOORE, T., ARUMUGAM, T., RAMACHANDRAN, V., AMOS, K. D., RIVERA, A., JI, B., EVANS, D. B. & LOGSDON, C. D. 2008a. Cancer-Associated Stromal Fibroblasts Promote Pancreatic Tumor Progression. *Cancer research,* 68**,** 918-926.

HWANG, Y. C., CHU, J. J. H., YANG, P. L., CHEN, W. & YATES, M. V. 2008b. Rapid identification of inhibitors that interfere with poliovirus replication using a cell-based assay. *Antiviral Research,* 77**,** 232-236.

ICHIKAWA-SHINDO, Y., SAKURAI, T., KAMIYOSHI, A., KAWATE, H., LINURNA, N., YOSHIZAWA, T., KOYAMA, T., FUKUCHI, J., LIMURO, S., MORIYAMA, N., KAWAKAMI, H., MURATA, T., KANGAWA, K., NAGAI, R. & SHINDO, T. 2008. The GPCR modulator protein RAMP2 is essential for angiogenesis and vascular integrity. *Journal of Clinical Investigation,* 118**,** 29-39.

ICHIKI, Y., KITAMURA, K., KANGAWA, K., KAWAMOTO, M., MATSUO, H. & ETO, T. 1994. DISTRIBUTION AND CHARACTERIZATION OF IMMUNOREACTIVE ADRENOMEDULLIN IN HUMAN TISSUE AND PLASMA. *Febs Letters,* 338**,** 6-10.

ICHINOSE, M. & SAWADA, M. 1996. Enhancement of phagocytosis by calcitonin gene-related peptide (CGRP) in cultured mouse peritoneal macrophages. *Peptides,* 17**,** 1405-1414.

IEMURA-INABA, C., NISHIKIMI, T., AKIMOTO, K., YOSHIHARA, F., MINAMINO, N. & MATSUOKA, H. 2008. Role of adrenomedullin system in lipid metabolism and its signaling mechanism in cultured adipocytes. *American Journal of Physiology-Regulatory Integrative and Comparative Physiology,* 295**,** R1376-R1384.

IIMURO, S., SHINDO, T., MORIYAMA, N., AMAKI, T., NIU, P., TAKEDA, N., IWATA, H., ZHANG, Y. L., EBIHARA, A. & NAGAI, R. 2004. Angiogenic effects of adrenomedullin in ischemia and tumor growth. *Circulation Research,* 95**,** 415-423.

INSEL, P. A. & OSTROM, R. S. 2003. Forskolin as a tool for examining adenylyl cyclase expression, regulation, and G protein signaling. *Cellular and Molecular Neurobiology,* 23**,** 305-314.

IOVINO, M., FEIFEL, U., YONG, C. L., WOLTERS, J. M. & WALLENSTEIN, G. 2004. Safety, tolerability and pharmacokinetics of BIBN4096BS, the first selective small molecule calcitonin gene-related peptide receptor antagonist, following single intravenous administration in healthy volunteers. *Cephalalgia,* 24**,** 645-656.

ISBERG, V., MORDALSKI, S., MUNK, C., RATAJ, K., HARPSØE, K., HAUSER, A. S., VROLING, B., BOJARSKI, A. J., VRIEND, G. & GLORIAM, D. E. 2016. GPCRdb: an information system for G protein-coupled receptors. *Nucleic Acids Research,* 44**,** D356-D364.

ISHIKAWA, T., CHEN, J., WANG, J. X., OKADA, F., SUGIYAMA, T., KOBAYASHI, T., SHINDO, M., HIGASHINO, F., KATOH, H., ASAKA, M., KONDO, T., HOSOKAWA, M. & KOBAYASHI, M. 2003. Adrenomedullin antagonist suppresses in vivo growth of human pancreatic cancer cells in SCID mice by suppressing angiogenesis. *Oncogene,* 22**,** 1238-1242.

ISHIMITSU, T., NISHIKIMI, T., SAITO, Y., KITAMURA, K., ETO, T., KANGAWA, K., MATSUO, H., OMAE, T. & MATSUOKA, H. 1994. PLASMA-LEVELS OF ADRENOMEDULLIN, A NEWLY IDENTIFIED HYPOTENSIVE PEPTIDE, IN PATIENTS WITH HYPERTENSION AND RENAL-FAILURE. *Journal of Clinical Investigation,* 94**,** 2158-2161.

ITABASHI, A., KASHIWABARA, H., SHIBUYA, M., TANAKA, K., MASAOKA, H., KATAYAMA, S. & ISHII, J. 1988. THE INTERACTION OF CALCITONIN GENE-RELATED PEPTIDE WITH ANGIOTENSIN-II ON BLOOD-PRESSURE AND RENIN RELEASE. *Journal of Hypertension,* 6**,** S418-S420.

IWASE, T., NAGAYA, N., FUJII, T., ITOH, T., ISHIBASHI-UEDA, H., YAMAGISHI, M., MIYATAKE, K., MATSUMOTO, T., KITAMURA, S. & KANGAWA, K. 2005. Adrenomedullin enhances angiogenic potency of bone marrow transplantation in a rat model of hindlimb ischemia. *Circulation,* 111**,** 356-362.

IYENGAR, S., OSSIPOV, M. H. & JOHNSON, K. W. 2017. The role of calcitonin gene-related peptide in peripheral and central pain mechanisms including migraine. *Pain,* 158**,** 543-559.

JAIN, R. K. 2003. Molecular regulation of vessel maturation. *Nature Medicine,* 9**,** 685-693.

JANZEN, W. P. 2014. Screening Technologies for Small Molecule Discovery: The State of the Art. *Chemistry & Biology,* 21**,** 1162-1170.

JARES-ERIJMAN, E. A. & JOVIN, T. M. 2003. FRET imaging. *Nature Biotechnology,* 21**,** 1387-1395.

JAVEED, N., SAGAR, G., DUTTA, S. K., SMYRK, T. C., LAU, J. S., BHATTACHARYA, S., TRUTY, M., PETERSEN, G. M., KAUFMAN, R. J., CHARI, S. T. & MUKHOPADHYAY, D. 2015. Pancreatic Cancer-Derived Exosomes Cause Paraneoplastic beta-cell Dysfunction. *Clinical Cancer Research,* 21**,** 1722-1733.

JIA, L. & LIU, X. D. 2007. The conduct of drug metabolism studies considered good practice (II): In vitro experiments. *Current Drug Metabolism,* 8**,** 822-829.

JIMENEZ-ANDRADE, J. M., BLOOM, A. P., STAKE, J. I., MANTYH, W. G., TAYLOR, R. N., FREEMAN, K. T., GHILARDI, J. R., KUSKOWSKI, M. A. & MANTYH, P. W. 2010. Pathological Sprouting of Adult Nociceptors in Chronic Prostate Cancer-Induced Bone Pain. *Journal of Neuroscience,* 30**,** 14649-14656.

JIN, D., HARADA, K., OHNISHI, S., YAMAHARA, K., KANGAWA, K. & NAGAYA, N. 2008. Adrenomedullin induces lymphangiogenesis and ameliorates secondary lymphoedema. *Cardiovascular Research,* 80**,** 339-345.

JOHNSTON, P. A. 2002. Cellular platforms for HTS: three case studies. *Drug Discovery Today,* 7**,** 353-363.

JUHASZ, G., ZSOMBOK, T., MODOS, E. A., OLAJOS, S., JAKAB, B., NEMETH, J., SZOLCSANYI, J., VITRAI, J. & BAGDY, G. 2003. NO-induced migraine attack: strong increase in plasma calcitonin gene-related peptide (CGRP) concentration and negative correlation with platelet serotonin release. *Pain,* 106**,** 461-470.

JUNG, J. 2014. Human Tumor Xenograft Models for Preclinical Assessment of Anticancer Drug Development. *Toxicological Research,* 30**,** 1-5.

KAAFARANI, I., FERNANDEZ-SAUZE, S., BERENGUER, C., CHINOT, O., DELFINO, C., DUSSERT, C., METELLUS, P., BOUDOURESQUE, F., MABROUK, K., GRISOLI, F., FIGARELLA-BRANGER, D., MARTIN, P. M. & OUAFIK, L. 2009. Targeting adrenomedullin receptors with systemic delivery of neutralizing antibodies inhibits tumor angiogenesis and suppresses growth of human tumor xenografts in mice. *Faseb Journal,* 23**,** 3424-3435.

KADMIEL, M., FRITZ-SIX, K., PACHARNE, S., RICHARDS, G. O., LI, M. Y., SKERRY, T. M. & CARON, K. M. 2011. Research Resource: Haploinsufficiency of Receptor Activity-Modifying Protein-2 (Ramp2) Causes Reduced Fertility, Hyperprolactinemia, Skeletal Abnormalities, and Endocrine Dysfunction in Mice. *Molecular Endocrinology,* 25**,** 1244-1253.

KAMITANI, S., ASAKAWA, M., SHIMEKAKE, Y., KUWASAKO, K., NAKAHARA, K. & SAKATA, T. 1999. The RAMP2/CRLR complex is a functional adrenomedullin receptor in human endothelial and vascular smooth muscle cells. *Febs Letters,* 448**,** 111-114.

KANO, H., KOHNO, M., YASUNARI, K., YOKOKAWA, K., HORIO, T., IKEDA, M., MINAMI, M., HANEHIRA, T., TAKEDA, T. & YOSHIKAWA, J. 1996. Adrenomedullin as a novel antiproliferative factor of vascular smooth muscle cells. *Journal of Hypertension,* 14**,** 209-213.

KAPOOR, K., ARULMANI, U., HEILIGERS, J. P. C., GARRELDS, I. M., WILLEMS, E. W., DOODS, H., VILLALON, C. M. & SAXENA, P. R. 2003. Effects of the CGRP receptor antagonist BIBN4096BS on capsaicin-induced carotid haemodynamic changes in anaesthetised pigs. *British Journal of Pharmacology,* 140**,** 329-338.

KATAOKA, Y., MIYAZAKI, S., YASUDA, S., NAGAYA, N., NOGUCHI, T., YAMADA, N., MORII, I., KAWAMURA, A., DOI, K., MIYATAKE, K., TOMOIKE, H. & KANGAWA, K. 2010. The First Clinical Pilot Study of Intravenous Adrenomedullin Administration in Patients With Acute Myocardial Infarction. *Journal of Cardiovascular Pharmacology,* 56**,** 413-419.

KATO, J. & KITAMURA, K. 2015. Bench-to-bedside pharmacology of adrenomedullin. *European Journal of Pharmacology,* 764**,** 140-148.

KATO, J., KOBAYASHI, K., ETOH, T., TANAKA, M., KITAMURA, K., IMAMURA, T., KOIWAYA, Y., KANGAWA, K. & ETO, T. 1996. Plasma adrenomedullin concentration in patients with heart failure. *Journal of Clinical Endocrinology & Metabolism,* 81**,** 180-183.

KATO, K., YIN, H., AGATA, J., YOSHIDA, H., CHAO, L. & CHAO, J. 2003. Adrenomedullin gene delivery attenuates myocardial infarction and apoptosis after ischemia and reperfusion. *American Journal of Physiology-Heart and Circulatory Physiology,* 285**,** H1506-H1514.

KELEG, S., KAYED, H., JIANG, X., PENZEL, R., GIESE, T., BUECHLER, M. W., FRIESS, H. & KLEEFF, J. 2007. Adrenomedullin is induced by hypoxia and enhances pancreatic cancer cell invasion. *International Journal of Cancer,* 121**,** 21-32.

KENAKIN, T., JENKINSON, S. & WATSON, C. 2006. Determining the potency and molecular mechanism of action of insurmountable antagonists. *Journal of Pharmacology and Experimental Therapeutics,* 319**,** 710-723.

KIM, W., MOON, S. O., SUNG, M. J., KIM, S. H., LEE, S., SO, J. N. & PARK, S. K. 2003. Angiogenic role of adrenomedullin through activation of Akt, mitogen-activated protein kinase, and focal adhesion kinase in endothelial cells. *Faseb Journal,* 17**,** 1937-+.

KINDLER, H. L., FRIBERG, G., SINGH, D. A., LOCKER, G., NATTAM, S., KOZLOFF, M., TABER, D. A., KARRISON, T., DACHMAN, A., STADLER, W. M. & VOKES, E. E. 2005. Phase II trial of bevacizurnab plus gemcitabine in patients with advanced pancreatic cancer. *Journal of Clinical Oncology,* 23**,** 8033-8040.

KITAMURA, K., KANGAWA, K., KAWAMOTO, M., ICHIKI, Y., NAKAMURA, S., MATSUO, H. & ETO, T. 1993a. ADRENOMEDULLIN - A NOVEL HYPOTENSIVE PEPTIDE ISOLATED FROM HUMAN PHEOCHROMOCYTOMA. *Biochemical and Biophysical Research Communications,* 192**,** 553-560.

KITAMURA, K., KANGAWA, K., KOJIMA, M., ICHIKI, Y., MATSUO, H. & ETO, T. 1994. COMPLETE AMINO-ACID-SEQUENCE OF PORCINE ADRENOMEDULLIN AND CLONING OF CDNA-ENCODING ITS PRECURSOR. *Febs Letters,* 338**,** 306-310.

KITAMURA, K., SAKATA, J., KANGAWA, K., KOJIMA, M., MATSUO, H. & ETO, T. 1993b. CLONING AND CHARACTERIZATION OF CDNA-ENCODING A PRECURSOR FOR HUMAN ADRENOMEDULLIN. *Biochemical and Biophysical Research Communications,* 194**,** 720-725.

KOBAYASHI, K., KITAMURA, K., HIRAYAMA, N., DATE, H., KASHIWAGI, T., IKUSHIMA, I., HANADA, Y., NAGATOMO, Y., TAKENAGA, M., ISHIKAWA, T., IMAMURA, T., KOIWAYA, Y. & ETO, T. 1996. Increased plasma adrenomedullin in acute myocardial infarction. *American Heart Journal,* 131**,** 676-680.

KONDOH, T., UETA, Y. & TORII, K. 2011. Pre-treatment of adrenomedullin suppresses cerebral edema caused by transient focal cerebral ischemia in rats detected by magnetic resonance imaging. *Brain Research Bulletin,* 84**,** 69-74.

KOYAMA, T., OCHOA-CALLEJERO, L., SAKURAI, T., KAMIYOSHI, A., ICHIKAWA-SHINDO, Y., IINUMA, N., ARAI, T., YOSHIZAWA, T., IESATO, Y., LEI, Y., UETAKE, R., OKIMURA, A., YAMAUCHI, A., TANAKA, M., IGARASHI, K., TORIYAMA, Y., KAWATE, H., ADAMS, R. H., KAWAKAMI, H., MOCHIZUKI, N., MARTINEZ, A. & SHINDO, T. 2013. Vascular Endothelial Adrenomedullin-RAMP2 System Is Essential for Vascular Integrity and Organ Homeostasis. *Circulation,* 127**,** 842-853.

KURASHIGE, C., HOSONO, K., MATSUDA, H., TSUJIKAWA, K., OKAMOTO, H. & MAJIMA, M. 2014. Roles of receptor activity-modifying protein 1 in angiogenesis and lymphangiogenesis during skin wound healing in mice. *Faseb Journal,* 28**,** 1237-1247.

KUREISHI, Y., KOBAYASHI, S., NISHIMURA, J., NAKANO, T. & KANAIDE, H. 1995. ADRENOMEDULLIN DECREASES BOTH CYTOSOLIC CA2+ CONCENTRATION AND CA2+-SENSITIVITY IN PIG CORONARY ARTERIAL SMOOTH-MUSCLE. *Biochemical and Biophysical Research Communications,* 212**,** 572-579.

KUSANO, S., KUKIMOTO-NIINO, M., AKASAKA, R., TOYAMA, M., TERADA, T., SHIROUZU, M., SHINDO, T. & YOKOYAMA, S. 2008. Crystal structure of the human receptor activity-modifying protein 1 extracellular domain. *Protein Science,* 17**,** 1907-1914.

KUWASAKO, K., SHIMEKAKE, Y., MASUDA, M., NAKAHARA, K., YOSHIDA, T., KITAURA, M., KITAMURA, K., ETO, T. & SAKATA, T. 2000. Visualization of the calcitonin receptor-

like receptor and its receptor activity-modifying proteins during internalization and recycling. *Journal of Biological Chemistry,* 275**,** 29602-29609.

LAMBERT, D. G. 2004. Drugs and receptors. *Continuing Education in Anaesthesia Critical Care & Pain,* 4**,** 181-184.

LASSEN, L. H., HADERSLEV, P., JACOBSEN, V. B., IVERSEN, H. K., SPERLING, B. & OLESEN, J. 2002. CGRP may play a causative role in migraine. *Cephalalgia,* 22**,** 54-61.

LASSEN, L. H., JACOBSEN, V. B., HADERSLEV, P. A., SPERLING, B., IVERSEN, H. K., OLESEN, J. & TFELT-HANSEN, P. 2008. Involvement of calcitonin gene-related peptide in migraine: regional cerebral blood flow and blood flow velocity in migraine patients. *Journal of Headache and Pain,* 9**,** 151-157.

LAWRENCE, T. S., BLACKSTOCK, A. W. & MCGINN, C. 2003. The mechanism of action of radios ensitization of conventional chemotherapeutic agents. *Seminars in Radiation Oncology,* 13**,** 13-21.

LEA, W. A. & SIMEONOV, A. 2011. Fluorescence polarization assays in small molecule screening. *Expert Opinion on Drug Discovery,* 6**,** 17-32.

LEFKOWITZ, R. J., ROTH, J. & PASTAN, I. 1970. RADIORECEPTOR ASSAY OF ADRENOCORTICOTROPIC HORMONE - NEW APPROACH TO ASSAY OF POLYPEPTIDE HORMONES IN PLASMA. *Science,* 170**,** 633-+.

LETIZIA, C., TAMBURRANO, G., ALO, P., PAOLONI, A., CALIUMI, C., MARINONI, E., DI IORIO, R. & D'ERASMO, E. 2001. Adrenomedullin, a new peptide, in patients with insulinoma. *European Journal of Endocrinology,* 144**,** 517-520.

LI, C. C., VERMEERSCH, S., DENNEY, W. S., KENNEDY, W. P., PALCZA, J., GIPSON, A., HAN, T. H., BLANCHARD, R., DE LEPELEIRE, I., DEPRE, M., MURPHY, M. G., VAN DYCK, K. & DE HOON, J. N. 2015a. Characterizing the PK/PD relationship for inhibition of capsaicin-induced dermal vasodilatation by MK-3207, an oral calcitonin gene related peptide receptor antagonist. *British Journal of Clinical Pharmacology,* 79**,** 831-837.

LI, D., PENG, J., XIN, H. Y., LUO, D., ZHANG, Y. S., ZHOU, Z., JIANG, D. J., DENG, H. W. & LI, Y. J. 2008. Calcitonin gene-related peptide-mediated antihypertensive and anti-platelet effects by rutaecarpine in spontaneously hypertensive rats. *Peptides,* 29**,** 1781-1788.

LI, H. Y., CUI, Z. M., CHEN, J., GUO, X. Z. & LI, Y. Y. 2015b. Pancreatic cancer: diagnosis and treatments. *Tumor Biology,* 36**,** 1375-1384.

LI, M. Y., WETZEL-STRONG, S. E., HUA, X. Y., TILLEY, S. L., OSWALD, E., KRUMMEL, M. F. & CARON, K. M. 2014. Deficiency of RAMP1 Attenuates Antigen-Induced Airway Hyperresponsiveness in Mice. *Plos One,* 9.

LI, M. Y., YEE, D., MAGNUSON, T. R., SMITHIES, O. & CARON, K. M. 2006. Reduced maternal expression of adrenomedullin disrupts fertility, placentation, and fetal growth in mice. *Journal of Clinical Investigation,* 116**,** 2653-2662.

LI, X., ASHANA, A. O., MORETTI, V. M. & LACKMAN, R. D. 2011. The relation of tumour necrosis and survival in patients with osteosarcoma. *International Orthopaedics,* 35**,** 1847-1853.

LIPINSKI, C. A., LOMBARDO, F., DOMINY, B. W. & FEENEY, P. J. 1997. Experimental and computational approaches to estimate solubility and permeability in drug discovery and development settings. *Advanced Drug Delivery Reviews,* 23**,** 3-25.

LIU, J. Q., BUTZOW, R., HYDEN-GRANSKOG, C. & VOUTILAINEN, R. 2009. Expression of adrenomedullin in human ovaries, ovarian sex cord-stromal tumors and cultured granulosa-luteal cells. *Gynecological Endocrinology,* 25**,** 96-103.

LOGAN, M., ANDERSON, P. D., SAAB, S. T., HAMEED, O. & ABDULKADIR, S. A. 2013. RAMP1 Is a Direct NKX3.1 Target Gene Up-Regulated in Prostate Cancer that Promotes Tumorigenesis. *American Journal of Pathology,* 183**,** 951-963.

LOUVET, C., LABIANCA, R., HAMMEL, P., LLEDO, G., ZAMPINO, M. G., ANDRE, T., ZANIBONI, A., DUCREUX, M., AITINI, E., TAIEB, J., FAROUX, R., LEPERE, C. & DE GRAMONT, A. 2005. Gemcitabine in combination with oxaliplatin compared with gemcitabine alone in locally advanced or metastatic pancreatic cancer: Results of a GERCOR and GISCAD phase III trial. *Journal of Clinical Oncology,* 23**,** 3509-3516.

LUNDSTROM, K. 2009. An Overview on GPCRs and Drug Discovery: Structure-Based Drug Design and Structural Biology on GPCRs. *G Protein-Coupled Receptors in Drug Discovery,* 552**,** 51-66.

LUO, G., CHEN, L., CONWAY, C. M., DENTON, R., KEAVY, D., SIGNOR, L., KOSTICH, W., LENTZ, K. A., SANTONE, K. S., SCHARTMAN, R., BROWNING, M., TONG, G., HOUSTON, J. G., DUBOWCHIK, G. M. & MACOR, J. E. 2012. Discovery of (5S,6S,9R)-5-Amino-6-(2,3-difluorophenyl)-6,7,8,9-tetrahydro-5H-cyclohepta[b]pyridin-9-yl 4-(2-oxo-2,3-dihydro-1H-imidazo[4,5-b]pyridin-1-yl)piperidine-1-carboxylate (BMS-927711): An Oral Calcitonin Gene-Related Peptide (CGRP) Antagonist in Clinical Trials for Treating Migraine. *Journal of Medicinal Chemistry,* 55**,** 10644-10651.

LUTTRELL, L. M. & LEFKOWITZ, R. J. 2002. The role of beta-arrestins in the termination and transduction of G-protein-coupled receptor signals. *Journal of Cell Science,* 115**,** 455-465.

LYNCH, T. & PRICE, A. 2007. The effect of cytochrome P450 metabolism on drug response, interactions, and adverse effects. *American Family Physician,* 76**,** 391-396.

MA, Q., YE, L. Y., LIU, H. X., SHI, Y. & ZHOU, N. M. 2017. An overview of Ca2+ mobilization assays in GPCR drug discovery. *Expert Opinion on Drug Discovery,* 12**,** 511-523.

MACARRON, R., BANKS, M. N., BOJANIC, D., BURNS, D. J., CIROVIC, D. A., GARYANTES, T., GREEN, D. V. S., HERTZBERG, R. P., JANZEN, W. P., PASLAY, J. W., SCHOPFER, U. & SITTAMPALAM, G. S. 2011. Impact of high-throughput screening in biomedical research. *Nature Reviews Drug Discovery,* 10**,** 188-195.

MAKI, T., IHARA, M., FUJITA, Y., NAMBU, T., MIYASHITA, K., YAMADA, M., WASHIDA, K., NISHIO, K., ITO, H., HARADA, H., YOKOI, H., ARAI, H., ITOH, H., NAKAO, K., TAKAHASHI, R. & TOMIMOTO, H. 2011. Angiogenic and Vasoprotective Effects of Adrenomedullin on Prevention of Cognitive Decline After Chronic Cerebral Hypoperfusion in Mice. *Stroke,* 42**,** 1122-1128.

MALLEE, J. J., SALVATORE, C. A., LEBOURDELLES, B., OLIVER, K. R., LONGMORE, J., KOBLAN, K. S. & KANE, S. A. 2002. Receptor activity-modifying protein 1 determines the species selectivity of non-peptide CGRP receptor antagonists. *Journal of Biological Chemistry,* 277**,** 14294-14298.

MALLENDER, W. D., BEMBENEK, M., DICK, L. R., KURANDA, M., LI, P., MENON, S., PARDO, E. & PARSONS, T. 2006. Biochemical Assays for High-throughput Screening. *In:* HÜSER , J. (ed.) *High-Throughput Screening in Drug Discovery.* Wiley-VCH Verlag GmbH & Co. KGaA, Weinheim, FRG.

MALVEZZI, M., BERTUCCIO, P., ROSSO, T., ROTA, M., LEVI, F., LA VECCHIA, C. & NEGRI, E. 2015. European cancer mortality predictions for the year 2015: does lung cancer have the highest death rate in EU women? *Annals of Oncology,* 26**,** 779-786.

MANTYH, P. W., CLOHISY, D. R., KOLTZENBURG, M. & HUNT, S. P. 2002. Molecular mechanisms of cancer pain. *Nature Reviews Cancer,* 2**,** 201-209.

MARCUS, R., GOADSBY, P. J., DODICK, D., STOCK, D., MANOS, G. & FISCHER, T. Z. 2014. BMS-927711 for the acute treatment of migraine: A double-blind, randomized, placebo controlled, dose-ranging trial. *Cephalalgia,* 34**,** 114-125.

MARINISSEN, M. J. & GUTKIND, J. S. 2001. G-protein-coupled receptors and signaling networks: emerging paradigms. *Trends in Pharmacological Sciences,* 22**,** 368-376.

MARINONI, E., DI IORIO, R., VILLACCIO, B., VELLUCCI, O., DI NETTA, T., SESSA, M., LETIZIA, C. & COSMI, E. V. 2005. Adrenomedullin in human male reproductive system.

European Journal of Obstetrics Gynecology and Reproductive Biology, 122**,** 195-198.

MARTINEZ, A., MILLER, M. J., UNSWORTH, E. J., SIEGFRIED, J. M. & CUTTITTA, F. 1995. EXPRESSION OF ADRENOMEDULLIN IN NORMAL HUMAN LUNG AND IN PULMONARY TUMORS. *Endocrinology,* 136**,** 4099-4105.

MARTINEZ, A., VOS, M., GUEDEZ, L., KAUR, G., CHEN, Z., GARAYOA, M., PIO, R., MOODY, T., STETLER-STEVENSON, W. G., KLEINMAN, H. K. & CUTTITTA, F. 2002. The effects of adrenomedullin overexpression in breast tumor cells. *Journal of the National Cancer Institute,* 94**,** 1226-1237.

MASAMUNE, A., WATANABE, T., KIKUTA, K. & SHIMOSEGAWA, T. 2009. Roles of Pancreatic Stellate Cells in Pancreatic Inflammation and Fibrosis. *Clinical Gastroenterology and Hepatology,* 7**,** S48-S54.

MATSON, B. C. & CARON, K. M. 2014. Adrenomedullin and endocrine control of immune cells during pregnancy. *Cellular & Molecular Immunology,* 11**,** 456-459.

MAYR, L. M. & BOJANIC, D. 2009. Novel trends in high-throughput screening. *Current Opinion in Pharmacology,* 9**,** 580-588.

MCGILLIS, J. P., HUMPHREYS, S., RANGNEKAR, V. & CIALLELLA, J. 1993. MODULATION OF B-LYMPHOCYTE DIFFERENTIATION BY CALCITONIN-GENE-RELATED PEPTIDE (CGRP) .1. CHARACTERIZATION OF HIGH-AFFINITY CGRP RECEPTORS ON MURINE 70Z/3 CELLS. *Cellular Immunology,* 150**,** 391-404.

MCGINNITY, D. F., SOARS, M. G., URBANOWICZ, R. A. & RILEY, R. J. 2004. Evaluation of fresh and cryopreserved hepatocytes as in vitro drug metabolism tools for the prediction of metabolic clearance. *Drug Metabolism and Disposition,* 32**,** 1247-1253.

MCINTYRE, T. A., HAN, C., XIANG, H., BAMBAL, R. & DAVIS, C. B. 2008. Differences in the total body clearance of lead compounds in the rat and mouse: Impact on pharmacokinetic screening strategy. *Xenobiotica,* 38**,** 605-619.

MCLATCHIE, L. M., FRASER, N. J., MAIN, M. J., WISE, A., BROWN, J., THOMPSON, N., SOLARI, R., LEE, M. G. & FOORD, S. M. 1998. RAMPs regulate the transport and ligand specificity of the calcitonin-receptor-like receptor. *Nature,* 393**,** 333-339.

MICHELINI, E., CEVENINI, L., MEZZANOTTE, L., COPPA, A. & RODA, A. 2010. Cell-based assays: fuelling drug discovery. *Analytical and Bioanalytical Chemistry,* 398**,** 227-238.

MICHELSEN, J., THIESSON, H., WALTER, S., OTTOSEN, P. D., SKOTT, O. & JENSEN, B. L. 2006. Tissue expression and plasma levels of adrenomedullin in renal cancer patients. *Clinical Science,* 111**,** 61-70.

MILLER, P. S., BARWELL, J., POYNER, D. R., WIGGLESWORTH, M. J., GARLAND, S. L. & DONNELLY, D. 2010. Non-peptidic antagonists of the CGRP receptor, BIBN4096BS and MK-0974, interact with the calcitonin receptor-like receptor via methionine-42 and RAMP1 via tryptophan-74. *Biochemical and Biophysical Research Communications,* 391**,** 437-442.

MIYAMOTO, N., TANAKA, R., SHIMOSAWA, T., YATOMI, Y., FUJITA, T., HATTORI, N. & URABE, T. 2009. Protein kinase A-dependent suppression of reactive oxygen species in transient focal ischemia in adrenomedullin-deficient mice. *Journal of Cerebral Blood Flow and Metabolism,* 29**,** 1769-1779.

MIYAO, Y., NISHIKIMI, T., GOTO, Y., MIYAZAKI, S., DAIKOKU, S., MORII, I., MATSUMOTO, T., TAKISHITA, S., MIYATA, A., MATSUO, H., KANGAWA, K. & NONOGI, H. 1998. Increased plasma adrenomedullin levels in patients with acute myocardial infarction in proportion to the clinical severity. *Heart,* 79**,** 39-44.

MIYASHITA, K., ITOH, H., ARAI, H., SUGANAMI, T., SAWADA, N., FUKUNAGA, Y., SONE, M., YAMAHARA, K., YURUGI-KOBAYASHI, T., PARK, K., OYAMADA, N., TAURA, D.,

TSUJIMOTO, H., CHAO, T. H., TAMURA, N., MUKOYAMA, M. & NAKAO, K. 2006. The neuroprotective and vasculo-neuro-regenerative roles of adrenomedullin in ischemic brain and its therapeutic potential. *Endocrinology,* 147**,** 1642-1653.

MIYASHITA, K., ITOH, H., SAWADA, N., FUKUNAGA, Y., SONE, M., YAMAHARA, K., YURUGI-KOBAYASHI, T., PARK, K. & NAKAO, K. 2003. Adrenomedullin provokes endothelial Akt activation and promotes vascular regeneration both in vitro and in vivo. *Febs Letters,* 544**,** 86-92.

MOORE, E. L., GINGELL, J. J., KANE, S. A., HAY, D. L. & SALVATORE, C. A. 2010. Mapping the CGRP receptor ligand binding domain: Tryptophan-84 of RAMP1 is critical for agonist and antagonist binding. *Biochemical and Biophysical Research Communications,* 394**,** 141-145.

MOORE, M. J., GOLDSTEIN, D., HAMM, J., FIGER, A., HECHT, J. R., GALLINGER, S., AU, H. J., MURAWA, P., WALDE, D., WOLFF, R. A., CAMPOS, D., LIM, R., DING, K., CLARK, G., VOSKOGLOU-NOMIKOS, T., PTASYNSKI, M. & PARULEKAR, W. 2007. Erlotinib plus gemcitabine compared with gemcitabine alone in patients with advanced pancreatic cancer: A phase III trial of the National Cancer Institute of Canada clinical trials group. *Journal of Clinical Oncology,* 25**,** 1960-1966.

MORENO, M. J., ABOUNADER, R., HEBERT, E., DOODS, H. & HAMEL, E. 2002. Efficacy of the non-peptide CGRP receptor antagonist BIBN4096BS in blocking CGRP-induced dilations in human and bovine cerebral arteries: potential implications in acute migraine treatment. *Neuropharmacology,* 42**,** 568-576.

MORFIS, M., TILAKARATNE, N., FURNESS, S. G. B., CHRISTOPOULOS, G., WERRY, T. D., CHRISTOPOULOS, A. & SEXTON, P. M. 2008. Receptor Activity-Modifying Proteins Differentially Modulate the G Protein-Coupling Efficiency of Amylin Receptors. *Endocrinology,* 149**,** 5423-5431.

MORIYAMA, T., OTANI, T. & MARUO, T. 2000. Expression of adrenomedullin by human granulosa lutein cells and its effect on progesterone production. *European Journal of Endocrinology,* 142**,** 671-676.

MULDERRY, P. K., GHATEI, M. A., BISHOP, A. E., ALLEN, Y. S., POLAK, J. M. & BLOOM, S. R. 1985. DISTRIBUTION AND CHROMATOGRAPHIC CHARACTERIZATION OF CGRP-LIKE IMMUNOREACTIVITY IN THE BRAIN AND GUT OF THE RAT. *Regulatory Peptides,* 12**,** 133-143.

NAGAYA, N. & KANGAWA, K. 2004. Adrenomedullin in the treatment of pulmonary hypertension. *Peptides,* 25**,** 2013-2018.

NAGAYA, N., KYOTANI, S., UEMATSU, M., UENO, K., OYA, H., NAKANISHI, N., SHIRAI, M., MORI, H., MIYATAKE, K. & KANGAWA, K. 2004. Effects of adrenomedullin inhalation on hemodynamics and exercise capacity in patients with idiopathic pulmonary arterial hypertension. *Circulation,* 109**,** 351-356.

NAGAYA, N., SALOH, T., NISHIKIMI, T., UEMATSU, M., FURUICHI, S., SAKAMAKI, F., OYA, H., KYOTANI, S., NAKANISHI, N., GOTO, Y., MASUDA, Y., MIYATAKE, K. & KANGAWA, K. 2000. Hemodynamic, renal, and hormonal effects of adrenomedullin infusion in patients with congestive heart failure. *Circulation,* 101**,** 498-503.

NAKAMURA, R., KATO, J., KITAMURA, K., ONITSUKA, H., IMAMURA, T., CAO, Y. N., MARUTSUKA, K., ASADA, Y., KANGAWA, K. & ETO, T. 2004. Adrenomedullin administration immediately after myocardial infarction ameliorates progression of heart failure in rats. *Circulation,* 110**,** 426-431.

NAKAMURA, R., KATO, J., KITAMURA, K., ONITSUKA, H., IMAMURA, T., MARUTSUKA, K., ASADA, Y., KANGAWA, K. & ETO, T. 2002. Beneficial effects of adrenomedullin on left ventricular remodeling after myocardial infarction in rats. *Cardiovascular Research,* 56**,** 373-380.

NAKATA, T., SEKI, N., MIWA, S., KOBAYASHI, A., SOEDA, J., NIMURA, Y., KAWASAKI, S. & MIYAGAWA, S. 2008. Identification of genes associated with multiple nodules in hepatocellular carcinoma using cDNA microarray: Multicentric occurrence or intrahepatic metastasis? *Hepato-Gastroenterology,* 55**,** 865-872.

NERI, B., CIPRIANI, G., GRIFONI, R., MOLINARA, E., PANTALEO, P., RANGAN, S., VANNINI, A., TONELLI, P., VALERI, A., PANTALONE, D., TADDEI, A. & BECHI, P. 2009. Gemcitabine Plus Irinotecan as First-Line Weekly Therapy in Locally Advanced and/or Metastatic Pancreatic Cancer. *Oncology Research,* 17**,** 559-564.

NIKITENKO, L. L., BLUCHER, N., FOX, S. B., BICKNEL, R., SMITH, D. M. & REES, M. C. P. 2006a. Adrenomedullin and CGRP interact with endogenous calcitonin-receptor-like receptor in endothelial cells and induce its desensitisation by different mechanisms. *Journal of Cell Science,* 119**,** 910-922.

NIKITENKO, L. L., FOX, S. B., KEHOE, S., REES, M. C. P. & BICKNELL, R. 2006b. Adrenomedullin and tumour angiogenesis. *British Journal of Cancer,* 94**,** 1-7.

NIKITENKO, L. L., MACKENZIE, I. Z., REES, M. C. P. & BICKNELL, R. 2000. Adrenomedullin is an autocrine regulator of endothelial growth in human endometrium. *Molecular Human Reproduction,* 6**,** 811-819.

NISHANT, T., SATHISH, K. D., ARUN, K. & PHANEENDRA, M. 2011. Role of Pharmacokinetic Studies in Drug Discovery. *Journal of Bioequivalence & Bioavailability,* 3**,** 263-267.

NISHIKIMI, T., SAITO, Y., KITAMURA, K., ISHIMITSU, T., ETO, T., KANGAWA, K., MATSUO, H., OMAE, T. & MATSUOKA, H. 1995. INCREASED PLASMA-LEVELS OF ADRENOMEDULLIN IN PATIENTS WITH HEART-FAILURE. *Journal of the American College of Cardiology,* 26**,** 1424-1431.

NORSKOV-LAURITSEN, L., THOMSEN, A. R. B. & BRAUNER-OSBORNE, H. 2014. G Protein-Coupled Receptor Signaling Analysis Using Homogenous Time-Resolved Forster Resonance Energy Transfer (HTRF) Technology. *International Journal of Molecular Sciences,* 15**,** 2554-2572.

NOZAKI, S., SISSONS, S., CHIEN, D. S. & SLEDGE, G. W., JR. 2003. Activity of biphenyl matrix metalloproteinase inhibitor BAY 12-9566 in a human breast cancer orthotopic model. *Clin Exp Metastasis,* 20**,** 407-12.

OEHLER, M. K., FISCHER, D. C., ORLOWSKA-VOLK, M., HERRLE, F., KIEBACK, D. G., REES, M. C. P. & BICKNELL, R. 2003. Tissue and plasma expression of the angiogenic peptide adrenomedullin in breast cancer. *British Journal of Cancer,* 89**,** 1927-1933.

OEHLER, M. K., NORBURY, C., HAGUE, S., REES, M. C. P. & BICKNELL, R. 2001. Adrenomedullin inhibits hypoxic cell death by upregulation of Bcl-2 in endometrial cancer cells: a possible promotion mechanism for tumour growth. *Oncogene,* 20**,** 2937-2945.

OHBAYASHI, H., SUITO, H., YOSHIDA, N., ILTO, Y., KUME, H. & YAMAKI, K. 1999. Adrenomedullin inhibits ovalbumin-induced bronchoconstriction and airway microvascular leakage in guinea-pigs. *European Respiratory Journal,* 14**,** 1076-1081.

OKUMURA, H., NAGAYA, N., ITOH, T., OKANO, I., HINO, J., MORI, K., TSUKAMOTO, Y., ISHIBASHI-UEDA, H., MIWA, S., TAMBARA, K., TOYOKUNI, S., YUTANI, C. & KANGAWA, K. 2004. Adrenomedullin infusion attenuates myocardial ischemia/reperfusion injury through the phosphatidylinositol 3-kinase/Akt-dependent pathway. *Circulation,* 109**,** 242-248.

OLESEN, J., DIENER, H., HUSSTEDT, I. W., GOADSBY, P. J., HALL, D., MEIER, U., POLLENTIER, S., LESKO, L. M. & CON, B. B. C. P. O. 2004. Calcitonin gene-related peptide receptor antagonist BIBN4096BS for the acute treatment of migraine. *New England Journal of Medicine,* 350**,** 1104-1110.

OUAFIK, L., SAUZE, S., BOUDOURESQUE, F., CHINOT, O., DELFINO, C., FINA, F., VUAROQUEAUX, V., DUSSERT, C., PALMARI, J., DUFOUR, H., GRISOLI, F., CASELLAS, P., BRUNNER, N. & MARTIN, P. M. 2002. Neutralization of adrenomedullin inhibits the growth of human glioblastoma cell lines in vitro and suppresses tumor xenograft growth in vivo. *American Journal of Pathology,* 160**,** 1279-1292.

OVERINGTON, J. P., AL-LAZIKANI, B. & HOPKINS, A. L. 2006. Opinion - How many drug targets are there? *Nature Reviews Drug Discovery,* 5**,** 993-996.

PADILLA, B. E., COTTRELL, G. S., ROOSTERMAN, D., PIKIOS, S., MULLER, L., STEINHOFF, M. & BUNNETT, N. W. 2007. Endothelin-converting enzyme-1 regulates endosomal sorting of calcitonin receptor-like receptor and beta-arrestins. *Journal of Cell Biology,* 179**,** 981-997.

PANDOL, S., EDDERKAOUI, M., GUKOVSKY, I., LUGEA, A. & GUKOVSKAYA, A. 2009. Desmoplasia of Pancreatic Ductal Adenocarcinoma. *Clinical Gastroenterology and Hepatology,* 7**,** S44-S47.

PANG, L., QI, J., GAO, Y., JIN, H. & DU, J. 2014. Adrenomedullin alleviates pulmonary artery collagen accumulationin rats with pulmonary hypertension induced by high blood flowLulu. *Peptides,* 54**,** 101-107.

PANTELOURIS, E. M. 1968. Absence of Thymus in a Mouse Mutant. *Nature,* 217**,** 370.

PAONE, D. V., SHAW, A. W., NGUYEN, D. N., BURGEY, C. S., DENG, J. Z., KANE, S. A., KOBLAN, K. S., SALVATORE, C. A., MOSSER, S. D., JOHNSTON, V. K., WONG, B. K., MILLER-STEIN, C. M., HERSHEY, J. C., GRAHAM, S. L., VACCA, J. P. & WILLIAMS, T. M. 2007. Potent, orally bioavailable calcitonin gene-related peptide receptor antagonists for the treatment of migraine: Discovery of N- (3R,6S)-6-(2,3-Difluorophenyl)-2-oxo-1-(2,2,2-trifluoroethyl)azepan-3 -yl -4-(2-oxo-2,3-dihydro-1H-imidazo 4,5-b pyridin-1-yl)piperidine-1-car boxamide (MK-0974). *Journal of Medicinal Chemistry,* 50**,** 5564-5567.

PARK, S. C., YOON, J. H., LEE, J. H., YU, S. J., MYUNG, S. J., KIM, W., GWAK, G. Y., LEE, S. H., LEE, S. M., JANG, J. J., SUH, K. S. & LEE, H. S. 2008. Hypoxia-inducible adrenomedullin accelerates hepatocellular carcinoma cell growth. *Cancer Letters,* 271**,** 314-322.

PAUS, R., HASLAM, I. S., SHAROV, A. A. & BOTCHKAREV, V. A. 2013. Pathobiology of chemotherapy-induced hair loss. *Lancet Oncology,* 14**,** E50-E59.

PAVEL, M. E., HOPPE, S., PAPADOPOULOS, T., LINDER, V., MOHR, B., HAHN, E. G., LOHMANN, T. & SCHUPPAN, D. 2006. Adrenomedullin is a novel marker of tumor progression in neuroendocrine carcinomas. *Hormone and Metabolic Research,* 38**,** 112-118.

PETERSEN, K. A., BIRK, S., DOODS, H., EDVINSSON, L. & OLESEN, J. 2004. Inhibitory effect of BIBN4096BS on cephalic vasodilatation induced by CGRP or transcranial electrical stimulation in the rat. *British Journal of Pharmacology,* 143**,** 697-704.

PETERSEN, K. A., BIRK, S., LASSEN, L. H., KRUUSE, C., JONASSEN, O., LESKO, L. & OLESEN, J. 2005. The CGRP-antagonist, BIBN4096BS does not affect cerebral or systemic haemodynamics in healthy volunteers. *Cephalalgia,* 25**,** 139-147.

PIERANTONI, C., PAGLIACCI, A., SCARTOZZI, M., BERARDI, R., BIANCONI, M. & CASCINU, S. 2008. Pancreatic cancer: Progress in cancer therapy. *Critical Reviews in Oncology Hematology,* 67**,** 27-38.

PIERCE, K. L., PREMONT, R. T. & LEFKOWITZ, R. J. 2002. Seven-transmembrane receptors. *Nature Reviews Molecular Cell Biology,* 3**,** 639-650.

POPIOLEK, M., NGUYEN, D. P., REINHART, V., EDGERTON, J. R., HARMS, J., LOTARSKI, S. M., STEYN, S. J., DAVOREN, J. E. & GRIMWOOD, S. 2016. Inositol Phosphate Accumulation in Vivo Provides a Measure of Muscarinic M-1 Receptor Activation. *Biochemistry,* 55**,** 7073-7085.

POTES, C. S., BOYLE, C. N., WOOKEY, P. J., RIEDIGER, T. & LUTZ, T. A. 2012. Involvement of the extracellular signal-regulated kinase 1/2 signaling pathway in amylin's eating inhibitory effect. *American Journal of Physiology-Regulatory Integrative and Comparative Physiology,* 302**,** R340-R351.

POYNER, D. R., SEXTON, P. M., MARSHALL, I., SMITH, D. M., QUIRION, R., BORN, W., MUFF, R., FISCHER, J. A. & FOORD, S. M. 2002. International Union of Pharmacology. XXXII. The mammalian calcitonin gene-related peptides, adrenomedullin, amylin, and calcitonin receptors. *Pharmacological Reviews,* 54**,** 233-246.

PRYSTAY, L., GAGNE, A., KASILA, P., YEH, L. A. & BANKS, P. 2001. Homogeneous cell-based fluorescence polarization assay for the direct detection of cAMP. *Journal of Biomolecular Screening,* 6**,** 75-82.

QI, Y. F., BU, D. F., DI NIU, D., SHI, Y. R., WANG, S. H., PANG, Y. Z., TANG, C. S. & DU, J. B. A. 2002. Effects of different peptide fragments derived from proadrenomedullin on gene expression of adrenomedullin gene. *Peptides,* 23**,** 1141-1147.

QIU, W. & SU, G. H. 2013. Development of Orthotopic Pancreatic Tumor Mouse Models. *Methods in molecular biology (Clifton, N.J.),* 980**,** 215-223.

QU, C. F., SONG, Y. J., RIZVI, S. M. A., LI, Y., SMITH, R., PERKINS, A. C., MORGENSTERN, A., BRECHBIEL, M. & ALLEN, B. J. 2005. In vivo and in vitro inhibition of pancreatic cancer growth by targeted alpha therapy using Bi-213-CHX.A"-C595. *Cancer Biology & Therapy,* 4**,** 848-853.

RAHIB, L., SMITH, B. D., AIZENBERG, R., ROSENZWEIG, A. B., FLESHMAN, J. M. & MATRISIAN, L. M. 2014. Projecting Cancer Incidence and Deaths to 2030: The Unexpected Burden of Thyroid, Liver, and Pancreas Cancers in the United States. *Cancer Research*.

RAMACHANDRAN, V., ARUMUGAM, T., HWANG, R. F., GREENSON, J. K., SIMEONE, D. M. & LOGSDON, C. D. 2007. Adrenomedullin is expressed in pancreatic cancer and stimulates cell proliferation and invasion in an autocrine manner via the adrenomedullin receptor, ADMR. *Cancer Research,* 67**,** 2666-2675.

RAMACHANDRAN, V., ARUMUGAM, T., LANGLEY, R., HWANG, R. F., VIVAS-MEJIA, P., SOOD, A. K., LOPEZ-BERESTEIN, G. & LOGSDON, C. D. 2009. The ADMR Receptor Mediates the Effects of Adrenomedullin on Pancreatic Cancer Cells and on Cells of the Tumor Microenvironment. *Plos One,* 4.

RAMOS, C. G., SUN, X., JOHNSON, E. B., NELSON, H. E. & BOSC, L. V. G. 2014. Adrenomedullin Expression in the Developing Human Fetal Lung. *Journal of Investigative Medicine,* 62**,** 49-55.

RANG, H. P. R. J. M. F. R. J. H. G. 2014. *Rang and Dale's Pharmacology*, Churchill Livingstone.

RAY, W. A., MURRAY, K. T., MEREDITH, S., NARASIMHULU, S. S., HALL, K. & STEIN, C. M. 2004. Oral erythromycin and the risk of sudden death from cardiac causes. *New England Journal of Medicine,* 351**,** 1089-1096.

RITTER, S. L. & HALL, R. A. 2009. Fine-tuning of GPCR activity by receptor-interacting proteins. *Nature Reviews Molecular Cell Biology,* 10**,** 819-830.

ROBINSON, S. D., AITKEN, J. F., BAILEY, R. J., POYNER, D. R. & HAY, D. L. 2009. Novel Peptide Antagonists of Adrenomedullin and Calcitonin Gene-Related Peptide Receptors: Identification, Pharmacological Characterization, and Interactions with Position 74 in Receptor Activity-Modifying Protein 1/3. *Journal of Pharmacology and Experimental Therapeutics,* 331**,** 513-521.

RODA, A., PASINI, P., MIRASOLI, M., MICHELINI, E. & GUARDIGLI, M. 2004. Biotechnological applications of bioluminescence and chemiluminescence. *Trends in Biotechnology,* 22**,** 295-303.

RODGERS, G. M., BECKER, P. S., BLINDER, M., CELLA, D., CHANAN-KHAN, A., CLEELAND, C., COCCIA, P. F., DJULBEGOVIC, B., GILREATH, J. A., KRAUT, E. H., MATULONIS, U. A., MILLENSON, M. M., REINKE, D., ROSENTHAL, J., SCHWARTZ, R. N., SOFF, G., STEIN, R. S., VLAHOVIC, G. & WEIR, A. B. 2012. Cancer- and Chemotherapy-Induced Anemia. *Journal of the National Comprehensive Cancer Network,* 10**,** 628-+.

ROH, J., CHANG, C. L., BHALLA, A., KLEIN, C. & HSU, S. Y. T. 2004. Intermedin is a calcitonin/calcitonin gene-related peptide family peptide acting through the calcitonin receptor-like receptor/receptor activity-modifying protein receptor complexes. *Journal of Biological Chemistry,* 279**,** 7264-7274.

ROSENFELD, M. G., MERMOD, J. J., AMARA, S. G., SWANSON, L. W., SAWCHENKO, P. E., RIVIER, J., VALE, W. W. & EVANS, R. M. 1983. PRODUCTION OF A NOVEL NEUROPEPTIDE ENCODED BY THE CALCITONIN GENE VIA TISSUE-SPECIFIC RNA PROCESSING. *Nature,* 304**,** 129-135.

RUDOLF, K., EBERLEIN, W., ENGEL, W., PIEPER, H., ENTZEROTH, M., HALLERMAYER, G. & DOODS, H. 2005. Development of human calcitonin gene-related peptide (CGRP) receptor antagonists. 1. Potent and selective small molecule CGRP antagonists. 1-N-2- 3,5-dibromo-N- 4-(3,4-dihydro-2(1H)-oxoquinazolin-3-yl)-1-piper idinyl carbonyl -D-tyrosyl -L-lysyl -4-(4-pyridinyl)piperazine: The first CGRP antagonist for clinical trials in acute migraine. *Journal of Medicinal Chemistry,* 48**,** 5921-5931.

RUNGE, S., WULFF, B. S., MADSEN, K., BRAUNER-OSBORNE, H. & KNUDSEN, L. B. 2003. Different domains of the glucagon and glucagon-like peptide-1 receptors provide the critical determinants of ligand selectivity. *British Journal of Pharmacology,* 138**,** 787-794.

RUSSELL, F. A., KING, R., SMILLIE, S. J., KODJI, X. & BRAIN, S. D. 2014. CALCITONIN GENE-RELATED PEPTIDE: PHYSIOLOGY AND PATHOPHYSIOLOGY. *Physiological Reviews,* 94**,** 1099-1142.

SAGAR, G., SAH, R. P., JAVEED, N., DUTTA, S. K., SMYRK, T. C., LAU, J. S., GIORGADZE, N., TCHKONIA, T., KIRKLAND, J. L., CHARI, S. T. & MUKHOPADHYAY, D. 2016. Pathogenesis of pancreatic cancer exosome-induced lipolysis in adipose tissue. *Gut,* 65**,** 1165-1174.

SAKATA, J., SHIMOKUBO, T., KITAMURA, K., NAKAMURA, S., KANGAWA, K., MATSUO, H. & ETO, T. 1993. MOLECULAR-CLONING AND BIOLOGICAL-ACTIVITIES OF RAT ADRENOMEDULLIN, A HYPOTENSIVE PEPTIDE. *Biochemical and Biophysical Research Communications,* 195**,** 921-927.

SALVATORE, C. A., HERSHEY, J. C., CORCORAN, H. A., FAY, J. F., JOHNSTON, V. K., MOORE, E. L., MOSSER, S. D., BURGEY, C. S., PAONE, D. V., SHAW, A. W., GRAHAM, S. L., VACCA, J. P., WILLIAMS, T. M., KOBLAN, K. S. & KANE, S. A. 2008. Pharmacological characterization of MK-0974 N- (3R, 6S)-6(2,3-difluorophenyl)-2-oxo-1-(2,2,2-trifluoroethyl)azepan-3-yl -4-(2-oxo-2,3-dihydro-1H-imidazo 4,5-b pyridin-1-yl)piperidine-1-carboxamide , a potent and orally Active calcitonin gene-related peptide receptor antagonist for the treatment of migraine. *Journal of Pharmacology and Experimental Therapeutics,* 324**,** 416-421.

SALVATORE, C. A., MOORE, E. L., CALAMARI, A., COOK, J. J., MICHENER, M. S., O'MALLEY, S., MILLER, P. J., SUR, C., WILLIAMS, D. L., ZENG, Z. Z., DANZIGER, A., LYNCH, J. J., REGAN, C. P., FAY, J. F., TANG, Y. S., LI, C. C., PUDVAH, N. T., WHITE, R. B., BELL, I. M., GALLICCHIO, S. N., GRAHAM, S. L., SELNICK, H. G., VACCA, J. P. & KANE, S. A. 2010. Pharmacological Properties of MK-3207, a Potent and Orally Active Calcitonin Gene-Related Peptide Receptor Antagonist. *Journal of Pharmacology and Experimental Therapeutics,* 333**,** 152-160.

SANTIEMMA, V., ROSSI, F., GUERRINI, L., MARKOUIZOU, A., PASIMENI, G., PALLESCHI, S. & FABBRINI, A. 2001. Adrenomedullin inhibits the contraction of cultured rat

testicular peritubular myoid cells induced by endothelin-1. *Biology of Reproduction,* 64**,** 619-624.

SATA, M., KAKOKI, M., NAGATA, D., NISHIMATSU, H., SUZUKI, E., AOYAGI, T., SUGIURA, S., KOJIMA, H., NAGANO, T., KANGAWA, K., MATSUO, H., OMATA, M., NAGAI, R. & HIRATA, Y. 2000. Adrenomedullin and nitric oxide inhibit human endothelial cell apoptosis via a cyclic GMP-independent mechanism. *Hypertension,* 36**,** 83-88.

SCHILD, H. O. 1949. PAX AND COMPETITIVE DRUG ANTAGONISM. *British Journal of Pharmacology and Chemotherapy,* 4**,** 277-280.

SCHINDLER, M. & DOODS, H. N. 2002. Binding properties of the novel, non-peptide CGRP receptor antagonist radioligand, H-3 BIBN4096BS. *European Journal of Pharmacology,* 442**,** 187-193.

SCHNEIDER, G. 2010. Virtual screening: an endless staircase? *Nature Reviews Drug Discovery,* 9**,** 273-276.

SCHOBER, M., JESENOFSKY, R., FAISSNER, R., WEIDENAUER, C., HAGMANN, W., MICHL, P., HEUCHEL, R. L., HAAS, S. L. & LOHR, J. M. 2014. Desmoplasia and Chemoresistance in Pancreatic Cancer. *Cancers,* 6**,** 2137-2154.

SCHOENAUER, R., ELS-HEINDL, S. & BECK-SICKINGER, A. G. 2017. Adrenomedullin - new perspectives of a potent peptide hormone. *Journal of Peptide Science,* 23**,** 472-485.

SCHOU, W. S., ASHINA, S., AMIN, F. M., GOADSBY, P. J. & ASHINA, M. 2017. Calcitonin gene-related peptide and pain: a systematic review. *Journal of Headache and Pain,* 18.

SEIBERT, H., MORCHEL, S. & GULDEN, M. 2002. Factors influencing nominal effective concentrations of chemical compounds in vitro: medium protein concentration. *Toxicology in Vitro,* 16**,** 289-297.

SEXTON, P. M., ALBISTON, A., MORFIS, M. & TILAKARATNE, N. 2001. Receptor activity modifying proteins. *Cellular Signalling,* 13**,** 73-83.

SHIBATA, Y., KASHIWAGI, B., ARAI, S., MAGARI, T., SUZUKI, K. & HONMA, S. 2006. Participation of adrenomedullin and its relation with vascular endothelial growth factor in androgen regulation of prostatic blood flow in vivo. *Urology,* 68**,** 1127-1131.

SHIMEKAKE, Y., NAGATA, K., OHTA, S., KAMBAYASHI, Y., TERAOKA, H., KITAMURA, K., ETO, T., KANGAWA, K. & MATSUO, H. 1995. ADRENOMEDULLIN STIMULATES 2 SIGNAL-TRANSDUCTION PATHWAYS, CAMP ACCUMULATION AND CA2+ MOBILIZATION, IN BOVINE AORTIC ENDOTHELIAL-CELLS. *Journal of Biological Chemistry,* 270**,** 4412-4417.

SHINDO, T., KURIHARA, Y., NISHIMATSU, H., MORIYAMA, N., KAKOKI, M., WANG, Y. H., IMAI, Y., EBIHARA, A., KUWAKI, T., JU, K. H., MINAMINO, N., KANGAWA, K., ISHIKAWA, T., FUKUDA, M., AKIMOTO, Y., KAWAKAMI, H., IMAI, T., MORITA, H., YAZAKI, Y., NAGAI, R., HIRATA, Y. & KURIHARA, H. 2001. Vascular abnormalities and elevated blood pressure in mice lacking adrenomedullin gene. *Circulation,* 104**,** 1964-1971.

SINCLAIR, S. R., KANE, S. A., XIAO, A., WILLSON, K., XU, Y., HICKEY, L., PALCZA, J., DE LEPELEIRE, I., VANMOLKOT, F., DE HOON, J. & MURPHY, M. G. 2007. MK-0974 oral CGRP antagonist inhibits capsaicin-induced increase in dermal microvascular blood flow. *Headache,* 47**,** 811-811.

SLACK, R. J., RUSSELL, L. J., HALL, D. A., LUTTMANN, M. A., FORD, A. J., SAUNDERS, K. A., HODGSON, S. T., CONNOR, H. E., BROWNING, C. & CLARK, K. L. 2011. Pharmacological characterization of GSK1004723, a novel, long-acting antagonist at histamine H-1 and H-3 receptors. *British Journal of Pharmacology,* 164**,** 1627-1641.

SMITH, D. A., DI, L. & KERNS, E. H. 2010. The effect of plasma protein binding on in vivo efficacy: misconceptions in drug discovery. *Nature Reviews Drug Discovery,* 9**,** 929-939.

STEENBERGH, P. H., HOPPENER, J. W. M., ZANDBERG, J., VISSER, A., LIPS, C. J. M. & JANSZ, H. S. 1986. STRUCTURE AND EXPRESSION OF THE HUMAN CALCITONIN CGRP GENES. *Febs Letters,* 209**,** 97-103.

STEPIEN, A., JAGUSTYN, P., TRAFNY, E. A. & WIDERKIEWICZ, K. 2003. Suppressing effect of the serotonin 5HT1B/D receptor agonist rizatriptan on calcitonin gene-related peptide (CGRP) concentration in migraine attacks. *Neurologia i neurochirurgia polska,* 37**,** 1013-23.

STRUMBERG, D., SCHULTHEIS, B., SCHEULEN, M. E., HILGER, R. A., KRAUSS, J., MARSCHNER, N., LORDICK, F., BACH, F., REUTER, D., EDLER, L. & MROSS, K. 2012. Phase II study of nimotuzumab, a humanized monoclonal anti-epidermal growth factor receptor (EGFR) antibody, in patients with locally advanced or metastatic pancreatic cancer. *Investigational New Drugs,* 30**,** 1138-1143.

SUZUKI, Y., HORIO, T., HAYASHI, T., NONOGI, H., KITAMURA, K., ETO, T., KANGAWA, K. & KAWANO, Y. 2004. Plasma adrenomedullin concentration is increased in patients with peripheral arterial occlusive disease associated with vascular inflammation. *Regulatory Peptides,* 118**,** 99-104.

TAKEI, Y., HYODO, S., KATAFUCHI, T. & MINAMINO, N. 2004. Novel fish-derived adrenomedullin in mammals: structure and possible function. *Peptides,* 25**,** 1643-1656.

TALLARIDA, R. J. 2007. Interactions between drugs and occupied receptors. *Pharmacology & Therapeutics,* 113**,** 197-209.

TANG, Y., LI, X. Q., HE, J. J., LU, J. G. & DIWU, Z. 2006. Real-time and high throughput monitoring of cAMP in live cells using a fluorescent membrane potential-sensitive dye. *Assay and Drug Development Technologies,* 4**,** 461-471.

TEPPER, S. J. & CLEVES, C. 2009. Telcagepant, a calcitonin gene-related peptide antagonist for the treatment of migraine. *Current Opinion in Investigational Drugs,* 10**,** 711-720.

TER HAAR, E., KOTH, C. M., ABDUL-MANAN, N., SWENSON, L., COLL, J. T., LIPPKE, J. A., LEPRE, C. A., GARCIA-GUZMAN, M. & MOORE, J. M. 2010. Crystal Structure of the Ectodomain Complex of the CGRP Receptor, a Class-B GPCR, Reveals the Site of Drug Antagonism. *Structure,* 18**,** 1083-1093.

TERWEE, J. A., CHIN, C. L., WATRIN, S., TELLO, R. F., RIEDER, N. J., LOWELL, J. D. & LATHAM-TIMMONS, D. 2011. Increased consistency and efficiency in routine potency testing by bioassay with direct use of cryopreserved (ready-to-plate) cells. *Journal of Immunological Methods,* 370**,** 65-74.

THE AMERICAN CANCER SOCIETY. 2016. *Risks of cancer surgery* [Online]. www.cancer.org: The American Cancer Society. Available: https://www.cancer.org/treatment/treatments-and-side-effects/treatment-types/surgery/risks-of-cancer-surgery.html [Accessed November 25 2017].

THOMAS, D. A., DUBNER, R. & RUDA, M. A. 1994. NEONATAL CAPSAICIN TREATMENT IN RATS RESULTS IN SCRATCHING BEHAVIOR WITH SKIN DAMAGE - POTENTIAL MODEL OF NONPAINFUL DYSESTHESIA. *Neuroscience Letters,* 171**,** 101-104.

TODA, M., SUZUKI, T., HOSONO, K., HAYASHI, I., HASHIBA, S., ONUMA, Y., AMANO, H., KURIHARA, Y., KURIHARA, H., OKAMOTO, H., HOKA, S. & MAJIMA, M. 2008. Neuronal system-dependent facilitation of tumor angiogenesis and tumor growth by calcitonin gene-related peptide. *Proceedings of the National Academy of Sciences of the United States of America,* 105**,** 13550-13555.

TOKUNAGA, N., NAGAYA, N., SHIRAI, M., TANAKA, E., ISHIBASHI-UEDA, H., HARADA-SHIBA, M., KANDA, M., ITO, T., SHIMIZU, W., TABATA, Y., UEMATSU, M., NISHIGAMI, K., SANO, S., KANGAWA, K. & MORI, H. 2004. Adrenomedullin gene transfer induces therapeutic angiogenesis in a rabbit model of chronic hind limb ischemia - Benefits of a novel nonviral vector, gelatin. *Circulation,* 109**,** 526-531.

TSUJIKAWA, K., YAYAMA, K., HAYASHI, T., MATSUSHITA, H., YAMAGUCHI, T., SHIGENO, T., OGITANI, Y., HIRAYAMA, M., KATO, T., FUKADA, S. I., TAKATORI, S., KAWASAKI, H., OKAMOTO, H., IKAWA, M., OKABE, M. & YAMAMOTO, H. 2007. Hypertension and dysregulated proinflarnmatory cytokine production in receptor activity-modifying protein 1-deficient mice. *Proceedings of the National Academy of Sciences of the United States of America,* 104**,** 16702-16707.

UDDMAN, R., EDVINSSON, L., EKMAN, R., KINGMAN, T. & MCCULLOCH, J. 1985. INNERVATION OF THE FELINE CEREBRAL VASCULATURE BY NERVE-FIBERS CONTAINING CALCITONIN GENE-RELATED PEPTIDE - TRIGEMINAL ORIGIN AND COEXISTENCE WITH SUBSTANCE-P. *Neuroscience Letters,* 62**,** 131-136.

UEZONO, Y., SHIBUYA, I., UEDA, Y., TANAKA, K., OISHI, Y., YANAGIHARA, N., UENO, S., TOYOHIRA, Y., NAKAMURA, T., YAMASHITA, H. & IZUMI, F. 1998. Adrenomedullin increases intracellular Ca2+ and inositol 1,4,5-trisphosphate in human oligodendroglial cell line KG-1C. *Brain Research,* 786**,** 230-234.

VAN BREEMEN, R. B. & LI, Y. 2005. Caco-2 cell permeability assays to measure drug absorption. *Expert Opinion on Drug Metabolism & Toxicology,* 1**,** 175-185.

VAN CUTSEM, E., VERVENNE, W. L., BENNOUNA, J., HUMBLET, Y., GILL, S., VAN LAETHEM, J. L., VERSLYPE, C., SCHEITHAUER, W., COSAERT, A. S. J. & MOORE, M. J. 2009. Phase III Trial of Bevacizumab in Combination With Gemcitabine and Erlotinib in Patients With Metastatic Pancreatic Cancer. *Journal of Clinical Oncology,* 27**,** 2231-2237.

VILARDAGA, J. P., DIPAOLO, E., BIALEK, C., DENEEF, P., WAELBROECK, M., BOLLEN, A. & ROBBERECHT, P. 1997. Mutational analysis of extracellular cysteine residues of rat secretin receptor shows that disulfide bridges are essential for receptor function. *European Journal of Biochemistry,* 246**,** 173-180.

VILLALON, C. M., CENTURION, D., VALDIVIA, L. F., DE VRIES, P. & SAXENA, P. R. 2002. An introduction to migraine: from ancient treatment to functional pharmacology and antimigraine therapy. 45th Annual Meeting of the Western-Pharmacology-Society, Jan 27-Feb 01 2002 Mazatlan, Mexico. 199-210.

VISA, M., ALCARRAZ-VIZAN, G., MONTANE, J., CADAVEZ, L., CASTANO, C., VILLANUEVA-PENACARRILLO, M. L., SERVITJA, J. M. & NOVIALS, A. 2015. Islet amyloid polypeptide exerts a novel autocrine action in beta-cell signaling and proliferation. *Faseb Journal,* 29**,** 2970-2979.

VON HOFF, D. D., ERVIN, T., ARENA, F. P., CHIOREAN, E. G., INFANTE, J., MOORE, M., SEAY, T., TJULANDIN, S. A., MA, W. W., SALEH, M. N., HARRIS, M., RENI, M., DOWDEN, S., LAHERU, D., BAHARY, N., RAMANATHAN, R. K., TABERNERO, J., HIDALGO, M., GOLDSTEIN, D., VAN CUTSEM, E., WEI, X. Y., IGLESIAS, J. & RENSCHLER, M. F. 2013. Increased Survival in Pancreatic Cancer with nab-Paclitaxel plus Gemcitabine. *New England Journal of Medicine,* 369**,** 1691-1703.

VONLAUFEN, A., JOSHI, S., QU, C. F., PHILLIPS, P. A., XU, Z. H., PARKER, N. R., TOI, C. S., PIROLA, R. C., WILSON, J. S., GOLDSTEIN, D. & APTE, M. V. 2008. Pancreatic stellate cells: Partners in crime with pancreatic cancer cells. *Cancer Research,* 68**,** 2085-2093.

VOSS, T., LIPTON, R. B., DODICK, D. W., DUPRE, N., GE, J. Y., BACHMAN, R., ASSAID, C., AURORA, S. K. & MICHELSON, D. 2016. A phase IIb randomized, double-blind,

placebo-controlled trial of ubrogepant for the acute treatment of migraine. *Cephalalgia,* 36**,** 887-898.

WANG, L. J., GALA, M., YAMAMOTO, M., PINO, M. S., KIKUCHI, H., SHUE, D. S., SHIRASAWA, S., AUSTIN, T. R., LYNCH, M. P., RUEDA, B. R., ZUKERBERG, L. R. & CHUNG, D. C. 2014. Adrenomedullin is a therapeutic target in colorectal cancer. *International Journal of Cancer,* 134**,** 2041-2050.

WANG, Z. Y., MA, W., CHABOT, J. G. & QUIRION, R. 2009. Cell-type specific activation of p38 and ERK mediates calcitonin gene-related peptide involvement in tolerance to morphine-induced analgesia. *Faseb Journal,* 23**,** 2576-2586.

WASHIMINE, H., ASADA, Y., KITAMURA, K., ICHIKI, Y., HARA, S., YAMAMOTO, Y., KANGAWA, K., SUMIYOSHI, A. & ETO, T. 1995. IMMUNOHISTOCHEMICAL IDENTIFICATION OF ADRENOMEDULLIN IN HUMAN, RAT, AND PORCINE TISSUE. *Histochemistry and Cell Biology,* 103**,** 251-254.

WATKINS, H. A., WALKER, C. S., LY, K. N., BAILEY, R. J., BARWELL, J., POYNER, D. R. & HAY, D. L. 2014. Receptor activity-modifying protein-dependent effects of mutations in the calcitonin receptor-like receptor: implications for adrenomedullin and calcitonin gene-related peptide pharmacology. *British Journal of Pharmacology,* 171**,** 772-788.

WAYBRIGHT, T. J., BRITT, J. R. & MCCLOUD, T. G. 2009. Overcoming Problems of Compound Storage in DMSO: Solvent and Process Alternatives. *Journal of Biomolecular Screening,* 14**,** 708-715.

WESTERMARK, G. T. 2011. Physiological and Pathophysiological Role of Islet Amyloid Polypeptide (IAPP, Amylin). *Betasys: Systems Biology of Regulated Exocytosis in Pancreatic Beta-Cells,* 2**,** 363-386.

WESTON, C., LU, J., LI, N. C., BARKAN, K., RICHARDS, G. O., ROBERTS, D. J., SKERRY, T. M., POYNER, D., PARDAMWAR, M., REYNOLDS, C. A., DOWELL, S. J., WILLARS, G. B. & LADDS, G. 2015. Modulation of Glucagon Receptor Pharmacology by Receptor Activity-modifying Protein-2 (RAMP2). *Journal of Biological Chemistry,* 290**,** 23009-23022.

WESTON, C., WINFIELD, I., HARRIS, M., HODGSON, R., SHAH, A., DOWELL, S. J., MOBAREC, J. C., WOODLOCK, D. A., REYNOLDS, C. A., POYNER, D. R., WATKINS, H. A. & LADDS, G. 2016. Receptor Activity-modifying Protein-directed G Protein Signaling Specificity for the Calcitonin Gene-related Peptide Family of Receptors. *Journal of Biological Chemistry,* 291**,** 21925-21944.

WILLIAMS, T. M., STUMP, C. A., NGUYEN, D. N., QUIGLEY, A. G., BELL, I. M., GALLICCHIO, S. N., ZARTMAN, C. B., WAN, B. L., DELLA PENNA, K., KUNAPULI, P., KANE, S. A., KOBLAN, K. S., MOSSER, S. D., RUTLEDGE, R. Z., SALVATORE, C., FAY, J. F., VACCA, J. P. & GRAHAM, S. L. 2006. Non-peptide calcitonin gene-related peptide receptor antagonists from a benzodiazepinone lead. *Bioorganic & Medicinal Chemistry Letters,* 16**,** 2595-2598.

WONG, H. K., CHEUNG, T. T. & CHEUNG, B. M. Y. 2012. Adrenomedullin and cardiovascular diseases. *JRSM cardiovascular disease,* 1.

WOOLLEY, M. J., WATKINS, H. A., TADDESE, B., KARAKULLUKCU, Z. G., BARWELL, J., SMITH, K. J., HAY, D. L., POYNER, D. R., REYNOLDS, C. A. & CONNER, A. C. 2013. The role of ECL2 in CGRP receptor activation: a combined modelling and experimental approach. *Journal of the Royal Society Interface,* 10.

WOSZCZEK, G. & FUERST, E. 2015. Ca2+ Mobilization Assays in GPCR Drug Discovery. *G Protein-Coupled Receptor Screening Assays: Methods and Protocols,* 1272**,** 79-89.

WYLLIE, D. J. A. & CHEN, P. E. 2007. Taking the time to study competitive antagonism. *British Journal of Pharmacology,* 150**,** 541-551.

WYON, Y., FRISK, J., LUNDEBERG, T., THEODORSSON, E. & HAMMAR, M. 1998. Postmenopausal women with vasomotor symptoms have increased urinary excretion of calcitonin gene-related peptide. *Maturitas,* 30**,** 289-294.

XIA, C. F., YIN, H., BORLONGAN, C. V., CHAO, J. & CHAO, L. 2006. Postischemic infusion of adrenomedullin protects against ischemic stroke by inhibiting apoptosis and promoting angiogenesis. *Experimental Neurology,* 197**,** 521-530.

XU, M., QI, F. F., ZHANG, S. S., MA, X. H., WANG, S., WANG, C. Y., FU, Y. & LUO, Y. Z. 2016. Adrenomedullin promotes the growth of pancreatic ductal adenocarcinoma through recruitment of myelomonocytic cells. *Oncotarget,* 7**,** 55043-55056.

YAMAUCHI, A., SAKURAI, T., KAMIYOSHI, A., ICHIKAWA-SHINDO, Y., KAWATE, H., IGARASHI, K., TORIYAMA, Y., TANAKA, M., LIU, T., XIAN, X., IMAI, A., ZHAI, L. Y., OWA, S., ARAI, T. & SHINDO, T. 2014. Functional differentiation of RAMP2 and RAMP3 in their regulation of the vascular system. *Journal of Molecular and Cellular Cardiology,* 77**,** 73-85.

YAP, T. A. & WORKMAN, P. 2012. Exploiting the Cancer Genome: Strategies for the Discovery and Clinical Development of Targeted Molecular Therapeutics. *Annual Review of Pharmacology and Toxicology, Vol 52,* 52**,** 549-+.

ZADOR, F., KIRALY, K., VARADI, A., BALOGH, M., FEHER, A., KOCSIS, D., ERDEI, A. I., LACKO, E., ZADORI, Z. S., HOSZTAFI, S., NOSZAL, B., RIBA, P., BENYHE, S., FURST, S. & AL-KHRASANI, M. 2017. New opioid receptor antagonist: Naltrexone-14-O-sulfate synthesis and pharmacology. *European Journal of Pharmacology,* 809**,** 111-121.

ZELLER, J., POULSEN, K. T., SUTTON, J. E., ABDICHE, Y. N., COLLIER, S., CHOPRA, R., GARCIA, C. A., PONS, J., ROSENTHAL, A. & SHELTON, D. L. 2008. CGRP function-blocking antibodies inhibit neurogenic vasodilatation without affecting heart rate or arterial blood pressure in the rat. *British Journal of Pharmacology,* 155**,** 1093-1103.

ZHAI, Y. F., CHEN, K. S., ZHONG, Y., ZHOU, B., AINSCOW, E., WU, Y. T. & ZHOU, Y. Y. 2016. An Automatic Quality Control Pipeline for High-Throughput Screening Hit Identification. *Journal of Biomolecular Screening,* 21**,** 832-841.

ZHANG, D., LUO, G., DING, X. & LU, C. 2012a. Preclinical experimental models of drug metabolism and disposition in drug discovery and development. *Acta Pharmaceutica Sinica B,* 2**,** 549-561.

ZHANG, J. H., CHUNG, T. D. Y. & OLDENBURG, K. R. 1999. A simple statistical parameter for use in evaluation and validation of high throughput screening assays. *Journal of Biomolecular Screening,* 4**,** 67-73.

ZHANG, R. & XIE, X. 2012. Tools for GPCR drug discovery. *Acta Pharmacologica Sinica,* 33**,** 372-384.

ZHANG, X. Q., GREEN, K. E., YALLAMPALLI, C. & DONG, Y. L. 2005. Adrenomedullin enhances invasion by trophoblast cell lines. *Biology of Reproduction,* 73**,** 619-626.

ZHANG, Y., XU, Y., MA, J., PANG, X. Y. & DONG, M. 2017. Adrenomedullin promotes angiogenesis in epithelial ovarian cancer through upregulating hypoxia-inducible factor-1 alpha and vascular endothelial growth factor. *Scientific Reports,* 7.

ZHANG, Z., GUAN, N., LI, T., MAIS, D. E. & WANG, M. 2012b. Quality control of cell-based high-throughput drug screening. *Acta Pharmaceutica Sinica B,* 2**,** 429-438.

ZHU, Y. J., WATSON, J., CHEN, M. J., SHEN, D. R., YARDE, M., AGLER, M., BURFORD, N., ALT, A., JAYACHANDRA, S., CVIJIC, M. E., ZHANG, L. T., DYCKMAN, A., XIE, J. N., O'CONNELL, J., BANKS, M. & WESTON, A. 2014. Integrating High-Content Analysis into a Multiplexed Screening Approach to Identify and Characterize GPCR Agonists. *Journal of Biomolecular Screening,* 19**,** 1079-1089.

ZUDAIRE, E., MARTINEZ, A. & CUTTITTA, F. 2003. Adrenomedullin and cancer. *Regulatory Peptides,* 112**,** 175-183.

ZUDAIRE, E., MARTINEZ, A., GARAYOA, M., PIO, R., KAUR, G., WOOLHISER, M. R., METCALFE, D. D., HOOK, W. A., SIRAGANIAN, R. P., GUISE, T. A., CHIRGWIN, J. M. & CUTTITTA, F. 2006. Adrenomedullin is a cross-talk molecule that regulates tumor and mast cell function during human carcinogenesis. *American Journal of Pathology,* 168**,** 280-291.